NASA TECHNICAL REPORT

NASA TR R-461

NASA TR R-461

REAL-TIME DETECTION AND DATA ACQUISITION SYSTEM FOR THE LEFT VENTRICULAR OUTLINE

Johan Hendrikus Christiaan Reiber

Ames Research Center
Moffett Field, Calif. 94035

NATIONAL AERONAUTICS AND SPACE ADMINISTRATION • WASHINGTON, D. C. • JUNE 1976

1 Report No. NASA TR R-461	2 Government Accession No	3 Recipient's Catalog No

4 Title and Subtitle	5 Report Date
REAL-TIME DETECTION AND DATA ACQUISITION SYSTEM FOR THE LEFT VENTRICULAR OUTLINE	June 1976
	6 Performing Organization Code

7 Author(s)	8 Performing Organization Report No
Johan Hendrikus Christiaan Reiber*	A-6292

	10 Work Unit No
9 Performing Organization Name and Address	970-23-30-16
Ames Research Center, NASA Moffett Field, California, 94035	11 Contract or Grant No
	13 Type of Report and Period Covered

12 Sponsoring Agency Name and Address	Technical Report
National Aeronautics and Space Administration Washington, D. C. 20546	14 Sponsoring Agency Code

15 Supplementary Notes

16 Abstract   Dynamic measurements of the left ventricular shape and size are of great importance in cardiovascular research and clinical practice. The usual method for acquiring these data requires that the left ventricular margin be outlined manually from television or cineradiographic images for on-line storage of the coordinates. Because of the large amounts of data required in left ventricular studies, this task is time consuming and tedious.

To automate the data acquisition procedure, a real-time contour detection and data acquisition system for the left ventricular outline has been developed using video techniques. The x-ray image of the contrast-filled left ventricle is stored for subsequent processing on film (cineangiogram), video tape or disc. The cineangiogram is converted into video format using a television camera. The video signal from either the TV camera, video tape or disc is the input signal to the system. The contour detection is based on a dynamic thresholding technique. Since the left ventricular outline is a smooth continuous function, for each contour side a narrow expectation window is defined in which the next borderpoint will be detected. A borderpoint is defined where the video signal crosses the reference level within the expectation window. Forced borderpoints are generated if the video signal does not cross the reference level within the expectation window. Each borderpoint is determined in a 12-bit format by counting 50-MHz clockpulses from the horizontal sync pulses to the borderpoint.

The center of the expectation window is defined as the average position of the centers of the expectation windows determined separately by the line and field extrapolation principles, respectively. The line extrapolation principle determines the center of the expectation window as a linear extrapolation from the borderpoints on the two previous lines in the same field and the field extrapolation principle as a linear extrapolation from corresponding borderpoints in one or two previous fields.

A computer interface has been designed and built for the online acquisition of the coordinates using a PDP-12 computer.

Results to date with the system have been very good. The advantage of this system over presently available systems is its potential for online, real-time acquisition of the left ventricular size and shape during angiocardiography.

17 Key Words (Suggested by Author(s))	18 Distribution Statement
Cineangiogram, Computer interface, Contour detection, Contourgraph, Digital computer, Dynamic geometry, Left ventricular angiography, Video disc recording, Videometry	Unlimited STAR Category - 54

19 Security Classif. (of this report)	20 Security Classif (of this page)	21 No of Pages	22 Price*
Unclassified	Unclassified	311	$9.25

Page intentionally left blank

Page intentionally left blank

ACKNOWLEDGMENTS

TABLE OF CONTENTS

A   proportionality factor ($0 \leq A \leq 1$), indicating equilibrium
position border point on background slope within distance
Δ from knee in linear border model

ACL   accumulator left border

ACR   accumulator right border

A_0 value of A for selected parameters (α_0, V_{c0})

AV   difference in consecutive border positions during simulated
aortic valve plane generation, expressed in 8-bit binary
format

a   upper level in the linear border model

BP_{equil} equilibrium position of border point

BP'_{equil} new equilibrium position of border point after dc level in
linear border model has changed from b to $b + c$ volts

BP''_{equil} new equilibrium position of border point after ventricular
slope in linear border model has changed from γ_1 to
γ_3 V/sec

BP'''_{equil} new equilibrium position of border point after background
slope in linear border model has changed from γ_2 to
γ_4 V/sec

BP(n)   position of border point on line n

BP(0)   initial position of a border point

BP(z)   z transform of BP(n)

b   dc level at the knee in the linear border model

b_{max} maximum value of b for all scan lines traversing the left
ventricle in a video field

b_{min} minimum value of b for all scan lines traversing the left ventricle in a video field

C   constant in formula describing maximum excursions of extreme points of the expectation window for zeroth order line extrapolation principle

$\left.\begin{array}{c} C_1 \\ C_2 \end{array}\right\}$ constants in formula describing $g_R(nT)$ for first-order line extrapolation principle

$\left.\begin{array}{c} C_3 \\ C_4 \end{array}\right\}$ constants in formula describing $g_L(nT)$ for first-order line extrapolation principle

c   incremental dc level in linear border model

c_N maximum allowable negative change in dc level in linear border model

c_n negative change in dc level in linear border model

c_p maximum allowable positive change in dc level in linear border model

c_1 maximum allowable positive change in dc level in linear border model such that the border point remains on the ventricular slope on first line with dc level changed

D   vertical distance between consecutive video lines, expressed in 50-MHz clock pulses

FE   field enable; binary operator indicating whether field extrapolation principle is selected or not

FF   field flag; binary operator indicating whether field extrapolation principle is applied or not

$F(x,y)$ function describing processed picture

$f_1(V_c)$ upper bound of α values as a function of V_c in linear border model

$f_2(V_c)$ lower bound of α values as a function of V_c in linear border model

$f_3(V_c)$ upper bound of α values as a function of V_c in linear border model with different dc level and ventricular slope from initial situation

$f_4(V_c)$ lower bound of α values as a function of V_c in linear border model with different dc level and ventricular slope from initial situation

$f(x,y)$ function describing original picture

$g_L(nT)$ position of forced border point at left-hand-side expectation window on line n in current field

$g_m(nT)$ position of border point on line n in field m

$g(nT)$ position of border point on line n in current field

$g_R(nT)$ position of forced border point at right-hand-side expectation window on line n in current field

$h[(n+1)T]$ center of the expectation window on line $(n+1)$ in current field, determined by the line extrapolation principle

$h_m[(n+1)T]$ center of the expectation window on line $(n+1)$ in field m, defined as the average position of the centers of the expectation windows determined separately by the line and field extrapolation principles

$h_{mF}[(n+1)T]$ center of the expectation window on line $(n+1)$ in field m determined by the field extrapolation principle

$h_{mL}[(n+1)T]$ center of the expectation window on line $(n+1)$ in field m determined by the line extrapolation principle

K	preset dc level for dynamical adjustment expectation window width
k	proportionality factor, determining amount of detail image to be mixed into original image
LBP	left-border point
LEPL	beginning point expectation window for left border
LEPR	end point expectation window for left border
LEWL	left-hand-side expectation window width for left border
LEWR	right-hand-side expectation window width for left border
LSPL1	left sample point for the left border at distance LSWL from LEPL
LSPL2	left sample point for the left border at distance LSWL/2 from LEPL
LSPR	right sample point for the left border at distance LSWR from detected border point
LSWL	left-hand-side sample window width for left border
LSWR	right-hand-side sample window width for left border
M	overall magnification function from face image intensifier to projection screen
MBR	memory buffer register
M(ACL)	contents accumulator left border
M(MBR)	contents memory buffer register
M_0	magnification factor at projected origin of calibration plate
M_1	slope of magnification function
N_1	pointer, gives address in field memory for border point in previous field
OP	outpulse generated at apex of left ventricle

q	electronic charge
RBP	right-border point
REPL	beginning point expectation window for right border
REPR	end point expectation window for right border
REWL	left-hand-side expectation window width for right border
REWR	right-hand-side expectation window width for right border
R_n	remainder of Taylor series
RSPL	left sample point for right border at distance RSWL from REPL
RSPR1	right sample point for right border at distance RSWR/2 from detected border point
RSPR2	right sample point for right border at distance RSWR from detected border point
RSWL	left-hand-side sample window width for right border
RSWR	right-hand-side sample window width for right border
r	correlation coefficient
SL	starting line; video line on which starting point SP is situated
SP	starting point; indicates start of the border detection algorithm within a video field
T	video line period (63.5 μsec)
T_D	time delay for image enhancement
V_c	manually adjustable dc level in formula for dynamic reference level
V_{c0}	assumed selected value for V_c
V_D	difference of sample levels on either side of a border measured at the same video line

V_{DIFF}	difference of original video signal and signal delayed over T_D sec
V_{equil}	equilibrium reference level at BP_{equil}
V'_{equil}	new equilibrium reference level at BP'_{equil} after dc level in linear border model has changed from b to $b + c$ volts
V''_{equil}	new equilibrium reference level at BP''_{equil} after ventricular slope in linear border model has changed from γ_1 to γ_3 V/sec
V'''_{equil}	new equilibrium reference level at BP'''_{equil} after background slope in linear border model has changed from γ_2 to γ_4 V/sec
V_{error}	error signal for additional adjustment of dynamic reference level
V_L	video sample level at left sample point in linear border model in equilibrium situation
$V_L(n+1)$	video sample level on line $(n + 1)$ at left sample point in linear border model
VL1	video sample level at LSPL1 on line $(n + 1)$ for left border
VL2	video sample level at LSPL2 on line $(n + 1)$ for left border
VR	video sample level at LSPR on line n for left border
V_R	video sample level at right sample point in linear border model in equilibrium situation
$V_R(n)$	video sample level on line n at right sample point in linear border model
$V_{ref}(n+1)$	calculated reference level on line $(n + 1)$

V_1 function for the ventricular slope in linear border model with slope γ_1 V/sec

V_1' function for the ventricular slope with dc level of $b + c$ volts and slope γ_1 V/sec in linear border model

V_2 function for the background area in linear border model with slope γ_2 V/sec

V_2' function for background area with dc level of $b + c$ volts and slope γ_2 V/sec in linear border model

$V_{2,DIFF}$ difference of V_{DIFF} and V_{DIFF} delayed over T_D sec

V_3 function for the ventricular slope with dc level of $b_{min} + c$ volts and slope γ_3 V/sec in linear border model

V_4 function for the background area with dc level of $b_{min} + c$ volts and slope γ_4 V/sec in linear border model

$V(s)$ Fourier transform of $v(t)$

$v(t)$ function describing video signal

$x0$ x coordinate of the origin of the external x-ray coordinate system

$x1$ x coordinate first lead bead position

$x2$ x coordinate second lead bead position

$y0$ y coordinate of the origin of the external x-ray coordinate system

$y1$ y coordinate first lead bead position

$y2$ y coordinate second lead bead position

α proportionality factor in formula for dynamic reference level $(0 \leq \alpha \leq 1)$

α_{min} minimum required value for α

α_0 assumed selected value for α

γ slope of ramp function

γ_1 initial ventricular slope in linear border model

γ_2 initial background slope in linear border model

γ_3 new ventricular slope in linear border model

γ_4 new background slope in linear border model

Δ one-sided sample window width, assuming a symmetrical window

Δ' dynamic one-sided sample window width, assuming a symmetrical window

Δ_L left-hand-side sample window width

Δ_R right-hand-side sample window width

$\Delta(nT)$ difference in horizontal position of border coordinates $g(nT)$ and $g[(n-1)T]$

δ direction coefficient biasing function for dynamic reference level parameters

ε one-sided expectation window width, assuming a symmetrical window

ε_L left-hand-side expectation window width

ε_R right-hand-side expectation window width

ζ amplitude standard video signal without synchronization pulses $(0.714 \pm 0.1 \text{ V})$

η amplitude synchronization pulse in standard video signal $(0.286 \text{ V nominal})$

θ angle between direction of the outline and video scan lines

σ   slope of maximum deviation function for zeroth-order line

         extrapolation principle

τ   time constant transient response for linear border model

∇   Laplacian operator

GLOSSARY OF MEDICAL TERMS USED

angiocardiography

roentgenography of the heart and great vessels after intravenous injection of opaque fluid

apex (cordis)

tip of the heart

atria

receiving chambers just prior to the cardiac ventricles

biplane x-ray system

x-ray system capable of recording two films simultaneously or nonsimultaneously and usually positioned at right angles (orthogonal)

cardiac

pertaining to the heart

catheterization (left ventricular)

the employment or passage of a catheter; in relation to the left ventricle the passage of a small catheter through blood vessels retrograde into the left heart chamber

cardiography

recording the heart's movements

cardiology

study of the heart and its functions

cineangiogram

motion picture of the passage of dye through the blood vessels

cardiovascular

pertaining to the heart and blood vessels

endocardial surface

inner surface of the heart wall

epicardial surface

outer surface of the heart wall

hemodynamic

pertaining to the movements involved in the circulation of the blood

left anterior oblique position (LAO)

position such that the left anterior quadrant of the chest wall is nearest the image intensifier; angle of rotation is usually specified

left ventricle	left heart chamber
left ventricular	pertaining to the left ventricle
myocardium	heart muscle
postero anterior	from back to front, or from the posterior (dorsal) to the anterior (ventral) surface; in roentgenology, denoting direction of the beam from the x-ray source to the beam exit surface
pulmonary	pertaining to the lungs
pulmonary artery	artery in which blood travels directly from the heart to the lungs
right anterior oblique position (RAO)	position such that the right anterior quadrant of the chest wall is nearest the image intensifier; angle of rotation is usually specified
transmural pressure	pressure across the wall of a cavity
ventricles	main pumping chambers of the heart

REAL-TIME DETECTION AND DATA ACQUISITION SYSTEM
FOR THE LEFT VENTRICULAR OUTLINE[*]

Johan Hendrikus Christiaan Reiber[**]

Ames Research Center

SUMMARY

Dynamic measurements of the left ventricular shape and size are of great importance in cardiovascular research and clinical practice. The usual method for acquiring these data requires that the left ventricular margin be outlined manually from television or cineradiographic images for on-line storage of the coordinates. Because of the large amounts of data required in left ventricular studies, this task is time consuming and tedious.

To automate the data acquisition procedure, a real-time contour detection and data acquisition system for the left ventricular outline has been developed using video techniques. The x-ray image of the contrast-filled left ventricle is stored for subsequent processing on film (cineangiogram), video tape or disc. The cineangiogram is converted into video format using a television camera. The video signal from either the TV camera, video tape or disc is the input signal to the system. The contour detection is based on a dynamic thresholding technique. Since the left ventricular outline is a smooth continuous function, for each contour side a narrow expectation window is defined in which the next borderpoint will be detected. A borderpoint is defined where the video signal crosses the reference level within the expectation window. Forced borderpoints are generated if the video signal does not cross the reference level within the expectation window. Each borderpoint is determined in a

12-bit format by counting 50-MHz clockpulses from the horizontal sync pulses to the borderpoint.

The center of the expectation window is defined as the average position of the centers of the expectation windows determined separately by the line and field extrapolation principles, respectively. The line extrapolation principle determines the center of the expectation window as a linear extrapolation from the borderpoints on the two previous lines in the same field and the field extrapolation principle as a linear extrapolation from corresponding border-points in one or two previous fields.

The reference level at which a borderpoint will be detected is calculated from local sampled video levels on a line-to-line basis. With three sample points per contour side, the calculated reference level can be adjusted where the video signal around the border differs from the assumed border model. A theoretical analysis of the reference level principle is given assuming this linearized border model. Using the difference of the sampled levels, a simple adjustment of the expectation window width can be applied advantageously in areas of low contrast.

A computer interface has been designed and built for the online acquisition of the coordinates using a PDP-12 computer. The eight most significant bits of an x coordinate are stored in memory. The y coordinate of a border-point is defined as its video line-number (8-bit format). The four remaining bits of each 12-bit data word are used as flag bits. Data transfers occur under control of the computer interface using direct memory access (DMA).

A quantitative evaluation of the success of the border algorithm was done using eight aluminum ellipses, four post-mortem casts and two series of left ventricular angiograms. The video detected outlines were compared with the

2

outlines determined manually by an experienced investigator, by calculating

image areas and the mean and standard deviations of the differences in the

outlines, after they had been corrected for linear and nonlinear magnification

(due to the recording and projection systems). This evaluation has shown that

the automatically detected outlines agree very well with the manually traced

outlines and that the reproducibility of the video system is much greater than

for manual tracings of the border.

Results to date with the system have been very good. The advantage of

this system over presently available systems is its potential for on-line, real-

time acquisition of the left ventricular size and shape during angiocardiography.

Page intentionally left blank

CHAPTER 1: INTRODUCTION

Statement of Problem

The function of myocardial muscle is to generate cyclic changes in tension and dimensions for the chamber walls to propel the required quantities of blood necessary to meet the circulatory needs of the body. Evaluating the status of cardiac function necessitates measurements of parameters such as length, tension, and the rates of changes of these parameters throughout individual cardiac cycles. The complex shape and configuration of the cardiac chambers preclude a description by simple geometric relationships or a specification by a relatively small number of dimensions.

Many methods for measuring cardiac chamber dimensions and volume in animals or man are known. However, angiocardiography has proven with time to be the most readily available, reliable method for these purposes (refs. 1-4). It provides information concerning the overall dynamic geometry of the atria or ventricles. Newer methods, such as radioisotope angiography, endocardial labeling with tantalum screws, and especially echo-ultrasound, are rapidly gaining ground. Despite these advances, angio-cardiography serves and will continue to serve as a standard for comparison for these methods.

Dynamic measurements of the size and shape of the left ventricular cavity and their correlation with simultaneously occurring pressure and flow events are very important in cardiovascular research. The left ventricular angiograms are obtained clinically during heart catheterization, whereby a catheter is inserted into the left ventricle through an artery from either the groin or the arm. This catheter may also have a

5

pressure-sensitive tip or an extra pressure catheter can be inserted. The left ventricular cavity is made roentgen opaque by injecting a suitable radiodense liquid (usually Renovist) into the intact left ventricle. A left ventricular shadow is generated at the face of the image intensifier by radiating the area with x-rays from an x-ray tube underneath the patient. A cine- and video camera are mounted on top of the image intensifier so that the information can be stored on film, video tape, and/or disc and can be viewed instantaneously on a TV monitor. The frame rate is normally between 30 and 60 frames/sec. By use of the Nyquist criterion, it has been shown that left ventricular volume and length can be adequately reproduced at 30 frames/sec (ref. 5).

Many methods and equations have been developed for determining heart size and shape from angiocardiograms (refs. 1 and 6-11). These methods are difficult to calibrate because there is no standard available for comparison; the absolute amount of blood in the left ventricle cannot be measured during life. Post-mortem casts are usually used to calibrate single-plane or biplane recordings, resulting in regression equations for a particular x-ray and optical processing chain (refs. 7 and 8). All volume data then must be corrected with these regression equations, which are valid only for this particular x-ray system. Large errors result if these corrections are not applied. For volume studies in man, single-plane cine techniques are recommended (ref. 9) because

    (1) it reduces the overall x-ray exposure to the patient,

    (2) more rapid filming is possible than with biplane large film angiocardiography,

    (3) the total amount of data to be processed is reduced,

(4) the cost of biplane x-ray equipment is prohibitive for most

laboratories.

Single-plane angiocardiography is useful for volume calculations

because the transverse chamber dimensions in man are nearly equal, which

is not the case for the canine left ventricle (ref. 9). The right ante-

rior oblique (RAO) position is recommended for calculation of volume

because the true spatial left ventricular length can be measured due to

the position of the heart within the chest. Forshortening of this major

chord usually occurs in the postero-anterior (PA) x-ray projection.

The availability of radiographic information concerning chamber

size and shape for clinical or investigative use within reasonable peri-

ods of time is limited. All methods for calculating left-ventricular

volume from angiocardiographic films are tedious and require the inter-

action of an experienced investigator to properly define chamber margins

even with films of excellent quality. Since the introduction of the

digital computer into the cardiovascular laboratory in the early sixties

(ref. 12), many aspects of the data processing have been automated.

Among others, the digital computer is used to

(1) store the coordinates of the obtained outlines from angiograms,

(2) correct the boundary points for linear and nonlinear

magnification,

(3) calculate spatial ventricular dimensions from biplane data or

sequential single-plane data from two different views (refs. 13

and 14),

(4) calculate left ventricular volume and relationships with other

parameters such as pressure,

(5) mathematically reconstruct the chamber as accurately as possible,

(6) display the results on a CRT viewing screen in the form of graphs, charts, or the constructed image of the heart chamber itself,

(7) sample analog haemodynamic parameters such as blood flow and pressure, in synchronization with the angiocardiographic data (ref. 15), and

(8) spatially track selected points and accurately describe their spatial motion over a cardiac cycle, using biplane filming and identification of discrete points in both sets of film (ref. 15).

The crucial part in the data acquisition and processing, however, is still to define and subsequently store the chamber margins in the digital computer. Manual and semiautomatic procedures using manual digitizers, electronic planimeters, or a flying spot scanner are currently in use. These methods require a considerable amount of interaction on the part of the investigator. In the last decade, many attempts have been made to automate this procedure and to come up with an automated border recognizer. As a result, several different approaches have been reported, of which the most important are described in chapter 2.

Left ventricular volume obtained from monoplane or biplane angiocardiograms has been demonstrated to be reasonably accurate and clinically useful (ref. 15). However, these conventional techniques are not adequate to determine the dynamic three-dimensional size and shape of the heart. Calculations of the shape and volume of the left ventricular

8

chamber from biplane cine- and video-roentgen silhouettes are conventionally based on two major unwarranted assumptions: (1) all cross sections of the ventricle oriented perpendicular to its long axis are elliptical and (2) the orthogonal silhouettes of each cross section were recorded when the ventricle was positioned so that the major and minor axes of each of its cross sections were perpendicular to the respective orthogonal beams of the biplane x-ray system. Most recently, computer graphics have been used for three-dimensional reconstruction of irregularly shaped, nonhomogeneous structures, such as the intact heart, using multiplanar roentgen projections (refs. 16-20).

To accurately reconstruct the three-dimensional shape and dimensions of the entire epicardial and endocardial surfaces of the heart, the roentgen opacity profiles of the video lines traversing the image of the heart are required. These profiles are obtained by analog-to-digital conversion and logarithmic transformation of the intensities at a large number of points across each video line traversing the heart and for at least 10 angles of view covering a range of 180°. By use of an algebraic reconstruction algorithm, the spatial distribution of roentgen opacities over the entire anatomic extent of the ventricles can be calculated. Needless to say, accurate on-line and real-time border recognition would be extremely helpful in obtaining the vast amount of data in the above described studies.

To quantitatively assess cardiac contractility and reserve capacity, the dynamic length/tension relationships must be determined, along with simultaneous measurements of intracardiac and transmural pressures. To accurately describe these relationships throughout the cardiac cycle,

techniques must be developed for determining the size and shape of the heart over its full anatomic extent at sufficiently frequent intervals of time.

This dissertation concentrates on a particular aspect of the complex data-acquisition system, that is, the research toward an on-line and real-time left ventricular boundary detector and the subsequent storage of that data in computer memory.

Statement of Purpose

This dissertation describes a real-time detection and data acquisition system for the left ventricular outline. The contour detection and acquisition occur at the video rate of 60 fields/sec. The total system has the potential for future on-line use. The capability of the system for detection of the left ventricular outline from angiocardiograms is illustrated. An evaluation of the system for determining the accuracy with which it detects the outlines compared with a manual digitizing method is given. Possible improvements and extensions for continuing research in this area are described.

The video technique for dynamic determinations of the dimensions and shapes of objects from roentgenographic data with particular reference to angiocardiography is called roentgen videometry.

Applying this technique to the roentgenographic image information requires that the input data be available in video format. The roentgenographic information is usually stored on film, video tape, or disc. For quantitative measurements of variations in either the dimensions or the luminosity of objects of interest in the x-ray images during dynamic angiography, conventional video cameras do not produce satisfactory images. Three characteristics of these cameras make them unsuitable for this purpose: (1) image integration and storage, (2) interlaced scanning, and (3) image retention. To avoid the degradation of temporal resolution, the use of noninterlaced scanning, synchronized 60/sec pulsed operation of the x-ray source and a camera with minimal image retention, such as image orthicon, lead monoxide vidicon, and silicon diode integrated target epicon are recommended (ref. 21).

To process individual film frames, a conventional camera can be used to convert the image into video format. Initially, large-film x-ray systems were used with film speeds of 6 to 12 films/sec. Advances in technology have allowed motion picture systems with speeds of 30-60 frames/sec, and for experimental use, even up to 270 and 540 frames/sec. The motion picture studies allow for beat-by-beat analysis of recorded events.

It was pointed out in the Introduction that calculating left ventricular volumes from angiocardiographic film is very tedious and

requires the interaction of an experienced investigator to define the outlines. The availability of computers in the cardiovascular laboratory has allowed reduction of the large volumes of data that result from the detection of the left ventricular outline. The crucial part in evaluating left ventricular angiograms is therefore the definition of the margin of the left ventricular chamber. Much research is done to automate this procedure. This chapter gives an overview of the most important systems that have been reported.

The videometry systems can be divided into three categories:

(1) Analog video processing - uses a video signal at 60 fields/sec from a video disc in the stop-action mode or from video converted cineangiograms. The operator interaction adjustments may consist of eliminating background structures, adjusting pedestal level, gain, or shading control.

(2) Digitized video processing - The video image is digitized and stored in a computer memory. Different border recognition algorithms can be applied.

(3) Light pen computer processing - The ventricular borders are traced with a light pen and the contour coordinates are stored in the computer for subsequent processing.

Analog Video Processing

One of the first reported systems was by the Mayo Clinic and used a biplane video angiographic system for dynamic measurements of the volume and shape of the left ventricle (refs. 16 and 22-28). A main feature of this system was the so-called video quantizer. Special electronic switching and delay circuitry allows one to record the orthogonal image

pairs side by side on the same video field. An operator interactive flying-spot scanner assembly is used to process the video signal for automated border recognition. The video signal that represents the anatomic structures surrounding the ventricular silhouette is adjusted to the same voltage level around the complete perimeter of the ventricular chamber to facilitate automatic electronic recognition of the ventricular borders. The adjustments consist of signal pedestal and signal gain, plus horizontal and vertical shade control for each video field. The flying-spot scanner assembly permits further improvement of the image by enabling the operator to manually brighten cardiac catheters, ribs, diaphragmatic borders of the liver, and other radiopaque structures superimposed on the cardiac borders and to darken filling defects in the ventricular chamber, particularly near the mitral valve. For this, the operator uses a pencil or eraser and direct visual feedback control by means of the video monitor. This manual shading technique frequently is not necessary when optimal x-ray penetration has been achieved.

The final interaction with the image at this stage is that the operator adjusts the video quantizer level so that, in his best judgment, the brightened spots marking the four border recognition points on the horizontal lines traversing the silhouettes of the ventricular chamber coincide with, as well as constitute, a complete brightened outline of the orthogonal borders of the chamber.

Four high-speed digital counters are used to measure the distance of the left ventricular silhouettes from the left edge of the television picture by counting 19-MHz clock pulses over these periods. These data are stored in real time in a digital computer for subsequent processing.

Another example of the use of an operator interactive border recognition system is to determine quantitatively the regional left-ventricular wall dynamics (ref. 29). Opacification of the left ventricle, adequate for wall thickness studies is achieved after the contrast material is injected into the main pulmonary artery. The video image contrast is adjusted at the time of analysis to provide for maximal signal/noise ratio of the epicardial and endocardial outlines for optimal border recognition. This adjustment is critical for reliable analyses and must be performed for each selected region of the ventricular wall. The videometry system then recognizes the endocardial and epicardial borders; only the selected segment gives reliable data.

A thresholding technique with constant threshold level was reported in 1970 by Covvey (ref. 30). Single cine frames are scanned by a vidicon camera and, with a special effect circuit, only the region around the ventricle is selected while the rest is blanked out. With this constant threshold level, only ventricles in pictures with exceptional contrast can be recognized.

The transit time of a horizontal video scan line through a cross section of the left ventricle is measured by counting 10-MHz clock pulses during the thresholding interval. These data are stored in a computer and the volume is calculated using Simpson's rule for the cylindrical disks, with height equal to the space between scan lines and diameter determined by the measured line width.

Another method that uses a video quantizer was described by Marcus and coworkers (refs. 31 and 32). Left ventricular angiograms taken in the RAO position at 60 frames/sec are projected with a flickerless

projector onto a Plumbicon television camera. A second television camera, the key camera,is used by a skilled operator to mask out noncontributing portions of the film and to shade selected areas so that the specified chamber can be identified accurately. The pictures are rotated so that the long axis of the opacified left ventricle is aligned horizontally on the television screen. A video planimeter with a variable threshold level is adjusted by the operator so that an accurate fit is obtain ᴄᴄ between the opacified area of the video planimeter and the area actually visualized. Three additional techniques aid in obtaining an accurate fit: (1) The extraneous background is eliminated by a mask that consists of a gray-on-black silhouette constructed slightly larger than the greatest area of the opacified ventricle in diastole. The mask is superimposed on the primary camera image by the key camera via a video keyer. (2) The operator can compensate for unequal distribution of contrast material in the ventricle by shading the television image either horizontally or vertically. (3) In any local area within the mask, density can be added or subtracted from the video image by blackening or whitening areas and superimposing these densities on the film camera image via a video mixer. This last technique is used to compensate for markedly uneven distribution of contrast material which sometimes occurs when unopacified blood from the left atrium enters the left ventricle.

The video planimeter determines the area of the opacified left ventricle on each cine frame by integrating the time that the gated television signal spends above the preset density threshold. A gated video comparator circuit determines when the video signal exceeds the threshold level. A second video planimeter determines the maximum

length of the left ventricle on each cine frame by measuring a gated horizontal band between the aortic valve and the left ventricular apex. The area and length are thus provided as analog signals, but are converted to digital format for subsequent processing. Volumes determined by this automated method compared with those obtained by manual planimetry using the area-length method gave a correlation coefficient of 0.96.

A later version of this system (ref. 32) required that the long axis of the ventricle be perpendicular to the television raster by rotating the television camera at the time of analysis. Each parallel section is assumed to be circular, and the ventricular volume, the sum of the volumes of the individual disks, can be determined by an electronic double-integration technique.

The real-time detection and data acquisition system for the left ventricular outline, which is proposed here, must be arranged in this analog video category. This system is based on a dynamic thresholding technique, whereby the reference level at which a border point is detected is calculated from local sampled video levels on a line-to-line basis. Detection of a border point is allowed only within a narrow expectation window that dynamically adapts to the left ventricular outline. The center of the expectation window on a particular line is determined by detected border positions on the previous two lines in the same field and by corresponding border points in the previous one or two fields.

Because of the fixed video scan direction, the projected left ventricle should preferably be oriented so that the longest chord is about perpendicular to the scan lines. At the average, the slope of the

left ventricular outline is then approximately perpendicular to the scan lines, thereby maximizing the density changes in the video signal at the scan lines traversing the left ventricle. This will result in a more accurate and stable detection process.

The system has been implemented so that no more than two contour points will occur on a video line traversing the left ventricle, one for the left border and one for the right border. In this context, left and right are defined with respect to the chord from the left-hand side of the designated aortic valve plane to the apex, as viewed by the investigator on a monitor screen. Allowing only one border point on a video line per contour side is justified by the fact that situations requiring more than one border point would only very seldom occur, even in nonoptimized left ventricular orientations.

An early prototype I contour detector is described in chapter 3. The computer interface for the data acquisition of the obtained contour information and the totally revised contour detector prototype II are described in the remaining chapters. An evaluation of the success of the applied border algorithm is also given.

Digitized Video Processing

. A threshold method based on statistical principles and heuristics to detect boundaries in radiographic images was reported by Chow and Kaneko (ref. 33). Their fundamental assumption, which has been empirically verified, is that the probability distribution of the intensity for any small region of the picture consisting solely of the object or the background is unimodal. The probability distribution of a small region containing a boundary is consequently a mixture of two unimodal

distributions and is generally bimodal. The histogram for such a region will therefore generally exhibit two peaks and a valley. The problem of determining the boundary reduces to that of ascertaining to which distribution each individual image point belongs. The valley point in the observed histogram, after certain smoothing operations, determines the threshold that separates the object and background. The thresholds are thus set dynamically according to local rather than global characteristics estimated from the observed intensity histograms. Before the boundary detection algorithm is applied to the scanned images, several operations are first performed: (1) the logarithmic transform to restore the radioactive absorption, (2) the subtraction of images with and without dye injection to remove irrelevant background, and (3) the averaging operation to suppress noise.

Kaneko and Mancini (ref. 34) describe a method for straight-line approximation for the boundary of the left ventricular chamber from consecutive video or cine frames, assuming that the boundary on a reference frame is available. This boundary on the reference frame may be detected manually through a light pen or by more sophisticated automated video densitometry methods (ref. 33). The previous boundary is divided into a set of segments along which local rectangular regions are set up on the present frame. The boundary on the present frame is then approximated by a set of straight lines which minimizes the square error in each rectangular region with the spatial derivative as its weight.

The idea of using the manually or (partially) automatically obtained boundary of the $(n-1)$th frame as an approximation for the boundary of the nth frame has resulted in another approach (ref. 35).

18

If the boundary search is restricted to a predetermined area of the pic-
ture, the likelihood of tracing boundaries of objects other than the ven-
tricle and contours that may occur inside the ventricle due to contrast
medium fluctuation and entering of new blood from the left atrium is
reduced. Three types of prior information are used: (1) location - the
search for the next boundary is restricted to some area around the previ-
ous boundary, (2) direction - only eight search directions at increments of
$45°$ are allowed, and (3) sign - using the center of gravity of the previous
boundary, the detection algorithm knows which side is inside or outside
the heart chamber. Only brightness transitions from bright to dark
moving from the inside to the outside are then accepted. After the new
boundary points are determined, a smoothing and filtering algorithm is
applied.

An approach that differs from previous work poses the problem of
outline or contour extraction as one of minimum cost tree searching
(ref. 36). It is "a completely automated procedure for the extraction
of the outline of the opacified left ventricle from digitized serial
angiocardiograms." The branch costs or metrics defined are indicative
of the likelihood that a particular branch lies on the true contour. The
branch metrics incorporate both local and global or contextual image
information. In this report, one obtained contour is shown and compared
with the outline extracted by a cardiologist. The computer-determined
outline lies in close relation to the manually determined contour, but
outside the outline determined by the cardiologist. Volume comparisons
are not given. This method determines the outline of the left ventricle
plus the aorta; at this stage, the algorithm does not search for the

aortic valve. However, a separate algorithm has been developed to find the aortic valve and the apex from the earlier obtained outline of the left ventricle plus aorta (ref. 37). This is done by looking at the amount of "turn" in the trace at each point along the aorta-ventricle boundary. The turning for a border point is estimated by fitting a directed straight line to the points immediately preceding this border point and another directed straight line to the points immediately following this point. The turn angle is then defined as the angle of the second directed line measured with respect to the first. The algorithm tracks the turning of the aorta-ventricle outline and uses this information to find the apex and to nominate points for the ends of the aortic valve line. The procedure for locating the apex is based on the expectation that it will be in a region of left turns somewhere near the center of the entire trace. The end points of the aortic valve line are indicated by a local extremum in the right-turn angles. The algorithm searches for local minimums in the turn angles that are more negative than -25°. An objective function is then evaluated for all possible pairings of candidate-right and candidate-left valve end points. This objective function is based on three traits of the aortic valve: (1) The valve line is one of the shortest lines that will connect the right and left boundaries of the ventricle-aorta outline. (2) The apex normally falls near the perpendicular bisector of the valve line or, in other words, the valve line is roughly perpendicular to the "centerline" of the ventricle-aorta silhouette. (3) There is usually a large right-turn angle at one or both of the valve line ends.

20

Two 20-frame series were processed and the algorithm located the valve line within 3 mm of the line selected by the cardiologist in all cases. The apex was also located within several millimeters of the point selected by the cardiologist in all cases. However, these results were obtained by applying the algorithm to outlines drawn by an experienced observer, who also preprocessed the film by filling in gaps in the outline and smoothing out irrelevant details.

An approach whereby a manually defined approximation of the left ventricular border is stored in computer memory and a computer algorithm detects a more precise border from the obtained data is described in references 38 and 39. The film is digitized by a flying-spot scanner, resulting in 64 gray levels over a 512 × 512 scan grid. An initial approximation to the image border is manually traced and stored in memory (ref. 40). The implemented algorithm assumes that the slope of the contrast transfer function across the image border is approximately zero for background and image areas and approaches a third-degree polynomial at the border area. Detecting the actual border points then requires the determination of a third-degree least-squares polynomial that fits the data in the border search interval; equating the second derivative of such a function to zero gives the point of inflection, where the maximal rate of contrast change occurs; this point is defined as the border coordinate for that interval. If the cubic approximation is not well defined (due to inadequate contrast change), then the border point is extrapolated from previously valid points.

The procedure now requires that a border search mask be defined by taking a given number of points on both sides of the trace that is

judged to define a region in which the actual border lies. The slopes of contiguous sections of the approximating line determine horizontal or vertical search directions, depending on whether the slope determined from the end points of each section is greater or less than 1. The computer algorithm determines the actual border points, which are displayed on a storage monitor for visual comparison with the manually traced outline. The computer contour is then used as the approximation to the border for the next data frame (instead of tracing an approximation) and the contour for the next image is calculated, etc., until all frames have been analyzed and the actual image border of each determined.

An algorithm has been developed by Clayton and coworkers that uses four separate border definition criteria (ref. 41). Again, a computer is used to process the video angiocardiographic recordings. A special interface is applied to transfer the video information, column by column, to the computer and a border definition algorithm is used to automatically obtain the border coordinates of the ventricular chamber for each video field (1/60 sec) during systole. To achieve maximum contrast of the radiographic image and to optimize ventricular mixing, the computer is programmed to control the dye injection by analyzing the ECG rhythm.

At the beginning of a sequence of fields, a table-top cursor controller is used to mark five points on the image: the right and left sides of the aortic valve, the extreme points on the left and right edges, and the apex. This information is used to determine the orientation of the major axis of the heart and to define the rectangular position of the image that should be digitized.

The algorithm is structured to combine various border definition criteria by forming a product. The terms of the product are based on a priori assumptions as well as information based on previous lines and fields from the same angiogram. The border algorithm searches for that point along a line in the quantized picture matrix which has the maximum probability of being the right or left border of the left ventricle. The search can be along either a horizontal or a diagonal line. The probability that a given point should be designated as the border is computed for each point using the product of four independent factors. The first term gives information concerning the location of black-to-white intensity transitions along the line. This term is the moving product of a normal frequency curve and the derivation of the discrete video levels for each point along the line, that is, a matched gradient filter. The maximum value of this term occurs where the set of points most closely fits the normal curve assumed for the gradient at the border.

The second term (video profile predictor) compares the video levels of the 10 points on either side of any point with the weighted values of the video levels adjacent to the determined border on previous lines. This term not only predicts the video level at the border point from the video level at previous border points, but also predicts the video intensity profile at the border from the profile shape at borders on previous lines.

The third term (location) is based on the assumption that the border is smooth and continuous from line to line. The predicted border location for a line is based on the direction computed from the border position on the previous two lines.

The last term (time sequence) predicts, for a given line, the location of the border in the current video field along the direction computed from the border positions on the equivalent lines in the previous two fields. The first field for a given sequence is manually entered to give the system the right initial conditions.

The apex is defined by requiring that the border cannot move outward whenever the left and right borders are within 15 points of each other. When the borders cross or are within 2 points of each other, the apex is closed. A 9-point parabolic smoothing algorithm is applied to the contour, and the aortic valve is then located by searching for the minimum distance between any of the first 20 points on the left border and any of the first 20 points on the right border.

By superimposing the computed border and the border determined by an experienced investigator on the TV monitor, good visual agreement between the two methods was found.

(Authors note: To determine accurately the success of the applied border algorithm, a quantitative evaluation is required. This remark is applicable to all systems described in this chapter. An evaluation method, applied to the detection and data acquisition system proposed in this report, is given in chapter 11.)

Another preliminary investigation in the border detection problem makes use of maximum likelihood estimations of boundary location (ref. 42). By use of a sophisticated, programmable film reader, part of the cine frame, as indicated by the operator with a light pen, is being digitized and the data are being stored in the computer; 64 levels of gray are recognized. To obtain density data, a line is constructed approximately

normal to the ventricular border through each initial point. Density readings are then obtained at each of n points equally divided on either side of the initial point. As a first approximation, a sharp discontinuity is assumed to exist at the boundary. Each sampled data point can then be written as one of the two constant densities plus an error term. A likelihood function is determined, and with least-squares estimates, the point most likely to be the boundary point is determined. A similar procedure can be derived if the data are assumed to consist of three line segments instead of two, thereby assuming the border optical density graph to be a linear function.

A method designed for use with a small computer in a clinical environment is described in reference 43. This method is based on a thresholding technique applied to the gradient of each point in the digitized image. An electronic window is positioned by the operator over the area to be processed. This section is digitized using 32 gray levels. To eliminate statistically independent electronic noise, spatial averaging or multiple digitization is applied. For each digitized point, the directional derivative is calculated using the 8 closest neighbors. To obtain a contour, this matrix of values of the gradient of the original picture function is examined for a selected minimum value. This procedure generally produces rather thick contours. To improve the resolution and to eliminate noise spikes and artifacts, a thinning algorithm is applied twice, followed by a gradient maximum following algorithm designed to eliminate all but the greatest values of the gradients remaining in the matrix. The final contour is not a continuous function, but gives a multiple of border points at each position along the actual ventricular boundary.

Light Pen Computer Processing

One of the first systems that used a computer to automate the
determination of volumes of cardiac chambers was reported in 1961 by
Baker and coworkers (ref. 12). This largely mechanical system can be
seen as an initial step toward a modern light-pen computer system. With
two 35-mm projectors, simultaneously recorded RAO and LAO images of
individual frames are projected side by side onto a tracing platform.
The contours are traced in black ink and small operational marks are
appropriately placed to instruct the scanner when to begin or stop mea-
surements. The slotted roller paper is moved forward and the next pair
of biplane data can be traced, etc. The paper now passes through a
scanner unit that uses the nonreflection of light to determine the drawn
borders and marks. The function of the scanner therefore is to measure
the diameters of the traced figures at 1-mm intervals and to transmit the
result to a photomultiplier tube which then transmits it to the computer.
The volumes of the individual cylindrical sections are calculated to
provide the total volume of the chamber.

Another system for on-line processing of the video image was
reported by Heintzen and coworkers (refs. 44-46). Byplay left ventricular
video angiocardiograms are stored on a video disc recorder and replayed
onto a TV monitor in a stop-action mode. Both projections are displayed
side by side on the monitor. The ventricular contours are successively
traced with a light pen and stored on a scan converter. The scan con-
verter reads out the stored information automatically. During each hori-
zontal scan, up to four counters are triggered by the heart boundary
pulses; the clock frequency is 10 MHz. Information corresponding to each

line of the contour stored in the buffer is read into a digital computer in real time and stored in an array. Unused portions or lines of each video field are used to simultaneously record analog data. In practice a horizontal white bar, the length of which is proportional to the actual intraventricular pressure, is superimposed in the video field in this way. This information can be stored in the computer simultaneously with the border tracing procedure, allowing automated processing of pressure-volume diagrams.

A volume angiography system for on-line computation of left ventricular angiograms utilizing a video disc recorder, a light pen unit, and a digital computer is described in reference 47. The goals of this system were to provide a clinical cardiac catheterization laboratory with an on-line method for determining left ventricular volumes at a reasonable cost, with readily available video components. The video disc recorder allows for immediate replay and stop-motion of ventricular angiograms on a video monitor. The light pen is used by a technician/physician operator to define the margins of the ventricular chamber and store the data directly in the digital computer. The computer applies preset magnification factors and calculates ventricular volume by use of the area-length method. Comparison of this system with conventional manual processing of cine-film has yielded a correlation coefficient of 0.99.

Page intentionally left blank

CHAPTER 3:   CONTOUR DETECTOR, PROTOTYPE I

The left ventricular contour detector prototype I was designed and
built at the Electronics Laboratory, Technological University, Delft,
The Netherlands, in cooperation with the Thorax Center, Erasmus
University, Rotterdam, The Netherlands (refs. 48-52). Using a model
of the left ventricle which sums given slices, volume was calculated
on-line with a special purpose calculator (ref. 53). A copy of this
prototype I was built at NASA-Ames Research Center for use in the Cardio-
vascular Research Laboratory. This device was then used as a working
tool for continuing research on the automated contour detection. The
basic principles of the prototype I contour detector are described here.

Basic Principles of the Contour Detector

Figure 1 is a block diagram of the system. The x-ray image of the
left ventricle is stored on film. This information is converted into
video format with a television camera. A left ventricular angiogram of
a dog is shown in figure 2. When the negative of conventional film is
used, the left ventricle appears as a bright structure against a dark
background. The video signal from the TV camera is the input signal to
the system. Before any contour algorithm is applied, several basic
operations are performed on the input signal to provide for a video sig-
nal with an improved signal/noise ratio and a restored dc level. The
signal is amplified, the synchronization pulses are stripped off, and a
1-MHz low-pass filter suppresses the upper frequencies which do not con-
tain relevant contour information. The filtered signal is then clamped
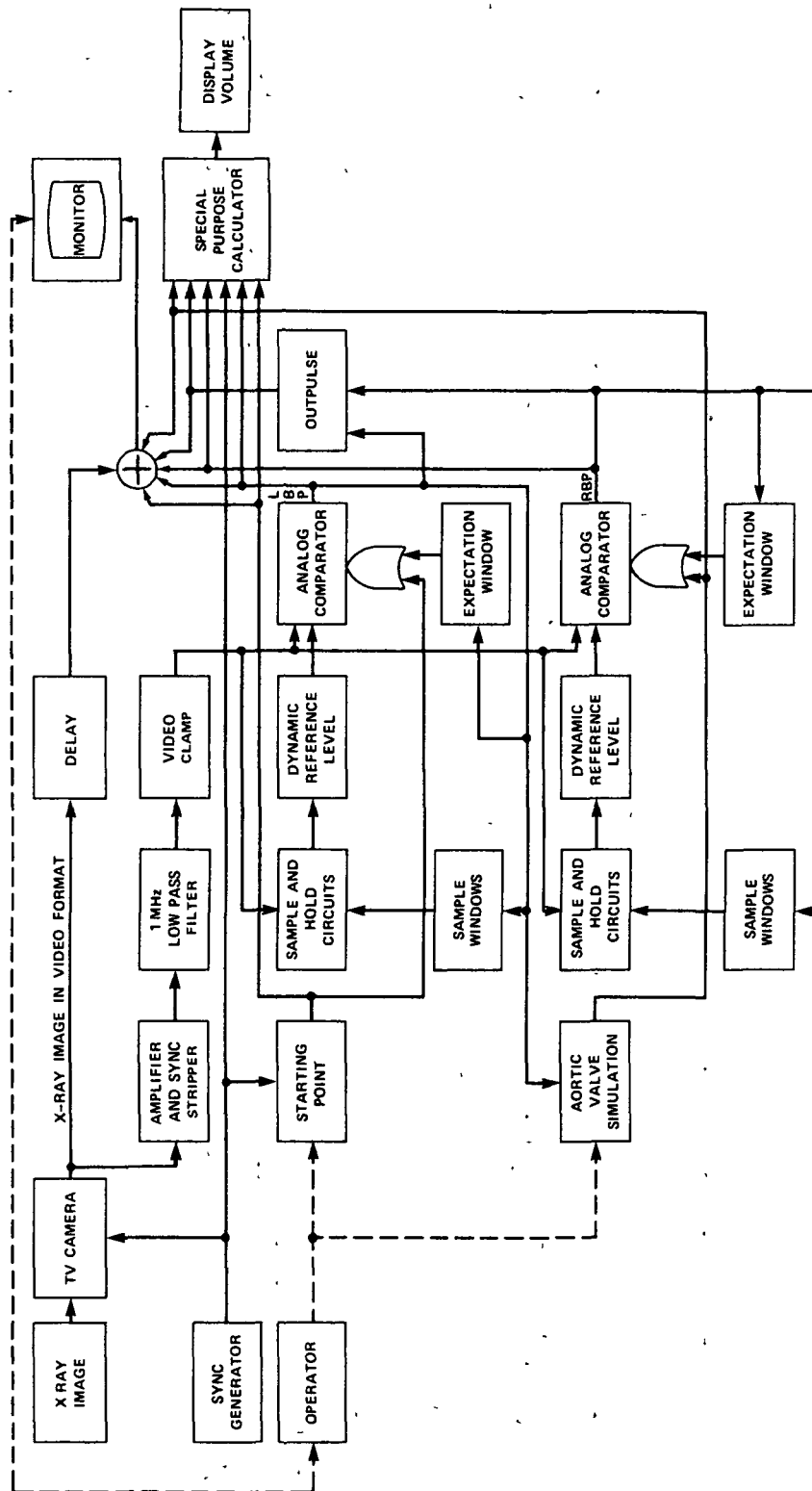for dc level restoration before it is applied to the analog comparators.

Figure 1.- Block diagram of contour detector prototype I.
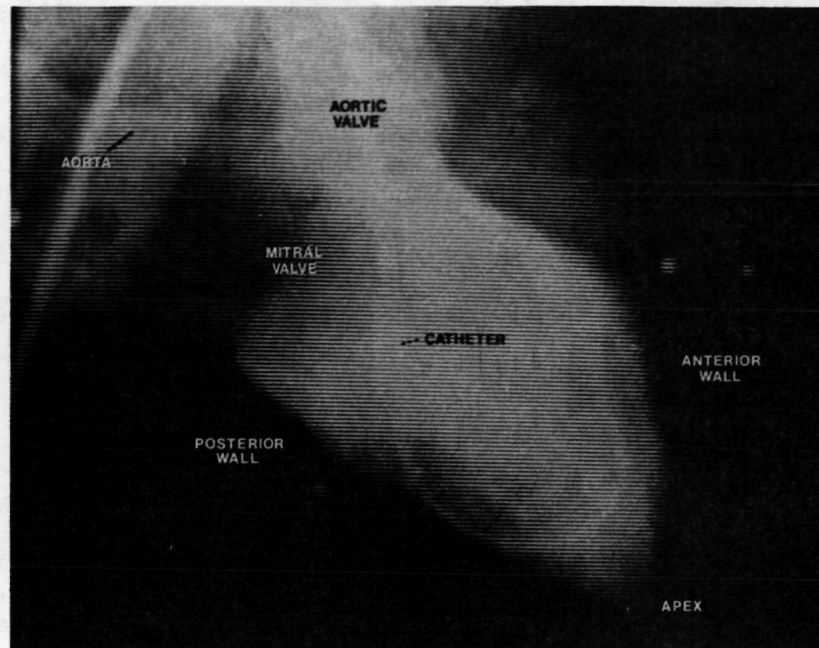
Figure 2.- Left ventricular angiogram of a dog.

For display and visual feedback, the input video signal passes through a delay line that equalizes the total delay of the low-pass filter and the logic circuitry involved in the contour detection. The delayed signal is then applied to a summation amplifier where the detected contour pulses are mixed into the video signal with the correct time relation. This total video signal is the output signal of the system and is used to display the x-ray image with the detected border on a TV monitor. The rest of the system is divided into two almost identical subsystems, one for the left border and one for the right border. In this context, left and right are defined with respect to the chord from the left-hand side of the aortic valve plane to the apex as viewed by the investigator on a monitor screen.

31

A contour can be defined as an image structure with a different brightness level on either side and with a high degree of coherence between its successive points. Such a contour can then be detected by applying a thresholding technique. An analog comparator is used which compares the video signal with a reference level. The comparator changes state as the video signal crosses the preset reference level, indicating the presence of a border point. Simply applying the level detection at a manually adjustable dc reference level would result in the detection of all the points in the picture with the same brightness level. To eliminate all but the actual left ventricular contour points, a starting point and expectation window are defined. The starting point can be manually positioned arbitrarily over the monitor screen with a joystick. This starting point indicates the position where the analog comparator for the left border is enabled for the first time during a video field. As soon as the video signal reaches the preset reference level, the first left-border point is detected. The starting point is usually positioned at the aortic valve plane. With a short fixed delay after the first left-border point has been detected, the first right-border point is generated which functions as the beginning point for the simulated aortic valve. The aortic valve plane is designated by the generation of a straight line, which separates the left ventricular chamber from the rest of the contrast-filled aorta. The generation is stopped as soon as the line encounters a preset reference level at the right border. The slope of the simulated aortic valve is manually adjustable with the joystick by rotating its central/shaft. Figure 3 shows a left ventricular cineangio-gram taken in a dog with the starting point positioned at the left side

32
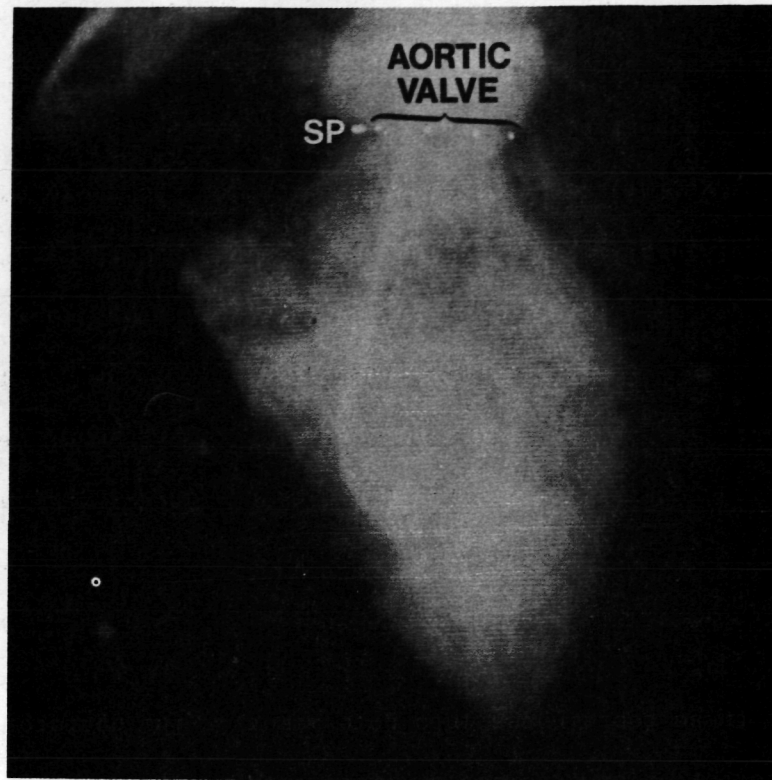
Figure 3.- Positions of the starting point (SP) and the simulated aortic valve.

of the aortic valve plane, which is designated by the generated straight line. The left ventricle has been oriented so that the longest chord is about perpendicular to the direction of the scan lines. It was explained in chapter 2, that this is the optimum orientation for the applied border detection algorithm.

The expectation window is a narrow window that dynamically adapts to the ventricular shape; the comparator is enabled during this expectation window period only. The center of the expectation window on line (n+1) is defined as having the same horizontal position as the border point BP(n) on the previous line (illustrated in fig. 4). The widths ε_L and ε_R of the left- and right-hand sides of the expectation window,

LINE n ——————— BP(n)

LINE (n+1) ———————

ϵ_L ϵ_R

→ t

EXPECTATION
WINDOW

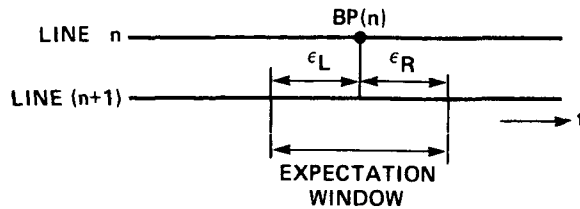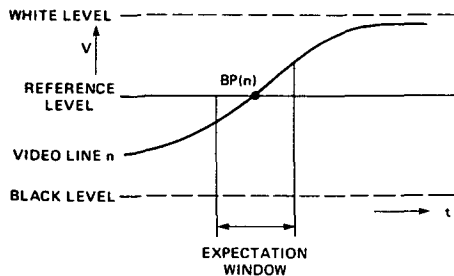Figure 4.- The center of the expectation window on line (n + 1) is defined as having the same horizontal position as the last detected border point BP(n) on the previous line n.

(a) A border point is detected where the video signal crosses the reference level.
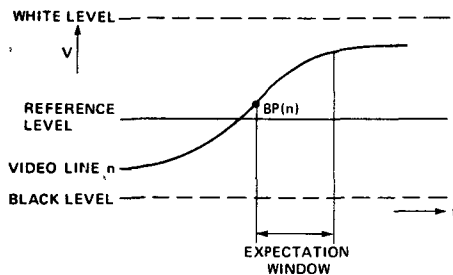
(b) A border point is detected at the beginning of the expectation window.
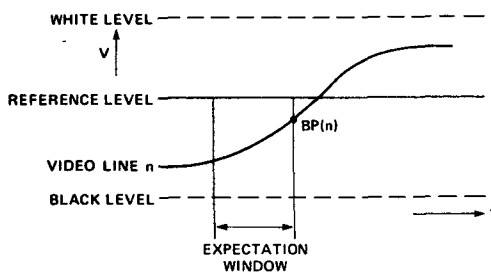
(c) A border point is generated at the end of the expectation window.

Figure 5.- Definition of the border points with respect to the expectation window.

respectively, are separately and manually adjustable. Clearly, this particular implementation of the expectation window principle is most effective when the major chord of the left ventricular cavity is about perpendicular to the scan direction of the video system.

In order to handle the case where the video signal does not cross the reference level within the expectation window, forced border points are generated. This may result from a sudden change in the video level at the border caused by intervening structures such as ribs or the diaphragm, or from a sudden position change in the actual left ventricular border from previous border points. The possible situations are illustrated in figure 5 for the left border. Figure 5(a) shows the

34

normal situation, where a border point is detected within the expectation window. Consider now the case, as illustrated in figure 5(b), that the actual contour has shifted to the left so that the video signal is already above the reference level at the beginning of the expectation window. A border point is then generated at the beginning of the expectation window as the comparator is enabled. In figure 5(c) the actual border has shifted to the right so that the video signal is below the reference level during the entire expectation window period. This situation is recognized by digital circuitry and a forced border point is then generated at the end of the expectation window.

The effects of making the expectation window widths too narrow is illustrated with the detected contours in figure 6. Figure 6(a) shows the situation where ε_L for the left border is too small. The system cannot follow the abrupt changes in the contour and instead approximates it with a straight line, the slope of which depends on ε_L. Figure 6(b) shows the situation where the right-hand side ε_R of the expectation window for the left border is too small. Again, the contour is approximated with a straight line wherever this situation is applicable. The slope of the line depends on ε_R. If the expectation window is too wide, detection is less stable because of intervening structures.

Detection of the right border occurs similarly. The detection is stopped and an outpulse generated at the ventricular apex when both borders come within a preset distance, manually adjustable from 200 nsec to 2 μsec.

Figure 7 shows an actual left ventricular angiogram whose margins have been detected using a constant reference level. Notice the error
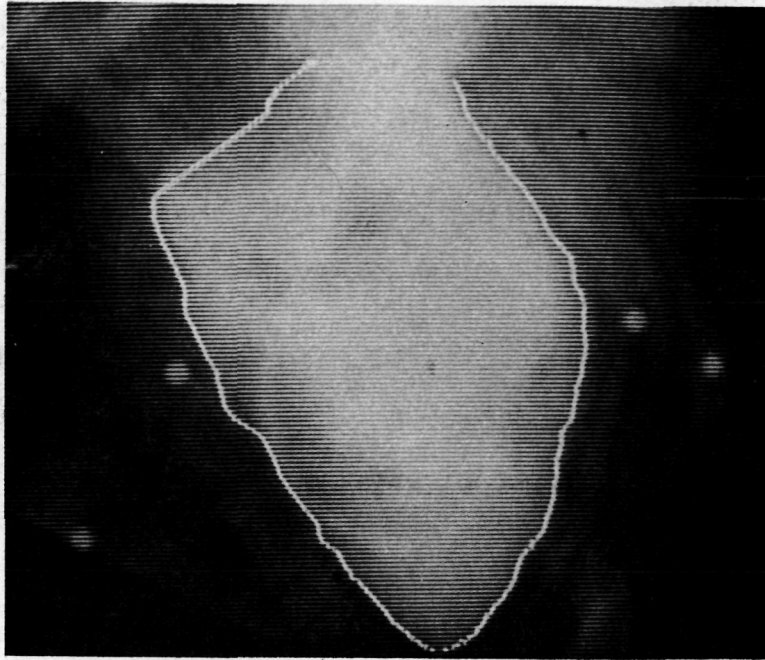
(a) Left-hand side of the expectation window for the left border is too narrow.
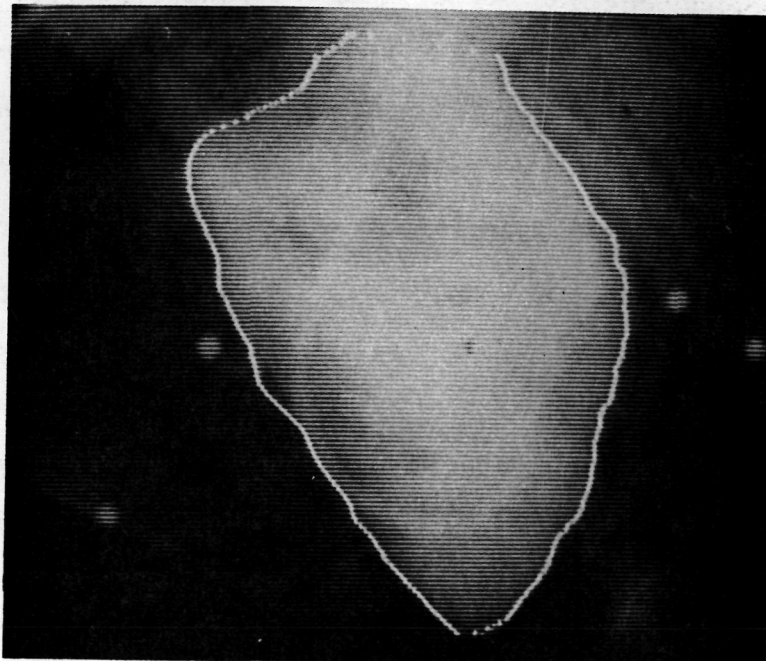
(b) Right-hand side of the expectation window for the left border is too narrow.

Figure 6.- Effects of too narrow expectation window widths on the detected contours.
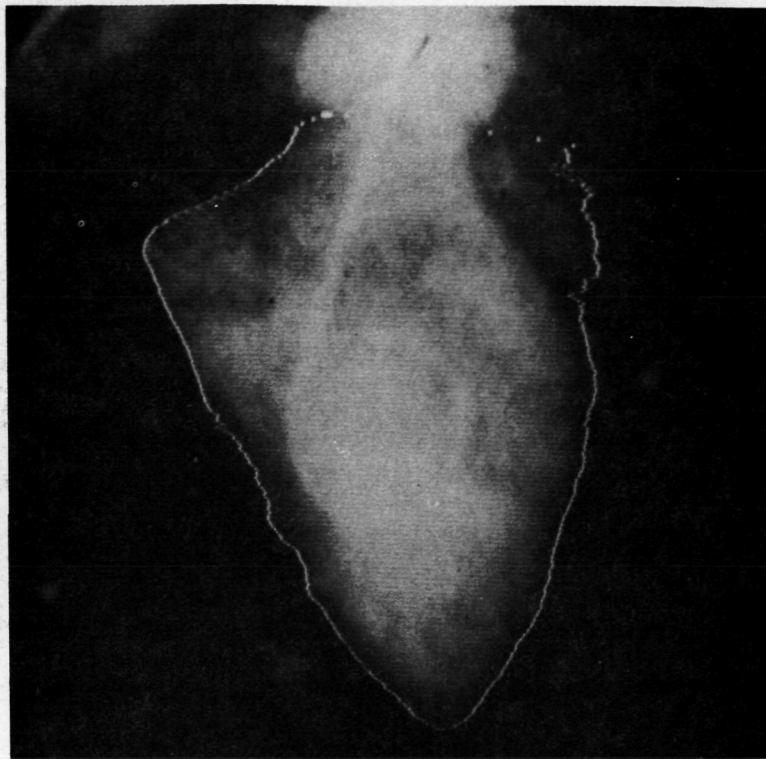
Figure 7.- Contour detection using a constant reference level.

present near the outflow tract. It is clear that the actual border

cannot be found in this way. This is remedied by use of a dynamic refer-

ence level (adjusted for each line) as described below.

Dynamic Reference Level

The constant reference level principle can be used satisfactorily

only if the brightness level is approximately constant along a ventricu-

lar border. However, in reality, this is seldom the case. The bright-

ness level changes along a border because of shading, nonhomogeneous

distribution of the contrast agent in the left ventricle, and overlapping

roentgen shadows from other organs and structures such as the diaphragm

and ribs.

A marked improvement is achieved by adjusting the reference level dynamically according to local brightness levels on a line-to-line basis. Two sample points are defined as shown in figure 8 for the left border.
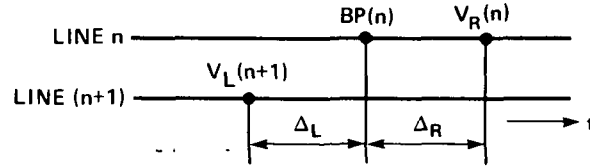
Figure 8.- Two sample points are defined for the determination of the reference level for the next line (n + 1) for the left border. The sample levels are denoted $V_R(n)$ and $V_L(n + 1)$, respectively.

With the detected border point on line n denoted by $BP(n)$, the video signal is sampled inside the ventricle at a distance Δ_R from $BP(n)$ on the same line and in the background area at a distance $T - \Delta_L$ from $BP(n)$ on line (n + 1), where T is the line period. This last sample point on line (n + 1) thus provides the most recent brightness information. The video samples are denoted $V_R(n)$ and $V_L(n + 1)$, respectively, as indicated in figure 8. The reference level for the border point on line (n + 1) is then calculated as

$$V_{ref}(n + 1) = \frac{\alpha}{2} \left[V_R(n) + V_L(n + 1)\right] + V_c \tag{1}$$

where α is a proportionality factor ($0 < \alpha < 1$) and V_c, a constant voltage level. A practical value for α is 0.8 to 0.9 and for the distances Δ_L and Δ_R, approximately 0.5 µsec. The time constant with which the reference level reaches a new final value after a disturbance depends on α. A larger α gives a larger time constant. Since the reference level for the first left- and right-border points cannot be computed from sample values, initial reference levels for these beginning points are set by the operator.

38

Figure 9 shows the detected contour for a left ventricular angiogram of a dog when applying the above described dynamic reference level principle. The obtained contour agrees well with the outline drawn by an experienced investigator.
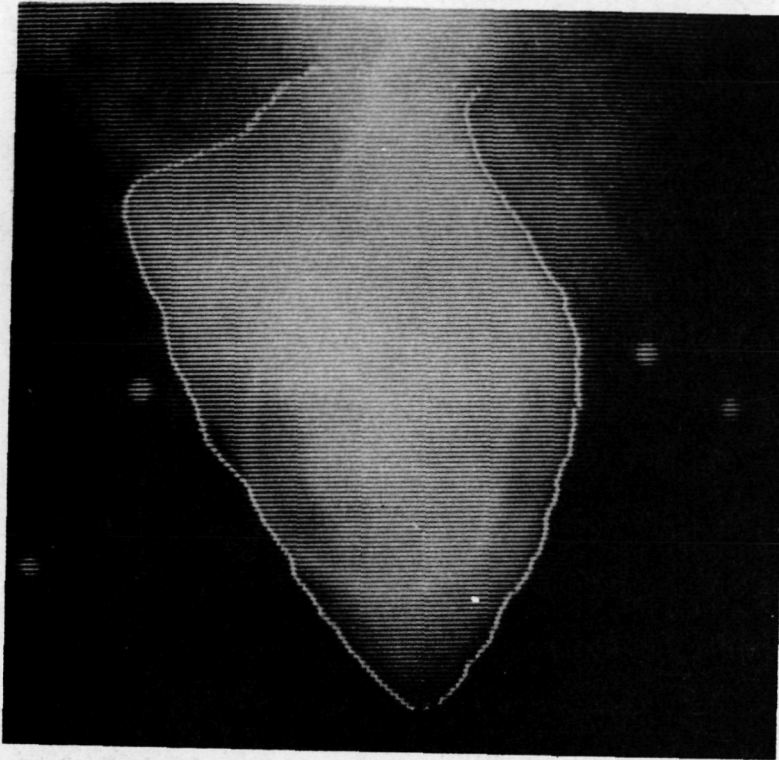
Figure 9.- Resulting contour for a left ventricular angiogram of a dog when applying the dynamic reference level principle.

Realization of the Contour Detector, Prototype I

After the description of the border algorithm, the realization of the system according to the block diagram in figure 1 should be relatively straightforward. The operator adjusts the position of the starting point, which enables the analog comparator for the left border and sets the initial reference level for the first left-border point. The analog comparator detects the first left-border point which defines the

39

expectation window and sample points for the next left-border point. The reference level is computed from the sample values, resulting in the second left-border point, etc. The first left-border point determines the beginning point of the simulated aortic valve, the slope of which is adjusted properly by the operator. The aortic valve generation is stopped as soon as the line encounters a preset reference level at the right border. This preset level is again set by the operator. Expectation windows and sample points are defined in the same way as for the left border. The detection is stopped and the outpulse is generated as soon as the distance between the left- and right-border points is smaller than the adjustable apex distance.

For volume calculations using a slices model (ref. 6), the diameter and volume of circular cross sections of the left ventricle, as sliced by the horizontal scan lines, are calculated from the detected border points by a special purpose calculator (ref. 53). The volumes of all the cross-sectional slices are added, providing an approximation of the left ventricular volume. The accuracy of the calculated volume according to this method is maximal when the longest chord of the ventricle is again about perpendicular to the direction of the scan lines.

For subsequent processing of the detected contour, it was decided to build a computer interface for on-line acquisition of these data. The computer interface design is described in chapter 4.

The computer interface is the link between the contour detector, which detects the left ventricular outline from angiograms in video format, and the computer, which enables one to do calculations using the border coordinates once they have been stored in memory. The basic function of the computer interface therefore is to convert the border coordinates to digital format and to transfer them to the computer memory. Designing the interface for a real-time interaction requires that the computer interface controls the information transfers to the computer instead of having the transfers under computer control.

Computer Interface Requirements

The PDP-12 computer in the Cardiovascular Research Laboratory at NASA-Ames Research Center is capable of doing input/output transfers under control of the external device on a cycle-stealing basis (ref. 54) - called direct memory access (DMA). The data break facility allows an I/O device to transfer information directly to or from the PDP-12 core memory using DMA. Generally, DMA is advantageous for high-speed I/O devices rather than transferring data through the accumulator under program control, which is slower and ties up the CPU. However, the data break device interface requires more control logic, resulting in higher hardware costs than a programmed transfer interface.

Data breaks are of two basic types: single cycle and three cycle. In a single-cycle data break, registers in the device (or device interface) specify the core memory address of each transfer and count the number of transfers to determine the end of data blocks. In the three-cycle

data break, two computer core memory locations perform these functions, simplifying the device interface by omitting two hardware registers.

To initiate a data break transfer of information, the interface control must

(a) specify the affected address in core memory,

(b) provide the data word by establishing the proper logic levels at the computer interface (assuming an input data transfer) or provide input gates and storage for the word (assuming an output data transfer),

(c) provide a logical signal to indicate direction of data word transfer,

(d) provide a logical signal to indicate single-cycle or three-cycle break operation, and

(e) request a data break by supplying a proper signal to the computer data break facility.

The transfer rate from the contour detector to the computer is relatively high. For each video-scan line (63.5 μsec) traversing the left ventricle, two coordinates must be transferred to the computer. During the time the CPU is not in a data break cycle requested by the contour detector, it should be able to service other devices connected to the computer, continue to execute the main program, and also transfer the stored border coordinates from core to disk storage once an interrupt signal is given (to be explained later). Therefore, the data break should be as short as possible and for that reason the single-cycle data break was chosen.

Figure 10 is a block diagram of the single-cycle data break transfer interface. The central processor unit (CPU) determines the order of

42
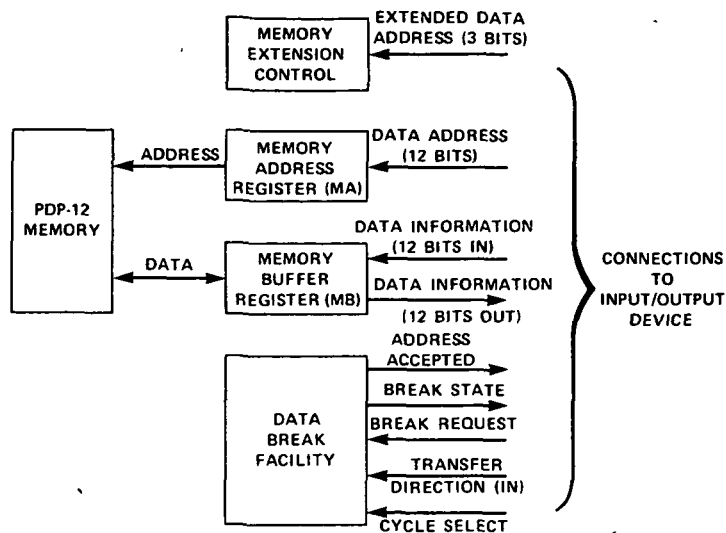
Figure 10.- Block diagram of the single-cycle data break transfer interface.

events in the PDP-12. CPU timing comprises a series of signal levels - designated time states - each of which is terminated by a time pulse (fig. 11). The duration of the CPU timing cycle is 1.6 µsec ± 20 percent. The cycle is divided into five time states ranging from 250 to 520 nsec in duration. The time pulses, approximately 100 nsec long, simultaneously terminate one time state and initiate the next. Time states are triggered by leading edges of time pulses; thus the duration of the pulse does not affect the length of the cycle. During a time state, operating conditions are established, the register gate inputs are
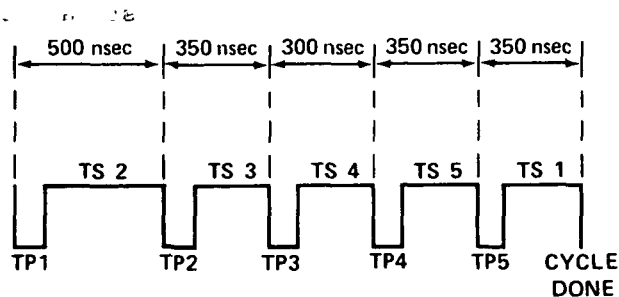
Figure 11.- Defined time states for the central processor unit (CPU).

enabled, and operations are performed on the data in the adders and shifters. Time pulses also synchronize CPU operations with memory operations as well as with I/O control.

The timing diagram of a single-cycle data break input transfer, can now be explained (fig. 12). The cycle select and the transfer direction do not change for this particular application, so these signals can be supplied from a stable dc source; this is hardwired in the interface.

The break request signal is sampled at 200 nsec before TP5 occurs. When the break request is recognized, the computer completes the current instruction, generates an address accept pulse at TP1, that is, at the beginning of the break cycle, to acknowledge receipt of the request, and then enters the break state to effect the transfer. The address accept pulse can be used in the device interface to clear the break request flip-flop, increment the content of the address register, etc. If the break request signal is removed before TP2 of the data break cycle, the computer performs the transfer and returns to programmed operation.

Design of Computer Interface

Figure 13 is a block diagram of the computer interface. The functions of the different blocks and the necessary input and output signals are described. Figure 14 is a photograph of the implemented computer interface. (Refer to this figure to clarify which operations the operator can perform and the kind of feedback he gets from the system.)

The design requirement for the computer interface is to determine the coordinates of the left ventricular border, as detected by the contour detector, over a number of video fields selected by the operator and to store these coordinates into core memory. The operator sets the

44

COMPUTER TIME | TP2 | TP3 | TP4 | TP5 | TP1 | TP2 | TP3 | TP4 | TP5 | TP1 | TP2 | TP3 | TP4 | TP5 | TP1 | TP2 | TP3

PREVIOUS CYCLE — BREAK CYCLE — NEXT CYCLE

BREAK REQUEST SIGNAL (INPUT TO PROCESSOR)
+3V / GND
SAMPLED AT OFF PAUSE BY PROCESSOR**
SIGNAL MUST GO TO +3V AT START OF ADDRESS ACCEPT PULSE IF NEXT CYCLE IS TO BE A BREAK

CYCLE SELECT (SAMPLE TO PROCESSOR)
3 CYCLE / 1 CYCLE
SAMPLED AT TP1
TYPICALLY HARDWIRED FOR A GIVEN DEVICE

B BREAK SIGNAL (OUTPUT TO I/O DEVICE)
+3V / GND
START OF BREAK CYCLE — END OF BREAK CYCLE

DATA ADDRESS INPUT LEVELS (INPUT TO PROCESSOR)
+3V / GND
EXT MEM ADDRESS READ
READ AT TP1 BY PROCESSOR
EARLIEST TIME POSSIBLE TO REMOVE ADDRESS IS AT START OF BREAK CYCLE

ADDRESS ACCEPT PULSE (OUTPUT TO I/O DEVICE)
+3V / GND
TP1 TP3

TRANSFER DIRECTION (INPUT TO PROCESSOR)
IN (+3V) / OUT (GND)
MUST BE SET UP AT TP2
CAN CHANGE ANYTIME AFTER TP3

*DATA SIGNAL INPUT TO MB (INPUT TO PROCESSOR)
AVAIL (+3V) / NOT AVAIL (GND)
LATEST POSSIBLE TIME TO SPECIFY INPUT DATA IS TP2
SAMPLED AT TP3 BY PROCESSOR

*OUTPUT DATA AVAILABLE IN MB (OUTPUT TO I/O DEVICE)
AVAIL (+3V) / NOT AVAIL (+3V)
AVAILABLE AT TP3 — TIME DURING WHICH DATA MUST BE STROBED BY I/O DEVICE

*SIGNAL NOT USED FOR INPUT TRANSFERS SHOWN FOR REFERENCE ONLY

**OFF PAUSE OCCURS 200 ns BEFORE TP5 IF IOP INSTRUCTION IN PROCESS OFF IOP SAMPLES BREAK REQUEST

Figure 12.– Timing diagram of a single-cycle data break input transfer.
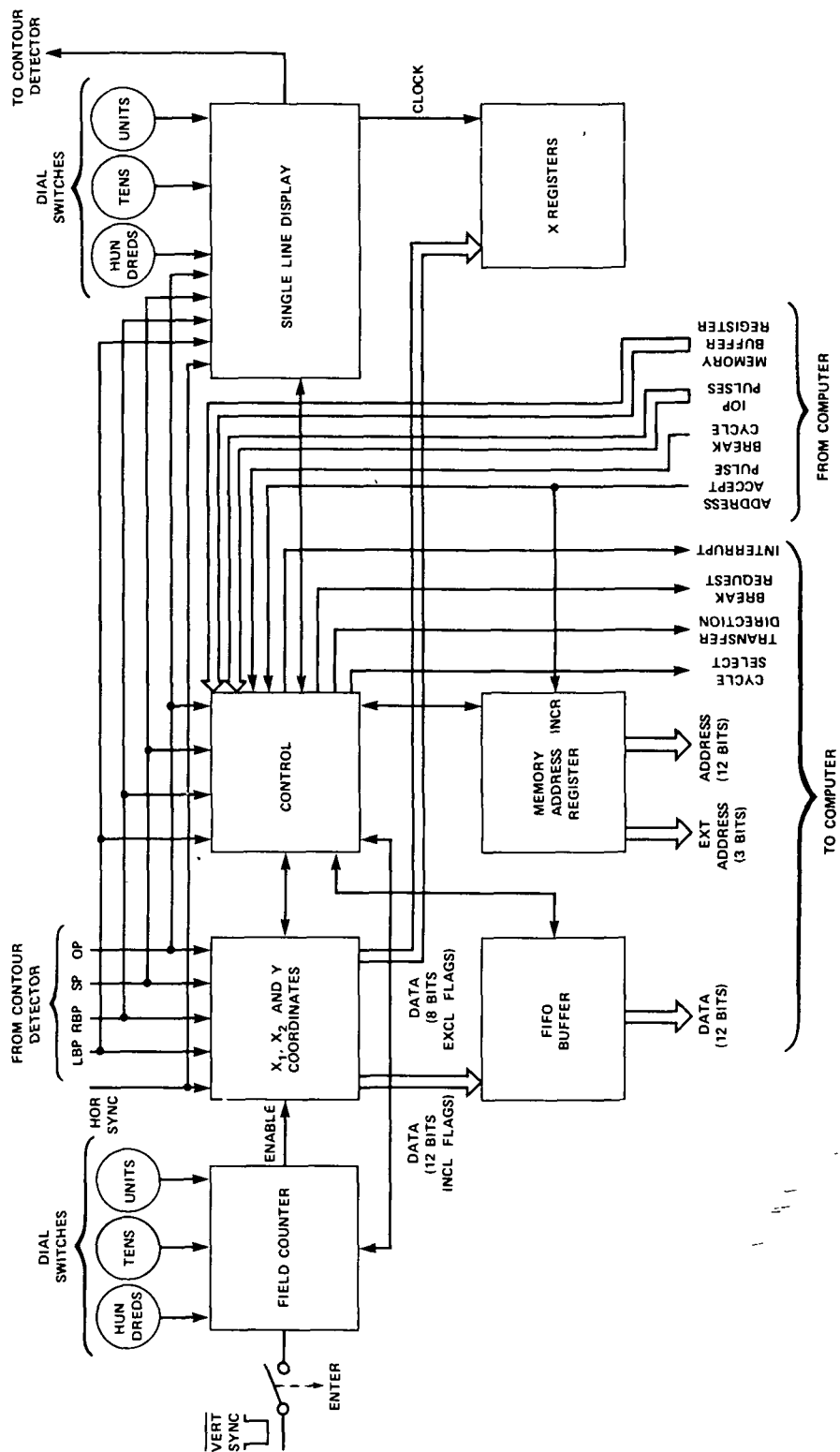
Figure 13.- Block diagram of computer interface.

46
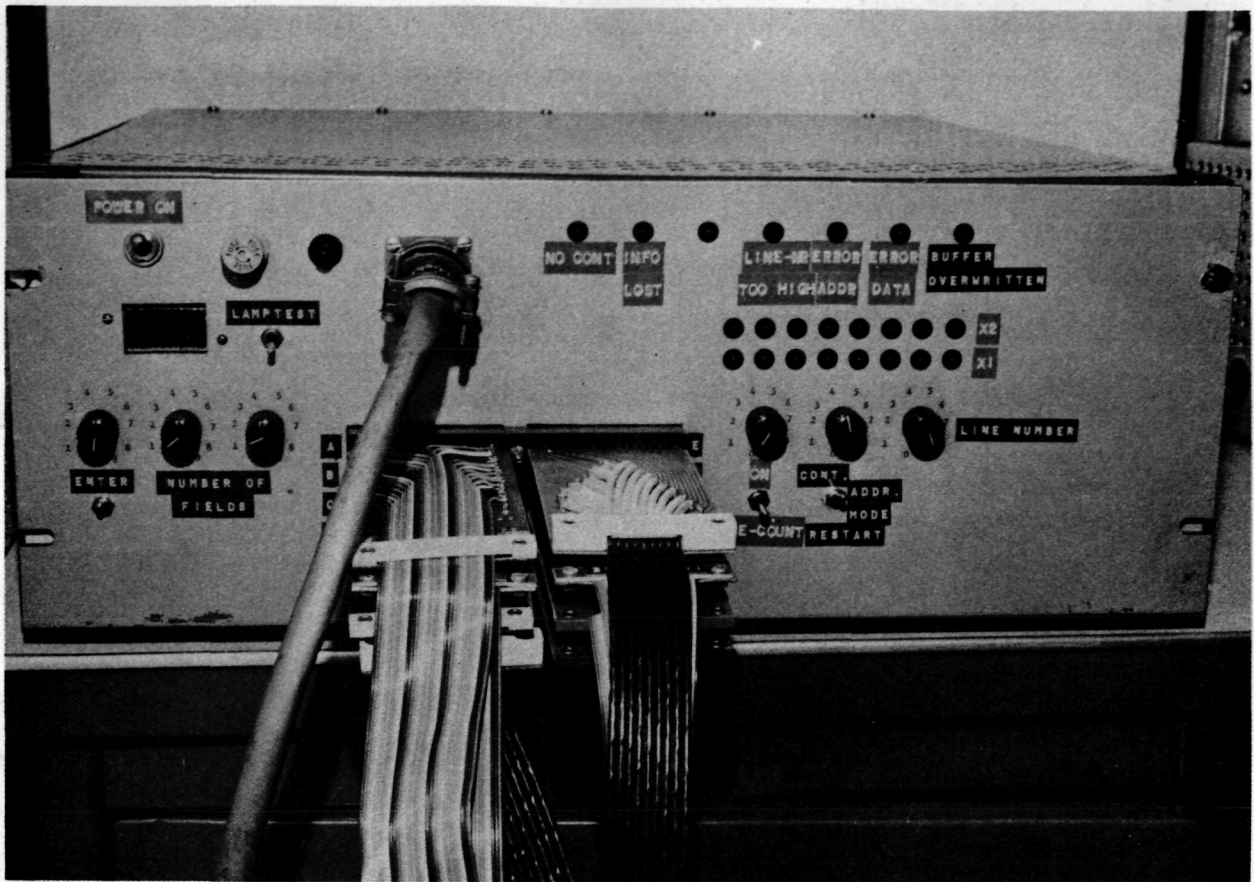
Figure 14.- Photograph of implemented computer interface.

desired number of video fields to be processed with the dial switches

connected to the block called "field counter" shown in figure 13. This

number can be selected between 0 and 399 to allow dynamic processing over

several consecutive heartbeats. For example, assume a heartrate of 80

per minute, that is, one heartbeat takes 3/4 sec. Since there are 60

video fields per second, to store the information on-line and in real

time during one heartbeat requires 45 video fields. With a catheteriza-

tion, only the first two or three heartbeats after the dye injection give

reliable data, so 135 fields would be sufficient if the processing cycle

is triggered at the right moment. The upper limit of 399 fields gives a

large safety margin that enables us to (1) store all the required data also at lower heartrates, (2) start the processing cycle slightly before the dye injection, and (3) stop at a moment when all the important data have been accumulated.

All flip-flops, which require an initial state at the start of a processing cycle, are initialized by a $\overline{\text{RESET}}$ pulse. There are three possible occurrences for generating this signal:

(1) when turning on the computer interface.

(2) manually from the computer console when the reformatting program is loaded from disk storage to core. This program converts the received data from the computer interface into the same format as generated by the manual outlining system, making both systems compatible. In a new version of the reformatting program, the $\overline{\text{RESET}}$ pulse will be generated under software control.

(3) immediately after the switch "enter" has been activated. This signals the beginning of a processing cycle.

The field counter counts the vertical synchronization pulses and selects the first occurring odd field after the "enter" switch has been closed, as the first field of the processing cycle. As a result, the processing cycle always begins in the same phase in the interlaced video system, allowing the operator to compare data of different processing cycles.

So long as the counted number of fields is less than the selected field number, the block called "x and y coordinates" is enabled by a control signal from the field counter. The processing is automatically stopped at the end of the field, which made the field counter state equal

48

to the selected number of fields. The processing can also be stopped manually before the end of the planned processing cycle is reached by returning the switch "enter" to the OFF position.

If the starting point for the contour detector has not been positioned properly, a contour might not be detected. This situation is defined when a left-border point on the starting line is missed. A control circuit in the interface checks this condition for each field and, if it is satisfied, an indicator light "no cont" (on the front panel) turns on and the processing cycle is stopped immediately.

In the present system, the processing cycle is started by manually closing the switch "enter." This works satisfactorily so long as the left ventricular outline is not detected on-line. However, it is clear that, with an improved on-line working contour detector, the processing cycle should be started automatically. This can be done by mixing a certain recognizable code into the video signal, for example, on the first video line of a field, at a moment determined by the dye injector. When replaying the video from tape or disc, this trigger moment can be recognized by a simple decoder circuit. The processing cycle is then halted when one of the following situations occur:

(a) when the switch "enter" is manually returned to the initial state,

(b) when the field counter state equals the selected number of fields, and

(c) when a signal is provided by the computer.

The function of the block "x and y coordinates" is to determine during a processing cycle: (1) the x1 and x2 coordinates for the left
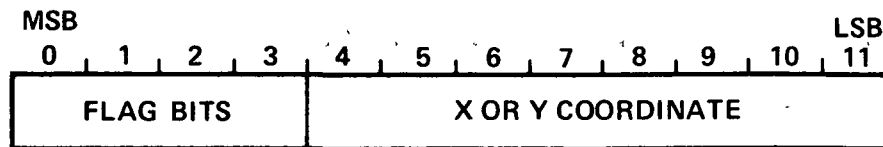
and right borders, respectively, on each line traversing the left ventricle and (2) the y coordinates of the starting point and the outpulse. The xl coordinate is a measure for the distance from the horizontal synchronization pulse to the left border and the x2 coordinate, from the horizontal synchronization pulse to the right border. The coordinates are determined by counting the number of clock pulses over these time periods. The clock pulses are 5-MHz pulses from a crystal-controlled oscillator with a temperature coefficient of ± 50 ppm/°C. The coordinates are expressed in an 8-bit binary format and the accuracy with which a border point is determined is then ± 1 bit. Because the oscillator is continuous (as distinct from a start-stop oscillator), the positive and negative errors due to the limited resolution are expected to cancel out at the average for area and volume calculations.

The y coordinate for a particular border point is defined as its video line number within this field, and is also given in eight bits. Only the y coordinates of the starting point and outpulse are stored in memory because all other y coordinates are just increments by one. These two y coordinates are stored after all the x coordinates for a field have been stored. The y coordinate of the outpulse, which is on the last line traversing the left ventricle, can be used advantageously to check the performance of the system by use of the "single-line display" (as explained later). The horizontal synchronization pulses function as clock pulses for the y-coordinate counter, which is cleared by the vertical synchronization pulse.

For area and volume calculations, only the distance between the border points on a video line could be used, instead of two x

50

coordinates per line. This would require only one 8-bit word per video line. However, there are several reasons why storage of the absolute coordinates was chosen. First, to accurately correct the detected outline back to actual dimensions, each border point must be corrected for linear and nonlinear magnification (explained in more detail in chapter 11). If one would store only relative coordinates, that is, the distance between the two points on a video line, then the nonlinearity in the magnification factor could not be accounted for, resulting in a less accurate determination of actual area and volume. Second, different volume calculation methods might be applied, some of which require absolute coordinates, others only relative coordinates. Storing absolute coordinates affords the flexibility to do so. The method used in the Cardiovascular Research Laboratory is the area/length volume calculation method, requiring the area of the left ventricle, which can be determined from relative coordinates, and the longest chord, which must be calculated from absolute coordinates (ref. 9). Third, to evaluate the success of the border algorithm (chapter 11), the detected contour is compared with the manually traced outline, given in absolute coordinates. The comparison is done with the PDP-12 by calculating for each method the distances from the coordinates to the chord, connecting the left-hand side of the aortic valve plane and the apex, and comparing corresponding distances. Clearly, absolute coordinates are required. Fourth, with the outline available in absolute coordinates, all existing software programs for analyzing, filing, and displaying contour data can be applied. Only one software reformatting program (chapter 11) is required to make the manual and video system compatible.

Each x and y coordinate is assigned a separate memory location. With these coordinates determined in an 8-bit format, the four remaining bits of each 12-bit word are used as flag bits. The 12-bit data word format is given in figure 15.

```
MSB                                              LSB
 0 | 1 | 2 | 3 | 4 | 5 | 6 | 7 | 8 | 9 | 10 | 11
┌───────────────────┬───────────────────────────┐
│                   │                           │
│    FLAG BITS      │     X OR Y COORDINATE      │
│                   │                           │
└───────────────────┴───────────────────────────┘
```

Bits 11-4:   x- or y-coordinate
Bit 3:   indicates x (bit = 0) or y (bit = 1) coordinate
Bit 2:   aortic valve beginning and end point
Bit 1:   discrete point for calibration
Bit 0:   x coordinates on selectable video line

Figure 15.- Computer interface, 12-bit data word format.

The most significant bit (bit 0) is made high for the x coordinates on a selected video line, which can be brightened on the monitor screen. The number of this line is determined with respect to the video line with the starting point, that is, the distance to the starting point is constant for a selected line. This allows an easy study of the left ventricular width during a heart cycle at a selected distance from the aortic valve. This feature is also used for test purposes since the x coordinates on this line are displayed on the front panel of the computer interface.

The second flag bit (bit 1) is made high for the x and y coordinate of a discrete point. The applied software program requires the positions of two discrete points on the image intensifier calibration plate. These discrete points are used to overlay obtained outlines accurately so that the changes in position, size, and shape of the left ventricle over a heart cycle can be determined. When the angio

52

information from the video disc is used, the positions of these points need be given only once during a left ventricular study. With the contour detector in the DISCRETE POINT mode, the coordinates of these points can be stored into memory by positioning the starting point at each discrete point and enabling the computer interface over a one-field period.

The third flag bit (bit 2) indicates the x coordinates of the beginning and end points of the aortic valve, as required by the software program. The two points are recognized in real time by the contour detector.

The last flag bit (bit 3) is high if the coordinate is a y coordinate. Because the y coordinates of the starting point and outpulse are the last coordinates to be sent to the computer for a particular field, these two bits also indicate the end of the data block for this field.

For error detection, a parity bit is assigned in the computer interface to each 12-bit data and address word. A more detailed description is given in the section on Error Detection, but some general comments on the implementation can be made at this point. The data parity bit is not stored in core because all 12 bits in a memory location have been assigned a different function and the PDP-12 does not have a hardwired error detection capability. The parity bits are transmitted with the data and address bits to the computer I/O multiplexer. Here new parity bits are generated and compared with the received parity bits. If the received and regenerated parity bits differ, an error has occurred during transmission. An error signal is then returned to the computer interface, and the indicator light "error data" or "error address" is turned on, whichever is applicable. A simple error detector code was chosen because

the occurrence of multiple errors is highly unlikely and the angiograms are stored on film, video tape, or disc for repeated processing in case of consistent errors.

Before being transmitted to the computer, the x and y coordinates, plus the assigned flag bits, are stored in a 64-word, first-in/first-out memory, which functions as a buffer memory between the rest of the computer interface and the computer. A first-in/first-out memory (FIFO) is a read/write data storage unit that automatically keeps track of the order in which data are entered into the memory, and reads out the data in the same order. This buffer can perform read and write operations at the two different rates simultaneously and completely independently. This allows one to write new data into the memory at the same time that the computer is reading data from the memory, without any synchronization between the two. Figure 16 illustrates the function of the FIFO as an asynchronous interface between the two systems. The buffer memory is built up with three 64 × 4-bit FIFO's. Four signals are used with the FIFO to control the reading and writing of data: shift-in (SI), input ready (IR), shift-out (SO), and
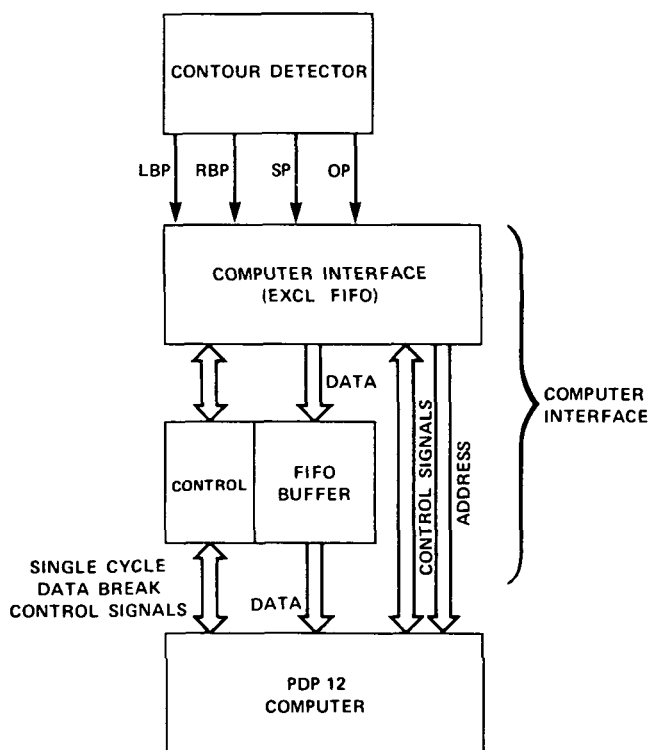
Figure 16.- A FIFO is used as an asynchronous buffer between the rest of the computer interface and the computer.

output ready, (OR). The device accepts a parallel word under control of the shift-in input. Data entered into the FIFO immediately ripples through the device to the outputs. Up to 64 words may be entered before any words are read from the memory. The stored words line up at the output end in the order in which they were written. A read command on the shift-out input (SO) causes the next to the last word of data to move to the output and all data shift one place down the stack. Input ready and output ready signals act as memory full and memory empty flags.

Data are written into the FIFO under control of the block called "control." During processing, a border point initiates the shift-in control signal if the input ready signal is high. When IR is low, then data reside in the first data register. New data may not be entered until these data have moved to the second register, indicated by IR going high. If a border point occurs while the IR is low, the low-to-high transition of IR initiates the write operation. An indicator light, "info lost," turns on when the FIFO has been filled completely and data are not read out in time to accept new data.

After a word has been stored in the FIFO, it falls through the FIFO; as it reaches the last register, the OR signal goes high, indicating that there is good stable data on the outputs. This OR-transition initiates a break request signal to the computer. The computer acknowledges the break cycle by sending an address accept pulse and the break cycle signal. According to the single-cycle data break input transfer timing diagram (fig. 12), the data are sampled at the rising edge of the address accept pulse, so that it can be shifted out of the FIFO after this moment. A

new break request is immediately given if data remain in the buffer. This reading of data is also under the control of the block "control."

The architecture of the PDP-12 in the Cardiovascular Research Laboratory presently allows up to three data break devices in either a three-cycle or single-cycle data break. The priority of a data break device is determined by cable location. Because of the relatively high data transmission rate, the contour detector interface must be assigned preferably the next to highest priority among the data break devices; the disk will normally have the highest priority. The RK8 disk presently used is a low-cost, random-access, removable mass-storage device. It uses the single-cycle data break and the transfer of data takes 16.7 μsec/word. The minimum, average, and maximum access times are 2.0 + 37 msec settle time, 134 msec, and 441 msec, respectively. The disk speed is 1500 ±30 rpm. The maximum block size per track is 4k (4096 words), divided over the upper and lower surface. A complete 4k of data can be transferred in just 80 msec. This suggests that, for future on-line acquisition of the border coordinates at 60 fields/sec, two 4k buffers should be assigned in core memory as intermediate storage.

The computed border coordinates of a minimum of eight video fields can be stored in one 4k buffer; the minimum time to fill a single buffer is therefore 8/60 sec = 133.33 msec. The maximum time required to store the contents of a buffer onto the disk, move the head to the next adjacent track, and wait until the beginning of this new track is 120 msec. An additional 13.33 msec is then left for software and electronic delay. The software routine should be designed to minimize the disk access time.

The simple calculation above shows that real-time, on-line acquisition of the border coordinates is possible with the present system. However, because of the relatively tight timing tolerances, the disk should be dedicated to the contour detector, because other disk accesses are not possible during the acquisition of the border coordinates. Instead of using this RK8 moving-head disk a fixed-head disk or a combination of a moving- and fixed-head disk is preferred for this real-time application, whereby the fixed-head disk is again dedicated to the contour detector. A fixed-head disk has a much lower access time, making the total system much more flexible.

The computer interface was originally designed for interfacing the contour detector I, which did not have the capability of on-line processing of the angiograms from the video disc/tape. Instead, cine frames were processed using the light table and TV camera, allowing smaller buffer sizes in core memory. In the present implementation, core addresses 4000_8 through 5777_8 are assigned to store the contour coordinates. As described before, the computer interface must specify the memory address for the single-cycle data break; the block "memory address register" provides this address at the correct moment. The address accept pulse functions as a clock pulse for the memory address counter. The memory address register has been designed so that two separate computer buffers can be used; the addresses of the beginning and end of each buffer are hardwired in the interface. In the present system, buffer I contains core addresses 4000_8 through 4777_8 and buffer II contains addresses 5000_8 through 5777_8. This memory configuration and the data transmission routes are shown in figure 17.
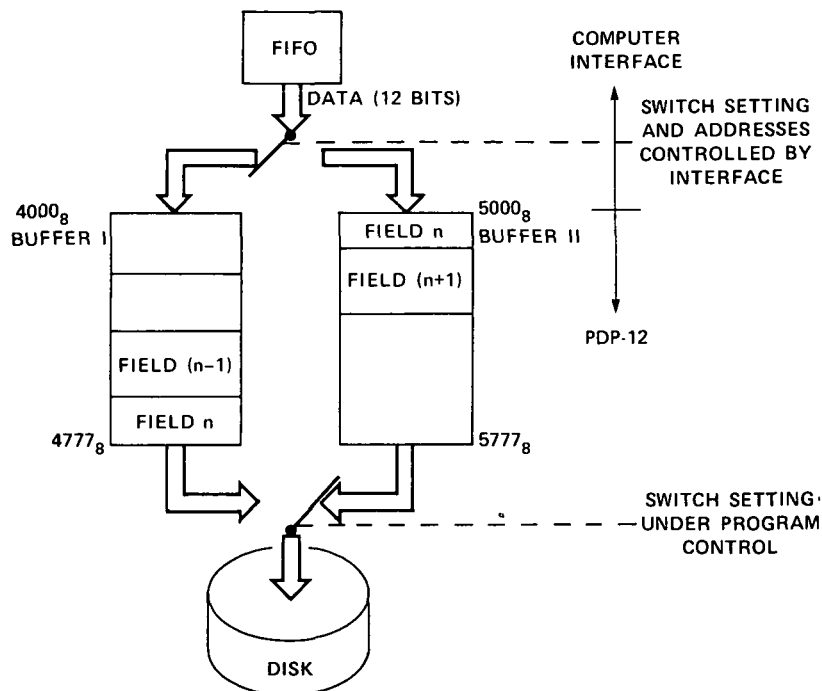
Figure 17.- In the PDP-12, two core buffers are assigned to store the contour coordinates. As soon as a buffer has been filled, its contents are transferred to the disk while incoming data are stored in the other buffer.

As soon as buffer I has been filled, the memory address counter is set at the beginning of the second buffer and an interrupt signal is generated which initiates transfer of the contents of buffer I to the disk, while buffer II is being filled simultaneously. In the same way, an interrupt is given when the second buffer is full; the address counter then returns to the first address in buffer I and the cycle repeats itself. As soon as all the information of a particular buffer has been transferred to the disk, the computer gives an IOP pulse that clears a flip-flop in the computer interface. If this IOP pulse is not received before the next interrupt is given, one of the buffers will be filled before the old information has been fully transferred to the disk. This

may result in loss of information, which is indicated by a front panel light "buffer overwritten."

The assigned 512 core memory locations per buffer will, on the average, be sufficient to store about two video fields. The last field in a buffer is generally segmented; the remainder is put on the new buffer. After all the selected fields have been processed, some data remain in one of the buffers because an interrupt is not given for this partially filled buffer. A software-generated command must then be given, which will initiate the transfer of this last data block to the disk.

The memory address counter is preset to 4000_8 by the first vertical synchronization pulse of the first processing cycle after a $\overline{\text{RESET}}$ pulse has been generated when (1) the power to the interface is turned on or (2) initiated from the computer console. This prevents the memory address counter from being preset each time the "enter" switch is activated.

If one has to process cine-film with a simple light table and a TV camera, the film frames cannot be accurately aligned so that the discrete points always have the same position in the defined video coordinate system. In this case, the two discrete points and the detected contour must be stored over a one-field period for each cine frame. The two discrete points will be entered first and then the contour. These discrete points are stored by changing the contour detector mode from CONTOUR to DISCRETE POINTS: only the starting point is displayed on the video monitor in this last mode. The starting point is then positioned at a discrete point and the computer interface is enabled over a one-field period. This results in the storage of the x and y coordinates of the starting

point. Because the memory address counter is not preset each time a
processing cycle is initiated, the discrete points and the contour are
stored in consecutive memory locations. This consecutively storing of
data also applies to all following processing cycles, until a new preset
signal is generated under the conditions described above.

When the angiocardiographic information from the video disc is used,
the positions of the discrete points need be given only once during a
ventricular study.

As explained before, a parity bit is generated in the computer
interface for the 12 address bits. This parity bit is compared with a
newly generated parity bit at the I/O multiplexer and the indicator light
"error address" comes on if the two parity bits differ.

Single-Line Display

As an extra feature, the "single-line display" was implemented. Its
purpose is to load the "registers x -coordinates" with the x1 and x2
coordinates of the border points on a particular video line (which can be
selected with dial switches) and to display this information on the front
panel. The selected line is brightened on the video monitor for visual
feedback.

When transferring the coordinates of the border points on such a
selected line to core, the most significant bit of the 12-bit data word
is made high. These coordinates can then be recognized when the contents
of core are examined to compare the computer-stored coordinates with the
coordinates displayed on the front panel of the interface. This check on
the data transmission performance was especially convenient during the
initial test periods. By positioning the selected line at the apex of

60

the left ventricle, one can also check whether the number of stored x coordinates per field equals twice the selected line number and equals twice the difference of the stored y coordinates of the starting point and outpulse plus two. The selected line number is defined with respect to the video line with the starting point. It was mentioned before that the single-line display also allows the study of left ventricular width at a selected distance from the aortic valve during a heart cycle.

The line is selected by the operator with three dial switches (fig. 13). Setting the switch "line count" (fig. 14) at the ON position enables this feature. Line number one is the line with the starting point. The selected line is brightened on the video monitor from the horizontal synchronization pulse to the left-border pulse and from the right-border pulse to the end of the line. This mixing occurs for each video field, so the selected line is continuously displayed independently of whether a processing cycle is initiated or not. If the selected line number is higher than the number of lines traversing the left ventricle, the line is brightened only from the outpulse to the end of the line and the indicator light "line number too high" turns on. This light turns off again as soon as the selected number is less than or equal to the number of lines traversing the left ventricle.

The x1 and x2 coordinates on the selected line are displayed on the front panel for each field of a processing cycle if the "single-line display" is enabled. At the end of the processing cycle, the displayed coordinates are the selected coordinates of the last processed field, which can then be compared with the core contents. This is done at the PDP-12 console using the EXAME and STEP EXAME switches.

Interrupts

An interrupt occurs when one of the buffers has been filled. This signals the computer to transmit the buffer contents to the disk. The transfer must be completed by the time the other buffer is filled with new data. The hardware in the computer interface detects the end of buffer condition, so the computer may be dedicated to its normal tasks until the interface interrupts.

The general way in which interrupts are handled by the Program Interrupt facility of the PDP-12 is described in this section. The interrupt facility is described mainly from the software point of view with a short discussion on the required hardware for the interface.

When a peripheral device requires service, it transmits an interrupt request signal to the computer. This signal interrupts the program currently underway and program control is then transferred to a specific memory location, in our case, address 0000. The contents of the program counter are stored in this location and after it has been determined which device initiated the interrupt, servicing of the I/O device can begin. When the service request has been completed, the interrupted program is resumed by returning to the location specified by the previously saved contents of the program counter.

When the end of a buffer is reached, a device flag is set in the computer interface, which causes the Program Interrupt Request bus to be grounded. Assuming the interrupt facility was turned on before (instruction ION), an interrupt occurs and the contents of the program counter are stored at address 0000. Address 0001 now typically contains a jump

indirect instruction to the flag check routine. A typical program that handles the interrupt requests is as follows:

Tag	Address	Instruction	Remarks
	1000	...	/Main program
	1001	...	/Main program continues
	1002	...	/Interrupt request occurs
		Interrupt occurs	
	0000		/Store PC (PC = 1003)
	0001	JMP I 0002	/Jump indirect to flag check routine
	0002	0100	/Address flag check routine
FLG CK	0100	IOT 6301	/Skip if device 30 is requesting
		SKP	/No – test next device
		JMP SR30	/Enter service routine 30
		IOT 6311	/Skip if device 31 is requesting
		SKP	
		.	
		.	
		.	
		.	
		.	
SR30	2000	...	/Service routine for interrupting device
	.	...	
	.	IOT 6302	/Clear device flag
	.	.	
	.	.	
	3003	ION	/Turn on interrupt facility
	3004	JMP I 0000	/Return to main program
	.		
	1003	...	/Main program continues

NOTE: The interrupt facility is turned off as soon as the interrupt request is recognized.

In most PDP-12 systems, numerous devices are connected to the program interrupt (PI) facility, so the routine beginning in core memory address 0001 must determine which device requested an interrupt. The function of the flag check routine therefore is to determine which device requires service by sequentially checking the flags of all equipment connected to the PI and to transfer program control to a service routine for the first device encountered that has its flag in the state required to request a program interrupt. In other words, when program interrupt requests can originate in numerous devices, each device flag connected to the PI must also be connected to the input/output skip (IOS). The IOS facility samples the conditions of I/O flags. Each device must be able to sample the select code, generated by the computer during an IOT instruction and, when selected, must be able to produce sequential IOT command pulses in accordance with the computer-generated IOP pulses. Circuits that perform these functions in the peripheral·device are called device selectors (DS). The format of an IOT instruction for the device with selection code 30₈ is shown in figure 18. To understand interrupt handling, it is important to know the information flow within the
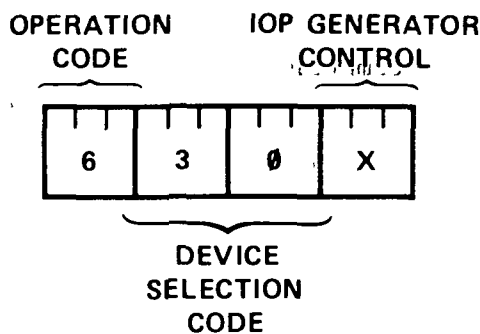

Figure 18.- Format of an IOT instruction for a device with selection code 30_8.

computer (see fig. 19).

All instructions stored in core memory as a program sequence are read into the memory buffer register (MB) and the instruction register (IR) for execution. The transfer of the operation (OP) code (the three most significant bits (bits 0, 1, and 2) of the
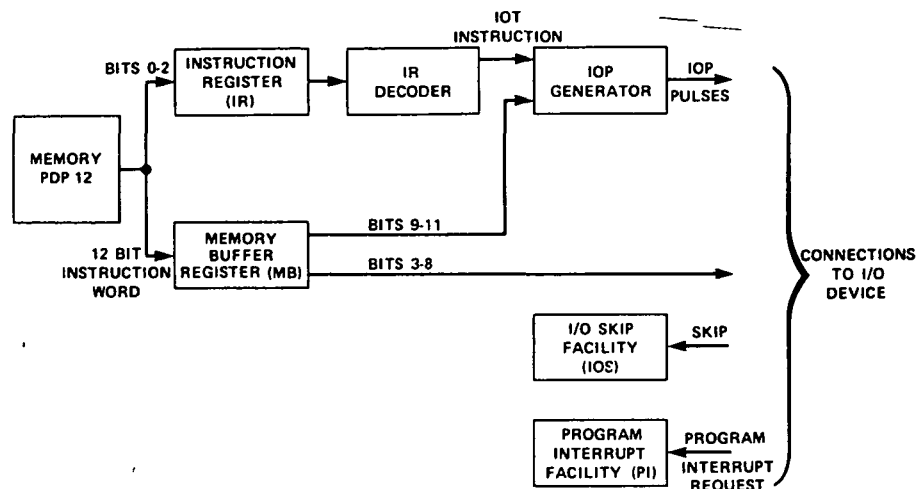
Figure 19.- Block diagram of programmed data transfer interface.

instruction) into the instruction register (IR) takes place and this OP

code is decoded to produce appropriate control signals. The computer,

upon recognition of the operation code as an IOT instruction, enters a

4.25-μsec expanded computer cycle and enables the IOP generator to pro-

duce time-sequenced IOP pulses as determined by the three least signifi-

cant bits of the instruction (bits 9, 10, and 11 in the MB). The IOP

pulses are generated according to the following table:

Instruction bit	IOP pulse	IOT pulse	Used primarily for but not restricted to
11	IOP 1	IOT 1	Sampling flags, skipping
10	IOP 2	IOT 2	Clearing flags, clearing AC
9	IOP 4	IOT 4	Reading buffers, loading buffers, and clearing buffers

These IOP pulses are bussed to device selectors in all peripheral

equipment.

Bits 3 through 8 of an IOT instruction serve as a device select code. Bus drivers in the processor buffer the 1 and 0 output signals of MB_{3-8} and distribute them to the interface connectors for bussed connection to all device selectors. Each DS is assigned a select code and is enabled only when the assigned code is present in the MB. The device selector implemented in the computer interface is shown in figure 20. Because the computer interface is assigned device number 30, the output of the six-input AND gate will be high only if an IOT 630X instruction is executed. When enabled, the device selector regenerates IOP pulses as IOT command pulses.
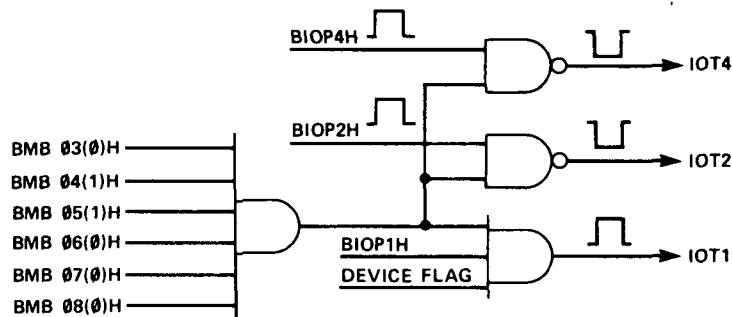

Figure 20.- Implementation of the device selector for the computer interface (device 30_8).

The way in which the flag check routine works can now be explained. The first instruction in this routine, the IOT 6301, will make the output of the AND gate in the device selector (fig. 20) for the computer interface high and, if the device flag is set, an IOT 1 pulse will occur, which drives the SKIP bus to ground. The state of the SKIP bus is sampled at the end of each IOT instruction. If the bus has been driven to ground, the contents of the program counter are incremented by 1, to advance the program count, without executing the instruction at the

current program count. In this manner, an IOT instruction can check the status of an I/O device flag and skip the next instruction if the device requires servicing.

The next instruction to be executed is then the JMP SR30, that is, a jump to the service routine for device 30. One of the instructions in this routine will be an IOT 6302, which generates an IOP 2 pulse for device 30. This signal can be used to clear the device flag. One of the last instructions of SR30 must be an ION instruction which, again, turns on the interrupt facility. A JMP I 0000 makes the program sequence return to the main program.

Suppose that another device wants to interrupt the program sequence during the time that the interrupt for device 30 is being handled. Because the interrupt facility was turned off as soon as the interrupt request from device 30 was recognized, the interrupt bus remains grounded until the interrupt facility is again turned on. A new interrupt immediately occurs and the contents of the program counter are again stored at address 0000. The whole cycle repeats itself, except that the flag check routine now skips the JMP SR30 instruction and, upon recognition of the requesting device, enters the service routine for this particular device.

The above described program interrupt facility was used for this particular application. In the PDP-12, a multilevel automatic priority interrupt can be applied if one wants to reduce the central processor overhead during the servicing of program interrupts (ref. 54). Up to 15 levels of interrupts can be accommodated with each level having a two-word vector address.

It is important to know when the contents of a buffer have been transferred to the disk. Every time the last word in a buffer is sent to the disk, an IOT 6304 instruction is executed. In the computer interface, a checking circuit has been implemented which receives this IOT 4 pulse. If no IOT 4 pulse is received between consecutive interrupt requests, the indicator light "buffer overwritten" comes on, as previously discussed.

Error Detection

In the general description of the computer interface, it was mentioned that single-error detection schemes are applied for the 12-bit data and address words. The method used was to add a single parity bit. This method is described in more detail here, along with a method for multiple-error detection (refs. 55 and 56).

It is important that at least a single error be detected so that processing can be repeated if it occurs. This is always possible since the angiograms are stored on film, video disc, or tape. With the high reliability of the integrated circuits and the short cable length over which the information is transmitted (<6 m), it is very unlikely that multiple errors will occur simultaneously. Adding an extra bit, the parity bit, to a word allows the detection of an error that affects only a single bit or an odd number of bits of the word. Generally, the error can be caused by hardware failures or noise on the transmission line.

The addition of a parity bit will guarantee that the minimum distance between any two words is at least 2. Generally, the following statement is valid: any set of binary words with minimum distance between words of at least 2 can be used as a single-error detecting code, and any single-error detecting code must have a minimum distance between

any two code words of at least 2. The distance D(x,y) between two words

x and y is the number of coordinates for which x and y are different,

as defined by Hamming (ref. 57).

The information to be placed into the parity bit position is chosen

so that the "parity word," consisting of the original system word plus

the parity bit, contains an odd number of ones (odd parity) or an even

number of ones (even parity). The function of a parity generator is to

examine the system word and to determine the logic level for this added

parity bit. Once the parity has been included, the "parity word" can be

examined after any transmission to determine if a failure or error has

occurred. The parity detection circuit (parity checker) generates a new

parity bit for the received 12 bits and, if the transmitted and new

parity bit differ, an error has occurred. The system control is then

informed that the system has not functioned properly. This parity scheme

will detect an odd number of errors, but fails if an even number of

errors occur.

In more error-prone situations, such as transmitting over a larger

distance or in a noisy environment, better schemes can be used. Although

this was not done in the implemented computer interface, one of the most

familiar schemes, the modified Hamming single-error correction and double-

error detection scheme, will be described.

The Hamming code for single-error correction is first described.

Single-error correction requires that redundant information be added to

the message information so that the bit number in error can be identified.

The necessary and sufficient condition for any set of binary words to be

a single-error correcting code is that the minimum distance between any

pair of words be 3. In the Hamming parity code, the redundant bits are called Hamming parity bits. The number of extra bits that must be added is found from the inequality $2^k \geq m + k + 1$, where k is the number of Hamming parity bits and m is the number of information bits. The total number of bits is then $n = m + k$ and the redundancy of the code is defined as $R = n/m = 1 + k/m$.

Figure 21 is a block diagram of a Hamming code single-error correction system for a 12-bit message word and the 5 required parity bits.
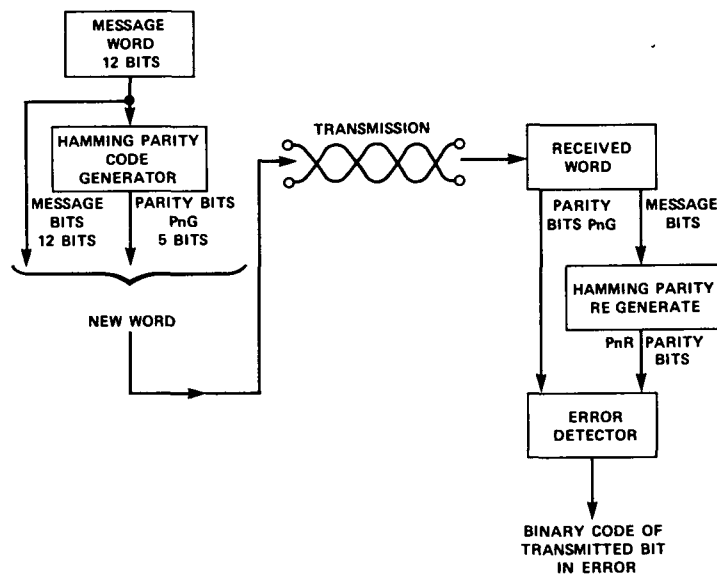
Figure 21.- Block diagram of a Hamming code single-error correction system.

The Hamming code generator calculates the 5 Hamming parity bits - P1G, P2G, P4G, P8G, and P16G (letter G indicates the parity bits calcu-lated by the parity generator) from the 12 message bits. The parity bits are usually placed in the bit positions corresponding to binary powers since they then enter into only one parity bit, making the formation of parity bit equations very straightforward. The 12 message bits are then

denoted M3, M5, M6, M7, M9, M10, M11, M12, M13, M14, M15, and M17. The
exact manner of generating the Hamming parity bits from the 12 message
bits is given in figure 22.

```
P1G P2G M3 P4G M5 M6 M7 P8G M9 M10 M11 M12 M13 M14 M15 P16G M17
 X       X      X      X      X       X       X       X           X
     X   X          X  X          X   X                X   X
             X   X  X  X                          X   X   X   X
                         X   X  X   X   X   X   X   X
                                                         X    X
```

P1G = M3 ⊕ M5 ⊕ M7 ⊕ M9 ⊕ M11 ⊕ M13 ⊕ M15 ⊕ M17
P2G = M3 ⊕ M6 ⊕ M7 ⊕ M10 ⊕ M11 ⊕ M14 ⊕ M15
P4G = M5 ⊕ M6 ⊕ M7 ⊕ M12 ⊕ M13 ⊕ M14 ⊕ M15
P8G = M9 ⊕ M10 ⊕ M11 ⊕ M12 ⊕ M13 ⊕ M14 ⊕ M15
P16G = M17

Figure 22.- Parity check table for a single-error correcting code with
12 message bits and 5 parity bits.

In figure 22, the X's placed in the table indicate which of the
message bits must be examined to generate the corresponding parity bit.
The necessary and sufficient conditions for a parity check table to
correspond to a single-error correcting code are that each column of the
table be distinct (no repeated columns) and that each column contains at
least one entry.

The Hamming parity detection circuit for this single-error correc-
tion system re-examines the input message bits exactly as the generator
did. The parity bits generated at the receiver - P1R, P2R, P4R, P8R,
and P16R - are then compared with the transmitted parity bits PnG (where
n represents 1, 2, 4, 8, and 16 for this example). Each combination of
parity bits (e.g., P1G transmitted and P1R received) is compared via an

Exclusive OR circuit. The result of this comparison forms a binary word that indicates the bit position of any single bit in error.

If a double error occurs, a correction is carried out according to the above explained scheme, but the wrong code word will be produced. For example, suppose that message bits M3 and M5 were in error; the regenerated parity bits P2R and P4R would then be different from the received parity bits P2G and P4G, indicating that message bit M6 was in error. By adding one additional parity bit over all the bits, one obtains the single-error correcting and double-error detecting capability; this is called the modified Hamming code, having a minimum distance of 4.

Referring to figure 22 and denoting the generated overall parity bit PGS, this yields

$$PGS = P1G \oplus P2G \oplus M3 \oplus P4G \oplus M5 \oplus M6 \oplus M7 \oplus P8G \oplus M9 \oplus M10 \oplus M11 \oplus M12 \oplus M13 \oplus M14 \oplus M15 \oplus P16G \oplus M17$$

Any single error in the resulting code will result in the same parity check violations as without PGS and, in addition, will violate the PGS parity bit. Any double error will *not* violate the PGS parity check, but will violate some of the P1G, P2G, P4G, P8G, or P16G parity bits, thus indicating that a double error has occurred.

The possible situations occurring when the modified Hamming code is used can be summarized as follows:

(1) If all equivalent G and R parity bits are the same, then there is no error.

(2) If for only one n the parity bits are unequal, then this parity bit is in error.

(3) If for more than one n the parity bits are unequal and PGS ≠ PRS, then a single error has occurred and the outputs of the Exclusive OR gates give the binary word of the bit in error.

(4) If for more than one n the parity bits are unequal and PGS = PRS, then a double error has occurred.

Therefore, a code that detects double errors, as well as corrects single errors, must consist of binary words having a minimum distance of 4.

Page intentionally left blank

CHAPTER 5: CONTOUR DETECTOR, PROTOTYPE II

Results with the contour detector prototype I were very encouraging. In many cases, rather accurate left ventricular outlines were obtained. An accurate outline is defined as one that coincides with the outline drawn by an experienced investigator. For these experiments, left ventricular cineangiograms were used. The film is placed on a light box and can be manually advanced with a film transport. The video camera is mounted vertically above the light box.

The outlines were generated on a frame-by-frame basis, whereby manual readjustments of the parameters were often necessary, especially the α and V_c parameters for the dynamic reference level. Also, limited border excursions from the direction perpendicular to the scan lines were only allowed because of the applied expectation window principle. The excursions are determined by the selected expectation window widths. However, the direction along a border is not everywhere the same. It is certainly very different at the mitral valve from the rest of the left border, if we take only this side as an example. This can result in inaccuracies, especially if the expectation window width is chosen fairly narrow. Because the left ventricle also makes a rotational movement during a heart cycle, the center of the expectation window must be determined in a way less dependent upon the vertical direction. With a real-time, on-line working contour detector as goal, it was obvious that improvements had to be found for the expectation window and dynamic reference level principles.

Because of the above mentioned reasons, a totally new contour detector has been built. Figure 23 is a block diagram of the prototype II
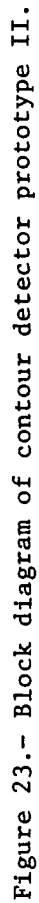
Figure 23.— Block diagram of contour detector prototype II.

contour detector. Although some of the basic principles used in the prototype I system have been applied in a more or less revised form again in the new system, the implementation of it has been changed completely. The prototype I was mainly based on analog circuit design with the expectation and sample-and-hold windows determined by time delays generated with monostable multivibrators, which are sensitive to temperature and power supply changes. The new system is based on a much more digital approach; using a 50-MHz clock, the border points, expectation, and sample points are determined in a 12-bit format. This approach allows a relatively easy and accurate correlation of video lines (chapter 6) and fields (chapter 7) and an adjustment of expectation window widths according to local brightness levels (chapter 10) which otherwise would not have been easily achievable. Whereas previously two sample-and-hold circuits per border side were used, in the new system three track-and-hold circuits per border side are used, allowing some additional adjustments of the reference level in case of irregular border signals.

With the border coordinates available in a 12-bit format in the contour detector, the design of the computer interface can also be simplified. The computer interface was originally designed for use with the first prototype system, whereby the x coordinates are calculated in the interface. For subsequent computer processing of the obtained data, the x coordinates need only be given in 8 bits. Therefore, the four least significant bits of a prototype II x coordinate can be deleted for the computer use.

Theoretical derivations and actual implementations of the system are discussed here and in the following chapters. In the remainder of this

chapter, the analog preprocessing circuitry is discussed. This part of the system is represented by the functional blocks in the upper part of the block diagram (fig. 23) - more specifically, the blocks "amplifier and sync stripper," "1-MHz low-pass filter Bessel," "video clamp," as well as the summation amplifier and the 400-nsec "delay line."

Video Analog Preprocessing

The actual implementation of the analog preprocessing circuitry is given in figure 24. The input video signal is assumed to be a standard video signal with an amplitude of 1 V including the negative going synchronization pulses (ref. 58). Because the synchronization pulses in the video signal have no important function in the border recognition algorithm, it is preferred to have a video signal without synchronization pulses at the input of the analog comparators. The synchronization pulses therefore are stripped off in the sync stripper. However, before this operation can be done, the video signal must be inverted and hard-clamped. The input video signal is inverted and amplified in OP AMP 1, which is an ultrafast FET input operational amplifier, extremely useful for video applications. Ideally, the gain of the input amplifier is given by $-R_F/R_1$; R_F is adjusted so that the amplitude of the signal from the blanking level to the reference white level is 1 V.

To restore the dc level in the video signal, the output signal of OP AMP 1 is hard-clamped. This clamping occurs during the back porch of the line synchronization pulses. Figure 25 is a detailed drawing of the video signal during the horizontal synchronization pulse.

Transistor Q3 is the clamping transistor that will be saturated when a clamp pulse turns it on. The collector is grounded so the video signal

78

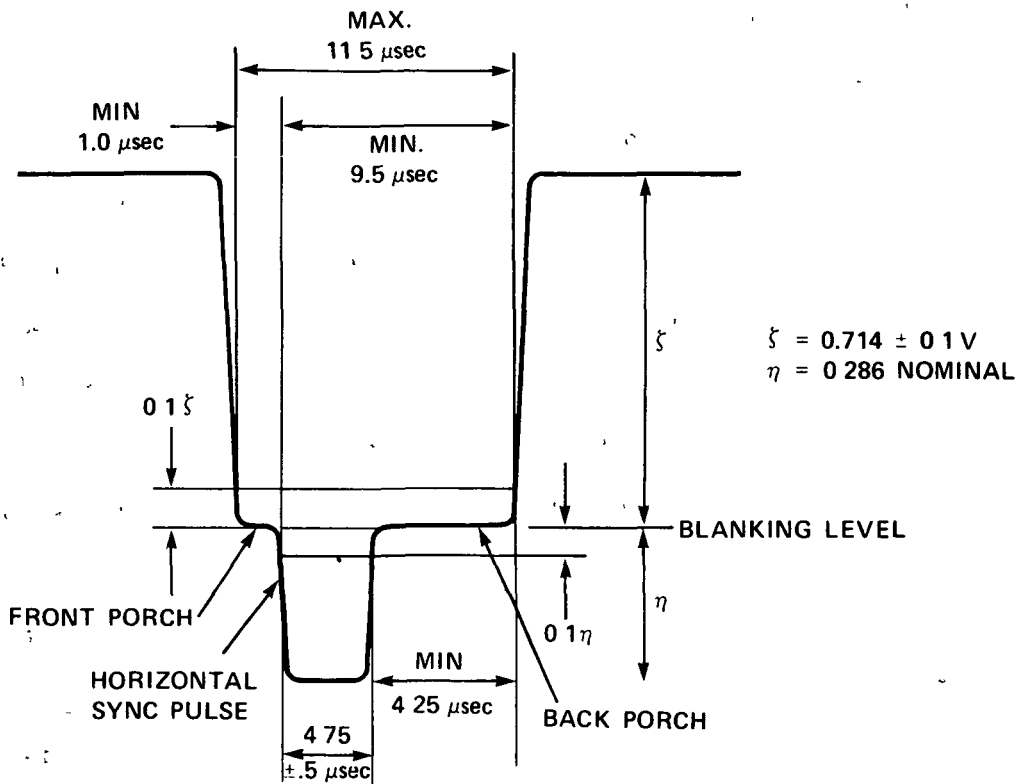Figure 24.- Video analog preprocessing circuitry.

79
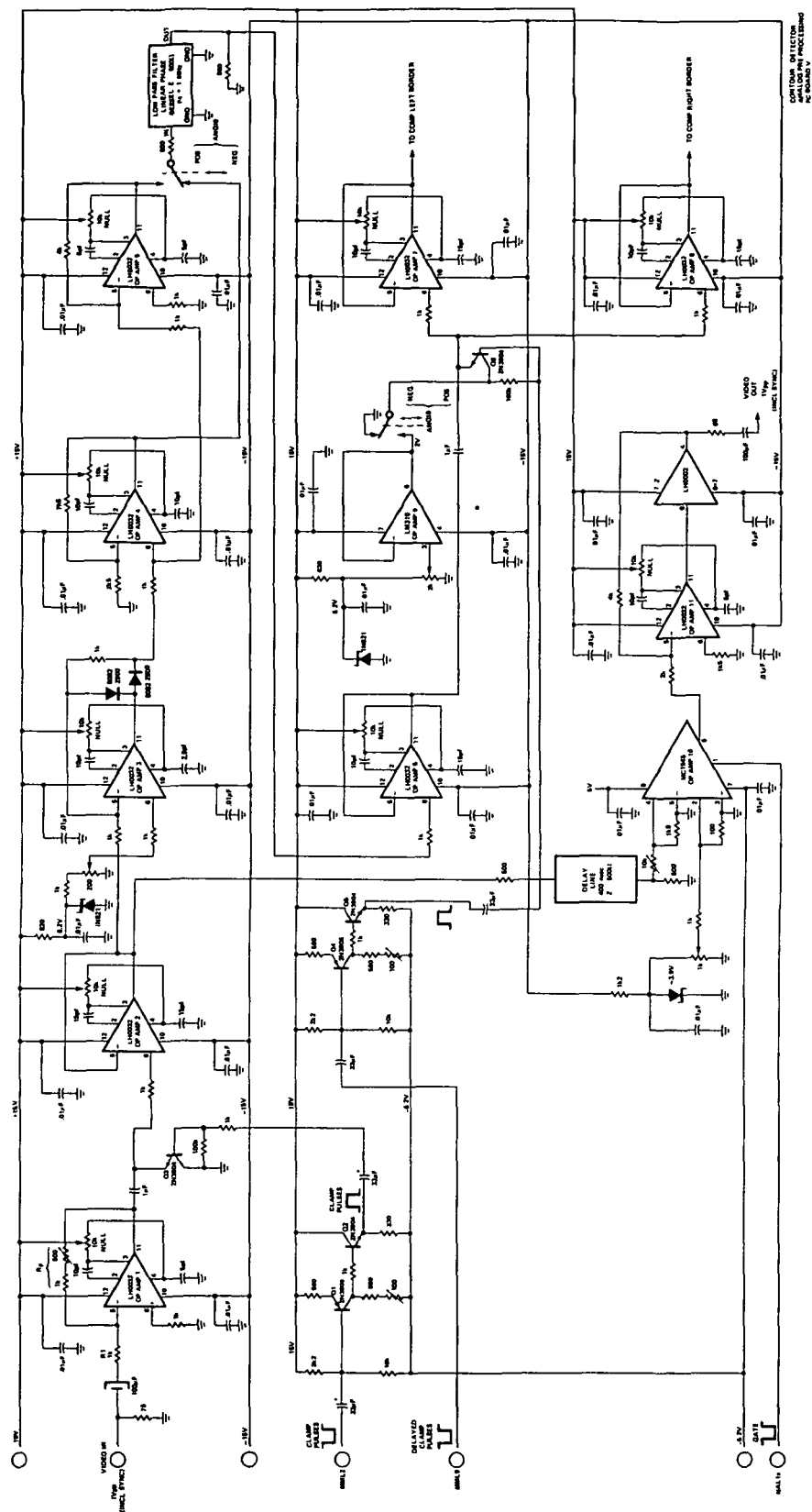
Figure 25.- Standard video signal with horizontal synchronization pulse.

will be clamped at a $V_{ce,sat}$ voltage drop above ground. The clamp

pulses are derived from the horizontal synchronization pulses.

OP AMP 2 functions as a high input impedance buffer for the clamped

video signal. From the output of this buffer, the signal branches over

two different routes. Following the upper route, the synchronization

pulses are stripped off in a precision limiter, implemented with opera-

tional amplifier OP AMP 3. (A detailed analysis of the precision limiter

is given in appendix B.) A convenient level to strip off the synchroniza-

tion pulses is at 0.1 η or approximately 30 mV below the blanking level

(fig. 25). It is then still possible to recognize visually the back

porch, which is important because the stripped video signal is again

clamped at the inputs of OP AMP's 7 and 8. Stripping at a level below

the blanking level also assures that a slight drift in the stripping

level, by whatever reasons, will not affect the information portion of the video signal.

The output signal from the precision limiter is connected to OP AMP's 4 and 5. OP AMP 4 amplifies the signal by a factor of +4 and OP AMP 5, by -4. These positive and negative amplifiers are needed so that cineangiograms (on negative of conventional film) can be used, as well as the information stored on video tape or disc. The amplification by a factor of 4 is necessary because a video signal with an amplitude of 2 V is desired at the comparator input. The signal is attenuated by a factor of 2 at the filter output because of the termination. The true format from the video disc shows a dark left ventricle against a bright background, while the cineangiogram provides a bright left ventricle against a dark background. The different video signals for a horizontal TV line traversing the left ventricle are given in figure 26. Figure 26(a) shows the signal from the video disc, while figure 26(b) shows the signal from the TV camera scanning a cineangiogram (negative).
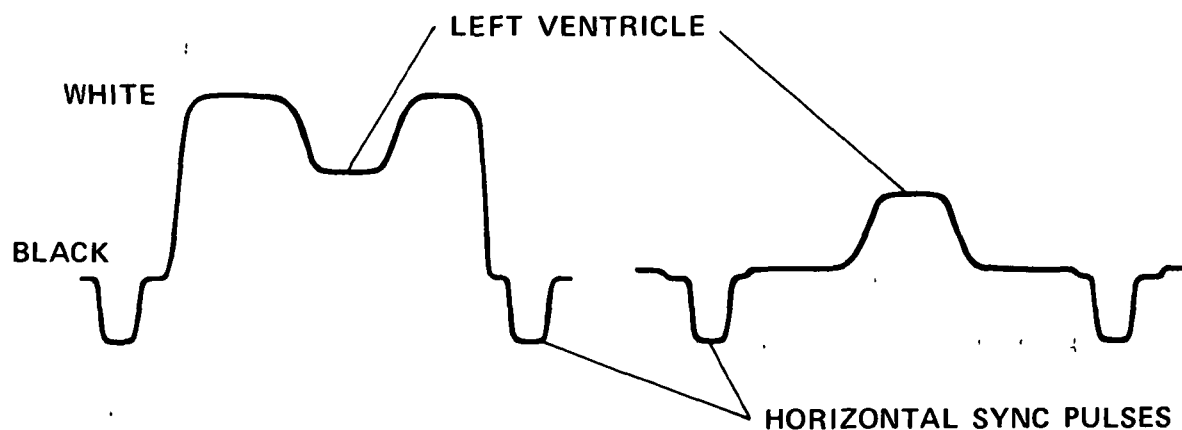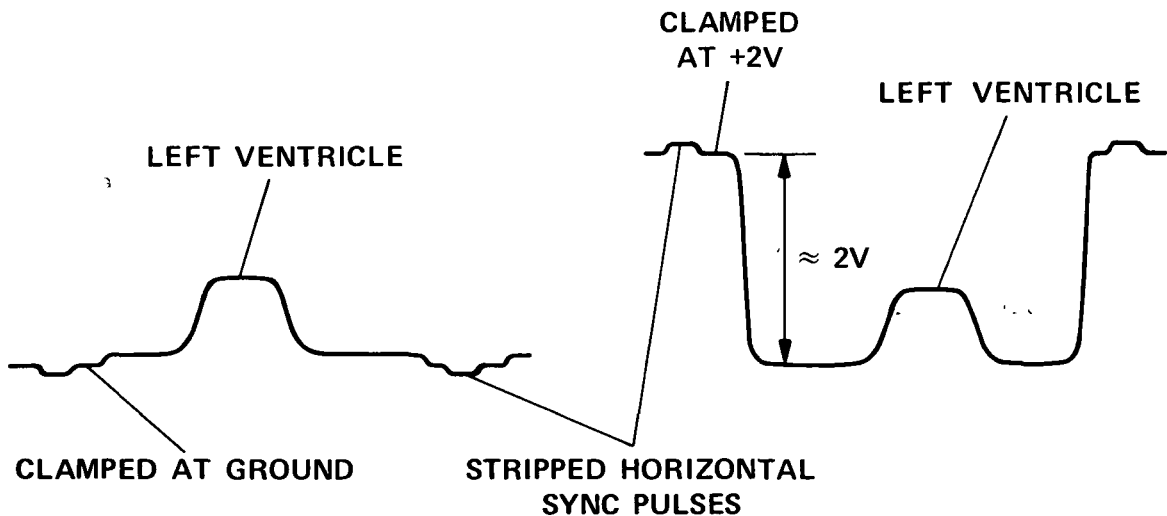

(a) Signal from the video disc.   (b) Signal from the TV camera scanning a negative cineangiogram.

Figure 26.- Video signal ot a horizontal line traversing the left ventricle.

The circuitry, which detects the left ventricular border, should always see the same format. Rather arbitrarily, but mainly because this was used in the first prototype of the contour detector, the brightened ventricle against a dark background, as provided by the negative of conventional film was defined, as the normalized format for the detection circuitry. Comparing the two formats in figures 26 then clarifies that inverting the video signal from the disc and clamping it at approximately +2 V will result in the same format for the detection algorithm. Figure 27(a) shows the video signal from the TV camera, clamped at ground and with the horizontal sync pulses stripped off. Figure 27(b) gives the final format for the video disc signal. In both cases, the left border is now characterized by a rising edge and the right border by a trailing edge. The video disc signal is inverted with OP AMP 5. With the switch at the input of the low-pass filter, the inverted or noninverted signal is selected.

(a) Processed signal from TV camera.   (b) Processed signal from video disc.
Figure 27.- Normalized video format for the detection algorithm.

82

The used filter is a low-pass filter with a cutoff frequency at 1 MHz, it is linear phase (Bessel function), and has a characteristic impedance of 500 Ω. The reasons for selecting this type of filter are described in appendix C. It is shown that frequencies above 1 MHz do not contain relevant border information so the signal/noise ratio can be improved by low-pass filtering at 1 MHz. Also, for video applications, the filter should have a pulse or step response with low overshoot, requiring a linear-phase-type filter.

This low-pass filter is terminated with its characteristic impedance and followed by a buffer. This buffer, OP AMP 6, does not load the filter and functions as a voltage source for the next clamp circuit. Transistor Q6 is the clamping transistor and the video signal is clamped at a $V_{ce,sat}$ voltage drop above ground for the video signal from the TV camera or at approximately +2 V for the video disc signal. The required clamping level is again selected with a switch. Because the filtered video signal is delayed over approximately 300 nsec, the clamp pulses for transistor Q6 must be delayed over the same time period. These delayed clamp pulses are again derived from the horizontal synchronization pulses.

Operational amplifiers OP AMP's 7 and 8 function as buffers; the output signals are the input signals to the comparators. OP AMP 7 is the buffer for the left-border comparator and OP AMP 8, for the right-border comparator.

In the lower route, the buffered video signal from OP AMP 2 is delayed over 400 nsec in a delay line to compensate for the total delay of the low-pass filter and the logic circuitry involved in the contour detection. This delay line is necessary because the detected contour

points and other control signals must be mixed into the video signal at the correct moments.

The MC 1545 is a gated, two-channel, differential amplifier used as a video switch. With the gate level high, the output is connected to channel A and with the gate signal low, to channel B. The open-loop gain of the MC 1545 is typically 18 dB. For a contour point or control signal to be mixed into the video signal, the gate level is made low, resulting in a "white" level pulse at the output.

The closed-loop configuration of OP AMP 11 and the LH0002 current amplifier functions as a -2 amplifier with a drive capability for 75 Ω coaxial cable. The "video out" signal has the standard format of 1-V peak-to-peak, including the synchronization pulses, and is applied to a video monitor to display the original x-ray picture with the detected contour points and/or control signals superimposed.

84

CHAPTER 6: LINE EXTRAPOLATION PRINCIPLE

The vital role of the expectation window principle in the left
ventricular contour detection is explained in chapter 3. In the contour
detector prototype I, the center of the expectation window on video line
(n + 1) is defined as having the same horizontal position as the last
detected border point on line n – defined as the zeroth-order line
extrapolation principle. The basic limitations of this principle are
that (1) only limited excursions from the direction perpendicular to the
video scan lines are allowed and (2) the center of the expectation window
is generally not a good approximation of the next border point.

In general, it is advantageous to make the width of the expectation
window as narrow as practically allowable to limit the excursions from
the actual border at those places along the border, where forced border
points are generated (e.g., because of intervening structures). On the
other hand, relatively wide expectation windows are often necessary
because the actual border may change appreciably from line to line, as at
the mitral valve. Therefore, the selected width of the window must
always be a compromise.

Clearly the zeroth-order line extrapolation principle works best if
the longest chord is about perpendicular to the scan lines. When using
cine film and a rotating light table, this orientation can always be
realized. To analyze a cine film over a complete cardiac cycle, the sys-
tem is set up properly with the longest chord about perpendicular to the
scan lines at diastole, after which the film can be advanced over the
entire cycle. Although the left ventricle may rotate over as much as

±20° during a cardiac cycle, additional rotations of the film to
compensate for this change in angular position is generally not necessary.

For left ventricular studies, the angiograms mostly are taken in the
RAO projection, in which the foreshortening of the longest chord is mini-
mal and the spinal column does not overlap the left ventricular shadow.
However, to process the stored images from video tape or disc, the orien-
tation is such that the longest chord is not perpendicular to the scan
lines, but may have an angle between 20° and 60°, with the direction
perpendicular to the scan lines. Since the video scan direction is fixed
and the analog information cannot be rotated once it is in video format,
the preferred orientation can be obtained only by either rotating the TV
camera on top of the image intensifier or rotating the patient with
respect to the x-ray system. Because of vibrations, the image intensi-
fier must be securely in position when the cine camera is used. However,
a left ventricular study has been done at Ames with the image intensifier
rotated over the required angle without any visible degradation. Despite
these possible solutions for rotating the angiograms, there is one impor-
tant objection against applying this in a research or clinical environ-
ment. During a catheterization, the cardiologist depends a great deal on
the video images to properly insert the catheters. Rotating the image
would therefore result in orientation problems.

Assuming that the orientation of the video disc stored angiograms
has not been optimized, relatively wide expectation windows must be
allowed for the zeroth-order line extrapolation principle. Also, the
center of the expectation window generally deviates more from the actual
margin compared with the vertical orientation. It is clear that an

improved expectation window principle must be found so that the center of the expectation window is a good approximation of the actual border point, independent of orientation.

The left ventricular contour being a smooth continuous function, the position of the border point on line (n + 1) can be approximated from the positions of detected border points on previous lines. It will be shown in the following section that this can be achieved by linearly extrapolating the border positions on lines (n - 1) and n. The zeroth-order extrapolation principle is also analyzed and both methods are compared.

First-Order Line Extrapolation Principle

Denote the left ventricular border function as $g(nT)$, where n is the video line number and T is the line period (63.5 μsec). The function $g(nT)$ is a measure for the distance from the horizontal sync pulse to the border point on line n. Using the Taylor series, the function value $g[(n + 1)T]$ can be written as

$$g[(n + 1)T] = g(nT) + T \cdot \frac{g'(nT)}{1!} + T^2 \cdot \frac{g''(nT)}{2!} + \ldots + T^n \cdot \frac{g^{(n)}(nT)}{n!} + R_n, \quad (2)$$

where R_n is the remainder of the Taylor series. Since the contour is a smooth continuous function and the distance T between video lines is small, this series expansion can generally be truncated after the first two terms, resulting in the linear function:

$$g[(n + 1)T] \approx g(nT) + T \cdot g'(nT) \quad (3)$$

The derivative at $t = nT$ can be approximated with

$$g'(nT) \approx \frac{g(nT) - g[(n - 1)T]}{T} \quad (4)$$

Substituting equation (4) into (3) gives

$$g[(n+1)T] \approx 2g(nT) - g[(n-1)T] \qquad (5)$$

This approximation of the position of $g[(n+1)T]$ is then defined as the center of the expectation window on line $(n+1)$, denoted by $h[(n+1)T]$; that is,

$$h[(n+1)T] \triangleq 2g(nT) - g[(n-1)T] \qquad (6)$$

This is referred to as the first-order line extrapolation principle. Once the border points on lines $(n-1)$ and n are known in binary format, the center of the expectation window on line $(n+1)$ can be calculated using equation (6). The determination of $h[(n+1)T]$ from $g(nT)$ and $g[(n-1)T]$ is illustrated in figure 28. The widths of the left- and right-hand sides of the expectation window are again denoted ε_L and ε_R, respectively; in the actual system, these widths are expressed in a 4-bit binary number.
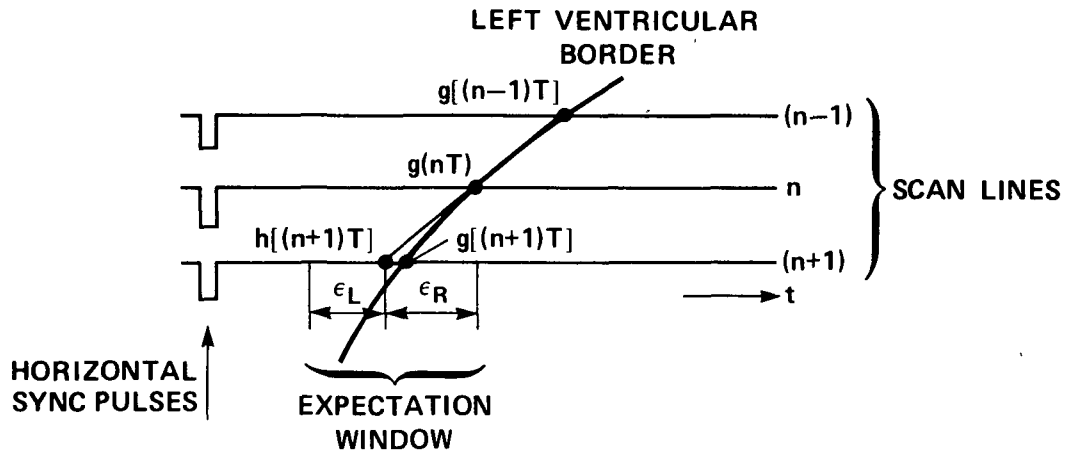

Figure 28.- The center $h[(n+1)T]$ of the expectation window on line $(n+1)$ is determined as a linear extrapolation from the border points $g(nT)$ and $g[(n-1)T]$ on the previous lines n and $(n-1)$, respectively.

In the implemented system, equation (6) is applied for both line extrapolation principles. Simply substituting $g(nT)$ for $g[(n-1)T]$ at

the time of calculation results in the position of the center of the expectation window according to the zeroth-order line extrapolation principle.

It was discussed in chapter 3 for the zeroth-order line extrapolation principle that straight-line approximation results in those areas where forced border points are generated at the beginning or end of the expectation window. This occurs when the video signal does not cross the reference level within the expectation window. The slope of the straight line is determined by the selected widths of the expectation window. It is certainly important to analyze what the maximum excursions from previous border points can be for the first-order case.

For simplicity, it is assumed that the expectation window is symmetrical about the center with half the width denoted ε ($\varepsilon > 0$). The maximum possible excursions can then be calculated by solving for $g(nT)$ from

$$\left| h[(n+1)T] - g[(n+1)T] \right| < \varepsilon \qquad \text{for all} \quad n \geq 0 \tag{7}$$

Substituting equation (6) into (7) gives

$$\left| 2g(nT) - g[(n-1)T] - g[(n+1)T] \right| < \varepsilon \tag{8}$$

or

$$\left| \{ g(nT) - g[(n-1)T] \} - \{ g[(n+1)T] - g(nT) \} \right| < \varepsilon \tag{9}$$

Define

$$\Delta(nT) \triangleq g(nT) - g[(n-1)T] \tag{10}$$

so that

$$\Delta[(n+1)T] = g[(n+1)T] - g(nT) \tag{11}$$

Substituting equations (10) and (11) into equation (9) yields

$$\left| \Delta[(n+1)T] - \Delta(nT) \right| < \varepsilon \tag{12}$$

89

The Δ functions can be approximated with

$$\Delta[(n+1)T] \approx g'[(n+1)T] \cdot T \qquad (13)$$

and

$$\Delta(nT) \approx g'(nT) \cdot T \qquad (14)$$

so that

$$\left| g'[(n+1)T] - g'(nT) \right| < \frac{\varepsilon}{T} \qquad (15)$$

Using the same approximation as in equations (13) and (14), we can write

$$g'[(n+1)T] - g'(nT) \approx g''[(n+1)T] \cdot T \qquad (16)$$

Substituting this into equation (15) gives

$$\left| g''[(n+1)T] \right| < \frac{\varepsilon}{T^2} \qquad (17)$$

or, to simplify the calculations,

$$\left| g''(nT) \right| < \frac{\varepsilon}{T^2} , \qquad n \geq +1 \qquad (18)$$

We are interested in the functions that satisfy this bound, that is, the functions for which

$$\left| g''(nT) \right| = \frac{\varepsilon}{T^2} , \qquad \varepsilon > 0 \qquad (19)$$

We will now distinguish two cases:

(1) The forced border points are generated at the end of the expectation window. The general solution to equation (19) can then be written as

$$g_R(nT) = \frac{\varepsilon}{2T^2} \cdot (nT)^2 + C_1 \cdot (nT) + C_2 , \qquad (20)$$

where C_1 and C_2 are constants.

(2) The forced border points are generated at the beginning of the expectation window, which yields

$$g_L(nT) = -\frac{\varepsilon}{2T^2} \cdot (nT)^2 + C_3 \cdot (nT) + C_4 \qquad (21)$$

with C_3 and C_4 constants.

Equations (20) and (21) are the general equations for a parabola.

Consider the case with initial conditions: $g(-T) = g(0) = 0$. In the actual system, a function $g(nT) = 0$ corresponds to the border position at the beginning of a scan line. However, in this chapter, we consider only position changes with respect to an initial condition. Taking zero as initial condition does not make the solutions less valuable. Substituting these conditions into equation (20) yields

$$C_1 = \frac{\varepsilon}{2T} \; ; \qquad C_2 = 0 \tag{22}$$

The function of the maximum excursions due to forced border points at the end of the expectation window is then

$$g_R(nT) = \frac{n\varepsilon(n+1)}{2} \tag{23}$$

Substituting the initial conditions into equation (21) yields

$$C_3 = -\frac{\varepsilon}{2T} \; ; \qquad C_4 = 0 \tag{24}$$

so that the function of the maximum excursions due to forced border points at the beginning of the expectation window is

$$g_L(nT) = -\frac{n\varepsilon(n+1)}{2} \tag{25}$$

These functions are plotted in figure 29 with solid lines. Note that the time axis is now vertical and the function value horizontal, in accordance with the TV scan. Assume now that the initial conditions are

$$g(0) = 0 \quad \text{and} \quad g(-T) = +\varepsilon \, , \quad \varepsilon > 0$$

Substituting these initial conditions into equation (20) gives

$$C_1 = -\frac{\varepsilon}{2T} \quad \text{and} \quad C_2 = 0 \tag{26}$$

so that

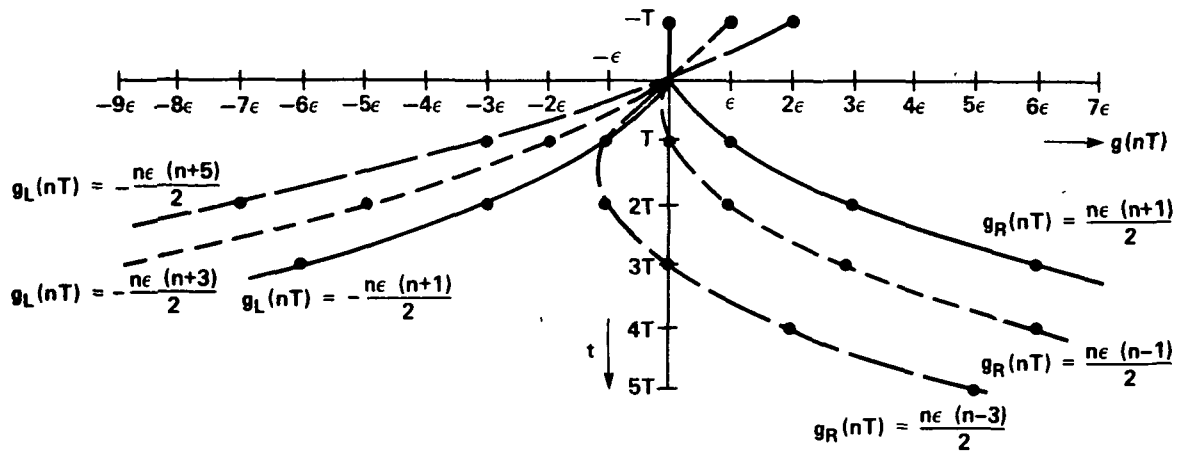$$g_R(nT) = \frac{n\varepsilon(n-1)}{2} \tag{27}$$

Figure 29.- Assuming a symmetrical expectation window with half the width denoted ϵ, the functions indicate the maximum possible excursions from different initial conditions.

and substituting into equation (21) gives

$$C_3 = -\frac{3\epsilon}{2T} \quad \text{and} \quad C_4 = 0 \tag{28}$$

so that

$$g_L(nT) = -\frac{n\epsilon(n+3)}{2} \tag{29}$$

These two functions are also plotted in figure 29 with dashed lines.

With initial conditions $g(0) = 0$ and $g(-T) = 2\epsilon$, the functions are

$$g_R(nT) = \frac{n\epsilon(n-3)}{2} \tag{30}$$

and

$$g_L(nT) = -\frac{n\epsilon(n+5)}{2} \tag{31}$$

These two functions are also plotted in figure 29. When ϵ_L is unequal to ϵ_R, the maximum excursions can easily be derived by substituting ϵ_L and ϵ_R, respectively, for ϵ in the derived formulas.

92

For the zeroth-order line extrapolation principle, the center $h[(n+1)T]$ of the expectation window on line $(n+1)$ is equal to the border position of $g(nT)$ on line n, delayed over one line period (fig. 30). In border coordinates, this can be written as

$$h[(n+1)T] = g(nT) \tag{32}$$

LEFT VENTRICULAR BORDER

g(nT)

g[(n+1)T]   h[(n+1)T]

n

(n+1)

t

ϵ_L ϵ_R

} SCAN LINES

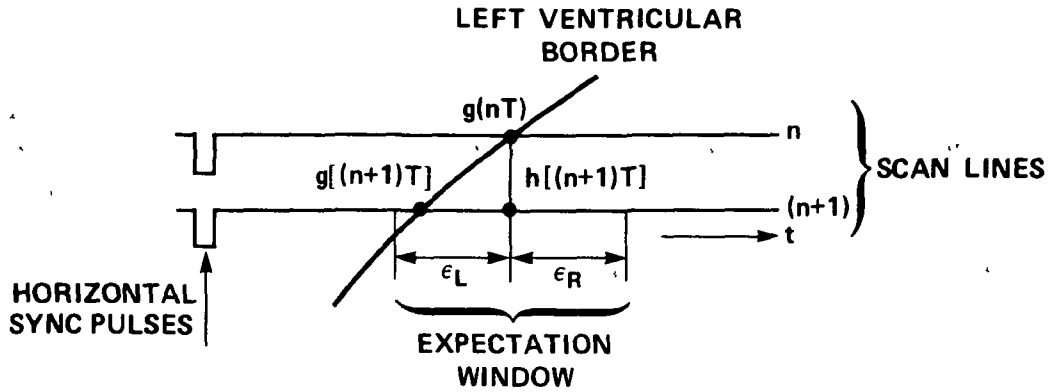**HORIZONTAL SYNC PULSES**

EXPECTATION WINDOW

Figure 30.- The center $h[(n+1)T]$ of the expectation window on line $(n+1)$ is defined as having the same horizontal position as the last detected border point on line n.

It was discussed in chapter 3 that the maximum excursions from previous border points are given by straight lines, the slopes of which are determined by the expectation window widths. In a way, similar to the analysis for the first-order case, the maximum possible excursions can be derived mathematically by solving for $g(nT)$ from

$$\left|h[(n+1)T] - g[(n+1)T]\right| < \epsilon , \quad \text{for all } n \geq 0 \tag{33}$$

assuming a symmetrical expectation window with half the width denoted ϵ ($\epsilon > 0$). Substituting equation (32) into (33) gives

$$\left|g[(n+1)T] - g(nT)\right| < \epsilon \tag{34}$$

Applying equations (11) and (13)

93

$$\Delta[(n+1)T] = g[(n+1)T] - g(nT) \approx g'[(n+1)T] \cdot T$$

yields

$$\left| g'(nT) \right| < \frac{\varepsilon}{T} \tag{35}$$

The maximum excursions are obtained by solving

$$\left| g'(nT) \right| = \frac{\varepsilon}{T} \tag{36}$$

The general solution can be written as

$$g(nT) = \pm \frac{\varepsilon}{T} \cdot (nT) + C \qquad \text{with} \quad \varepsilon > 0 \tag{37}$$

This is a straight line as previously mentioned. For the initial condition $g(0) = 0$, the solution is

$$g(nT) = \pm \frac{\varepsilon}{T} \cdot (nT) \tag{38}$$

This function is plotted in figure 31. The function $g(nT)$ is now independent of the value of the border function at $t = -T$. However,
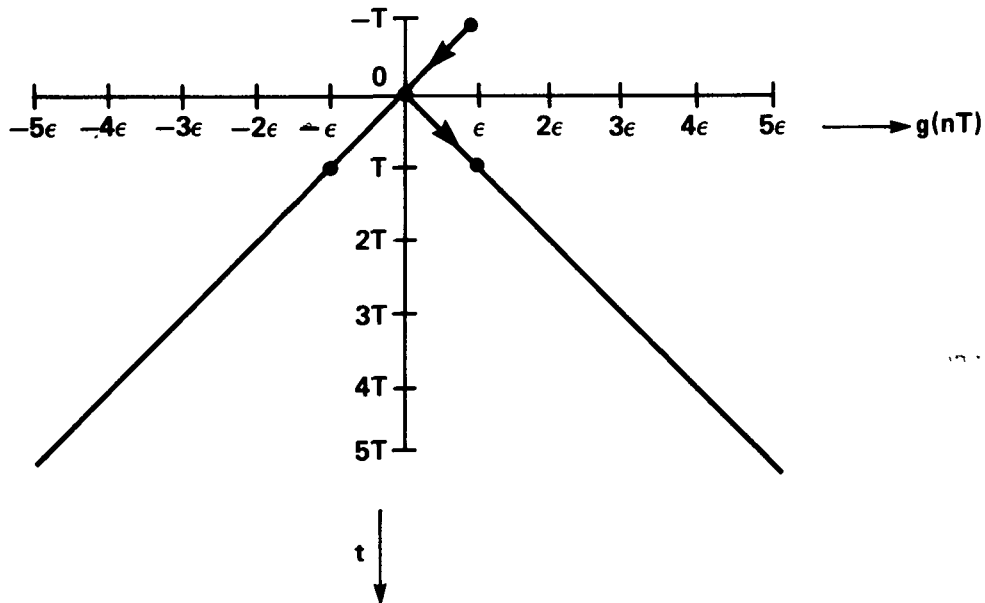
Figure 31.- Assuming a symmetrical expectation window with half the width denoted ε, the functions of maximum possible excursions are given by straight lines with slope $\sigma = \pm\varepsilon/T$.

94

because of the restricted expectation window excursions, the possible

value of g(-T) must be between +ε and -ε if g(0) = 0 is to be true.

The arrows in figure 31 indicate the maximum allowed changes in border

positions from t = -T to +T. Equation (38) can also be written as

$$g(nT) = \sigma nT \tag{39}$$

where

$$\sigma \triangleq \pm \frac{\varepsilon}{T} \tag{40}$$

In figure 31, the time axis is vertical and the function values are

plotted horizontally, as for a video display. For $\sigma = 0$, a vertical line

in the video image results and for $\sigma = \pm\infty$, a horizontal line results.

For a given sample period T, the slope σ is a linear function of ε.

A greater ε means that the system will be able to follow segments of

the left ventricular border, which are more horizontally oriented; how-

ever, a greater ε also increases the possibility of tracking an

intervening structure.

The left- and right-hand sides of the expectation window are gener-

ally not equal. Distinguishing ε_L and ε_R, the functions for the maximum

possible excursions are

$$g_L(nT) = -\frac{\varepsilon_L}{T} \cdot (nT) \tag{41}$$

and

$$g_R(nT) = +\frac{\varepsilon_R}{T} \cdot (nT) \tag{42}$$

Comparing the functions in figures 29 and 31, which have the same ε,

shows that the zeroth-order approximation is restricted in its ability to

track rapidly changing border functions. For a particular degree of

excursions from previous border points, smaller window widths can be

allowed using the first-order line extrapolation principle.

Note that the maximum excursions of the border functions for systems with other values of the sampling period   T   can easily be derived from figures 29 and 31. The plot for another value of   T   follows from these figures if they are compressed vertically or expanded with unchanged   ε axis. This will be the case for higher and lower resolution systems, respectively.

The step and ramp responses of both principles are described in the next section, using the   z   transform.

First-Order Line Extrapolation Principle in the   z   Domain

Transfer function- Equation (6), $h[(n+1)T] = 2g(nT) - g[(n-1)T]$, can be transformed (assuming initial conditions to be zero) into the   z domain as

$$zH(z) = 2G(z) - z^{-1}G(z) \tag{43}$$

This results in the transfer function

$$\frac{H(z)}{G(z)} = \frac{1}{z} \cdot \frac{2z-1}{z} \tag{44}$$

Note that $2g(nT) - g[(n-1)T]$ is calculated on line   n, but is used for line $(n+1)$. This one-line period delay is taken care of with the factor $1/z$. Figure 32 is a block diagram of this first-order approximation system.
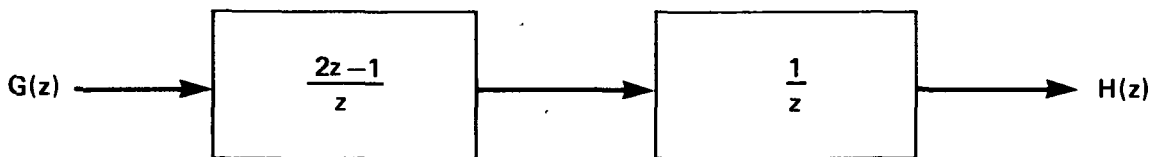

$$G(z) \longrightarrow \boxed{\frac{2z-1}{z}} \longrightarrow \boxed{\frac{1}{z}} \longrightarrow H(z)$$

Figure 32.- Block diagram of the first-order line extrapolation
principle in the   z   domain.

Step response- If the border position changes abruptly from one line to the other, the centers of the expectation windows can be determined by calculating the step response. Let $G(z) = z/(z-1)$ (unity input step), then

$$H(z) = \frac{z}{z-1} \cdot \frac{2z-1}{z^2} = 2z^{-1} + z^{-2} + z^{-3} + \dots \tag{45}$$
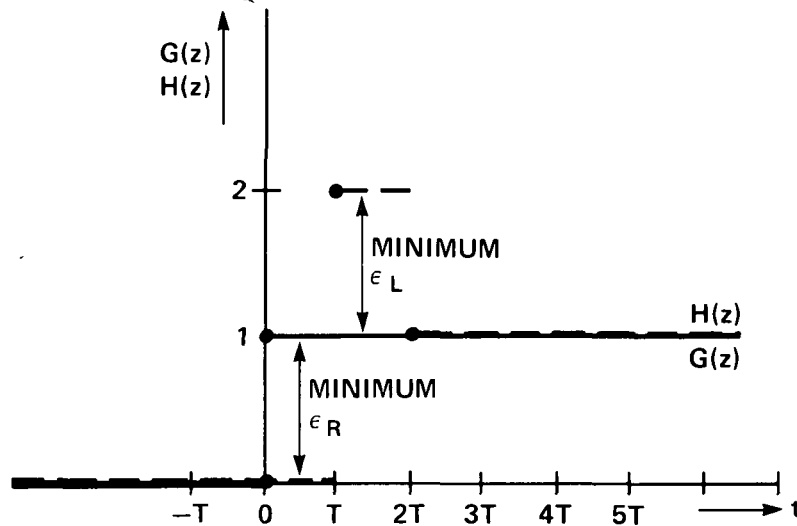
This function is plotted in figure 33.

Figure 33.- Step response, first-order line extrapolation principle.

A 100 percent overshoot occurs in the positioning of the centers of the expectation windows. There are other approximation methods which give a smaller overshoot, but these have the disadvantage that there is a finite error (delay) in the ramp response (ref. 51). These methods are also much more complex to implement.

In the calculation of this step response, it is assumed that the actual border points are detected, which means that one must allow for the left- and right-hand sides, ε_L and ε_R, respectively, of the expectation window, a minimum width equal to the step in the function $g(nT)$.

This is because g(nT) represents the detected contour and not the actual

border.   If it is assumed that the expectation window widths satisfy

these minimum requirements, the detected border equals the actual border.

If the widths ϵ_L and ϵ_R are smaller than the minimum required widths,

forced border points are generated, resulting in less overshoot

(described in more detail in the section on forced border points).

The assumption of the expection window widths satisfying the minimum

required widths must be made for all calculated step and ramp response in

this chapter.

Ramp response- In an identical way, the ramp response can be deter-

mined in case the border positions change linearly.   The ramp function

with slope γ in the z domain is

$$G(z) = \gamma \frac{Tz}{(z - 1)^2} \tag{46}$$

Therefore,

$$H(z) = \frac{\gamma Tz}{(z - 1)^2} \cdot \frac{2z - 1}{z^2} = \gamma T(2z^{-2} + 3z^{-3} + 4z^{-4} + \ldots) \tag{47}$$
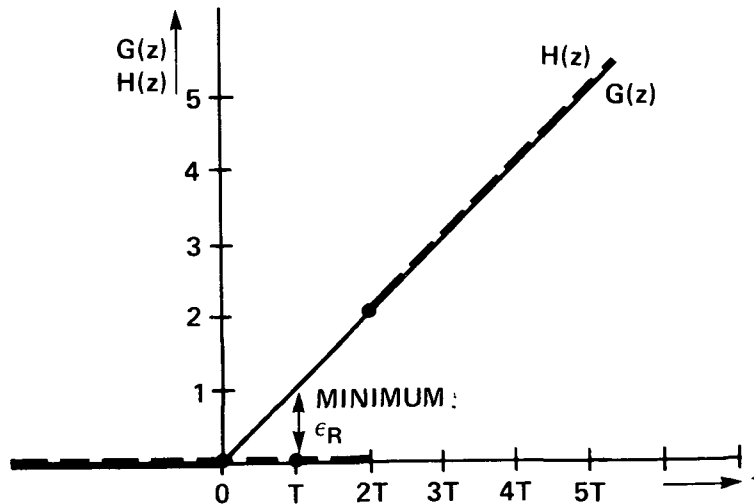
as shown in figure 34.

Figure 34.- Ramp response, first-order line extrapolation principle.

The minimum required one-sided width of the expectation window is $\varepsilon_R = \gamma T$, as indicated in the figure. In this case, there is no requirement for ε_L.

Zeroth-Order Line Extrapolation Principle in the z Domain

Transfer function- In this case, the center of the expectation window on line $(n+1)$ is simply determined by delaying the position of the border point on line n by one line period. The transfer function is therefore

$$\frac{H(z)}{G(z)} = \frac{1}{z} \tag{48}$$
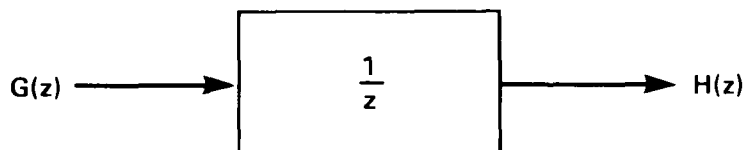
The block diagram is given in figure 35.

Figure 35.- Block diagram of the zeroth-order line extrapolation principle in the z domain.

Step response- The response to a step function is a delay over T:

$$H(z) = \frac{1}{z} \cdot \frac{z}{z-1} = z^{-1} + z^{-2} + z^{-3} + \ldots \tag{49}$$

This step response is shown in figure 36. For this zeroth-order approximation, no overshoot occurs in the position of the center of the expectation window. As explained before, this calculation of $H(z)$ is valid
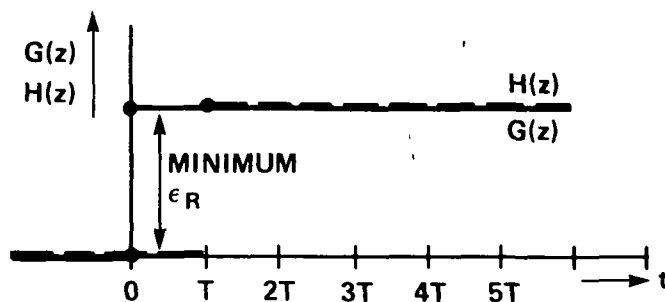

Figure 36.- Step response, zeroth-order line extrapolation principle.

only for a minimum width ε_R for the right-hand side of the expectation window equal to the step in the actual border function. If the selected ε_R is less than this minimum required width, forced border points are generated and the final value is reached under a straight line, the slope of which is determined by ε_R. For the assumed positive step, there is no requirement for ε_L.

Ramp response- The response to a ramp function $G(z) = \gamma [Tz/(z-1)^2]$ is

$$H(z) = \frac{\gamma Tz}{(z-1)^2} \cdot \frac{1}{z} = \gamma T(z^{-2} + 2z^{-3} + 3z^{-4} + 4z^{-5} + \ldots) \qquad (50)$$
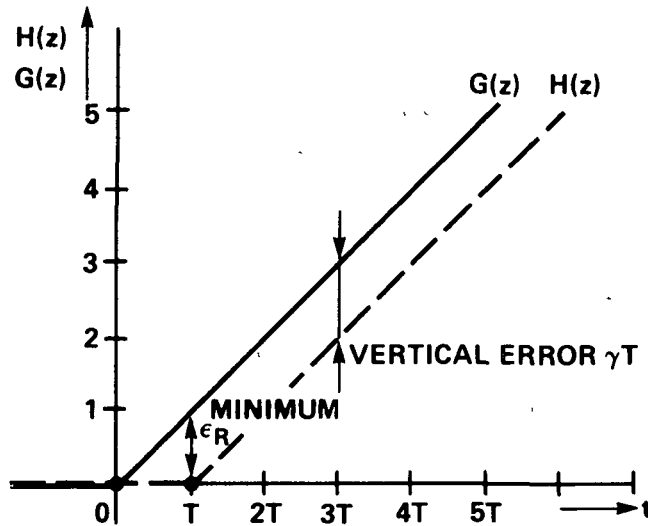
as shown in figure 37.

Figure 37.- Ramp response, zeroth-order line extrapolation principle.

The "vertical" error can be calculated by applying the formula for the final value of the error function. The error function $F(z)$ is

$$F(z) = H(z) - G(z) = G(z) \cdot \left(\frac{1-z}{z}\right) \qquad (51)$$

The vertical error is then

100

$$\lim_{z \to 1} \frac{z-1}{z} \, F(z) = \lim_{z \to 1} \frac{z-1}{z} \cdot \frac{\gamma Tz}{(z-1)^2} \cdot \frac{1-z}{z} = -\gamma T \qquad (52)$$

The minus sign indicates that, for the ramp function, the centers of the expectation window are always delayed with respect to the border points. This delay is linearly dependent on the slope of the ramp.

The required minimum width ε_R is again equal to γT, the same requirement as for the ramp response of the first-order expectation window principle.

Effects of forced border points on step and ramp responses- If no border points are detected within the expectation window, forced border points are generated at one side of the window (as explained in the description of the contour detector prototype I). The effects of the applied forced border points on both expectation window principles are determined in this section.

Effects on first-order line extrapolation principle- Consider the case in which there is a step change in the actual border and the width ε_R is less than the required width as determined in figure 33. Forced border pulses are then generated at the end of the expectation window. The resulting positions of the border points and the centers of the expectation windows are shown in figure 38. In figures 38 through 41, the detected border points are indicated by X's and the resulting centers of the expectation windows by dots.

The overshoot of the centers of the expectation windows in figure 38 is less than in figure 33, where $\varepsilon_R \geq$ amplitude step. However, with less overshoot it takes longer to settle down. For a ramp function, the situation is illustrated in figure 39. Again some over- and undershoots

of the centers of the expectation windows occur, but the actual border is fairly well approximated.
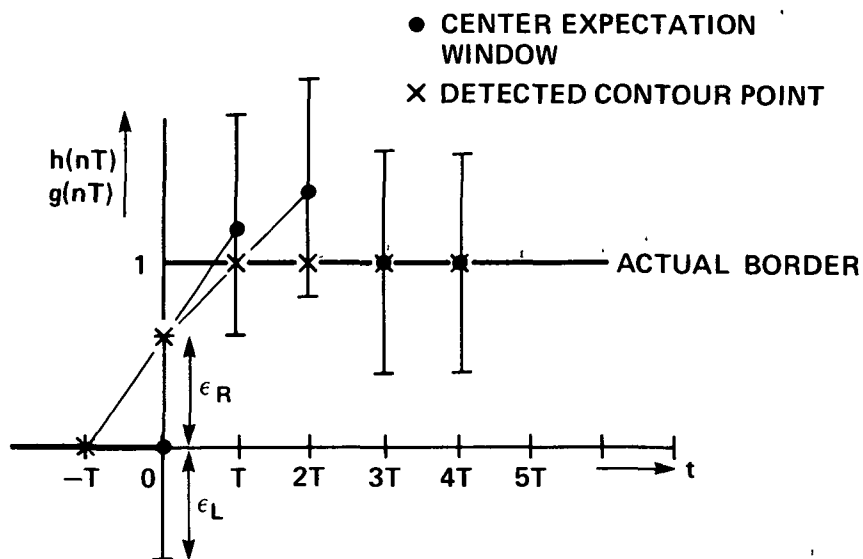

● CENTER EXPECTATION WINDOW
✕ DETECTED CONTOUR POINT

Figure 38.- Step response, first-order line extrapolation principle with ε_R less than step in border function.
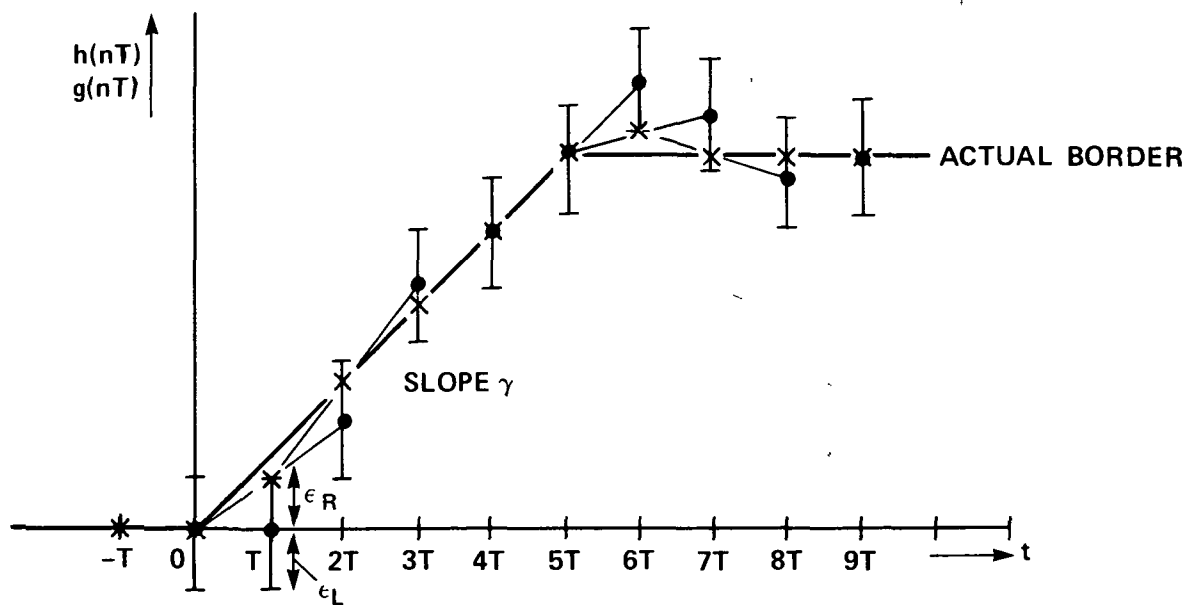

Figure 39.- Ramp response, first-order line extrapolation principle with $\varepsilon_R < \gamma T$.
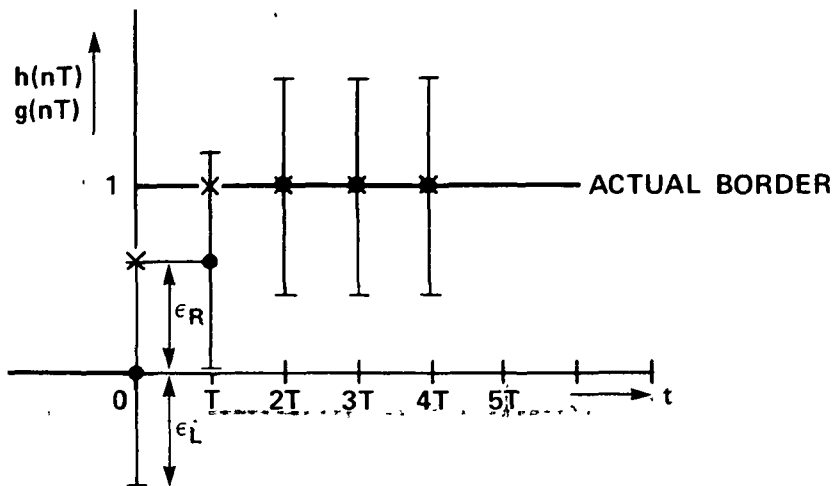
Figure 40.- Step response, zeroth-order line extrapolation principle with ϵ_R less than step in border function.
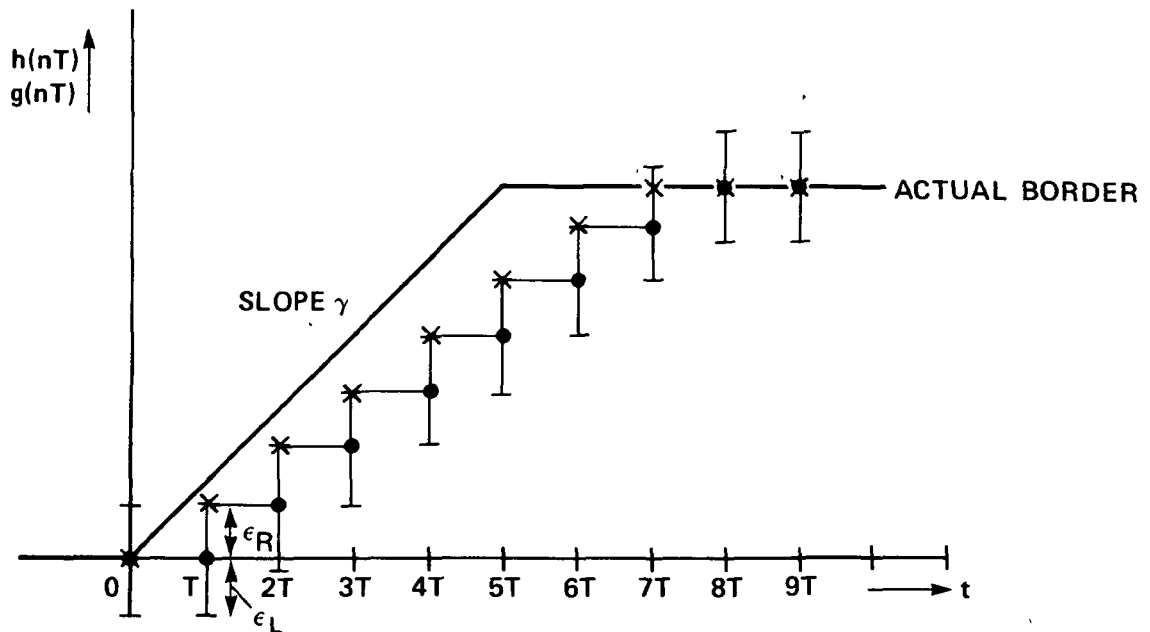

Figure 41.- Ramp response, zeroth-order line extrapolation principle with $\epsilon_R < \gamma T$.

Effects on zeroth-order line extrapolation principle- The step response is shown in figure 40. The scale used is the same as in figure 38. There is no overshoot in the positions of the centers

of the expectation windows. So long as forced border points are generated, the centers are on a straight line, the slope of which is determined by the width ϵ_R.

For a ramp function the situation is illustrated in figure 41. The contour is now approximated with a straight line and the distance between the actual and forced border points increases with time. A comparison of figure 41 with figure 39 clarifies the improved tracking capability of the first-order line extrapolation principle.

CHAPTER 7: FIELD EXTRAPOLATION PRINCIPLE

The fact that the ventricular contour is a smooth, continuous function is used in chapter 6 to determine the center of the expectation window as a linear extrapolation from the border points on the two previous lines. The spatial movement of the left ventricle during a heart cycle is also a smooth, continuous function with time (ref. 15), suggesting that the last or last two fields are used as an approximation for the border in the current field. This will be especially advantageous for detecting the contours during systole when contrast is usually very low. At those instances, the human eye often is not capable of detecting the correct location of the margin. The investigator then approximates the outline as accurately as possible by scanning the whole cycle or part of the cycle a few times to ascertain the spatial movement of the ventricle. He then returns to the low-contrast frames and, with the information stored in his own memory, he draws the outline where he thinks it should be. Although a human being has a much greater capability than a relatively simple machine of extracting the relevant information from a series of pictures and of using this to approximate the next picture, applying the information of only the last two fields is a first approximation to this complex problem.

Similar to the zeroth- and first-order line extrapolation principles for the determination of the center of the expectation window from the border points on previous lines in the same field, we can define zeroth- and first-order field extrapolation principles using corresponding border points in previous fields. The zeroth-order field extrapolation principle then considers only the last field.

Applying both extrapolation principles simultaneously, the center of the expectation window $h_m[(n+1)T]$ on line $(n+1)$ in field m is then defined as the average position of the centers of the expectation windows determined separately by the line and field extrapolation methods.

Clearly, this field extrapolation principle is another important step toward implementation of an on-line processing system. For this purpose, the left ventricular angiograms must be stored on video tape/disc and these recordings, instead of cineangiograms, are used to process the data. This combined extrapolation principle is, of course, also applicable when a single frame of a cineangiogram is processed off-line using a TV camera and a light table. Although this will have a stabilizing effect on the contour detection, because it averages out slight differences between consecutive fields, this was not the original reason for applying the field extrapolation principle.

Defining the Center of the Expectation Window Using Both the Line
and Field Extrapolation Principle

The numbering of the scan lines in the odd and even fields is defined as shown in figure 42. For simplicity, it has been assumed that the field retrace time for the odd field is equal to zero and, for the even field, is equal to the retrace time of the last line in this frame. In reality, the number of scan lines per field is less than 256 because of the actual field retrace time. The first complete line in each field is assigned line number 1; this number is incremented by one for each following line. For memory addressing purposes, the even field is
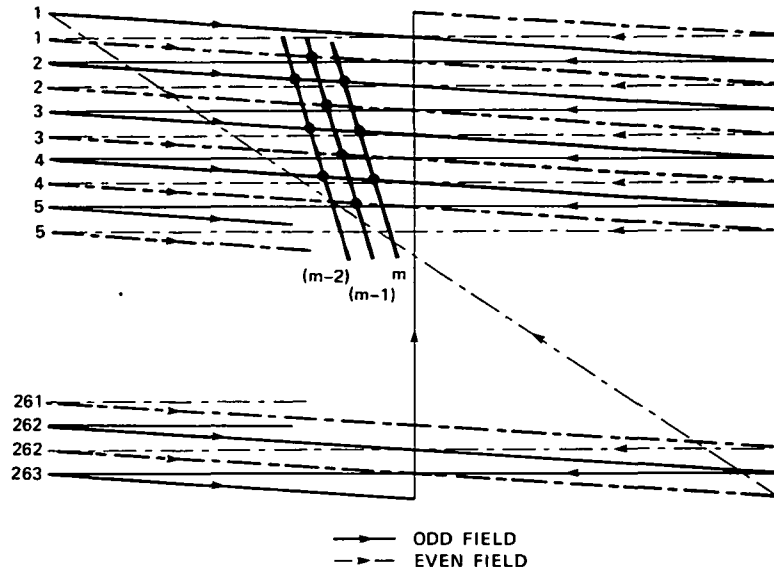
Figure 42.- Numbering of the scan lines in a video frame as defined,
for the field extrapolation principle.

distinguished by adding 512 (= 2^9) to the line number. A moving **straight**
line is shown at its positions in fields (m - 2) to the current field **m.**

A border point is denoted as $g_m(nT)$, where m refers to the **field**
number and n, to the line number; therefore, $g_{(m-1)}[(n-1)T]$ is **the**
border position on line (n - 1) in field (m - 1). If only the line **extrap-**
olation principle is applied, the center of the expectation window **on**
line (n + 1) in field m is given as

$$h_{mL}[(n+1)T] = 2g_m(nT) - g_m[(n-1)T] \qquad (53)$$

To calculate the center of the expectation window using the field
extrapolation principle, we must distinguish between even and odd **fields.**
Assuming field m is an odd field, the center of the expectation **window**
is defined as

$$h_{mF}[(n+1)T] = 2g_{(m-1)}(nT) - g_{(m-2)}[(n+1)T] \qquad (54)$$

If field m is an even field, $h_{mF}[(n+1)T]$ is defined as

107

$$h_{mF}[(n+1)T] = 2g_{(m-1)}[(n+1)T] - g_{(m-2)}[(n+1)T] \qquad (55)$$

Applying both extrapolation principles simultaneously results in:

Field m is odd field:

$$h_m[(n+1)T] = \frac{2g_m(nT) - g_m[(n-1)T] + 2g_{(m-1)}(nT) - g_{(m-2)}[(n+1)T]}{2} \qquad (56)$$

Field m is even field:

$$h_m[(n+1)T] = \frac{2g_m(nT) - g_m[(n-1)T] + 2g_{(m-1)}[(n+1)T] - g_{(m-2)}[(n+1)T]}{2} \qquad (57)$$

Note that $h_m[(n+1)T]$ is calculated shortly after $g_m(nT)$ has been detected, so that the line number at that moment is n. The zeroth-order field extrapolation principle can be applied by substituting $g_{(m-1)}(nT)$ and $g_{(m-1)}[(n+1)T]$ in equations (56) and (57), respectively, instead of $g_{(m-2)}[(n+1)T]$. The center of the expectation window can thus be determined in four different ways by selecting independently the zeroth- and first-order line and field extrapolation principles, respectively.

The determination of the center of the expectation window using the first-order line and field extrapolation principles is illustrated in figure 43. The left ventricular contour is shown at its different positions in fields (m-2) through m. It is assumed that the current field m is an odd field. The center of the expectation window determined by only the line extrapolation principle from $g_m(nT)$ and $g_m[(n-1)T]$ is denoted $h_{mL}[(n+1)T]$. Applying only the field extrapolation principle results in $h_{mF}[(n+1)T]$, as calculated from $g_{(m-1)}(nT)$ and $g_{(m-2)}[(n+1)T]$. The actual center $h_m[(n+1)T]$ on line (n+1) in field m is then

108

Figure 43.- The center $h_m[(n+1)T]$ of the expectation window on line $(n+1)$ in field m is defined as the average position of the centers $h_{mL}[(n+1)T]$ and $h_{mF}[(n+1)T]$ of the expectation windows, determined separately by the line and field extrapolation methods, respectively.

defined as the average value of $h_{mL}[(n+1)T]$ and $h_{mF}[(n+1)T]$. Assuming

figure 43 shows the left border of the left ventricular contour, the

left-hand side of the expectation window is denoted LEPL and the right-

hand side, LEPR. The distance from LEPL to $h_m[(n+1)T]$ is denoted LEWL.

Generally, a sample point LSPL is defined at a distance LSWL from LEPL.

The other sample point to the right of the border is denoted LSPR. The

positions of the expectation and sample points are described in more

detail in chapter 8. However, at this point it is important to know how

the positions of LSPL and LEPL are calculated from $h_m[(n+1)T]$. As

explained in chapter 8, LEPR is determined from the position of LEPL and

LSPR from $g_m[(n+1)T]$. Note that the expectation and sample window

widths are determined in a 4-bit binary format.

Implementation

The circuitry used to calculate the center of the expectation

window $h_m[(n+1)T]$ for the left and right borders has been implemented

separately. The calculation for both borders can be done simultaneously

109

during the horizontal synchronization pulse, requiring only one control

unit. However, calculating the center of the expectation window for the

right border requires an extra time state to handle the aortic valve

simulation. The design of the memory configuration for the left border

and the required timing are described with actual circuit diagrams, a

flow chart, and a timing diagram. The actual implementation of the

control unit will not be described.

The left-border coordinates of the last two fields are stored in a

1k × 13 bit static   n MOS random access memory (RAM) with an access and

cycle time of 500 nsec maximal (chapter 5, fig. 23). With each coordi-

nate available in a 12-bit format, the thirteenth bit is used as a con-

trol bit, which is zero, if there is no border point on a scan line and one if there is a border point. The implemented memory configuration is shown schematically in figure 44. Storing the 13 bits present at the DATA IN input at a location specified by the 10-bit address is accomplished by having the READ/WRITE and CONTROL ENABLE inputs both low. Reading data from a specified memory location occurs when the READ/WRITE input is high and the CONTROL ENABLE low. After the DATA OUT outputs have sta-bilized, these data can be loaded

Figure 44.- Memory configuration
for storing the left-border
coordinates of two fields.

into the memory buffer register MBR. Using tri-state buffers, this information can be applied to the B-bus of the left-border arithmetic unit during the appropriate time periods to calculate the center of the expectation window.

The actual circuitry for the field memory is shown in figure 45. The eight least significant bits of the address are determined by counting the scan lines during a video field using 4-bit counters COCC1 and COCC2. The counter outputs are connected to the inputs of an 8-bit adder (ADCC1 and ADCC2), which adds a 1 to the address when $g_{(m-2)}[(n+1)T]$ and $g_{(m-1)}[(n+1)T]$ need to be accessed. The 9th bit of the address is always zero and the most significant bit can be $\emptyset$ or 1, depending on whether one wants to access the coordinates of an odd or even field, respectively. Therefore, the detected border coordinates in an odd field will always be stored in the lower half of the memory and the coordinates in an even field in the upper half. Note that the nine least significant bits must be used for the video line number if a 625-line video scan is used, as for European systems.

The memory buffer register (MBR) consists of four 4-bit bidirectional universal shift registers, SRCC1-SRCC4, which enable one to load data, shift left and right, and inhibit the clock. BUCC1 through BUCC3 are the tri-state buffers that apply the data to the B-bus of the arithmetic unit at the appropriate times.

Figure 46 is a flow chart of the complete procedure used to calculate the center of the expectation window on line $(n+1)$ in field m. The processing cycle is completed in 2.75 μsec, divided into 11 time states of 250 nsec each, as shown in the timing diagram in figure 47.
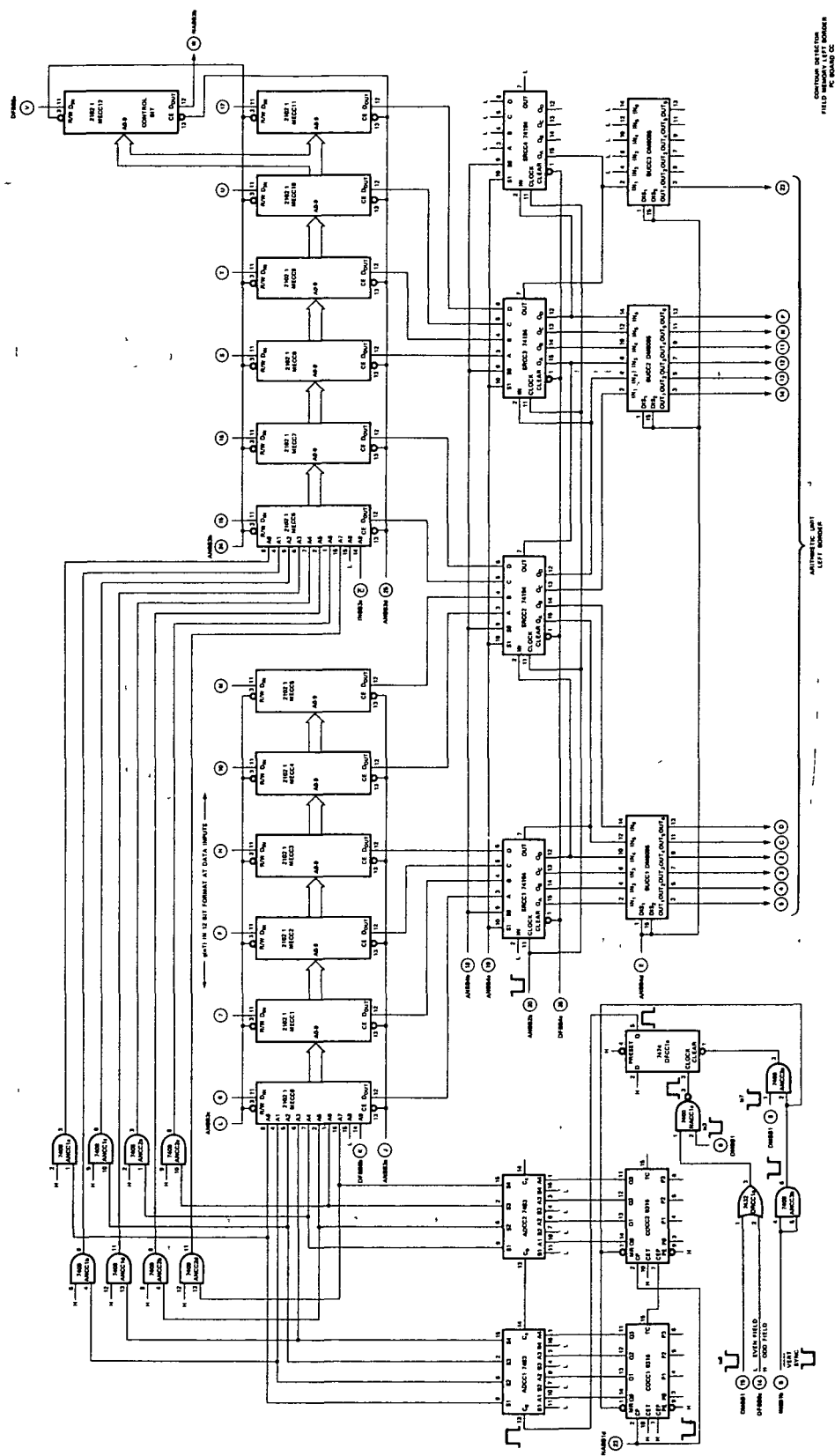
111

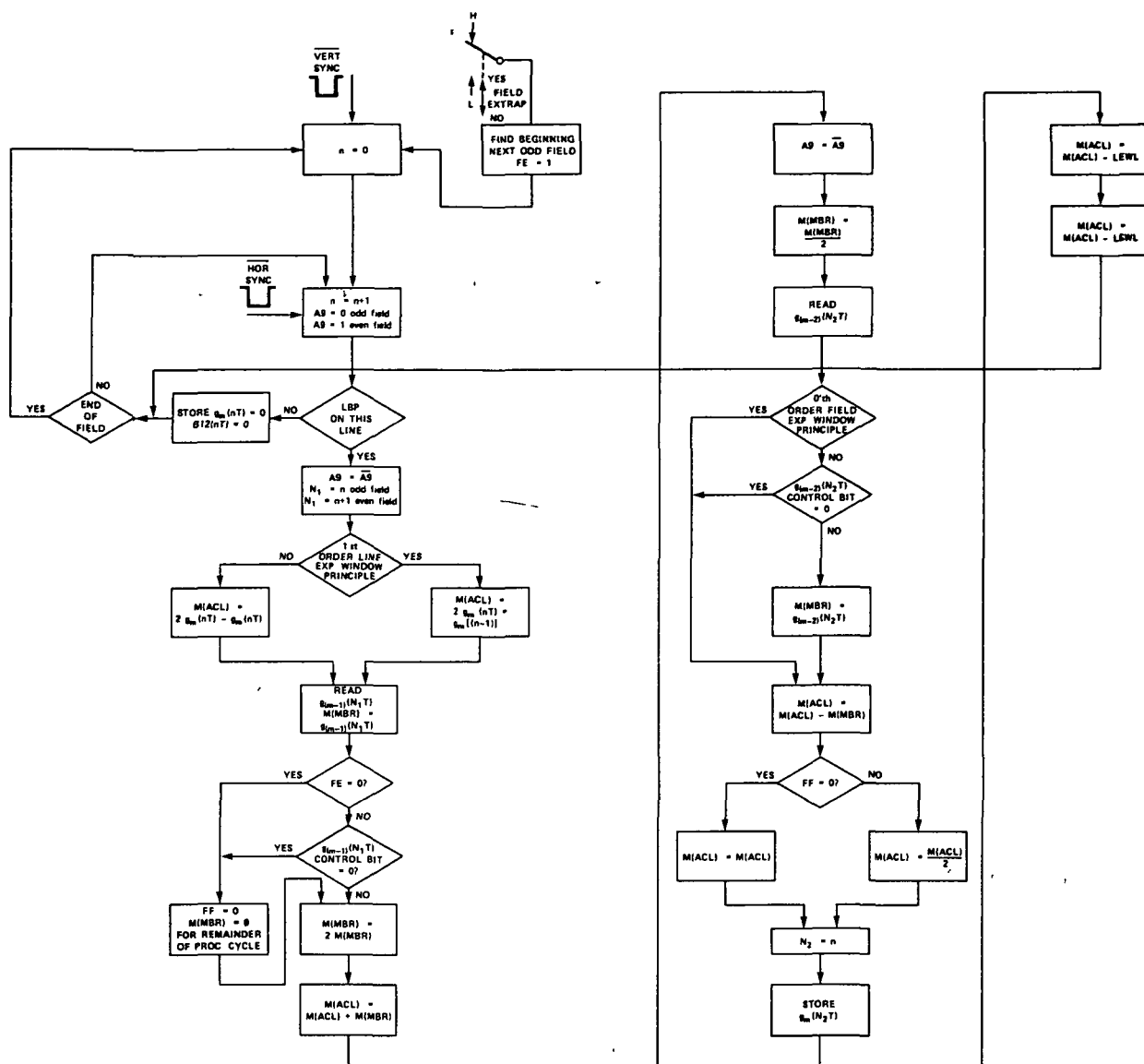Figure 45.- Implementation of the field memory for the left border.

Figure 46.- Flow chart for calculating the center of the expectation window using the line and field extrapolation principles.
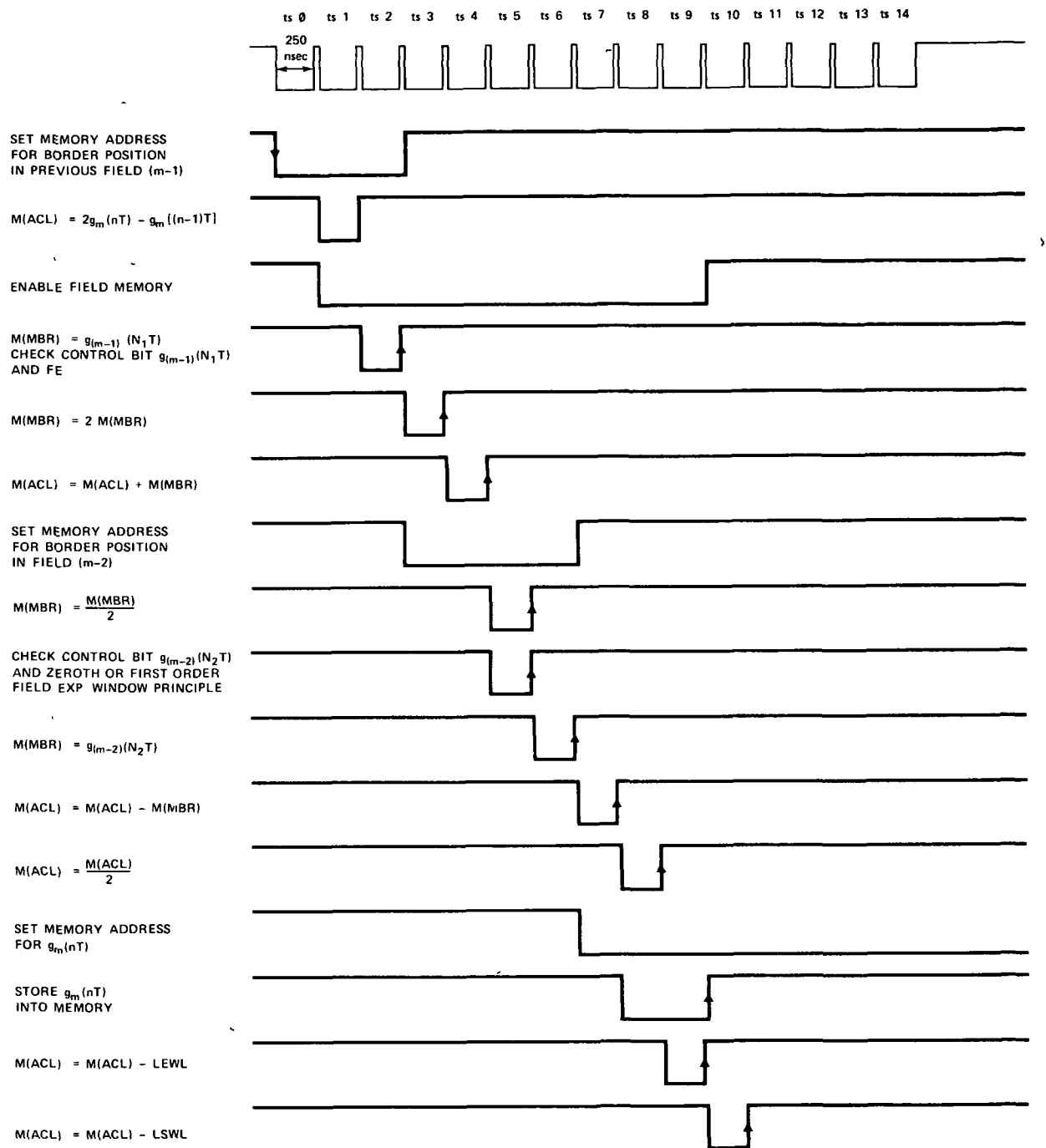
Figure 47.- Timing diagram for calculating the center of the expectation window.

This diagram indicates which manipulations are done during which time states. The comments in figure 47 are given for the case in which the first-order extrapolation principles are used with the control bits unequal to zero. The complete flow diagram is described below; at the same time references are made to the timing diagram.

The field extrapolation principle is enabled by activating a switch shown at the top of the flow diagram. So long as this switch has not been activated, the center of the expectation window is determined using the line extrapolation principle only (this will be clarified later on). To always start in the same phase after having activated the switch, the first complete odd field after this moment is defined as the first field with FE (field enable) = 1. The most significant address bit A9 is made low at the beginning of each video line in an odd field to access the lower half of the 1k memory and is made high at the beginning of each video line in an even field. The first full line in a field after the occurrence of the vertical synchronization pulse is assigned the value n = 1.

The calculation of the center of the expectation window $h_m[(n+1)T]$ is only carried out if a left-border point has been detected at the current line n. If no left-border point has been detected during a scan line, then $g_m(nT) = 0$ is stored into memory with a corresponding control bit equal to zero, indicating that all zeros have been stored at this location. This is not explicitly shown in the timing diagram. As a result, all scan lines not traversing the left ventricle are assigned a control bit equal to zero. Because of the vertical movement of the entire left ventricle over a heart cycle plus its contraction and

ejection movements, it is important to know if actual contour points were detected at the selected video lines in the previous fields.

Assuming a left-border point has been detected, the most significant address bit is inverted at the beginning of time-state $ts\emptyset$ to access the border coordinate in the previous field. Also, a 1 is added to the address if the current field is an even field (compare eqs. (54) and (55)). During time state $ts1$, the center of the expectation window is calculated according to the line extrapolation principle as $2g_m(nT) - g_m[(n-1)T]$. This calculation is done in the arithmetic unit for the left border in the same way as described for the right border in chapter 8. The result is stored in four 4-bit shift registers of the same type as used for the memory buffer register (fig. 45). This 16-bit register is referred to as ACL (accumulator left border) and its contents as $M(ACL)$; therefore,

$$M(ACL) = 2g_m(nT) - g_m[(n-1)T] \qquad (58)$$

If the zeroth-order line extrapolation is selected, $g_m(nT)$ is substituted for $g_m[(n-1)T]$ and the result is

$$M(ACL) = 2g_m(nT) - g_m(nT) = g_m(nT) \qquad (59)$$

The field memory is enabled at the beginning of time state $ts1$ and, with the correct address applied, $g_{(m-1)}(N_1T)$ is read and stored into the memory buffer register at the end of $ts2$, that is

$$M(MBR) = g_{(m-1)}(N_1T) \qquad (60)$$

where $N_1 = n$ if the current field is an odd field and $N_1 = n + 1$ for an even field. At the end of $ts2$, it is also checked if the field extrapolation principle was not selected ($FE = 0?$) and if the control bit for $g_{(m-1)}(N_1T)$ is equal to zero. If the answer to one or both of these

116

questions is true, then the MBR is cleared for the remainder of this processing cycle. This situation is referred to as FF: = 0. This means that the center of the expectation window will be determined only by the line extrapolation principle. Independent of whether the data in the MBR are unequal to zero or not, the contents of MBR are shifted over one position to the right at the end of ts3, which yields $M(MBR): = 2M(MBR)$. These new data are added to the contents of the accumulator during ts4. Assuming that one had selected the first-order line extrapolation principle and activated the field extrapolation switch, the contents of ACL would be

$$M(ACL) = 2g_m(nT) - g_m[(n-1)T] + 2g_{(m-1)}(N_1T) \qquad (61)$$

At the beginning of ts3, the address is set for the reading of the data from field $(m-2)$ during a later time state. The most significant address bit A9 is again inverted, thus giving it the initial value it had at the beginning of the video line, and a 1 is added to the current line number. The next step during ts5 is to shift the data in the MBR one position to the left, resulting again in

$$M(MBR) = g_{(m-1)}(N_1T) \qquad (62)$$

Meanwhile, the coordinate $g_{(m-2)}[(n+1)T]$ is read from memory, but not yet loaded into the MBR. At the end of ts5, the system checks whether the zeroth-order field expectation window principle was selected and whether the control bit for $g_{(m-2)}[(n+1)T]$ is equal to zero. If the answer to one or both of these checks is true, then the zeroth-order field extrapolation will be applied. The border coordinate $g_{(m-2)}[(n+1)T]$ will not be stored in the MBR, but the old data $g_{(m-1)}(N_1T)$ are subtracted from the accumulator contents during ts7.

117

If this is not the case, then $g_{(m-2)}[(n+1)T]$ is stored in the MBR at

the end of ts2 and the contents of MBR are subtracted from the

accumulator contents.

Earlier, the conditions were described for which the MBR was

cleared for the remainder of the processing cycle (FF = 0). It is clear

that, under these conditions, the contents of MBR do not change even if

one wants to load $g_{(m-2)}[(n+1)T]$, because MBR remains cleared

independently of the clock pulse.

These same conditions are also important for the next step. If

FF = 0, the accumulator contains the center of the expectation window

calculated according to the line extrapolation principle only. For this

condition, the clock to the accumulator is inhibited during ts8 and

nothing happens. If FF ≠ 0, then the accumulator contains the sum of

the centers of the expectation windows as calculated according to the

line and field extrapolation principles separately. To obtain the

average of these centers, the contents of the accumulator are shifted

one position left during ts8, resulting in

$$M(ACL) = h_m[(n+1)T] \tag{63}$$

At the beginning of ts7, the extra 1 in the memory address is removed

and the last detected border point $g_m(nT)$ is stored in memory during

ts8 and ts9.

The expectation window width LEWL is subtracted from $h_m[(n+1)T]$

during ts9 and the result is stored in the accumulator. As explained

in chapter 8 for the right border, these data are also stored in D flip-

flop registers; these data then represent the left-hand side LEPL of the

expectation window. Similarly, the sample window width LSWL is

118

subtracted from the contents of the accumulator during ts10 and stored in ACL at the end of ts10. The final result is then that the accumulator contains the position of LSPL for the next video line in the current field.

The processing cycle for calculating LEPL and LSPL on the next video line (n + 1) in the current field m is now complete and we return to the beginning of the flow chart for the next processing cycle. If line n was not the last line in the video field, then the address is incremented by one and bit A9 is reset to zero if the current field is an odd field and set to one for an even field. With n being the last line in the field, the line counter is reset during the vertical synchronization pulse and the whole cycle is repeated.

Page intentionally left blank

CHAPTER 8: IMPLEMENTATION OF EXPECTATION AND

SAMPLE POINTS

In chapter 7, the center of the expectation window $h_m[(n+1)T]$ on line $(n+1)$ in field m was defined as:

Field m is odd field:

$$h_m[(n+1)T] = \frac{2g_m(nT) - g_m[(n-1)T] + 2g_{(m-1)}(nT) - g_{(m-2)}[(n+1)T]}{2} \quad (64)$$

Field m is even field:

$$h_m[(n+1)T] = \frac{2g_m(nT) - g_m[(n-1)T] + 2g_{(m-1)}[(n+1)T] - g_{(m-2)}[(n+1)T]}{2}$$

$$(65)$$

Formulas (64) and (65) are given for the general case that the center is determined using both the first-order line and field extrapolation principle. The zeroth-order line extrapolation principle can be applied by substituting $g_m(nT)$ for $g_m[(n-1)T]$ at the time of the calculation. Similarly, the zeroth-order field extrapolation can be applied by substituting $g_{(m-1)}(nT)$ and $g_{(m-1)}[(n+1)T]$ in equations (64) and (65), respectively, for $g_{(m-2)}[(n+1)T]$. These features have been implemented in the actual system, allowing an instantaneous comparison of the different principles.

The values of the border positions are determined in digital format by counting clock pulses from the horizontal synchronization pulses to these border points. The required clock frequency can be derived by considering the possibly occurring errors and the required accuracy. The maximum error, which can occur in the determination of a border point, is ±1 bit. The calculation of the center of the expectation

121

window, according to each extrapolation principle separately, results in a maximum error of ±3 bits for each principle. Because $h_m[(n+1)T]$ is defined as the average of these two centers, the maximum possibly occurring error in $h_m[(n+1)T]$ is again ±3 bits. The position of $h_m[(n+1)T]$ on line $(n+1)$ is found by comparing the state of a position counter with the calculated value of $h_m[(n+1)T]$. Another ±1-bit error is possible here, resulting in a total maximum error of ±4 clock periods.

Thus a high count frequency is required if one wants the center of the expectation window to be a good approximation of the next border point under all circumstances. This is especially true in areas of low contrast, where the expectation window width is automatically narrowed down (chapter 10) under the assumption that the next border points are detected or generated as forced border points in a direction determined by previous border points. Therefore, an overall accuracy of ±80 nsec was assumed, resulting in a clock period of 20 nsec or a clock frequency of 50 MHz.

With the required accuracy in mind, the temperature stability of the clock pulse oscillator is certainly important. Assume that we allow the number of counted pulses over one line period ($= 57\,\mu$sec) to be off by no more than one count. The time period used, 57 μsec, is the time from the rising edge of the inverted horizontal synchronization pulse on a line until the trailing edge of this pulse at the end of the line. The number of clock pulses for each 57 μsec is

$$\frac{57\times10^{-6}}{20\times10^{-9}} = 2850 \tag{66}$$

so that

122

$$\Delta T = \frac{1}{2850} \times 20 \text{ nsec} = 7.02 \times 10^{-12} \text{ sec} \tag{67}$$

and

$$\Delta f \approx 17.5 \text{ kHz} \tag{68}$$

Assuming a temperature range of $\pm 10°$ C in the ventilated system, this requires a $\Delta f/°C = 35$ ppm/°C. With a maximum number of clock pulses per line of 2850, the coordinates of the contour for use in the contour detector are determined in a 12-bit format.

Applying formulas (64) and (65), the center of the expectation window is also determined in a 12-bit format. However, we also must determine the beginning and end points of the expectation window to enable the comparator, and the sample points to calculate the dynamic reference level.

If it is assumed, for simplicity, that only the first-order line extrapolation principle is applied, the beginning and end points of the expectation window on line $(n+1)$ are shown in figure 48 for the left
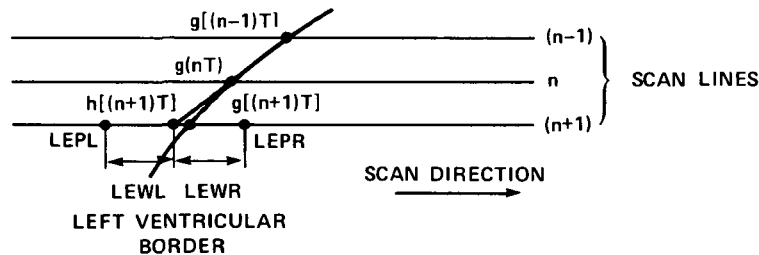
Figure 48.- Positioning of beginning point LEPL and end point LEPR of the expectation window on line $(n+1)$ for the left border.

border. These points are denoted LEPL and LEPR, respectively, where the first letter refers to left (L) or right (R) border, EP to expectation point, and the last letter to the left- (L) or right- (R) hand side of

123

expectation window, respectively. According to the way the system has been implemented, these beginning and end points are defined as

$$LEPL = h[(n+1)T] - LEWL \qquad (69)$$

and

$$LEPR = LEPL + LEWL + LEWR \qquad (70)$$

that is, LEPR is determined from the position of LEPL (W in LEWL and LEWR refers to window). Note that the assigned value of a point in digital format increases, from left to right in figure 48.

Three sample points are defined for the left border, as illustrated in figure 49 (explained in more detail in chapter 10). The sample points are denoted LSPR, LSPL1, and LSPL2, respectively, where the first letter again refers to the left (L) or right (R) border, SP to sample point, and the last letter to the left (L) or right (R) side of the border, respectively. Assuming the last detected border point is g(nT) on line n, the video signal is sampled on the same line at a distance LSWR from g(nT) and on the next line (n+1) at distances LSWL and LSWL/2 before the left-hand side of the expectation window LEPL, respectively (SW refers to sample window). The video samples at the
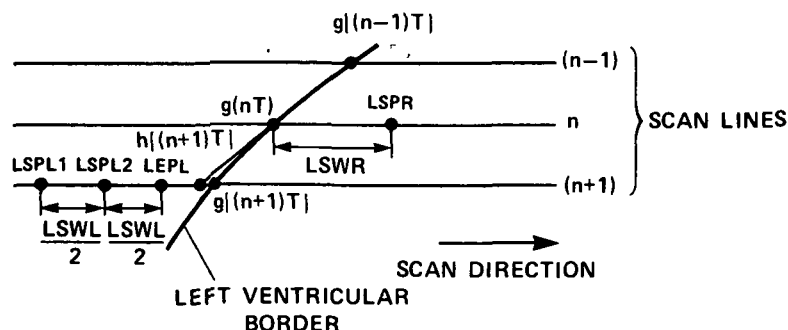

Figure 49.- Three sample points (LSPR, LSPL1, and LSPL2) are defined to determine the reference level for the next line (n + 1) for the left border.

124

three defined sample points are used to calculate the reference level for line $(n+1)$. After $g[(n+1)T]$ has been detected, a sample point LSPR at a distance LSWR from $g[(n+1)T]$ is again defined for calculating the reference level for line $(n+2)$, etc.

Sample point LSPR is determined from the detected border point $g(nT)$ on line n as

$$LSPR = g(nT) + LSWR \qquad (71)$$

and sample point LSPL1 is calculated from LEPL as

$$LSPL1 = LEPL - LSWL \qquad (72)$$

In the implemented system, sample point LSPL2 is derived from LSPL1 as

$$LSPL2 = LSPL1 + \frac{LSWL}{2} \qquad (73)$$

The window width LSWL should always be chosen so that there is enough time left for the track-and-hold amplifier to acquire an accurate sample of the video signal at LSPL2 and for the analog circuitry (chapter 10) to determine the new reference level from the video samples, before the comparator is enabled at LEPL. From the specifications for the track-and-hold amplifier and from measurements, it was determined that the minimum allowable width for LSWL is 400 nsec. This restriction does not apply for LSWR because the sampled level at LSPR is not used until the samples at LSPL1 and LSPL2 are available.

The width of the defined expectation and sample windows are separately and manually adjustable in the implemented system using 12-position rotary switches. The selected position of a switch is converted into a 4-bit number with the circuitry in figure 50.

The selected switch position is not directly converted into binary format, but initially into the reflected binary or Gray code. The Gray
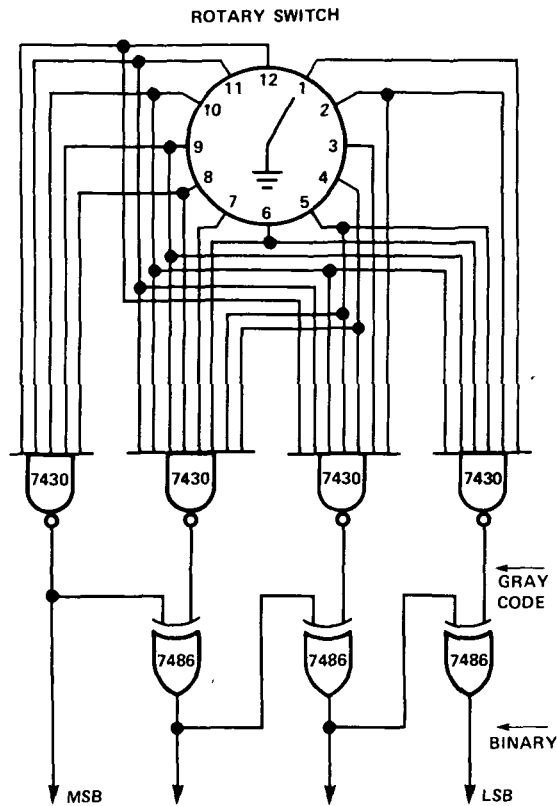
125

ROTARY SWITCH

Figure 50.- Conversion of a selected rotary switch position into 4-bit binary format.

code is a unit distance code, which means that only one bit at a time can change when incrementing or decrementing the decimal equivalent with one. This code is extremely useful for converting shaft positions into binary format. In straight binary, it is possible to enter incorrect or invalid states during switching. For example, going from binary $0111(7_{10})$ to $1000(8_{10})$ results in $1111(15_{10})$ during the time that the switch contact overlaps both positions. It is assumed here that make-before-break-type switches are used; otherwise, the state 0000 would occur during switching.

Implementing the circuitry in figure 50 for each parameter, the selected window widths LEWL, LEWR, LSWL, and LSWR are available in binary format.

So far, the derived formulas all applied to the left border. The formulas for the right border can be derived similarly, except that an extra term must be included to generate the designated aortic valve plane. The aortic valve width AV is defined as the horizontal distance between two consecutive aortic valve points referred to the same line. The width AV is available in an 8-bit format; AV = 0000 0000 results in a generated valve plane perpendicular to the scan lines and AV = 1111 1111 results in a position change of aortic valve points from line to line of 255×20 nsec = 5.1 μsec. However, assuming that such a big change from line to line will not occur under practical circumstances, the AV has been implemented so that AV = 1001 1110 is the greatest value which corresponds to a maximum change of 3.16 μsec from line to line.

The aortic valve which AV is manually adjustable with the third potentiometer in the joystick. Rotating the shaft of the joystick changes the dc voltage level at the input of an 8-bit A/D converter; the circuitry is given in figure 51. The analog voltage is sampled each 16.67 msec during the vertical synchronization pulse.

The positions of the expectation and sample points during the aortic valve simulation are given in figure 52. So long as this simulated valve plane is generated, the field extrapolation principle is inhibited and only the zeroth-order line extrapolation principle is applied, necessary for the generation of a straight line.

The beginning point REPL of the expectation window on line (n + 1) is determined by
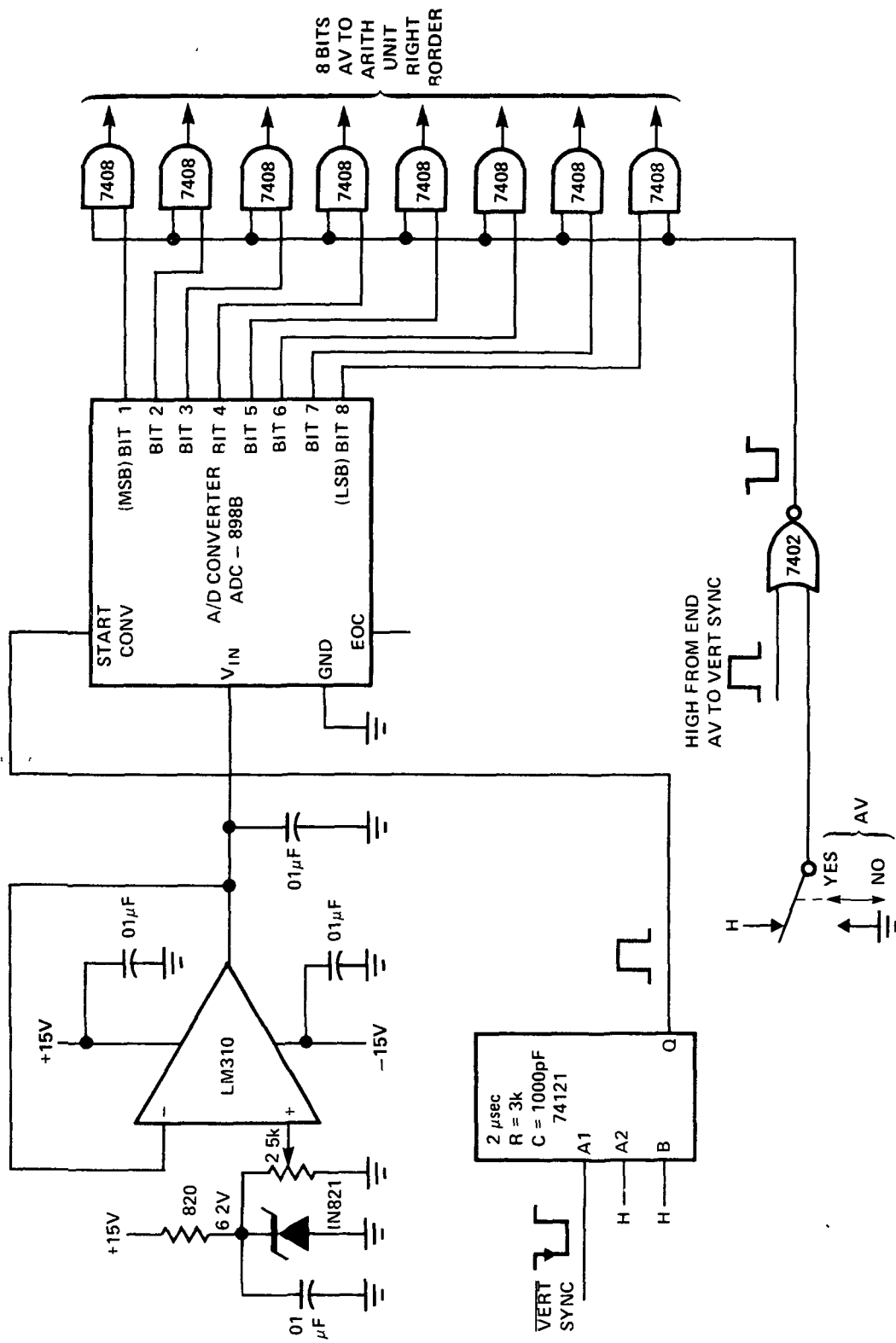
$$REPL = g(nT) + AV - REWL \qquad (74)$$

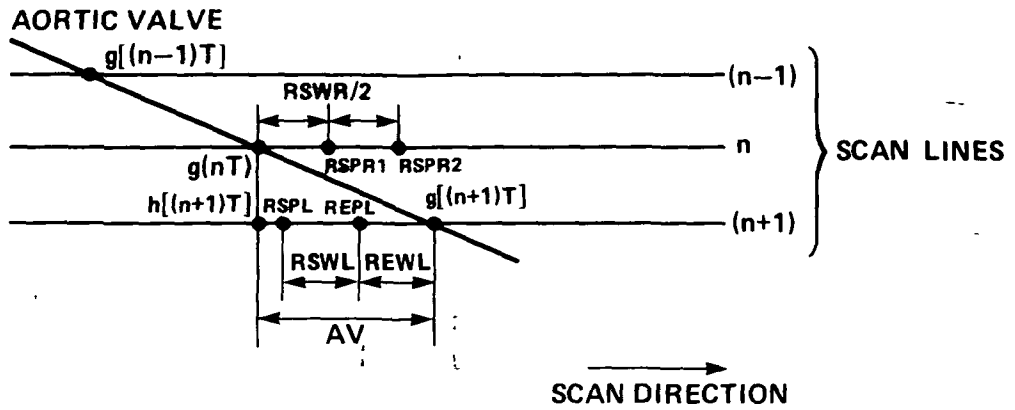Figure 51.- Aortic valve width as determined in an 8-bit format.

Figure 52.- Definition of expectation and sample points during the generation of the simulated aortic valve plane.

The end point of the expectation window during the aortic valve plane generation is defined as

$$REPR = REPL + REWL \qquad (75)$$

Because the left ventricular cavity is now the left of the right border, the three sample points RSPL, RSPR1, and RSPR2 necessary for calculating the reference level on line $(n+1)$ are defined as shown in figure 52. Sample point RSPL is defined as

$$RSPL = g(nT) + AV - REWL - RSWL = REPL - RSWL \qquad (76)$$

Sample points RSPR1 and RSPR2 on line n are derived from $g(nT)$ as

$$RSPR1 = g(nT) + RSWR \qquad (77)$$

and

$$RSPR2 = g(nT) + \frac{RSWR}{2} \qquad (78)$$

In the present implementation of the system, the dynamic reference level is not applied to the right-border comparator during the aortic valve plane generation, but instead a dc preset reference level (chapter 10). However, it is explained in chapter 12 that the end of the simulated aortic valve plane can be determined from these video samples.

129

During the aortic valve simulation, the analog comparator for the right border is enabled from REPL until the aortic valve point at g(nT) + AV. If the comparator does not encounter a point with the same brightness level as the preset reference level during this period, then the aortic valve point is defined as the contour point. However, if a point occurs with the correct reference level within the defined expectation window, then this point is defined as the first right-border point and the aortic valve simulation is stopped. Because of the sudden direction changes, the center of the expectation window for the second right-border point is always calculated using the zeroth-order line extrapolation principle. The field extrapolation principle is also again applicable for the second right-border point. From this point, each of the four possible combinations of line and field extrapolation principles can be applied by the appropriate selection of the MODE switches (fig. 53).

The general formulas for the expectation and sample points after the aortic valve simulation period can be derived from formulas (74), (75), and (76). For the general case with the center of the expectation window denoted $h_m[(n+1)T]$, equation (74) becomes

$$REPL = h_m[(n+1)T] + AV - REWL \qquad (79)$$

The end point REPR is defined as

$$REPR = REPL + REWL + REWR \qquad (80)$$

Equation (76) can now be written as

$$RSPL = h_m[(n+1)T] + AV - REWL - RSWL \qquad (81)$$

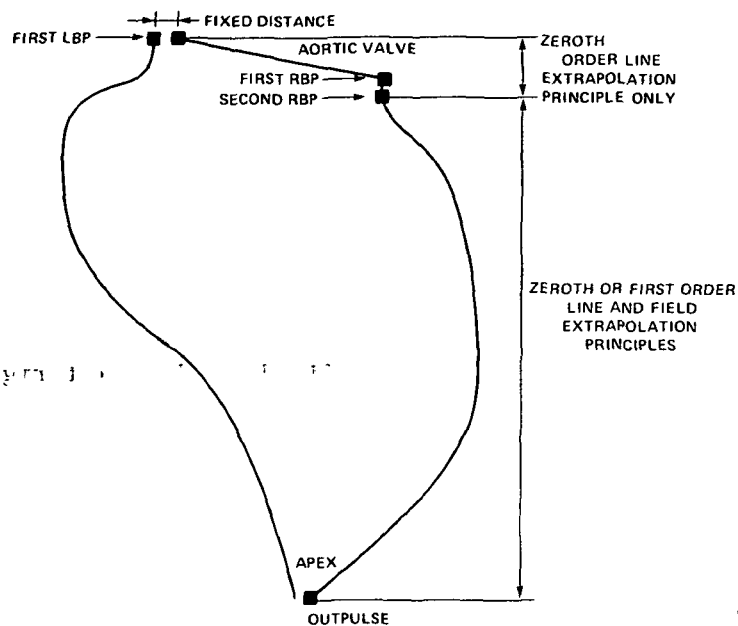The formulas for RSPR1 and RSPR2 remain, of course, unchanged.

130

Figure 53.- Applicable line and field extrapolation principles for the right border.

In order that the timing for the right-border arithmetic unit remains unchanged, the term AV is always included but is made equal to zero outside the aortic valve simulation period.

In the remainder of this chapter, the implementation of the circuitry to determine the expectation and sample points for the right border is described.

Arithmetic Unit

The arithmetic unit for the right border was designed as shown schematically in figure 54. Using tri-state buffers, the addends are all applied to the A-bus, and the augends or subtrahends to the B-bus.
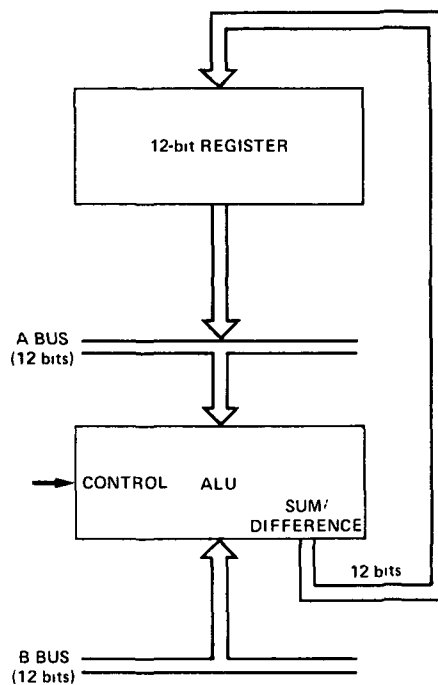
131

Figure 54.- Simplified block diagram of the implemented
arithmetic unit.

The result of an arithmetic addition or subtraction is stored in a

12-bit register and can be applied again to the A-bus for the next

arithmetic operation.

The implementation of the arithmetic unit for the right border is

shown in figure 55. This unit calculates the positions of the points

REPL and RSPL in a 12-bit format. An identical unit has been built for

the left border; this unit is somewhat simpler because it need not carry

out the calculation for the simulated aortic valve.

After the right-border point g(nT) has been detected, its 12-bit

coordinate is available at the inputs of DFZ1 through DFZ3 and BUZ3,

BUZ4, and BUZ7f. Consider the case when the zeroth-order line extrapo-

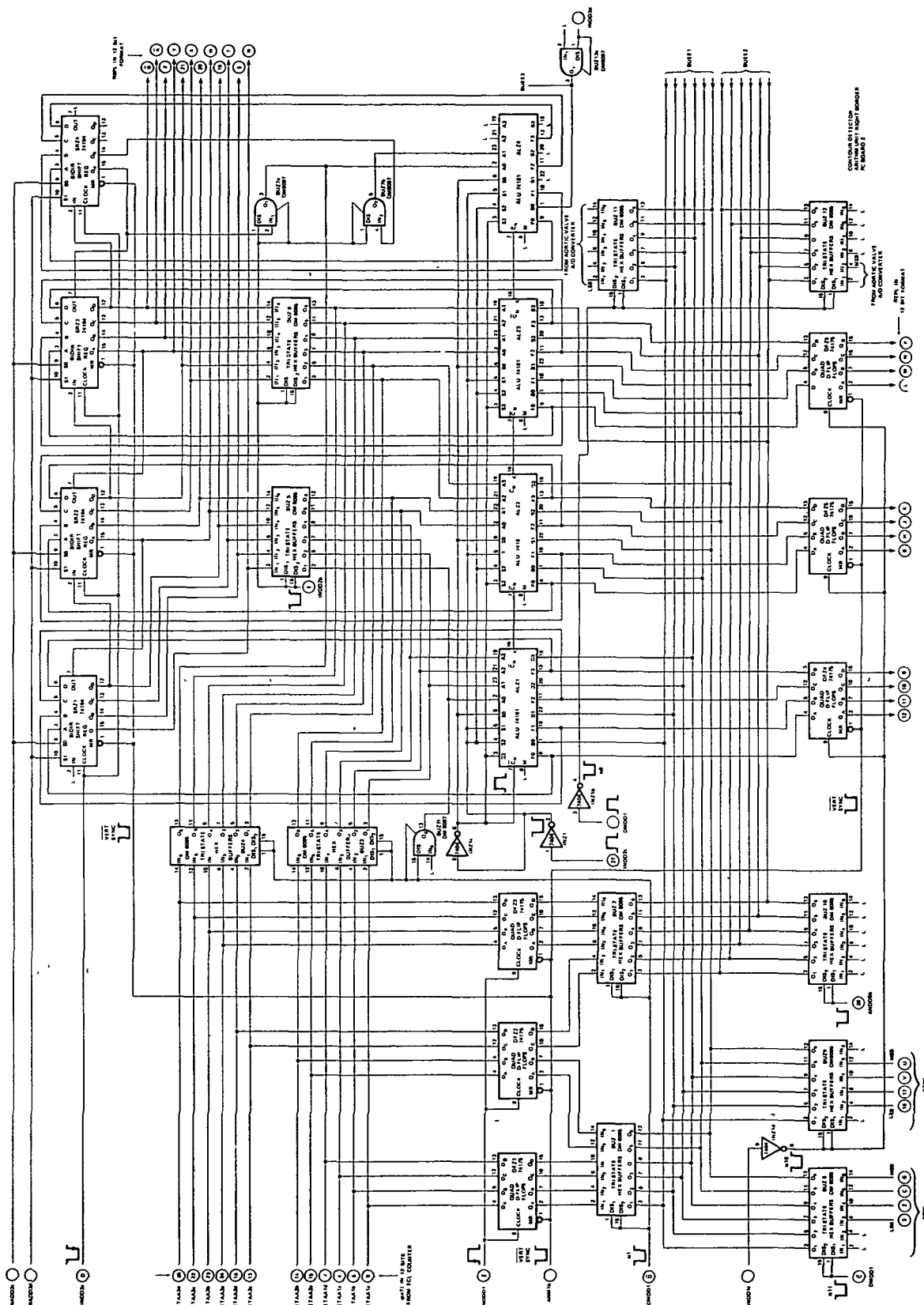lation principle is selected. This occurs during the aortic valve

132

Figure 55.- Arithmetic unit for the right border.

133

simulation period and after that if manually chosen. At the start of time state ts1 (fig. 47, chapter 7), the 12 bits are stored in the D flip-flop registers DFZ1, DFZ2, and DFZ3. With the tri-state buffers BUZ1, BUZ2, BUZ3, BUZ4, and BUZ7f enabled during ts1, $2g(nT)$ is applied to the A-inputs of the ALU, consisting of ALZ1 through ALZ4, and $g(nT)$ to the B-inputs. The ALU control being set for subtraction, the resulting $2g(nT) - g(nT)$ is stored at the rising edge of ts1 into the shift registers SRZ1 through SRZ4. These four shift registers are referred to as ACR (accumulator right border).

For the first-order line extrapolation principle, $2g(nT)$ is again applied to the A-bus during ts1 through the appropriate tri-state buffers. However, at this moment, $g(nT)$ is not stored in flip-flop registers DFZ1, DFZ2, and DFZ3. During ts1, the information in these registers is then still $g[(n - 1)T]$ from the previous line and this coordinate is applied to the B-bus. At the end of ts1, the resulting $2g(nT) - g[(n - 1)T]$ is stored in the accumulator.

The contents of the accumulator can be applied to the A-bus through tri-state buffers BUZ5, BUZ6, BUZ7a, and BUZ7b at the appropriate time states as defined in figure 47 for additional additions and subtractions.

The four bits representing REWL are connected to the inputs of the tri-state buffer BUZ9. By shifting the four bits of REWL one position to the right at the inputs of BUZ9, the expectation window can be adjusted in steps of 40 nsec. Similarly, the four bits representing RSWL are connected to the inputs of tri-state buffer BUZ8. These four bits are now shifted up two positions so that the position of RSWL is adjustable in steps of 80 nsec.

After the position of REPL has been calculated in the arithmetic unit, this information is stored in flip-flop registers DFZ4 through DFZ6. At the end of the processing cycle, the position of RSPL is stored in the accumulator.

It has been explained that one extra addition must be carried out for the right border because of the simulated aortic valve. The 8 bits representing the valve width are applied to the B-bus through tri-state buffers BUZ11 and BUZ12.

The control circuitry has been designed so that the system always starts in the zeroth-order line extrapolation mode at the starting line and at least two aortic valve points are generated, thereby eliminating any initial condition problems. Without this preventive measure, actual right-border points (as distinguished from aortic valve points) could be detected near the left-border points. This would result in erroneous border points and a halt in the detection process caused by the outpulse mechanism.

So far, it has been explained how the coordinates of the expectation point REPL and the sample point RSPL on line $(n+1)$ are calculated from the available coordinates on previous lines and in previous fields. The position determination on a scan line of these points, as well as the points REPR, RSPR1, and RSPR2, is described in the next section. This has been implemented with digital comparators and 50-MHz counters. At the same time, it will be shown how the 12-bit coordinate of a detected border point is determined.

Position Determination of Expectation and Sample Points

When this system was implemented, no synchronous Schottky TTL, 50-MHz counters were available on the market. Except for this, the total delay resulting from the digital comparison and from required control logic implemented with Schottky TTL would be more than one clock period. To compensate for the extra time delays, additional logic would be required. This compensation would especially be important as the window widths decrease, which occurs, for example, when the expectation window width is adjusted dynamically according to local brightness levels (chapter 10).

For these reasons, the ECL 10k logic family was chosen to determine the positions of the expectation and sample points. This family proved very successful for this particular application. The wired OR capability could be used advantageously in the digital comparator and, because of the "constant current" switching behavior, there is very low noise generation compared with the large "spikes" associated with Schottky TTL. The ECL 10k family involves somewhat more work because the wire connections must be terminated with the characteristic impedance of the line. At these high speeds, the wires behave like transmission lines requiring correct resistive terminations. However, a careful design and implementation resulted in a very reliable system.

The implementation of the circuitry to determine the positions of points REPL and RSPL and the 12-bit coordinate of the border point on each scan line is given in figure 56.

Basically, this circuitry works as follows. The data stored in the flip-flop registers and the accumulator of the right-border arithmetic

Figure 56.- Implemented circuitry for determining g(nT), REPL, and RSPL for the right border.

137

unit, representing REPL and RSPL, respectively, are connected to the inputs of TTL-to-ECL translators TEAA1-TEAA3 and TEAA4-TEAA6, respectively. From the beginning of a scan line until the position of RSPL has been determined, the 12 bits representing RSPL are applied to one side of a 12-bit comparator through the translators. The 12-bit comparator is implemented with Exclusive OR gates XOAA1-XOAA4 and NOR gate ORAA2b. The other side of the comparator is connected to the outputs of the 50-MHz counters COAA1-COAA3. These counters start counting the clock pulses at the rising edge of the horizontal synchronization pulse for the scan lines traversing the left ventricle. As soon as the contents of the counter equal the 12-bit data word for RSPL, the output of the digital comparator becomes high. This signal is connected to the D inputs of flip-flops DFAA1b and DFAA1a. Inverted 50-MHz clock pulses, slightly delayed with respect to the clock pulses at the clock inputs of the counters, function as sample pulses for flip-flops DFAA1a and DFAA1b. The clock input of DFAA1a is disabled as long as flip-flop DFAA1b is in the initial condition. Flip-flop DFAA1b is then set at the rising edge of the sample pulse, indicating the position of RSPL. The other set of translators is now enabled, applying the 12 bits for REPL to the digital comparator, whose output becomes low again. The counters continue to count and the output of the comparator becomes high again as the state of the counters equals the 12-bit data word for REPL. Flip-flop DFAA1a is then set, indicating the position of REPL. With the Q-output of DFAA1a high, the analog comparator is enabled and the sample pulses are disabled.

138

As the video signal crosses the reference level, the comparator changes state and the output of LRAA1a becomes high (fig. 57). This resets the flip-flops and the counter stops counting clock pulses. The state of the counter thus represents the border coordinate on this particular line and this information is applied through ECL to TTL translators ETAA1-ETAA3 to the arithmetic unit (fig. 55).

The analog comparator is also enabled during the horizontal synchronization pulses. It then returns to the initial condition with the true output high. Since no REPL and RSPL values have been calculated for the starting line SL, the analog comparator is enabled on this line by setting flip-flop DFAA1a with the starting point (SP) signal. So far we have determined the positions of RSPL and REPL and the detected border coordinate in 12 bits. The positions of the points REPR, RSPR1, and RSPR2 are found with the circuitry in figure 57.

Basically, the positions of these three points are determined in a way as described for figure 56. A digital comparator is used which compares the state of a 50-MHz counter with a data word, giving the position of this particular point with respect to a predetermined point. The output of the comparator becomes high when both binary words applied to the comparator are identical. The comparator output signal is sampled with inverted 50-MHz clock pulses, slightly delayed with respect to the counter clock pulses. The low-to-high transition of the Q-output of the sample flip-flop then indicates the position of this particular point.

Counters COAB3 and COAB4 have been implemented to determine the position of the right-hand side REPR of the expectation window. The
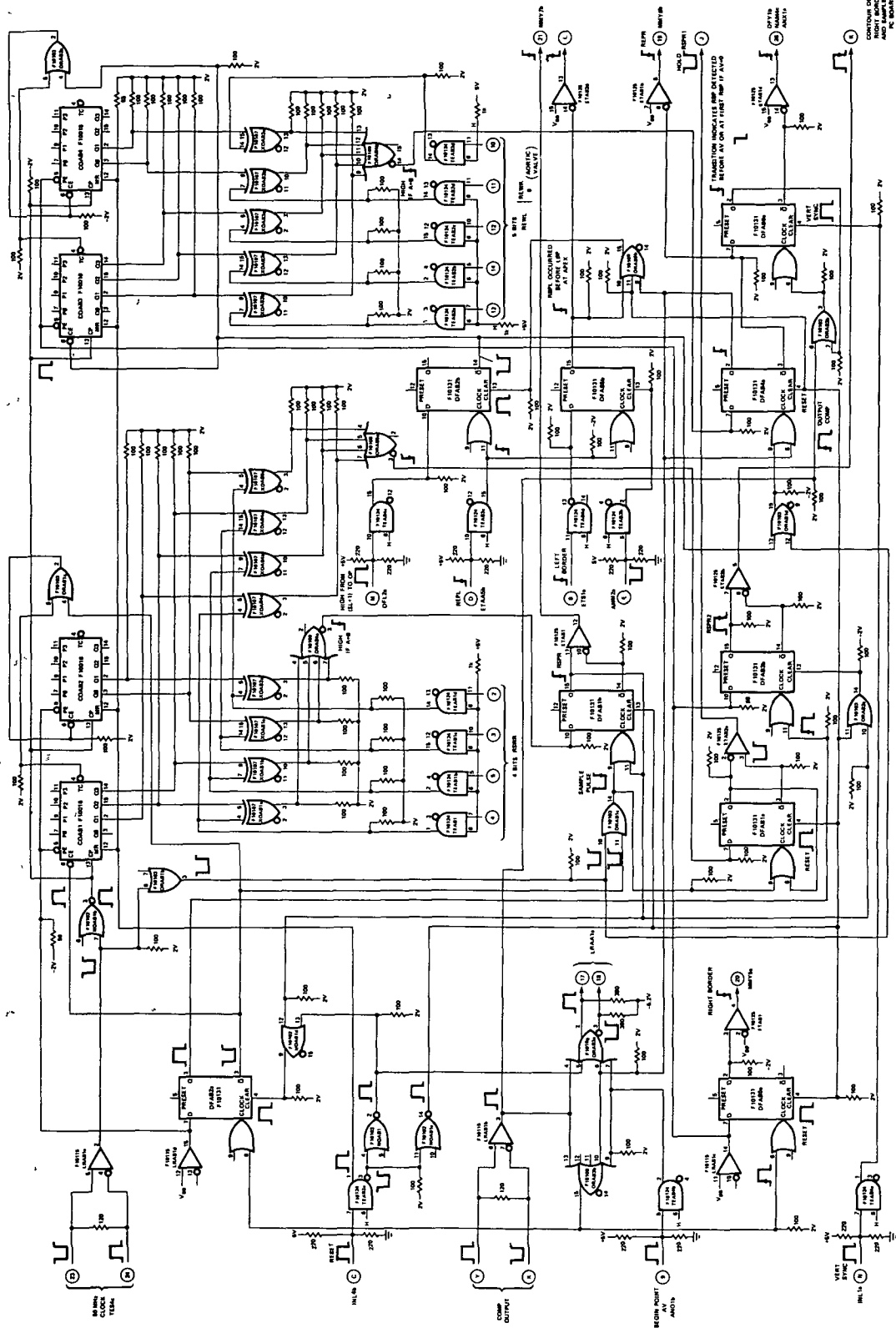
139

Figure 57.- Implemented circuitry used to determine the positions of points REPR, RSPR1, and RSPR2 for the right border.

140

counters are enabled immediately after REPL has been detected. A 5-bit data word, representing REWL + REWR, is applied to the other side of the comparator. The term REWR is made equal to zero during the aortic valve simulation period (compare eqs. (75) and (80)).

Flip-flop DFAB6a determines when the first right-border point after the aortic valve simulation period is detected. The output signal from the analog comparator for the right border functions as the clock signal for this flip-flop. If the analog comparator changes state before REPR has been detected, that is, before DFAB4a is set, then flip-flop DFAB6a is set, indicating the end of the simulated aortic valve plane.

The position of a right-border point is indicated by the low-to-high transition of the Q output of flip-flop DFAB5a, which is cleared during the horizontal synchronization pulse. The clock signal for this flip-flop is the output signal from ORAB3b, which is the OR function of several possible border-indicating signals.

The border point is defined at the first low-to-high transition per video line of one of the input signals of ORAB3b. This occurs when: (1) the comparator changes state as the video signal crosses the reference level, or (2) when the flip-flop DFAB4a is set, indicating the position of REPR (this results in a forced border pulse at the end of the expectation window), or (3) when the beginning point of the aortic valve is generated.

The same OR function plus the reset pulse during the horizontal synchronization pulse is generated with OR gate ORAB3a; this signal is applied to the circuitry in figure 56 as a reset for the flip-flops, thereby disabling the analog comparator and the clock pulses.

Before describing the circuitry used to determine the positions of sample points RSPR1 and RSPR2, the required control signals for the sample-and-hold amplifiers are discussed. The sampled values at RSPR1 and RSPR2 must be stored until the next border point has been detected. This means that the time from g(nT) until RSPR1 and RSPR2, respectively, is available only as settling time for the amplifier in the TRACK mode. According to the specifications, we should allow at least a 200-nsec acquisition time. Therefore, we have assumed a lowest limit for RSWR of 240 nsec (rotary switch set at 3), resulting in a minimum time period of 120 nsec between g(nT) and RSPR1. Another sample/hold amplifier is then required for RSPR1 to sample the video signal accurately at this point (fig. 58). The first S/H amplifier R11 is in the TRACK mode from the horizontal sync pulse until RSPR1 and holds the video sample from this point until the end of the scan line. The second S/H amplifier R12 samples the output voltage of R11 and holds this value until the
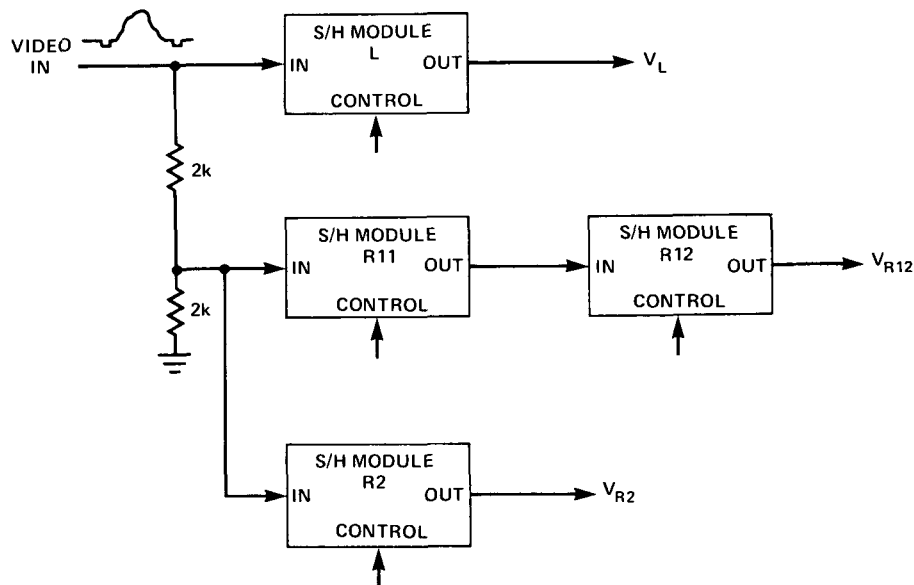

Figure 58.- Video samples for calculating the reference level of the right border are obtained with four sample/hold amplifiers.

142

detected border point g[(n + 1)T] on the next line. The required

control signals for the sample/hold amplifiers for the right border are
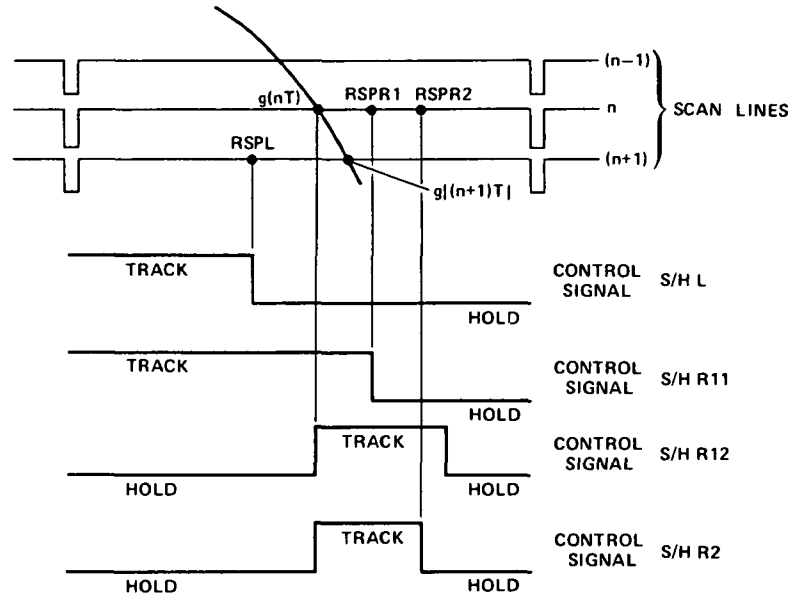
given in figure 59.

Figure 59.- Required control signals for the sample/hold amplifiers
for the right border.

These necessary control signals for S/H amplifiers R11 and R2 are

implemented with the circuitry in figure 57. Counters COAB1 and COAB2

are enabled immediately after a right-border point has been detected and

are used to determine the positions of RSPR1 and RSPR2. The digital

comparator for RSPR1 consists of XOAB4a-XOAB4c, XOAB5a, and ORAB5a and

for RSPR2, XOAB1a-XOAB1c, XOAB2a, and ORAB4a. Both comparators have the

four bits representing RSWR in common. By connecting the other inputs

of the comparators to the appropriate outputs of the counters, each unit

of RSWR corresponds to a time period of 80 nsec. In exactly the same

way as described for the expectation points, the comparator outputs are

sampled with 50-MHz sample pulses and the positions of RSPR1 and RSPR2

are determined. The control signals for S/H amplifiers R11 and R2 are generated with flip-flops DFAB1a and DFAB3b, respectively. The control signal for amplifier R12 has been realized using monostable multivibrators (not shown in fig. 57).

One part of figure 57 has not yet been discussed – flip-flop DFAB5b and associated gates connected to it. This flip-flop is used to detect whether a REPL occurs before a left-border point has been detected. If this is true, then the outpulse is generated. Border points are no longer allowed on this line because the left and right margins could cross each other at this point. By clearing the flip-flop from the vertical synchronization pulse until the end of the aortic valve, care has been taken that no REPL is detected before a left-border point at the beginning of the simulated aortic valve plane, where the distance between both margins also can be small. Other reasons for generating an outpulse are described in the following section.

Outpulse Mechanism

The contour detection is halted during a video field as soon as the outpulse occurs. The implementation of this outpulse mechanism is shown in figure 60. An outpulse is generated for the following reasons:

(1) If no left-border point (LBP) has been detected on a video line during the period from the starting point SP until the outpulse OP. If this is true, then flip-flop DFM2a is set.

(2) If no right-border point (RBP) has been detected on a video line during the period from the starting point SP until the outpulse or if the right-border point occurs before the left-border point on a scan line. For this condition, flip-flop DFM1a is set by the last
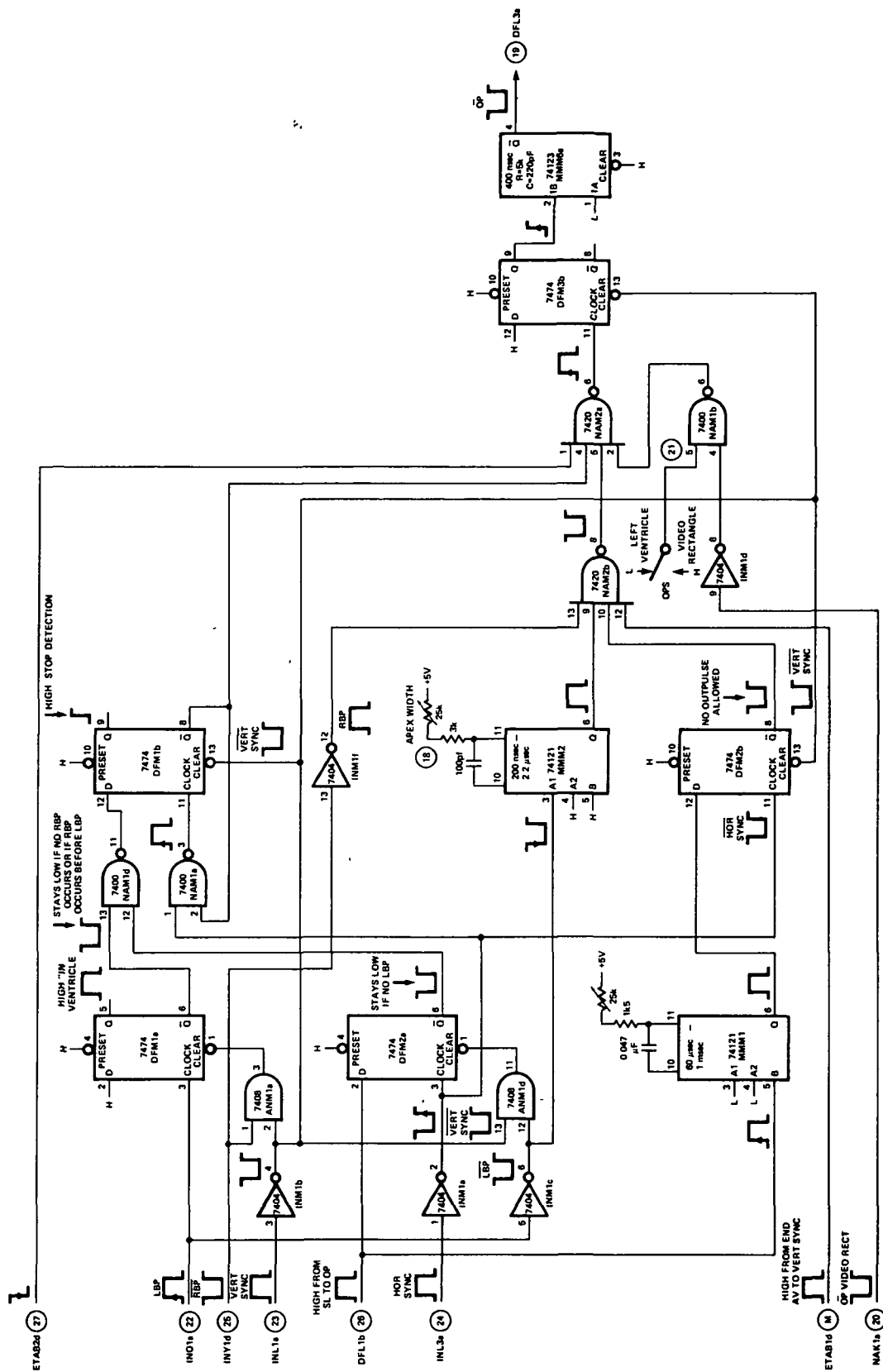
144

Figure 60.– Implementation of outpulse mechanism.

145

detected left-border point. The status of this flip-flop and flip-flop DFM2a is sampled at the end of each scan line and flip-flop DFM1b is set if one of the conditions mentioned above is satisfied.

(3) If the distance between LBP and RBP at the apex is less than a preset distance, manually adjustable from 200 nsec to 2.2 μsec with mono-stable multivibrator MMM2. A pulse occurs at the output of NAND-gate NAM2b if this condition is satisfied. The pulse is inhibited during the aortic valve generation period, during which both borders can come within this distance of each other.

A contour detector mode is selectable in which no simulated aortic valve is generated. The analog comparator for the right border is then enabled by the first left-border point and the first right-border point is detected, where the video signal crosses a preset reference level. This mode can be used advantageously with the video rectangle for test purposes. The pulse at the output of NAM2b is then inhibited over an adjustable number of scan lines, starting at the scan line with the starting point. This has been implemented with monostable multivibrator MMM1 and flip-flop DFM2b.

(4) If the left-hand side of the expectation window REPL for the right border at the apex occurs before a left-border point has been detected (as explained in fig. 57). The appropriate control signal is applied to NAND-gate NAM2a (input point 1).

(5) If the video rectangle generator (appendix A) is used, then an outpulse is generated at the end of the last line of the rectangle. This outpulse can be selected with switch OPS. Using this outpulse, the border detection on an actual left ventricular image can be halted

wherever desired by changing the parameters of the rectangle. This is used to advantage during certain design and checking procedures.

Flip-flop DFM3b is set at the first occurring low-to-high transition of the output signal from NAM2a during a video field. The change in state of DFM3b triggers monostable multivibrator MMM6a, resulting in a 400-nsec wide outpulse OP, which halts the border detection algorithm.

Page intentionally left blank

In chapter 8, three sample points were defined for the determination of the reference level for line $(n+1)$ for the left border (again illustrated in fig. 61). With the detected border point on line n
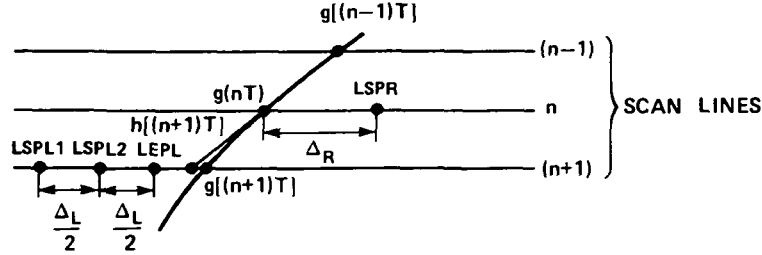

Figure 61.- Three sample points LSPR, LSPL1, and LSPL2 are defined to determine the reference level for the next line $(n+1)$ for the left border.

denoted $g(nT)$, the video signal is sampled inside the ventricle at a distance Δ_R from $g(nT)$ on the same line, and in the background area at distances Δ_L and $\Delta_L/2$, respectively, before the left-hand side of the expectation window on line $(n+1)$. The reference level for the border point on line $(n+1)$ is then calculated as

$$V_{ref}(n+1) = \frac{\alpha}{2}\left(VR + \frac{VL1}{2} + \frac{VL2}{2}\right) + V_c \tag{82}$$

where α is a proportionality factor, V_c is a constant voltage level, VR is the video sample at LSPR, and VL1 and VL2 are the video samples at LSPL1 and LSPL2, respectively. By taking the average value of VL1 and VL2, either side of the contour has the same weight. The function of the two sample points at the background area is explained in more detail in chapter 10.

By use of a waveform monitor, the video signal at the left

ventricular border was studied. This study showed that the border area

can be approximated with linear functions (fig. 62). To gain more
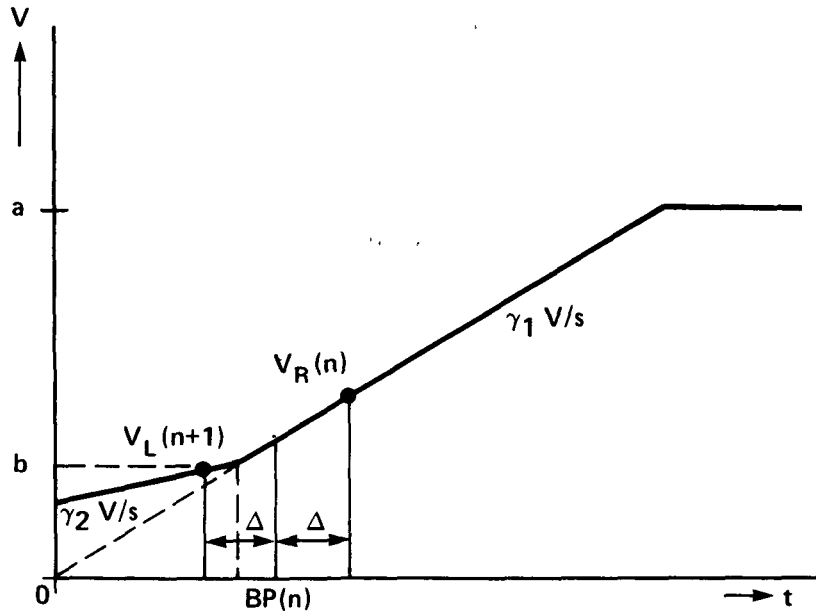

Figure 62.- Linearized border model for left border.

insight into the detection process and to find an optimum solution so

that, under all reasonable conditions, an acceptable border point will be

detected, a line periodic video signal is assumed. This signal changes

linearly with a slope of γ_2 V/sec over the background area and with a

slope of γ_1 V/sec beyond the actual border, with $0 \leq \gamma_2 < \gamma_1$. It is

assumed that the straight line with slope γ_1 V/sec goes through $(0,0)$.

To simplify the calculations, one left sample point is assumed and both

sample points have the same distance Δ to the border point. The

sampled voltage level on line n at $t = BP(n) + \Delta$ is denoted $V_R(n)$ and

the sampled voltage level on line $(n+1)$ at $t = BP(n) + T - \Delta$ is denoted

$V_L(n+1)$.

150

With this linearized border model, the effects on deviations from the equilibrium situation are determined. This analysis will provide us with the requirements the different parameters must satisfy for an acceptable and stable contour under varying conditions.

Determination of the Equilibrium Situation

A border point is said to be acceptable if it occurs on the ventricular slope within a distance Δ from the knee in the border model. This results in one sample point on the ventricular slope and the other in the background area. The function for the left ventricular slope can be written as

$$V_1 = \gamma_1 t \tag{83}$$

and the function for the background slope as

$$V_2 = \gamma_2 t + b\left(1 - \frac{\gamma_2}{\gamma_1}\right) \tag{84}$$

where $\gamma_1 > \gamma_2$. Because γ_2 will generally be relatively small, it is always assumed that $\gamma_1 > \gamma_2$. The position of the border point BP_{equil} in the equilibrium situation can be derived by substituting the formulas for the sample levels $V_R(n)$ and $V_L(n+1)$ in the equation for the reference level

$$V_{ref}(n+1) = \frac{\alpha}{2}\left[V_R(n) + V_L(n+1)\right] + V_c \tag{85}$$

with $BP(n)$ as the unknown variable, and solving for $BP(n)$ with $V_{ref}(n+1)$ equal to the reference level for $BP(n)$. The sample levels are

$$V_R(n) = \gamma_1[BP(n) + \Delta] \tag{86}$$

$$V_L(n+1) = \gamma_2[BP(n) - \Delta] + b\left(1 - \frac{\gamma_2}{\gamma_1}\right) \tag{87}$$

151

if it is assumed that

$$\frac{b}{\gamma_1} \le BP(n) \le \frac{b}{\gamma_1} + \Delta \tag{88}$$

Substituting equations (86) and (87) into (85) and solving for $BP(n)$
with $V_{ref}(n+1) = \gamma_1 \cdot BP(n)$ yields

$$BP_{equil} = \frac{\frac{\alpha}{2} (\Delta\gamma_1 + b)\left(1 - \frac{\gamma_2}{\gamma_1}\right) + V_c}{\gamma_1 \left[1 - \frac{\alpha}{2} \cdot \left(1 + \frac{\gamma_2}{\gamma_1}\right)\right]} \tag{89}$$

and the final reference level

$$V_{equil} = \frac{\frac{\alpha}{2} (\Delta\gamma_1 + b)\left(1 - \frac{\gamma_2}{\gamma_1}\right) + V_c}{1 - \frac{\alpha}{2} \left(1 + \frac{\gamma_2}{\gamma_1}\right)} \tag{90}$$

For what range of α values is the denominator positive? The equation

$$1 - \frac{\alpha}{2} \left(1 + \frac{\gamma_2}{\gamma_1}\right) > 0 \tag{91}$$

gives

$$0 < \alpha < \frac{2}{1 + \frac{\gamma_2}{\gamma_1}} \tag{92}$$

For $\gamma_2 < \gamma_1$, the denominator will always be positive for $\alpha < 1$. For
the equilibrium situation, we require that

$$b < V_{equil} < b + \Delta\gamma_1 \tag{93}$$

Substituting equation (90) into (93) and solving for α yields

$$\frac{b - V_c}{\frac{\Delta}{2} (\gamma_1 - \gamma_2) + b} < \alpha < 1 - \frac{V_c}{b + \Delta\gamma_1} \tag{94}$$

Because α is always greater than zero,

$$V_c < b \tag{95}$$

152

The functions

$$f_1(V_c) = 1 - \frac{V_c}{b + \Delta\gamma_1} \tag{96}$$

and

$$f_2(V_c) = \frac{b - V_c}{\frac{\Delta}{2}(\gamma_1 - \gamma_2) + b} \tag{97}$$

and the allowed ranges for α and V_c are given in figure 63. The function $\alpha = 1 - (V_c/b)$, is independent of the possible changes in slopes
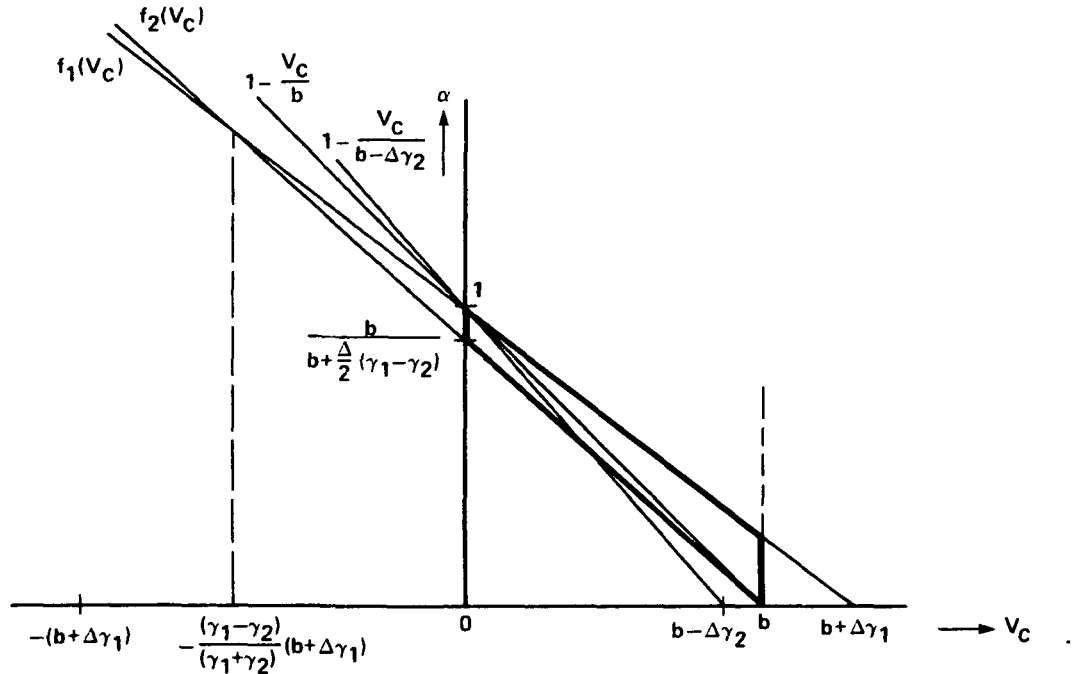

Figure 63.- Allowed region of α and V_c values for detecting a stable contour point using the border model in figure 62.

γ_1 and γ_2 and connects both extreme biasing points. A bias point on or near this function seems to be a reasonable choice. Changing the bias point on this function from $\alpha = 0$, $V_c = b$ to $\alpha = 1$, $V_c = 0$ means that one goes from a constant reference level at $\alpha = 0$, $V_c = b$ to the point where the reference level is determined as the average of the sampled levels. As a result, the deviation of the equilibrium reference level

from the knee voltage of b volts increases with increasing α. (The
question of the bias line is discussed later in more detail.) The tran-
sient responses from initial conditions unequal to the equilibrium
position are discussed in the following sections.

Transient Responses Toward the Equilibrium Situation

Transient response for an initial condition within the acceptable
range of border positions- Consider the case for an initial border point
position, denoted by BP(0), satisfying

$$\frac{b}{\gamma_1} < BP(0) < \frac{b}{\gamma_1} + \Delta \qquad (98)$$

and a reference level $V_{ref}(1) \neq V_{equil}$, where V_{equil} is given by
equation (90). What is the transient response toward the equilibrium
situation?

Because of the line periodicity, this can be derived from the
following equation:

$$BP(n+1) = \frac{1}{\gamma_1} \cdot V_{ref}(n+1) = \frac{1}{\gamma_1} \left\{ \frac{\alpha}{2} [V_R(n) + V_L(n+1)] + V_c \right\} \qquad (99)$$

which applies for an initial condition above as well as below the
equilibrium position within the indicated range. Substituting the
sampled levels on lines n and (n+1), respectively, gives

$$BP(n+1) = \frac{1}{\gamma_1} \left(\frac{\alpha}{2} \left\{ \gamma_1 [BP(n) + \Delta] + \gamma_2 [BP(n) - \Delta] + b\left(1 - \frac{\gamma_2}{\gamma_1}\right) \right\} + V_c \right) \qquad (100)$$

Applying the z transform with $z[\dot{BP}(n)] \triangleq BP(z)$ and solving for BP(z)
yields

$$BP(z) = \frac{zBP(0)}{z - \frac{\alpha}{2}\left(1 + \frac{\gamma_2}{\gamma_1}\right)} + \frac{\frac{\alpha}{2}\left(\Delta + \frac{b}{\gamma_1}\right)\left(1 - \frac{\gamma_2}{\gamma_1}\right) + \frac{V_c}{\gamma_1}}{z - \frac{\alpha}{2}\left(1 + \frac{\gamma_2}{\gamma_1}\right)} \cdot \frac{z}{z - 1} \qquad (101)$$

154

Transforming back to the time domain

$$BP(n) = BP(0) \cdot e^{n \ln \frac{\alpha}{2}\left(1+\frac{\gamma_2}{\gamma_1}\right)} + \frac{\frac{\alpha}{2}(\Delta\gamma_1 + b)\left(1-\frac{\gamma_2}{\gamma_1}\right) + V_c}{\gamma_1\left[1-\frac{\alpha}{2}\left(1+\frac{\gamma_2}{\gamma_1}\right)\right]} \left[1 - e^{n \ln \frac{\alpha}{2}\left(1+\frac{\gamma_2}{\gamma_1}\right)}\right]$$

(102)

Check – initial condition at $n = 0$: $BP(n = 0) = BP(0)$

final value at $n = \infty$:

$$BP(n = \infty) = \frac{\frac{\alpha}{2}(\Delta\gamma_1 + b)\left(1-\frac{\gamma_2}{\gamma_1}\right) + V_c}{\gamma_1\left[1-\frac{\alpha}{2}\left(1+\frac{\gamma_2}{\gamma_1}\right)\right]}$$

Again this is the equilibrium position as given by equation (89).

The transient response is an exponential function with time constant

$$\tau = \frac{-1}{\ln \frac{\alpha}{2}\left(1+\frac{\gamma_2}{\gamma_1}\right)}$$

(103)

Under the assumption that $\gamma_2 < \gamma_1$ and $0 \leq \alpha < 1$, it follows that

$$0 \leq \frac{\alpha}{2}\left(1+\frac{\gamma_2}{\gamma_1}\right) < 1$$

(104)

which results in a negative exponent in the exponential function. If $\gamma_2 \ll \gamma_1$, the time constant τ can be approximated with $\tau = -1/\ln(\alpha/2)$. A small value of α results in a small value for τ and thus a fast response. A $\gamma_2 \neq 0$ increases the response time. A relatively large value for τ results for values of α close to 1. This is allowed because sudden position changes are also limited by the expectation window width.

Transient response for an initial condition with both sample points

on the ventricular slope- Consider the case with an initial condition

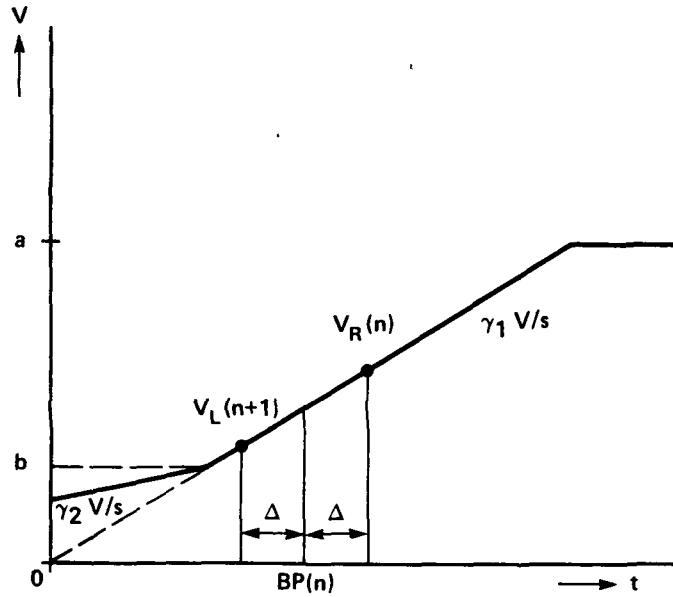such that both sample points are on the left ventricular slope (fig. 64).

Figure 64.- Initial condition with both sample points on the
ventricular slope.

What we need then is a mechanism, which "pulls" the border point back to

the equilibrium situation as defined by equation (89). This can be

derived by solving for the equilibrium reference voltage, in this case

with both sample points on the slope, and requiring that

$$V_{equil} < b + \Delta\gamma_1 \tag{105}$$

As soon as a border point is within a distance Δ from b/γ_1, the rest

of the trajectory is described by equation (102). Substituting

$$V_R(n) = \gamma_1[BP(n) + \Delta] \tag{106}$$

and

$$V_L(n+1) = \gamma_1[BP(n) - \Delta] \tag{107}$$

156

into equation (85) with

$$V_{ref}(n+1) = \gamma_1 BP(n) \qquad (108)$$

gives

$$\frac{\alpha}{2} \{\gamma_1 [BP(n) + \Delta] + \gamma_1 [BP(n) - \Delta]\} + V_c = \gamma_1 \cdot BP(n) \qquad (109)$$

Solving for BP(n) yields

$$BP_{equil} = \frac{V_c}{\gamma_1 (1 - \alpha)} \qquad (110)$$

and

$$V_{equil} = \frac{V_c}{1 - \alpha} \qquad (111)$$

This equilibrium level should be chosen so that this situation with both sample points on the slope changes to the situation with one sample point on the slope and the other at the dark level (as indicated in fig. 62). This requires that

$$V_{equil} < b + \Delta\gamma_1 \qquad (112)$$

Because $0 < \alpha < 1$, $(1 - \alpha)$ in equation (111) is positive and, from equations (111) and (112), it follows that:

$$\alpha < 1 - \frac{V_c}{b + \Delta\gamma_1} \qquad (113)$$

the same upper limit as found in equation (94). This shows that if α satisfies this condition, there is a "pulling" mechanism that changes the situation with both sample points on the ventricular slope to the stable situation with one sample point on the slope and the other in the background area. The transient response can be derived similarly as done in the previous section.

Substituting the sampled levels on lines n and (n+1), respectively, into equation (99) gives, for BP(n+1),

$$BP(n+1) = \frac{1}{\gamma_1}\left(\frac{\alpha}{2}\{\gamma_1[BP(n)+\Delta]+\gamma_1[BP(n)-\Delta]\}+V_c\right) \qquad (114)$$

Applying the z transform with the initial condition denoted $BP(0)$ and solving for $BP(z)$ yields

$$BP(z) = BP(0)\cdot\frac{z}{z-\alpha}+\frac{V_c}{\gamma_1}\cdot\frac{z}{(z-1)(z-\alpha)} \qquad (115)$$

Transforming back to the time domain yields

$$BP(n) = BP(0)\cdot e^{n\ln\alpha}+\frac{V_c}{\gamma_1(1-\alpha)}\left(1-e^{n\ln\alpha}\right) \qquad (116)$$

Check - initial condition at $n=0$: $BP(n=0)=BP(0)$

final value at $n=\infty$: $BP(n=\infty)=V_c/\gamma_1(1-\alpha)$

The transient response is shown in figure 65. The trajectory is a decreasing exponential function with time constant $\tau=-1/\ln\alpha$, which is independent of Δ and γ_1. A value of α close to 1 again results in a large time constant.

Given an initial condition $BP(0)>b/\gamma_1+\Delta$, the trajectory back to the equilibrium situation is described by equation (116) so long as $BP(n)>b/\gamma_1+\Delta$ and by equation (102) for $BP(n)<b/\gamma_1+\Delta$.
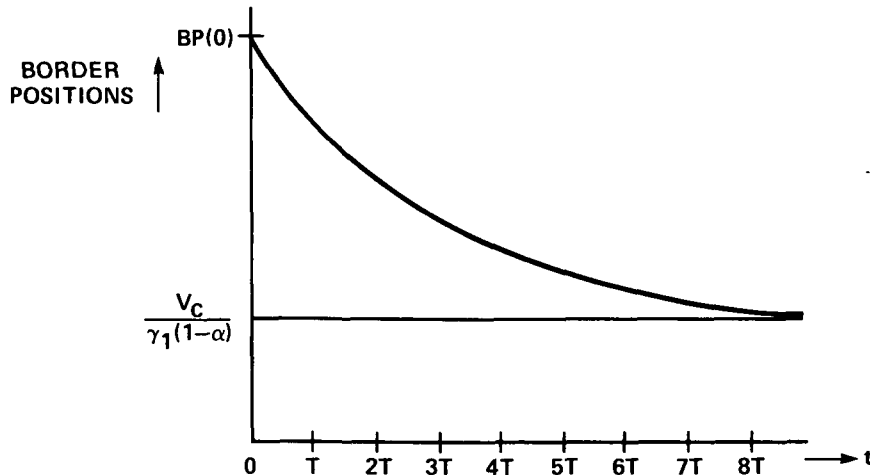

Figure 65.- Transient response from an initial condition $BP(0)$ to the equilibrium border position at $BP_{equil}=V_c/\gamma_1(1-\alpha)$.

Transient response for an initial condition with both sample points on background slope- In this case, a mechanism is needed that "drives" the border point back to the equilibrium situation as defined by equation (89) (fig. 66). This can be derived by solving for the equilibrium
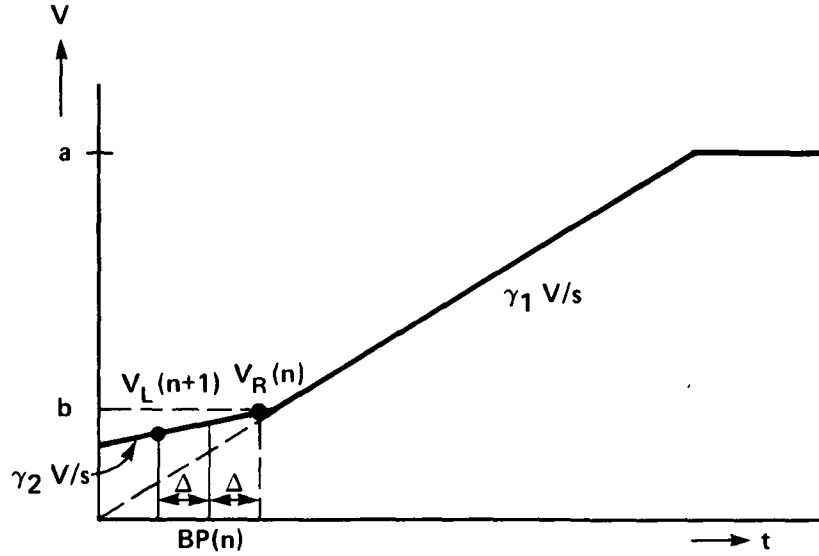

Figure 66.- Initial condition with both sample points on the background slope.

reference voltage, in this case with both sample points on the background function, and requiring that

$$V_{equil} > b - \gamma_2 \Delta \tag{117}$$

As soon as the reference level becomes greater than $b - \gamma_2 \Delta$ during the transient response, the situation changes because the right sample point then will be on the ventricular slope. Before considering this situation, the requirement for equation (117) is determined. Substituting

$$V_R(n) = \gamma_2 [BP(n) + \Delta] + b\left(1 - \frac{\gamma_2}{\gamma_1}\right) \tag{118}$$

and

$$V_L(n+1) = \gamma_2 [BP(n) - \Delta] + b\left(1 - \frac{\gamma_2}{\gamma_1}\right) \tag{119}$$

159

into equation (85) with

$$V_{ref}(n+1) = \gamma_2 \cdot BP(n) + b\left(1 - \frac{\gamma_2}{\gamma_1}\right) \tag{120}$$

and solving for BP(n) yields

$$BP_{equil} = \frac{V_c}{\gamma_2(1-\alpha)} - \frac{b}{\gamma_2}\left(1 - \frac{\gamma_2}{\gamma_1}\right) \tag{121}$$

and

$$V_{equil} = \frac{V_c}{1-\alpha} \tag{122}$$

This equilibrium level then should be chosen so that this situation with both sample points on the background slope changes to the situation with one sample point on the ventricular slope and the other in the background area. Solving for α from equations (117) and (122) yields

$$\alpha > 1 - \frac{V_c}{b - \Delta\gamma_2} \tag{123}$$

Plotting this function in figure 63 shows that the allowed region of α and V_c values is now much smaller under the conditions of equation (123). However, the bias line $\alpha = 1 - (V_c/b)$ always satisfies this requirement.

The transient response can be derived in a manner similar to the other cases. Since the border point is now on the background slope, the transient response can be derived from

$$BP(n+1) = \frac{1}{\gamma_2} \cdot V_{ref}(n+1) - b\left(\frac{1}{\gamma_2} - \frac{1}{\gamma_1}\right)$$

$$= \frac{1}{\gamma_2}\left\{\frac{\alpha}{2}\left[V_R(n) + V_L(n+1)\right] + V_c\right\} - b\left(\frac{1}{\gamma_2} - \frac{1}{\gamma_1}\right) \tag{124}$$

Substituting equations (118) and (119) into (124) gives

$$BP(n+1) = \alpha \cdot BP(n) - (1-\alpha)b\left(\frac{1}{\gamma_2} - \frac{1}{\gamma_1}\right) + \frac{V_c}{\gamma_2} \tag{125}$$

Applying the z transform with the initial condition denoted BP(0) and solving for BP(z) yields

160

$$BP(z) = \frac{z}{z - \alpha} \cdot BP(0) + \left[\frac{V_c}{\gamma_2} - (1 - \alpha)b\left(\frac{1}{\gamma_2} - \frac{1}{\gamma_1}\right)\right] \cdot \frac{z}{(z - 1)(z - \alpha)} \quad (126)$$

Transforming back to the time domain

$$BP(n) = BP(0) \cdot e^{n \ln \alpha} + \left[\frac{V_c}{\gamma_2(1 - \alpha)} - \frac{b}{\gamma_2}\left(1 - \frac{\gamma_2}{\gamma_1}\right)\right]\left(1 - e^{n \ln \alpha}\right) \quad (127)$$

Check – initial condition at $n = 0$: $BP(n = 0) = BP(0)$

final value at $n = \infty$: $BP(n = \infty) = \frac{V_c}{\gamma_2(1 - \alpha)} - \frac{b}{\gamma_2}\left(1 - \frac{\gamma_2}{\gamma_1}\right)$

The transient response is again an exponential function with time con-

stant $\tau = -1/\ln \alpha$. Equation (127) is applicable so long as both sample

points are on the background slope.

Transient response for an initial condition with

$(b/\gamma_1) - \Delta < BP(0) < (b/\gamma_1) -$ In the previous section, the transient

response and the requirements for the "driving" mechanisms were derived

for the case with two sample points on the background slope.

This was valid until point $BP(n) = (b/\gamma_1) - \Delta$. After this point has been
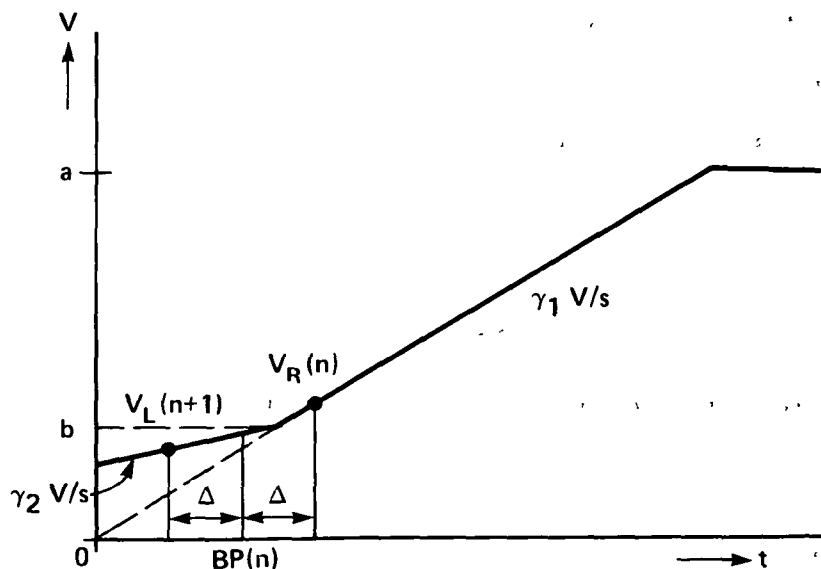

Figure 67.- Initial condition with $(b/\gamma_1) - \Delta < BP(0) < (b/\gamma_1)$.

reached, the situation changes because one sample point is now on the
ventricular slope and we must determine the new requirements for reaching
the equilibrium situation as defined by equation (89). This will be
done by deriving the conditions under which an equilibrium situation
with $(b/\gamma_1) - \Delta < BP_{equil} < (b/\gamma_1)$ can occur (fig. 67). The sample voltages
are now:

$$V_R(n) = \gamma_1 [BP(n) + \Delta] \tag{128}$$

and

$$V_L(n+1) = \gamma_2 [BP(n) - \Delta] + b\left(1 - \frac{\gamma_2}{\gamma_1}\right) \tag{129}$$

The reference level is

$$V_{ref}(n+1) = \gamma_2 \cdot BP(n) + b\left(1 - \frac{\gamma_2}{\gamma_1}\right) \tag{130}$$

Substituting these formulas into equation (85) and solving for $BP(n)$
yields

$$BP_{equil} = \frac{\frac{\alpha}{2}(\Delta\gamma_1 + b)\left(1 - \frac{\gamma_2}{\gamma_1}\right) - b\left(1 - \frac{\gamma_2}{\gamma_1}\right) + V_c}{\gamma_2\left[1 - \frac{\alpha}{2}\left(1 + \frac{\gamma_1}{\gamma_2}\right)\right]} \tag{131}$$

We want to determine the requirements for an equilibrium position so
that

$$\frac{b}{\gamma_1} - \Delta < BP_{equil} < \frac{b}{\gamma_1} \tag{132}$$

Therefore, define

$$BP_{equil} = \frac{b}{\gamma_1} - A\Delta \tag{133}$$

with $0 \le A \le 1$. Solving for A from equations (131) and (133) gives

$$A = \frac{(1 - \alpha)b - \frac{\alpha}{2}\Delta\gamma_1\left(1 - \frac{\gamma_2}{\gamma_1}\right) - V_c}{\Delta\gamma_2\left[1 - \frac{\alpha}{2}\left(1 + \frac{\gamma_1}{\gamma_2}\right)\right]} \tag{134}$$

The denominator in equation (134) is negative for

$$\alpha \ge \frac{2\gamma_2}{\gamma_1 + \gamma_2} \tag{135}$$

162

while the numerator is negative for

$$\alpha \geq \frac{b - V_c}{b + \frac{\Delta\gamma_1}{2}\left(1 - \frac{\gamma_2}{\gamma_1}\right)} \tag{136}$$

To solve for $0 \leq A \leq 1$, distinguish two cases:

(I) $\alpha \geq \dfrac{2\gamma_2}{\gamma_1 + \gamma_2}$ and $\alpha \geq \dfrac{b - V_c}{b + \frac{\Delta\gamma_1}{2}\left(1 - \frac{\gamma_2}{\gamma_1}\right)}$

Under these conditions, A is positive but the numerator and denominator are negative. Solving for $A \leq 1$ yields

$$\alpha \leq 1 - \frac{V_c}{b - \Delta\gamma_2} \tag{137}$$

The allowed region for α and V_c, so that an equilibrium condition is obtained under the above conditions, is shown in figure 68.
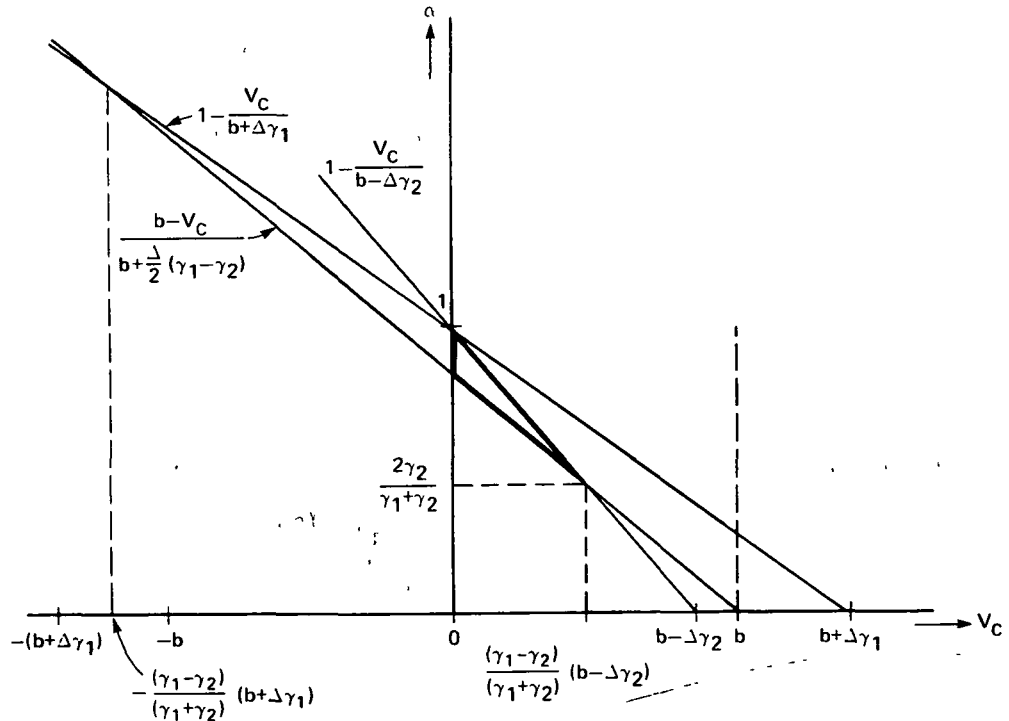

Figure 68.- Region of α and V_c values for which a labile equilibrium with $(b/\gamma_1) - \Delta < \overline{BP}_{equil} < (b/\gamma_1)$ is possible.

(II)
$$\alpha \leq \frac{2\gamma_2}{\gamma_1 + \gamma_2} \quad \text{and} \quad \alpha \leq \frac{b - V_c}{b + \frac{\Delta\gamma_1}{2}\left(1 - \frac{\gamma_2}{\gamma_1}\right)}$$

Under these conditions, A is positive because both the numerator and

denominator of A are positive. Solving for $A \leq 1$ yields

$$\alpha \geq 1 - \frac{V_c}{b - \Delta\gamma_2} \tag{138}$$

However, this region is outside the defined region in figure 63 so a

bias point is not acceptable here.

Assuming an initial border point with $(b/\gamma_1) - \Delta \leq BP(0) \leq (b/\gamma_1)$ and

a set of parameters (α, V_c) within the defined region in figure 63, but

outside the region of equation (137), the calculated $V_{ref}(n+1)$ is

always greater than $V_{ref}(n)$ during the time that $(b/\gamma_1) - \Delta < BP(n) < (b/\gamma_1)$.

This then provides the "driving" mechanism for the border point to return

to a position on the ventricular slope.

An equilibrium situation can occur under the conditions given in

the first case. The required set of parameters (α, V_c) for a particular

A is obtained by solving for α from equations (131) and (133), which

results in

$$\alpha = -\frac{V_c}{b + \frac{\Delta}{2}(\gamma_1 - \gamma_2) - \frac{A\Delta}{2}(\gamma_1 + \gamma_2)} + \frac{(b - A\Delta\gamma_2)}{b + \frac{\Delta}{2}(\gamma_1 - \gamma_2) - \frac{A\Delta}{2}(\gamma_1 + \gamma_2)} \tag{139}$$

a set of straight lines with direction coefficient

$$\delta = -\frac{1}{b + \frac{\Delta}{2}(\gamma_1 - \gamma_2) - \frac{A\Delta}{2}(\gamma_1 + \gamma_2)} \tag{140}$$

For the limits $A = 0, 1$, respectively, equation (139) simplifies to

164

A = 0:

$$\alpha = \frac{b - V_c}{b + \frac{\Delta\gamma_1}{2}\left(1 - \frac{\gamma_2}{\gamma_1}\right)} \qquad \text{(equals eq. (97))} \qquad (141)$$

A = 1:

$$\alpha = 1 - \frac{V_c}{b - \Delta\gamma_2} \qquad \text{(equals eq. (123))} \qquad (142)$$

All lines defined by equation (139) have the point $\alpha = 2\gamma_2/(\gamma_1 + \gamma_2)$, $V_c = (b - \Delta\gamma_2)[(\gamma_1 - \gamma_2)/(\gamma_1 + \gamma_2)]$ in common (fig. 68). It follows from equation (140) that an increasing value of A corresponds to an increasing absolute value of slope δ.

Consider the case for a particular α_0 and V_{c0} and for an equilibrium position with $0 \le A_0 \le 1$. The corresponding bias line that satisfies these parameters is then, from equation (139),

$$\alpha_0 = -\frac{V_{c0}}{b + \frac{\Delta}{2}(\gamma_1 - \gamma_2) - A_0\frac{\Delta}{2}(\gamma_1 + \gamma_2)} + \frac{b - A_0\Delta\gamma_2}{b + \frac{\Delta}{2}(\gamma_1 - \gamma_2) - A_0\frac{\Delta}{2}(\gamma_1 + \gamma_2)} \qquad (143)$$

However, it can be shown that this is a labile equilibrium. If, for some reason, the border point changes position and becomes BP(n) = $(b/\gamma_1) - A\Delta$, with A < A_0, then the equilibrium requirements associated with this new position correspond to an (α, V_c) function with a smaller absolute slope than the slope defined by equation (143). The newly calculated $V_{ref}(n + 1)$ is therefore higher than the equilibrium reference level associated with this new position and the position of the border point continues to increase until an equilibrium situation with $BP_{equil} > (b/\gamma_1)$ is reached. Similarly, if the position of the border point changes and becomes BP(n) = $(b/\gamma_1) - A\Delta$ with $A_0 < A \le 1$, then the equilibrium requirements associated with this new position correspond to an (α, V_c) function with a greater absolute slope than the

165

slope defined by equation (143). The newly calculated $V_{ref}(n+1)$ is then lower than this new equilibrium reference level would be and the position of the border point continues to decrease until an equilibrium situation with $BP_{equil} < (b/\gamma_1) - \Delta$ is reached.

Summarizing: if a border point is detected on the background slope with $(b/\gamma_1) - \Delta < BP(n) < (b/\gamma_1)$, then this situation is stable only if the existing α and V_c satisfy equation (134) for the corresponding value of A at this point. If the selected α and V_c correspond to an equilibrium position $(b/\gamma_1) - \Delta < BP_{equil} < BP'(n)$, then the position of the border point increases until a stable point is detected with $BP_{equil} > (b/\gamma_1)$. On the other hand, if α and V_c correspond to an equilibrium position $BP(n) < BP_{equil} < (b/\gamma_1)$, then the position of the border point decreases until a stable point is detected with $BP_{equil} < (b/\gamma_1) - \Delta$. However, a detected border point on the background slope will always return to the ventricular slope by requiring that

$$\alpha \geq 1 - \frac{V_c}{b - \Delta\gamma_2} \qquad (144)$$

The transient response from an initial condition $BP(0)$ can again be derived from equation (124). Substituting equation (128) and (129) into (124) gives

$$BP(n+1) = \frac{\alpha}{2}\left(1 + \frac{\gamma_1}{\gamma_2}\right) \cdot BP(n) + \frac{\alpha}{2}(\Delta\gamma_1 + b)\left(\frac{1}{\gamma_2} - \frac{1}{\gamma_1}\right) + \frac{V_c}{\gamma_2} - b\left(\frac{1}{\gamma_2} - \frac{1}{\gamma_1}\right) \qquad (145)$$

Applying the z transform with the initial condition denoted $BP(0)$ and solving for $BP(z)$ yields

166

$$BP(z) = \frac{zBP(0)}{z - \frac{\alpha}{2}\left(1 + \frac{\gamma_1}{\gamma_2}\right)} + \frac{\left\{\left[\frac{\alpha}{2}(\Delta\gamma_1 + b) - b\right]\left(\frac{1}{\gamma_2} - \frac{1}{\gamma_1}\right) + \frac{V_c}{\gamma_2}\right\}z}{\left[z - \frac{\alpha}{2}\left(1 + \frac{\gamma_1}{\gamma_2}\right)\right](z - 1)} \qquad (146)$$

Transforming back to the time domain,

$$BP(n) = BP(0)e^{n \ln \frac{\alpha}{2}\left(1 + \frac{\gamma_1}{\gamma_2}\right)}$$

$$+ \frac{\left[\frac{\alpha}{2}(\Delta\gamma_1 + b) - b\right]\left(1 - \frac{\gamma_2}{\gamma_1}\right) + V_c}{\gamma_2\left[1 - \frac{\alpha}{2}\left(1 + \frac{\gamma_1}{\gamma_2}\right)\right]}\left[1 - e^{n \ln \frac{\alpha}{2}\left(1 + \frac{\gamma_1}{\gamma_2}\right)}\right] \qquad (147)$$

Check - initial condition at $n = 0$: $BP(n = 0) = BP(0)$

final value at $n = \infty$: $BP(n = \infty) = \dfrac{\left[\frac{\alpha}{2}(\Delta\gamma_1 + b) - b\right]\left(1 - \frac{\gamma_2}{\gamma_1}\right) + V_c}{\gamma_2\left[1 - \frac{\alpha}{2}\left(1 + \frac{\gamma_1}{\gamma_2}\right)\right]}$

The time constant is given by

$$\tau = \frac{-1}{\ln \frac{\alpha}{2}\left(1 + \frac{\gamma_1}{\gamma_2}\right)} \qquad (148)$$

which is negative for $\alpha > 2\gamma_2/(\gamma_1 + \gamma_2)$. For $\alpha > 2\gamma_2/(\gamma_1 + \gamma_2)$, $e^{n \ln(\alpha/2)[1 + (\gamma_1/\gamma_2)]}$ is an exponential increasing function with time, which again shows the instability of an equilibrium position in the indicated range in figure 68. Only if

$$\frac{\left[\frac{\alpha}{2}(\Delta\gamma_1 + b) - b\right]\left(1 - \frac{\gamma_2}{\gamma_1}\right) + V_c}{\gamma_2\left[1 - \frac{\alpha}{2}\left(1 + \frac{\gamma_1}{\gamma_2}\right)\right]} = BP(0) \qquad (149)$$

then

$$BP(n) = BP(0) \qquad \text{for all } n \geq 0 \qquad (150)$$

If

167

$$BP(0) < \frac{\left[\frac{\alpha}{2}(\Delta\gamma_1 + b) - b\right]\left(1 - \frac{\gamma_2}{\gamma_1}\right) + V_c}{\gamma_2\left[1 - \frac{\alpha}{2}\left(1 + \frac{\gamma_1}{\gamma_2}\right)\right]} \tag{151}$$

for a particular α and V_c, then $BP(n)$ is an increasing function with time, and if

$$BP(0) > \frac{\left[\frac{\alpha}{2}(\Delta\gamma_1 + b) - b\right]\left(1 - \frac{\gamma_2}{\gamma_1}\right) + V_c}{\gamma_2\left[1 - \frac{\alpha}{2}\left(1 + \frac{\gamma_1}{\gamma_2}\right)\right]} \tag{152}$$

for a particular α and V_c, then $BP(n)$ is a decreasing function with time. For $\alpha < 2\gamma_2/(\gamma_1 + \gamma_2)$, the time constant is positive, indicating that a stable operating point with $(b/\gamma_1) - \Delta < BP_{equil} < (b/\gamma_1)$ is possible under the necessary conditions. However, it has been explained that these conditions do not meet the requirements for a stable operating point at $(b/\gamma_1) < BP_{equil} < (b/\gamma_1) + \Delta$. Therefore, this possible stable operating point with $(b/\gamma_1) - \Delta < BP_{equil} < (b/\gamma_1)$ will never occur.

Effects of Changes in Parameter Values

dc level changes with c volts- The voltage level at the knee in the border model is referred to as the dc level (fig. 69). We will assume that the border model for line n has the original dc level, but line $(n+1)$ has been shifted over c volts. The equilibrium reference level for line n is given by

$$V_{equil} = \frac{\frac{\alpha}{2}(\Delta\gamma_1 + b)\left(1 - \frac{\gamma_2}{\gamma_1}\right) + V_c}{1 - \frac{\alpha}{2}\left(1 + \frac{\gamma_2}{\gamma_1}\right)} \tag{90}$$

The new functions for the border model are

$$V_2' = \gamma_2 t + b\left(1 - \frac{\gamma_2}{\gamma_1}\right) + c \qquad \text{(background area)} \tag{153}$$
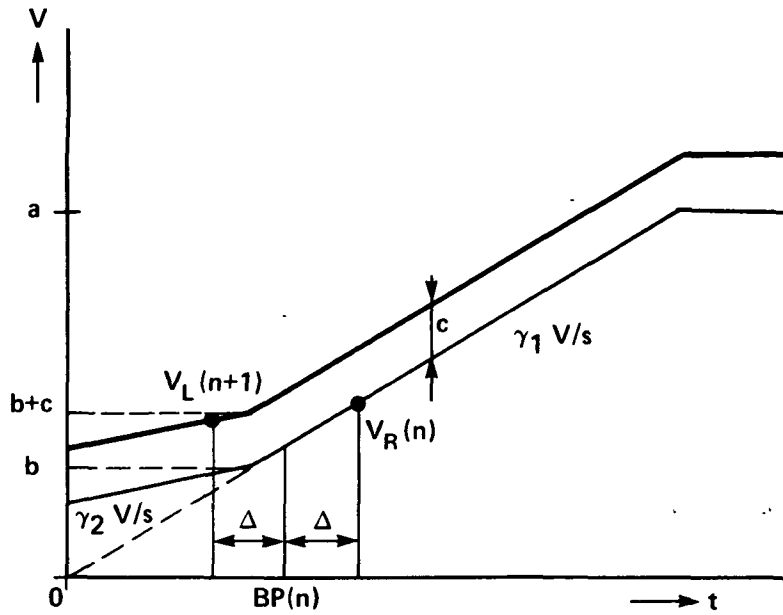
168

Figure 69.- Border model has been shifted upward over c volts, starting with line (n + 1).

$$V_1' = \gamma_1 t + c \qquad \text{(ventricular border)} \qquad (154)$$

Assuming that the dc shift will remain in effect for all scan lines following line (n + 1), we can calculate a new equilibrium reference level for this new situation. This new equilibrium level V'_{equil} can be computed under the assumption that

$$b + c < V'_{equil} < b + c + \Delta\gamma_1 \qquad (155)$$

Solving this inequality yields the maximum allowable value of c. The new sample levels in the equilibrium situation are

$$V_R = \gamma_1 (BP'_{equil} + \Delta) + c \qquad (156)$$

$$V_L = \gamma_2 (BP'_{equil} - \Delta) + b\left(1 - \frac{\gamma_2}{\gamma_1}\right) + c , \qquad (157)$$

169

where the border point in the new situation is denoted BP'_{equil}. The new equilibrium level can be written

$$V'_{equil} = \gamma_1 \cdot BP'_{equil} + c \qquad (158)$$

Substituting these formulas into equation (85) and solving for BP'_{equil} yields

$$BP'_{equil} = \frac{\frac{\alpha}{2}(\Delta\gamma_1 + b)\left(1 - \frac{\gamma_2}{\gamma_1}\right) + (\alpha - 1)c + V_c}{\gamma_1\left[1 - \frac{\alpha}{2}\left(1 + \frac{\gamma_2}{\gamma_1}\right)\right]} \qquad (159)$$

and the new equilibrium reference level,

$$V'_{equil} = \frac{\frac{\alpha}{2}(\Delta\gamma_1 + b + c)\left(1 - \frac{\gamma_2}{\gamma_1}\right) + V_c}{\left[1 - \frac{\alpha}{2}\left(1 + \frac{\gamma_2}{\gamma_1}\right)\right]} \qquad (160)$$

The equilibrium reference level then shifts over

$$V'_{equil} - V_{equil} = \frac{\frac{\alpha}{2}c\left(1 - \frac{\gamma_2}{\gamma_1}\right)}{\left[1 - \frac{\alpha}{2}\left(1 + \frac{\gamma_2}{\gamma_1}\right)\right]} \qquad (161)$$

so that

$$\left|V'_{equil} - V_{equil}\right| < |c| \qquad \text{for all } \alpha < 1 \qquad (162)$$

The equilibrium border position shifts over

$$BP'_{equil} - BP_{equil} = \frac{(\alpha - 1)c}{\gamma_1\left[1 - \frac{\alpha}{2}\left(1 + \frac{\gamma_2}{\gamma_1}\right)\right]} \qquad (163)$$

where $BP'_{equil} - BP_{equil}$ is negative for positive c and positive for negative c. Ideally, we would like to have $BP'_{equil} - BP_{equil}$ equal to zero; but this requires that $\alpha = 1$, which is not acceptable for several reasons. We have calculated before that the time constant for transient responses with both sample points on the same slope is given by

170

$\tau = -1/\ln\,\alpha$. With $\alpha = 1$, this goes to infinity. It was also calculated that the equilibrium reference level in these cases is $V_c/(1-\alpha)$. With V_c finite, this means that the reference level goes to infinity for $\alpha = 1$. Therefore, we will always require $\alpha < 1$, resulting in a negative $BP'_{equil} - BP_{equil}$ for c positive and a positive $BP'_{equil} - BP_{equil}$ for c negative. For a stable situation it is required that

$$b + c < V'_{equil} < b + c + \Delta\gamma_1 \tag{164}$$

Substituting equation (160) and solving for α gives

$$\frac{b + c - V_c}{\frac{\Delta\gamma_1}{2}\left(1 - \frac{\gamma_2}{\gamma_1}\right) + b + c} < \alpha < 1 - \frac{V_c}{b + c + \Delta\gamma_1} \tag{165}$$

We now must distinguish between a positive and negative value of c.

Positive c– Because $V'_{equil} - V_{equil} < c$, solve for the left-hand side of inequality (164) to determine the maximum allowable value of c, that is,

$$b + c < \frac{\frac{\alpha}{2}\,(\Delta\gamma_1 + b + c)\left(1 - \frac{\gamma_2}{\gamma_1}\right) + V_c}{\left[1 - \frac{\alpha}{2}\left(1 + \frac{\gamma_2}{\gamma_1}\right)\right]} \tag{166}$$

If the maximum allowable positive change in dc level is c_p, then

$$c_p = \frac{\frac{\alpha}{2}\,\Delta\gamma_1\left(1 - \frac{\gamma_2}{\gamma_1}\right) + V_c}{1 - \alpha} - b \tag{167}$$

The values of c_p as a function of α are shown in figure 70. The α value for which $c_p = 0$ equals the lower bound in the inequality in equation (94), as it should be. Choosing this α value allows only a negative c. Similarly, the maximum allowable value of c_p is
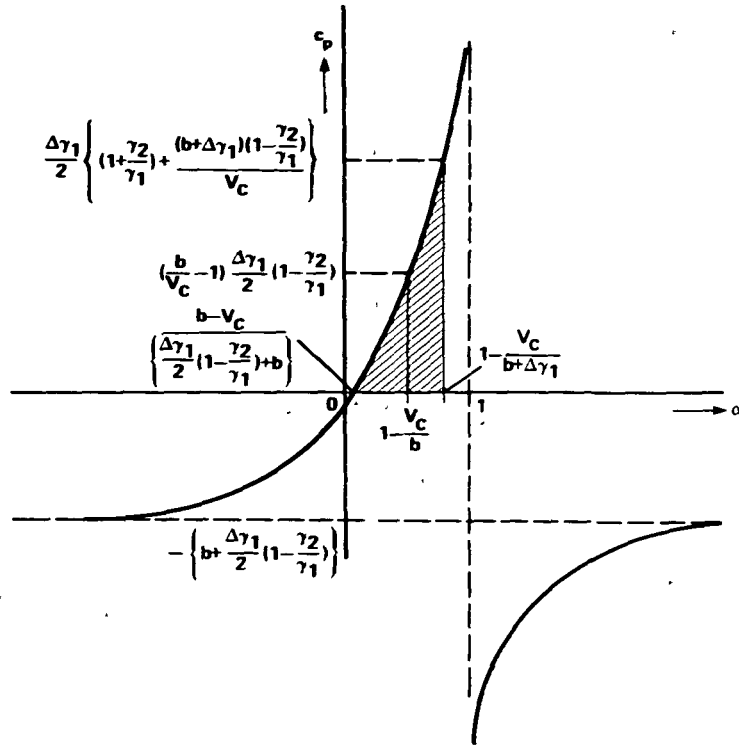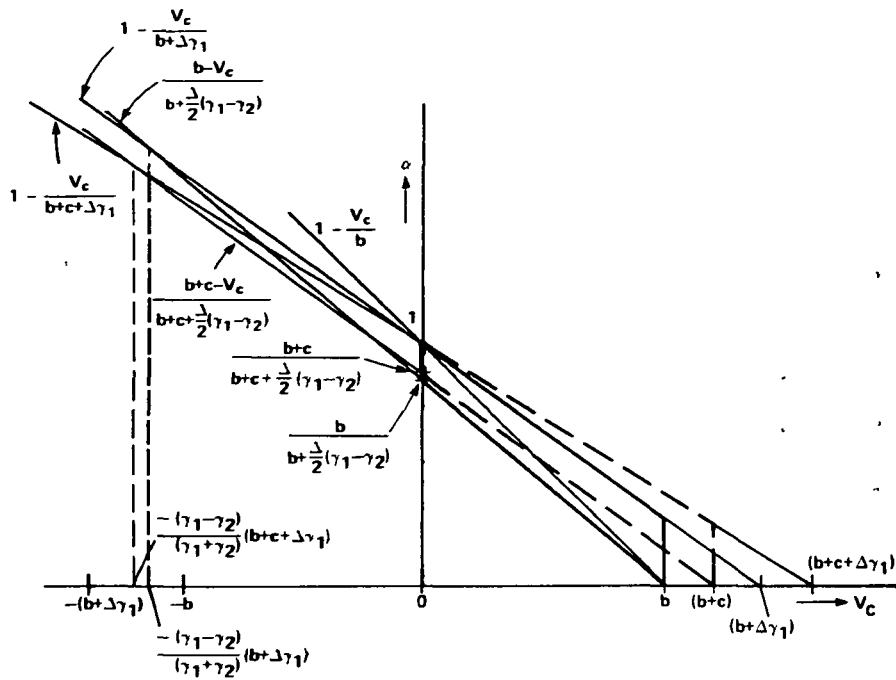
171

Figure 70.- The function $c_p = f(\alpha)$ gives the maximum allowable positive change in dc level as a function of α.

determined by the upper limit $\alpha = 1 - [V_c/(b + \Delta\gamma_1)]$ in equation (94); in this case, no negative c is allowed. Choosing $\alpha = 1 - (V_c/b)$ results in a maximum allowable value of

$$c_p = \left(\frac{b}{V_c} - 1\right) \frac{\Delta\gamma_1}{2} \left(1 - \frac{\gamma_2}{\gamma_1}\right) \tag{168}$$

Figure 71 shows the region of (α, V_c) values that satisfy equation (165) and the original region defined by equation (94), respectively. The α and V_c parameters should be chosen so that the bias point belongs to both regions under varying c. It can easily be seen from figure 71 that $c_p = 0$ for

$$\alpha = \frac{b - V_c}{\frac{\Delta\gamma_1}{2} \left(1 - \frac{\gamma_2}{\gamma_1}\right) + b} \tag{169}$$

172

$1 - \dfrac{V_c}{b+\Delta\gamma_1}$

$\dfrac{b-V_c}{b+\frac{1}{2}(\gamma_1-\gamma_2)}$

$1 - \dfrac{V_c}{b+c+\Delta\gamma_1}$

$1 - \dfrac{V_c}{b}$

$\dfrac{b+c-V_c}{b+c+\frac{1}{2}(\gamma_1-\gamma_2)}$

$\dfrac{b+c}{b+c+\frac{1}{2}(\gamma_1-\gamma_2)}$

$\dfrac{b}{b+\frac{1}{2}(\gamma_1-\gamma_2)}$

$-\dfrac{(\gamma_1-\gamma_2)}{(\gamma_1+\gamma_2)}(b+c+\Delta\gamma_1)$

$-(b+\Delta\gamma_1)$ $-b$

$-\dfrac{(\gamma_1-\gamma_2)}{(\gamma_1+\gamma_2)}(b+\Delta\gamma_1)$

b $(b+c)$

$(b+\Delta\gamma_1)$

$(b+c+\Delta\gamma_1)$

$\longrightarrow V_c$

C POSITIVE

Figure 71.– Allowed range of α and V_c values changes when the dc level shifts upward over c volts.

The maximum allowable c_p decreases with increasing V_c and with increasing slope γ_2. It increases with increasing slope γ_1.

Negative c– Because $\left| V'_{equil} - V_{equil} \right| < |c|$ for negative c, we now must solve for the right-hand side of equation (164), that is,

$$\frac{\frac{\alpha}{2}(\Delta\gamma_1 + b + c)\left(1 - \frac{\gamma_2}{\gamma_1}\right) + V_c}{\left[1 - \frac{\alpha}{2}\left(1 + \frac{\gamma_2}{\gamma_1}\right)\right]} < b + c + \Delta\gamma_1 \qquad (170)$$

Defining

$$c_n \triangleq -c > 0 \qquad (171)$$

equation (170) can be written as

173

$$\frac{\frac{\alpha}{2}\,(\Delta\gamma_1 + b - c_n)\left(1 - \frac{\gamma_2}{\gamma_1}\right) + V_c}{\left[1 - \frac{\alpha}{2}\left(1 + \frac{\gamma_2}{\gamma_1}\right)\right]} < b - c_n + \Delta\gamma_1 \qquad (172)$$

If the absolute value of the maximum allowable negative change in dc

level is c_N, then

$$c_N = \Delta\gamma_1 + b - \frac{V_c}{1 - \alpha} \qquad (173)$$

The values of c_N as a function of α are shown in figure 72. The α

value for which $c_N = 0$ equals the upper bound in the inequality in
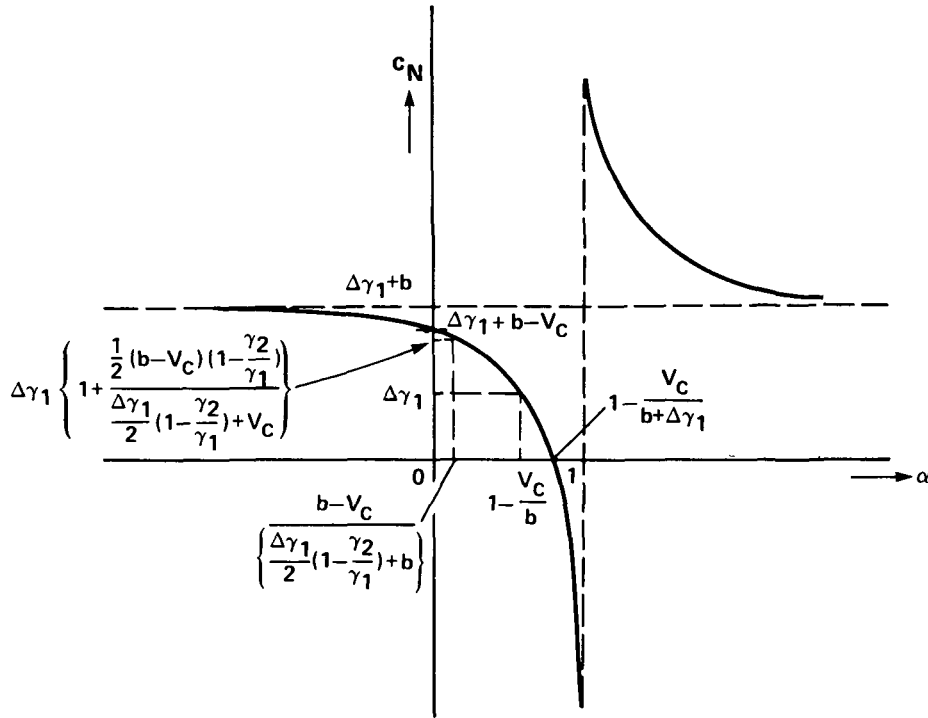

Figure 72.- The function $c_N = f(\alpha)$ gives the maximum allowable negative
change in dc level as a function of α.

equation (94). Choosing this α value allows only a positive c.

Similarly, for

$$\alpha = \frac{b - V_c}{\frac{\Delta\gamma_1}{2}\left(1 - \frac{\gamma_2}{\gamma_1}\right) + b} \qquad \text{(lower bound in eq. (94))}$$

174

the maximum c_N allowed is

$$c_N = \Delta\gamma_1 \left[1 + \frac{\frac{1}{2}(b - V_c)\left(1 - \frac{\gamma_2}{\gamma_1}\right)}{\frac{\Delta\gamma_1}{2}\left(1 - \frac{\gamma_2}{\gamma_1}\right) + V_c} \right] \tag{174}$$

no positive c is allowed for this α value. Choosing $\alpha = 1 - (V_c/b)$ results in a maximum allowable value of $c_N = \Delta\gamma_1$ which is independent of V_c, b, and γ_2.

The allowed region of (α, V_c) values which satisfies equation (165) with negative c and the original region according to equation (94), respectively, are shown in figure 73. As shown in this figure, the maximum allowable $c_N = \Delta\gamma_1$ for $\alpha = 1 - (V_c/b)$.
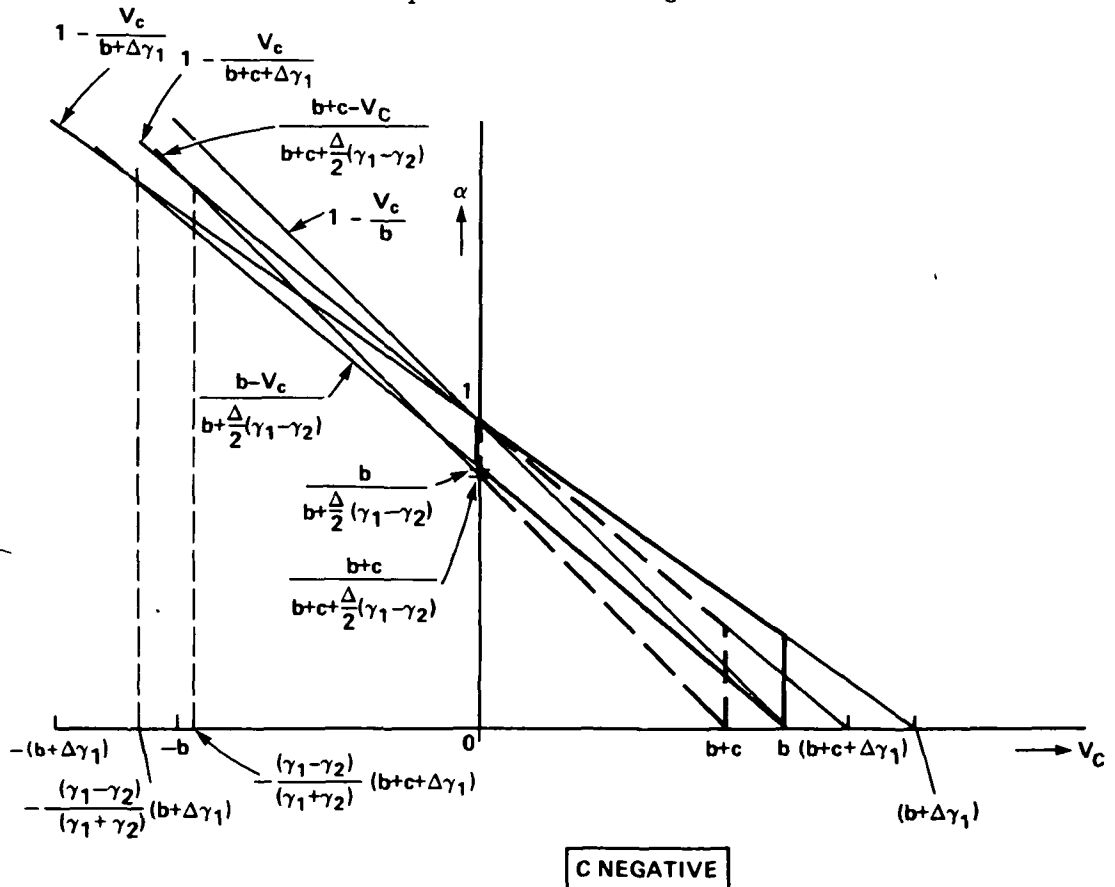

Figure 73.- The allowed range of α and V_c values changes when the dc level shifts downward over c volts.

175

Comparing the maximum allowable values for c_p and c_N with $\alpha = 1 - (V_c/b)$ shows that c_p increases with decreasing V_c while C_N remains constant. For $C_N > \Delta\gamma_1$, there is no point on the bias line $\alpha = 1 - (V_c/b)$ which satisfies equation (165). However, for any $c > 0$, we can find a bias point on this line that satisfies equation (165). This point can also be derived easily from figures 70 and 72, which suggests that one should measure the minimum value of b, denoted b_{min}, for all scan lines traversing the left ventricle in a video image and define the bias line as

$$\alpha = 1 - \frac{V_c}{b_{min}} \tag{175}$$

We certainly have no a priori knowledge of b_{min} for a particular field, but this value can be approximated very well with the measured $[(VL1/2) + (VL2/2)]_{min}$ of the previous field. Implementing $V_c = b_{min}(1 - \alpha)$ then requires only an adjustment of the α factor for the appropriate choice of the reference levels.

The maximum occurring c_p per video field then determines the required value of α. Assuming constant slopes γ_2 and γ_1, a minimum and maximum dc level of b_{min} and b_{max}, respectively, the minimum required value for α then follows from:

$$c_p = b_{max} - b_{min} = \frac{\alpha_{min}}{2(1 - \alpha_{min})} \Delta\gamma_1 \left(1 - \frac{\gamma_2}{\gamma_1}\right) \tag{176}$$

With this α_{min} value, an equilibrium level of b_{max} volts results at those lines with the highest dc level and an equilibrium level of

$$V_{equil} = \frac{\frac{\alpha_{min}}{2} (\Delta\gamma_1 + b_{min})\left(1 - \frac{\gamma_2}{\gamma_1}\right) + b_{min}(1 - \alpha_{min})}{1 - \frac{\alpha_{min}}{2} \left(1 + \frac{\gamma_2}{\gamma_1}\right)} \tag{177}$$

176

for the scan lines with the lowest dc level. If $\alpha > \alpha_{min}$, an overall higher reference level results, that is, the detected border will deviate more from the desired border.

It is also important to know the magnitude of the initial change in reference level and border position at line $(n+1)$. It is assumed that the border model on line n has a dc level of b volts, where $b \geq b_{min}$, and the dc level for line $(n+1)$ has been shifted over c volts. The calculation will be set up using the general notation with α and V_c without initially using the suggested relationship $\alpha = 1 - (V_c/b_{min})$. The sample voltages for lines n and $(n+1)$ are, respectively,

$$V_R(n) = V_{equil} + \Delta\gamma_1 \qquad (178)$$

and

$$V_L(n+1) = \gamma_2(BP_{equil} - \Delta) + b\left(1 - \frac{\gamma_2}{\gamma_1}\right) + c \qquad (179)$$

Substituting formulas (89) and (90) for BP_{equil} and V_{equil}, respectively, into (178) and (179) and $V_R(n)$ and $V_L(n+1)$ in the formula for $V_{ref}(n+1)$ yields

$$V_{ref}(n+1) = \frac{\frac{\alpha}{2}(\Delta\gamma_1 + b)\left(1 - \frac{\gamma_2}{\gamma_1}\right) + V_c}{\left[1 - \frac{\alpha}{2}\left(1 + \frac{\gamma_2}{\gamma_1}\right)\right]} + \frac{\alpha}{2}c \qquad (180)$$

The initial change in reference voltage $V_{ref}(n+1)$ compared with V_{equil} then equals

$$V_{ref}(n+1) - V_{equil} = \frac{\alpha}{2}c \qquad (181)$$

which is independent of the slopes and the sampling distance Δ. If c is positive, what will be the requirement on c such that

$$V_{ref}(n+1) \geq b + c \ ? \tag{182}$$

This means that the new border point on line $(n+1)$ remains on the ventricular slope. If the maximum allowable positive change in dc level, satisfying equation (182) is denoted c_1, then substituting equation (180) into (182) and solving for c_1 yields:

$$c_1 = \frac{\frac{\alpha}{2} \Delta\gamma_1 \left(1 - \frac{\gamma_2}{\gamma_1}\right) - b(1 - \alpha) + V_c}{\left(1 - \frac{\alpha}{2}\right)\left[1 - \frac{\alpha}{2}\left(1 + \frac{\gamma_2}{\gamma_1}\right)\right]} \tag{183}$$

The values of c_1 as a function of α are shown in figure 74. Comparing c_p (eq. (167)) and c_1 (eq. (183)) shows, that for $\alpha > 2\gamma_2 / (\gamma_1 + \gamma_2)$,
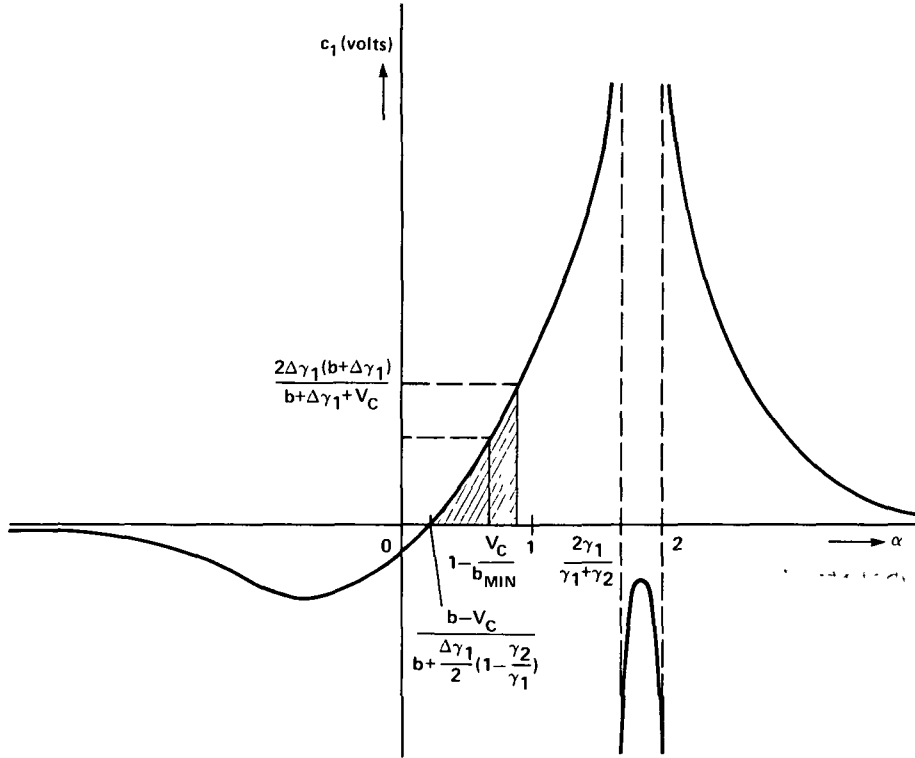

Figure 74.- The function $c_1 = g(\alpha)$ gives the maximum allowable positive change in dc level so that the border point remains on the ventricular slope on line $(n+1)$.

$$c_p > c_1 \tag{184}$$

Under the same condition $\alpha > 2\gamma_2/(\gamma_1 + \gamma_2)$, it is true that, for a particular c,

$$V'_{equil} - V_{equil} > V_{ref}(n+1) - V_{equil} \tag{185}$$

so the initial change in reference level is smaller than the final change under this condition. Assuming $\alpha > 2\gamma_2/(\gamma_1 + \gamma_2)$ and α satisfies $\alpha = 1 - (V_c/b_{min})$, the maximum allowable value for c can be determined so that $BP(n+1)$ remains on the ventricular slope. Substituting $V_c = (1-\alpha)b_{min}$ into equation (183) yields

$$c_1 = \frac{\frac{\alpha}{2} \Delta\gamma_1 \left(1 - \frac{\gamma_2}{\gamma_1}\right) - (1-\alpha)(b - b_{min})}{\left(1 - \frac{\alpha}{2}\right)\left[1 - \frac{\alpha}{2}\left(1 + \frac{\gamma_2}{\gamma_1}\right)\right]} \tag{186}$$

For parameter b, the allowable change in dc level is maximum if $b = b_{min}$, which gives

$$c_1 = \frac{\frac{\alpha}{2} \Delta\gamma_1 \left(1 - \frac{\gamma_2}{\gamma_1}\right)}{\left(1 - \frac{\alpha}{2}\right)\left[1 - \frac{\alpha}{2}\left(1 + \frac{\gamma_2}{\gamma_1}\right)\right]} \tag{187}$$

Returning to the general case with c_1 defined by equation (183), the new position of the border point on line $(n+1)$ can be derived from

$$BP(n+1) = \frac{V_{ref}(n+1) - c_1}{\gamma_1} \tag{188}$$

Substituting equation (180) yields

$$BP(n+1) = \frac{\frac{\alpha}{2}(\Delta\gamma_1 + b)\left(1 - \frac{\gamma_2}{\gamma_1}\right) + V_c}{\gamma_1\left[1 - \frac{\alpha}{2}\left(1 + \frac{\gamma_2}{\gamma_1}\right)\right]} + \frac{\left(\frac{\alpha}{2} - 1\right)c_1}{\gamma_1} \tag{189}$$

and

$$BP(n+1) - BP_{equil} = -\frac{\left(1 - \frac{\alpha}{2}\right)c_1}{\gamma_1} \tag{190}$$

The one-sided expectation window width should normally be greater than this possibly occurring change in border position. If this is not the case, then the position of $BP(n+1)$ will be determined by the beginning of the expectation window.

If $c_1 < c < c_p$ with $\alpha \geq 2\gamma_2/(\gamma_1 + \gamma_2)$, then $BP(n+1)$ will occur on the background slope. What are the requirements that the border point will return to its equilibrium position as defined by equation (160)? It was explained earlier that the required α and V_c depend on the particular initial condition of the border point on the background slope, but there is a minimum requirement that the border point always returns to the ventricular slope. This requirement can be derived by observing the situation with an equilibrium position at $BP_{equil} = (b/\gamma_1) - \Delta$. The new equation for the upward-shifted background slope is

$$V_2' = \gamma_2 t + b\left(1 - \frac{\gamma_2}{\gamma_1}\right) + c \tag{191}$$

If $BP(n) = (b/\gamma_1) - \Delta$, the new sample levels will be

$$V_R(n) = b + c \tag{192}$$

and

$$V_L(n+1) = \gamma_2\left(\frac{b}{\gamma_1} - 2\Delta\right) + b\left(1 - \frac{\gamma_2}{\gamma_1}\right) + c \tag{193}$$

Solving for $V_{ref}(n+1) = b + c - \Delta\gamma_2$ yields

$$\alpha = 1 - \frac{V_c}{b + c - \Delta\gamma_2} \tag{194}$$

180

With $\alpha \geq 1 - V_c/(b + c - \Delta\gamma_2)$, the border point will always return to the equilibrium position on the ventricular slope. With $c \geq 0$, it will be clear from equation (194) that the allowed region of α values will be limited under these circumstances. If $\alpha = 1 - (V_c/b_{min})$, then $\alpha \geq 1 - V_c/(b + c - \Delta\gamma_2)$ will be satisfied only for

$$c < \Delta\gamma_2 - (b - b_{min}) \qquad (195)$$

For $b = b_{min}$, the maximum allowable positive change is only $\Delta\gamma_2$ and for, $b = b_{min} + \Delta\gamma_2$, no positive change at all is allowed. In reality, the situation with $BP = (b/\gamma_1) - \Delta$ is avoided by the use of the expectation window, which has a one-sided width $\varepsilon < \Delta$. This means that from one line to the next the maximum possible change in border position is only ε; it is thereby important that the center of the expectation window approximates the next border position as accurately as possible. This favors again the first-order extrapolation principle over the zeroth-order principle. Also, the dc level changes from line to line will generally be relatively small so that $c < c_1$ is usually satisfied.

In situations for which the border points tend to fall off toward $BP = (b/\gamma_1) - \Delta$, because of a sudden positive change in dc level, the instability can be avoided by the use of the dynamic expectation window (chapter 10). This will limit the excursions from previous border points so that a stable contour can again be obtained.

It follows from equations (167) and (183) that, for $\alpha < 2\gamma_2/(\gamma_1 + \gamma_2)$,

$$c_p < c_1 \qquad (196)$$

and

$$V'_{equil} - V_{equil} < V_{ref}(n + 1) - V_{equil} \qquad (197)$$

181

The initial change in reference level is greater than the final change under this condition. Satisfying the conditions for c_p results in a stable contour point for $BP(n+1)$ with no extra requirements. The effects of changes in the dc level are summarized as follows. Assuming that the lowest dc level for a particular image is at b_{min} volts and $\alpha = 1 - (V_c/b_{min})$, then the maximum allowable positive change in dc level such that the detected border point remains on the ventricular slope is given by

$$c_p = \frac{\frac{\alpha}{2} \Delta\gamma_1 \left(1 - \frac{\gamma_2}{\gamma_1}\right)}{1 - \alpha} \tag{198}$$

If the reference level on line n is b volts, then the maximum allowable positive change such that the border point on line $(n+1)$ remains on the ventricular slope is given by

$$c_1 = \frac{\frac{\alpha}{2} \Delta\gamma_1 \left(1 - \frac{\gamma_2}{\gamma_1}\right) - (1 - \alpha)(b - b_{min})}{\left(1 - \frac{\alpha}{2}\right)\left[1 - \frac{\alpha}{2}\left(1 + \frac{\gamma_2}{\gamma_1}\right)\right]} \tag{199}$$

for $\alpha > 2\gamma_2/(\gamma_1 + \gamma_2)$. Figures 70 and 74 show that the maximum values of c_p and c_1 increase with increasing α. Under these conditions, the detected border points are near $(b+c)/\gamma_1$ for the scan lines with the highest dc levels and at a somewhat higher level for the lowest dc levels.

Ventricular slope changes from γ_1 *to* γ_3 *V/sec-* Assume that the dc level is $b_{min} + c$ volts ($c \geq 0$) and the slope on line n is γ_1 V/sec and on line $(n+1)$ and all following lines, γ_3 V/sec (fig. 75). For simplicity, $b \triangleq b_{min}$. The equation for the new border function is

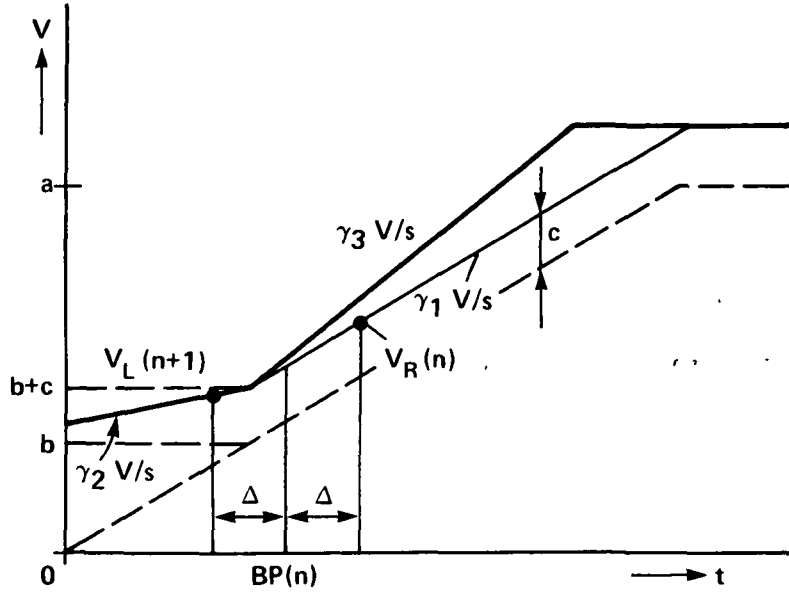$$V_3 = \gamma_3 t + b\left(1 - \frac{\gamma_3}{\gamma_1}\right) + c \tag{200}$$

182

Figure 75.- Left ventricular slope changes from γ_1 to γ_3 V/sec.

The new equilibrium position BP''_{equil} can again be derived by substituting

$$V_R = \gamma_3 (BP''_{equil} + \Delta) + b\left(1 - \frac{\gamma_3}{\gamma_1}\right) + c \qquad (201)$$

$$V_L = \gamma_2 (BP''_{equil} - \Delta) + b\left(1 - \frac{\gamma_2}{\gamma_1}\right) + c \qquad (202)$$

and

$$V''_{equil} = \gamma_3 \cdot BP''_{equil} + b\left(1 - \frac{\gamma_3}{\gamma_1}\right) + c \qquad (203)$$

into equation (85), assuming $(b/\gamma_1) < BP''_{equil} < (b/\gamma_1) + \Delta$. Solving for BP''_{equil} yields

$$BP''_{equil} = \frac{\frac{\alpha}{2} (\Delta\gamma_3 + b)\left(1 - \frac{\gamma_2}{\gamma_3}\right) + (\alpha - 1)c + V_c}{\gamma_3 \left[1 - \frac{\alpha}{2} \left(1 + \frac{\gamma_2}{\gamma_3}\right)\right]} + b\left(\frac{1}{\gamma_1} - \frac{1}{\gamma_3}\right) \qquad (204)$$

Check - for $\gamma_3 = \gamma_1$:

183

$$BP''_{equil} = \frac{\frac{\alpha}{2}(\Delta\gamma_1 + b)\left(1 - \frac{\gamma_2}{\gamma_1}\right) + (\alpha - 1)c + V_c}{\gamma_1\left[1 - \frac{\alpha}{2}\left(1 + \frac{\gamma_2}{\gamma_1}\right)\right]} = BP'_{equil} \qquad \text{(see eq. (159))}$$

The equilibrium reference voltage for BP''_{equil} follows from equation (204) as

$$V''_{equil} = \gamma_3 \cdot BP''_{equil} + b\left(1 - \frac{\gamma_3}{\gamma_1}\right) + c = \frac{\frac{\alpha}{2}(\Delta\gamma_3 + b + c)\left(1 - \frac{\gamma_2}{\gamma_3}\right) + V_c}{1 - \frac{\alpha}{2}\left(1 + \frac{\gamma_2}{\gamma_3}\right)} \qquad (205)$$

What are the requirements in this case for

$$b + c < V''_{equil} < b + c + \Delta\gamma_3 ? \qquad (206)$$

Since equations (205) and (206) are identical to equations (160) and (164), if we replace γ_3 by γ_1, the solution for equation (206) follows simply from equation (165) by replacing γ_1 with γ_3, that is,

$$\frac{b + c - V_c}{\frac{\Delta\gamma_3}{2}\left(1 - \frac{\gamma_2}{\gamma_3}\right) + b + c} < \alpha < 1 - \frac{V_c}{b + c + \Delta\gamma_3} \qquad (207)$$

Consider the case for $c = 0$. Equation (207) then simplifies to

$$\frac{b - V_c}{\frac{\Delta\gamma_3}{2}\left(1 - \frac{\gamma_2}{\gamma_3}\right) + b} < \alpha < 1 - \frac{V_c}{b + \Delta\gamma_3} \qquad (208)$$

Referring to figure 63, it is clear that

$$f_3(V_c) = 1 - \frac{V_c}{b + \Delta\gamma_3} \qquad (209)$$

rotates around the point $\alpha = 1$, $V_c = 0$ with varying slope γ_3. Similarly,

$$f_4(V_c) = \frac{b - V_c}{\frac{\Delta\gamma_3}{2}\left(1 - \frac{\gamma_2}{\gamma_3}\right) + b} \qquad (210)$$

rotates around the point $\alpha = 0$, $V_c = b$ with varying γ_3 and γ_2.

Therefore, $\alpha = 1 - (V_c/b)$ satisfies equation (208) for all γ_2 and

$\gamma_3 > \gamma_2$; this follows also from equation (205). Substituting $c = 0$ and

$V_c = (1 - \alpha)b$ into equation (205) results in

$$V''_{equil} = b + \frac{\frac{\alpha}{2}\, \Delta\gamma_3 \left(1 - \frac{\gamma_2}{\gamma_3}\right)}{1 - \frac{\alpha}{2}\left(1 + \frac{\gamma_2}{\gamma_3}\right)} \tag{211}$$

For all $\gamma_3 > \gamma_2$ and $\alpha < 1$, it follows that

$$0 < \frac{\frac{\alpha}{2}\, \Delta\gamma_3 \left(1 - \frac{\gamma_2}{\gamma_3}\right)}{1 - \frac{\alpha}{2}\left(1 + \frac{\gamma_2}{\gamma_3}\right)} < \Delta\gamma_3 \tag{212}$$

which again satisfies equation (206). Now consider the case for $c > 0$.

Assuming that the bias point (α, V_c) is chosen on line $\alpha = 1 - (V_c/b)$,

equation (205) can be written

$$V''_{equil} = b + \frac{\frac{\alpha}{2}\, (\Delta\gamma_3 + c) \left(1 - \frac{\gamma_2}{\gamma_3}\right)}{1 - \frac{\alpha}{2}\left(1 + \frac{\gamma_2}{\gamma_3}\right)} \tag{213}$$

Requiring again that $b + c < V''_{equil}$, this yields

$$c < \frac{\frac{\alpha}{2}\, (\Delta\gamma_3 - \Delta\gamma_2)}{1 - \alpha} = \frac{\frac{\alpha}{2}\, \Delta\gamma_3 \left(1 - \frac{\gamma_2}{\gamma_3}\right)}{1 - \alpha} \tag{214}$$

or

$$\alpha > \frac{c}{c + \frac{\Delta\gamma_3}{2}\left(1 - \frac{\gamma_2}{\gamma_3}\right)} = \frac{c}{c + \frac{\Delta\gamma_3}{2} - \frac{\Delta\gamma_2}{2}} \tag{215}$$

The requirement $V''_{equil} < b + c + \Delta\gamma_3$ is always satisfied for $\alpha < 1$ and

$\gamma_3 > \gamma_2$. It follows from equation (215) that, for a particular value of

c, a larger α is required for a decreasing slope γ_3 and a smaller α

is required for an increasing slope γ_3. This follows also from fig-

ure 76, which shows the allowed area for α and V_c according to
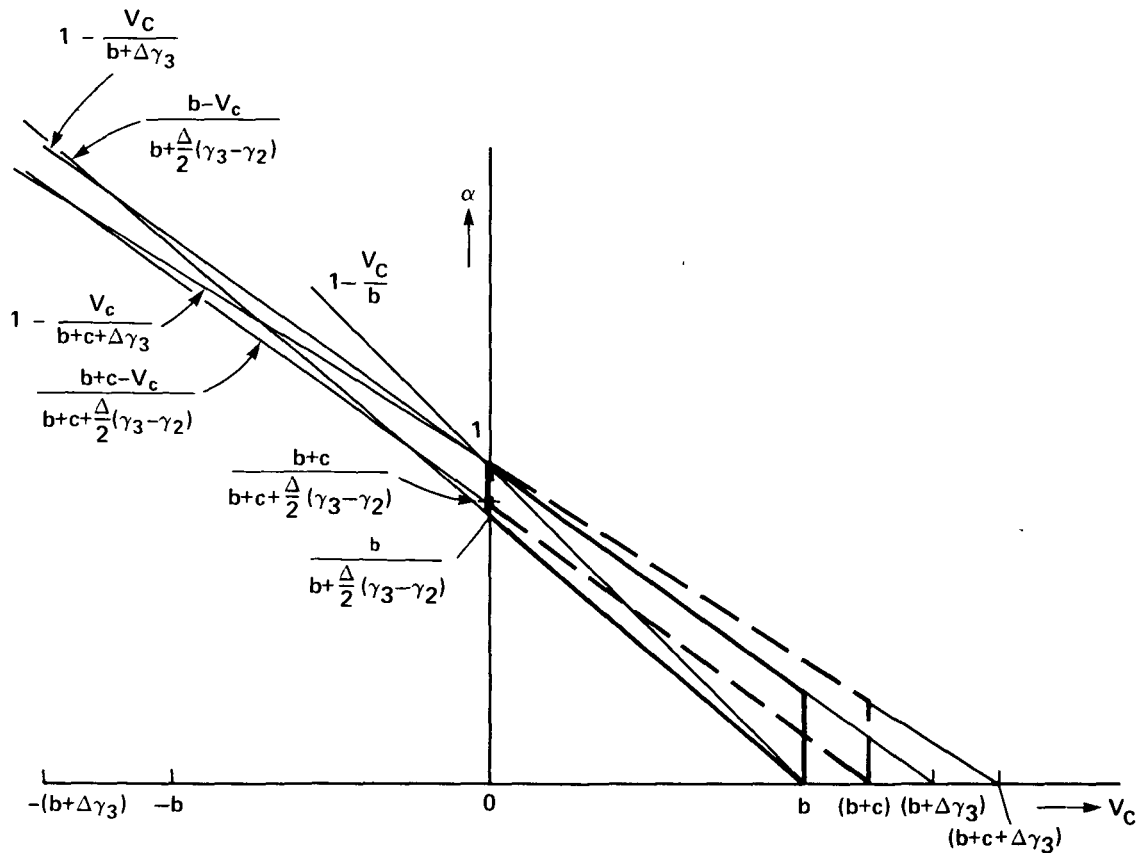
Figure 76.- Allowed region of α and V_c values for a ventricular slope of γ_3 V/sec and a shift in dc level of c volts.

equation (207) with $c = 0$ and $c > 0$. With a required bias point on line $\alpha = 1 - (V_c/b)$ within the indicated regions, an increasing α is clearly needed with decreasing slope γ_3 and a decreasing α is needed with increasing slope γ_3 because the slope of

$$\alpha = \frac{b + c - V_c}{\frac{\Delta\gamma_3}{2}\left(1 - \frac{\gamma_2}{\gamma_3}\right) + b + c} \qquad \text{changes (see eq. (207))}$$

A maximum $\alpha = 1$ is required if $\gamma_3 = \gamma_2$. Assuming a constant background slope γ_2, the α should be chosen on the biasing line $\alpha = 1 - (V_c/b)$ so that an equilibrium reference level of $b + c$ volts is obtained for maximum c and minimum γ_3.

186

What will be the initial change in border position after the slope has changed to γ_3 V/sec? The reference level for line $(n+1)$ has not changed and is still equal to the equilibrium level V'_{equil} as given by equation (160) with $V_c = b(1-\alpha)$, that is,

$$V_{ref}(n+1) = b + \frac{\frac{\alpha}{2}(\Delta\gamma_1 + c)\left(1 - \frac{\gamma_2}{\gamma_1}\right)}{1 - \frac{\alpha}{2}\left(1 + \frac{\gamma_2}{\gamma_1}\right)} \tag{216}$$

which means that $V_{ref}(n+1) > b+c$, independent of the change in slope, because it was assumed that $V'_{equil} > b+c$. Only the position of the border point on line $(n+1)$ changes. The new border point on line $(n+1)$ then will be

$$BP(n+1) = \frac{V_{ref}(n+1) - b\left(1 - \frac{\gamma_3}{\gamma_1}\right) - c}{\gamma_3} = \frac{b}{\gamma_1} + \frac{\frac{\alpha}{2}\Delta\gamma_1\left(1 - \frac{\gamma_2}{\gamma_1}\right) + (\alpha - 1)c}{\gamma_3\left[1 - \frac{\alpha}{2}\left(1 + \frac{\gamma_2}{\gamma_1}\right)\right]} \tag{217}$$

The equilibrium position on line n can be obtained from equation (159) by substituting $V_c = b(1-\alpha)$, that is,

$$BP'_{equil} = \frac{b}{\gamma_1} + \frac{\frac{\alpha}{2}\Delta\gamma_1\left(1 - \frac{\gamma_2}{\gamma_1}\right) + (\alpha - 1)c}{\gamma_1\left[1 - \frac{\alpha}{2}\left(1 + \frac{\gamma_2}{\gamma_1}\right)\right]} \tag{218}$$

The initial change in border position is therefore

$$BP(n+1) - BP'_{equil} = \left(\frac{1}{\gamma_3} - \frac{1}{\gamma_1}\right)\left[\frac{\frac{\alpha}{2}\Delta\gamma_1\left(1 - \frac{\gamma_2}{\gamma_1}\right) + (\alpha - 1)c}{1 - \frac{\alpha}{2}\left(1 + \frac{\gamma_2}{\gamma_1}\right)}\right] \tag{219}$$

For $\gamma_3 > \gamma_1$,

$$BP(n+1) - BP'_{equil} < 0 \tag{220}$$

and for $\gamma_3 < \gamma_1$,

$$BP(n+1) - BP'_{equil} > 0 \tag{221}$$

The final change in border position after the slope has changed to γ_3 is then

$$BP''_{equil} - BP'_{equil} = \frac{\frac{\alpha}{2}\Delta\gamma_3\left(1 - \frac{\gamma_2}{\gamma_3}\right) + (\alpha - 1)c}{\gamma_3\left[1 - \frac{\alpha}{2}\left(1 + \frac{\gamma_2}{\gamma_3}\right)\right]} - \frac{\frac{\alpha}{2}\Delta\gamma_1\left(1 - \frac{\gamma_2}{\gamma_1}\right) + (\alpha - 1)c}{\gamma_1\left[1 - \frac{\alpha}{2}\left(1 + \frac{\gamma_2}{\gamma_1}\right)\right]} \quad (222)$$

Background slope changes from γ_2 *to* γ_4 *V/sec-* Assume that the dc level is $b_{min} + c$ volts ($c \geq 0$) and the background slope on line n is γ_2 V/sec and on line (n + 1) and all following lines, γ_4 V/sec (fig. 77).
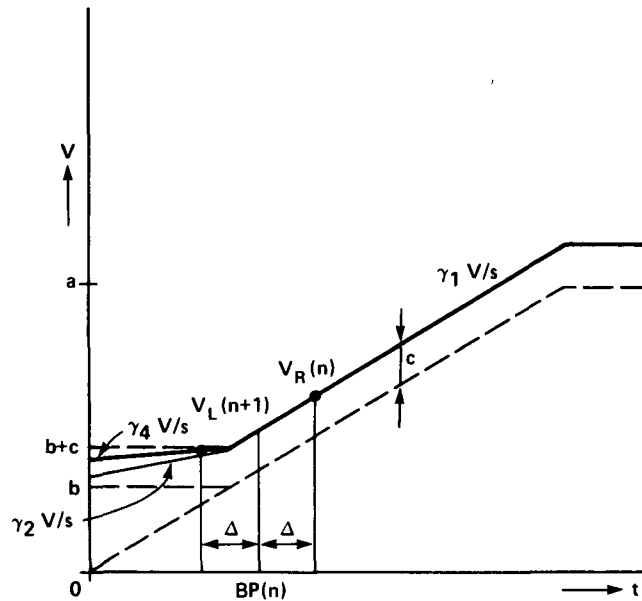

Figure 77.- Background slope changes from γ_2 to γ_4 V/sec.

The ventricular slope is γ_1 V/sec. For simplicity, $b = b_{min}$. The equation for the new background function is

$$V_4 = \gamma_4 t + b\left(1 - \frac{\gamma_4}{\gamma_1}\right) + c \quad (223)$$

The equilibrium level follows simply from equation (160) by substituting γ_4 for γ_2, that is,

188

$$V'''_{equil} = \frac{\frac{\alpha}{2}(\Delta\gamma_1 + b + c)\left(1 - \frac{\gamma_4}{\gamma_1}\right) + V_c}{\left[1 - \frac{\alpha}{2}\left(1 + \frac{\gamma_4}{\gamma_1}\right)\right]} \qquad (224)$$

With the bias point on line $\alpha = 1 - (V_c/b)$, this becomes

$$V'''_{equil} = b + \frac{\frac{\alpha}{2}(\Delta\gamma_1 + c)\left(1 - \frac{\gamma_4}{\gamma_1}\right)}{1 - \frac{\alpha}{2}\left(1 + \frac{\gamma_4}{\gamma_1}\right)} \qquad (225)$$

So far we have assumed that

$$b + c < V'''_{equil} < b + c + \Delta\gamma_1 \qquad (226)$$

The position BP'''_{equil} can then be derived using the formula $V_1 = \gamma_1 t + c$, which results in

$$BP'''_{equil} = \frac{b}{\gamma_1} + \frac{\frac{\alpha}{2}\Delta\gamma_1\left(1 - \frac{\gamma_4}{\gamma_1}\right) + (\alpha - 1)c}{\gamma_1\left[1 - \frac{\alpha}{2}\left(1 + \frac{\gamma_4}{\gamma_1}\right)\right]} \qquad (227)$$

If equation (224) is used for V'''_{equil}, the requirements for satisfying equation (226) are

$$\frac{b + c - V_c}{\frac{\Delta\gamma_1}{2}\left(1 - \frac{\gamma_4}{\gamma_1}\right) + b + c} < \alpha < 1 - \frac{V_c}{b + c + \Delta\gamma_1} \qquad (228)$$

Consider the case for $c = 0$. Equation (228) then simplifies to

$$\frac{b - V_c}{\frac{\Delta\gamma_1}{2}\left(1 - \frac{\gamma_4}{\gamma_1}\right) + b} < \alpha < 1 - \frac{V_c}{b + \Delta\gamma_1} \qquad (229)$$

Referring again to figure 63, clearly $\alpha = 1 - (V_c/b)$ satisfies equation (229) for all γ_1 and $0 \le \gamma_4 < \gamma_1$. For $c > 0$ and $\alpha = 1 - (V_c/b)$, the formula for V'''_{equil} is given by equation (225). Solving for $b + c < V'''_{equil}$ yields

$$\alpha > \frac{c}{c + \frac{\Delta\gamma_1}{2}\left(1 - \frac{\gamma_4}{\gamma_1}\right)} = \frac{c}{c + \frac{\Delta\gamma_1}{2} - \frac{\Delta\gamma_4}{2}} \qquad (230)$$

or

$$c < \frac{\frac{\alpha}{2}(\Delta\gamma_1 - \Delta\gamma_4)}{1 - \alpha} \qquad (231)$$

Equation (230) shows that, for a particular value of c, a larger α is needed with increasing slope γ_4 and a smaller α, with decreasing slope γ_4 (fig. 71). The required value of α is determined by the intersection of $\alpha = 1 - (V_c/b)$ and

$$\alpha = \frac{b + c - V_c}{\frac{\Delta\gamma_1}{2}\left(1 - \frac{\gamma_4}{\gamma_1}\right) + b + c} \ .$$

The intersection of the last function with the ordinate axis is given by

$$\alpha = \frac{b + c}{b + c + \frac{\Delta}{2}(\gamma_1 - \gamma_4)} \ .$$

Changing γ_2 makes this intersection point occur higher or lower on the ordinate axis. A slope $\gamma_4 > \gamma_2$ results in a higher intersection point with the α axis and therefore also a higher intersection point with the unchanged function of $\alpha = 1 - (V_c/b)$. This results in the requirement for a higher value of α. Assuming a constant ventricular slope γ_1, the α value should be chosen on the biasing line $\alpha = 1 - (V_c/b)$ so that an equilibrium reference level of $b + c$ volts is obtained for maximum c and maximum γ_4.

What will be the initial change in border position after the slope has changed to γ_4 V/sec? The equilibrium position on line n, with $\alpha = 1 - (V_c/b)$, is given by equation (218) as

$$BP'_{equil} = \frac{b}{\gamma_1} + \frac{\frac{\alpha}{2}\,\Delta\gamma_1\left(1 - \frac{\gamma_2}{\gamma_1}\right) + (\alpha - 1)c}{\gamma_1\left[1 - \frac{\alpha}{2}\left(1 + \frac{\gamma_2}{\gamma_1}\right)\right]}$$

The sample levels on lines n and $(n+1)$ are

$$V_R(n) = \gamma_1(BP'_{equil} + \Delta) + c \tag{232}$$

$$V_L(n+1) = \gamma_4(BP'_{equil} - \Delta) + b\left(1 - \frac{\gamma_4}{\gamma_1}\right) + c \tag{233}$$

Substituting these equations into equation (85) gives the new reference level on line $(n+1)$:

$$V_{ref}(n+1) = b + \frac{\frac{\alpha}{2}(\Delta\gamma_1 + c)\left(1 - \frac{\gamma_4}{\gamma_1}\right) + \frac{\alpha^2}{2\gamma_1}(\Delta\gamma_1 + c)(\gamma_4 - \gamma_2)}{1 - \frac{\alpha}{2}\left(1 + \frac{\gamma_2}{\gamma_1}\right)} \tag{234}$$

Check – for $\gamma_4 = \gamma_2$ this results in

$$V_{ref}(n+1) = b + \frac{\frac{\alpha}{2}(\Delta\gamma_1 + c)\left(1 - \frac{\gamma_2}{\gamma_1}\right)}{1 - \frac{\alpha}{2}\left(1 + \frac{\gamma_2}{\gamma_1}\right)} = V'_{equil}$$

The initial change in voltage level is therefore

$$V_{ref}(n+1) - V'_{equil} = \frac{\frac{\alpha}{2\gamma_1}(1 - \alpha)(\Delta\gamma_1 + c)(\gamma_2 - \gamma_4)}{1 - \frac{\alpha}{2}\left(1 + \frac{\gamma_2}{\gamma_1}\right)} \tag{235}$$

for which

$$V_{ref}(n+1) - V'_{equil} > 0 \quad \text{for} \quad \gamma_4 < \gamma_2 \tag{236}$$

and

$$V_{ref}(n+1) - V'_{equil} < 0 \quad \text{for} \quad \gamma_4 > \gamma_2 \tag{237}$$

Thus, $V_{ref}(n+1)$ decreases when slope γ_4 increases and increases when γ_4 decreases since $V_L(n+1)$ changes accordingly. The final difference between V'''_{equil} and V'_{equil} is

191

$$V'''_{equil} - V'_{equil} = \frac{\frac{\alpha}{2}(1-\alpha)\left(\Delta + \frac{c}{\gamma_1}\right)(\gamma_2 - \gamma_4)}{\left[1 - \frac{\alpha}{2}\left(1 + \frac{\gamma_4}{\gamma_1}\right)\right]\left[1 - \frac{\alpha}{2}\left(1 + \frac{\gamma_2}{\gamma_1}\right)\right]} \tag{238}$$

Comparing $V_{ref}(n+1) - V'_{equil}$ and $V'''_{equil} - V'_{equil}$ results in

$$\left[V_{ref}(n+1) - V'_{equil}\right] - \left(V'''_{equil} - V'_{equil}\right) = \frac{\frac{\alpha^2}{4\gamma_1}(1-\alpha)(\Delta\gamma_1 + c)(\gamma_4 - \gamma_2)\left(1 + \frac{\gamma_4}{\gamma_1}\right)}{\left[1 - \frac{\alpha}{2}\left(1 + \frac{\gamma_2}{\gamma_1}\right)\right]\left[1 - \frac{\alpha}{2}\left(1 + \frac{\gamma_4}{\gamma_1}\right)\right]}$$

$$\tag{239}$$

which shows that the initial change in reference level is always less

than the final change.

192

CHAPTER 10: DYNAMIC REFERENCE LEVEL

As shown in chapter 9, an acceptable border point is detected under all reasonable conditions if the reference level is calculated according to the formula

$$V_{ref}(n+1) = \frac{\alpha}{2} \left[V_R(n) + V_L'(n+1) \right] + V_c \qquad (85)$$

In the contour detector prototype II, two sample points are defined in the background area. For the left border, the new formula for the reference level is

$$V_{ref}(n+1) = \frac{\alpha}{2} \left(VR + \frac{VL1}{2} + \frac{VL2}{2} \right) + V_c \qquad (82)$$

where VR is the video sample on the ventricular slope of LSPR (line n) and VL1 and VL2 are the video samples on the background slope at LSPL1 and LSPL2, respectively (chapter 8, fig. 49). These last two samples are taken on line (n+1).

The two sample points LSPL1 and LSPL2 are important in areas of low contrast where the actual video signal may be different from the assumed border model. At those places, the slope γ_2 often becomes negative, resulting in a reference level that is too high as calculated from equation (82). This situation is characterized by VL1 > VL2 and is recognized in the system. Under this condition, an error term $V_{error} = (VL1/2) - (VL2/2)$ is determined and subtracted from the term $(VL1/2) + (VL2/2)$ in the formula for the reference level. The effect is that the reference level is determined as if the border signal had a background slope of $\gamma_2 = 0$. On these bases, the final formula for the reference level can be written as

$$V_{ref}(n+1) = \frac{\alpha}{2}\left(\frac{VL1}{2}+\frac{VL2}{2}-V_{error}+VR\right)+V_c \tag{240}$$

where

$$\left. \begin{aligned} V_{error} &= \frac{VL1}{2}-\frac{VL2}{2}, &&\text{if } \frac{VL1}{2}>\frac{VL2}{2} \\ &= 0, &&\text{if } \frac{VL1}{2}<\frac{VL2}{2} \end{aligned} \right\} \tag{241}$$

The calculated value for the reference level on each line is based on a border model for which $VR-[(VL1/2)+(VL2/2)]>K$, where K is a dc voltage level. Because of intervening structures, situations occur where $VR-[(VL1/2)+(VL2/2)]<K$. This situation is recognized and, to avoid large excursions from previous points, the width of the expectation window is automatically made much smaller on the video lines satisfying this condition.

The implementation of the circuitry that calculates the dynamic reference level for the left border on a line-to-line basis and the dynamical adjustment of the expectation window are described here. The circuit diagram is given in figure 78.

Implementation of the Dynamic Reference Level

The sampled voltage level at LSPR must be held over almost a full line period until the next border point $g[(n+1)T]$ has been detected. Only the short period from $g(nT)$ until LSPR is then available for the track-and-hold amplifier to settle to the new sample level. This width LSWR is manually adjustable from 80 to 960 nsec in steps of 80 nsec. In most cases, an optimum border detection is achieved with LSWR equal to approximately 560 nsec. However, sometimes this width must be much smaller. For the used sample/hold modules in this particular

194

Figure 78.- Implementation of the circuitry for calculating the dynamic reference level.

195

application, an acquisition time of at least 200 nsec should be maintained for an accurate sampling of the video signal at LSPR. Therefore, the sampling at LSPR is done with two sample/hold modules LR1 and LR2; the control signals for the resulting four sample/hold amplifiers for the left border are shown in figure 79.
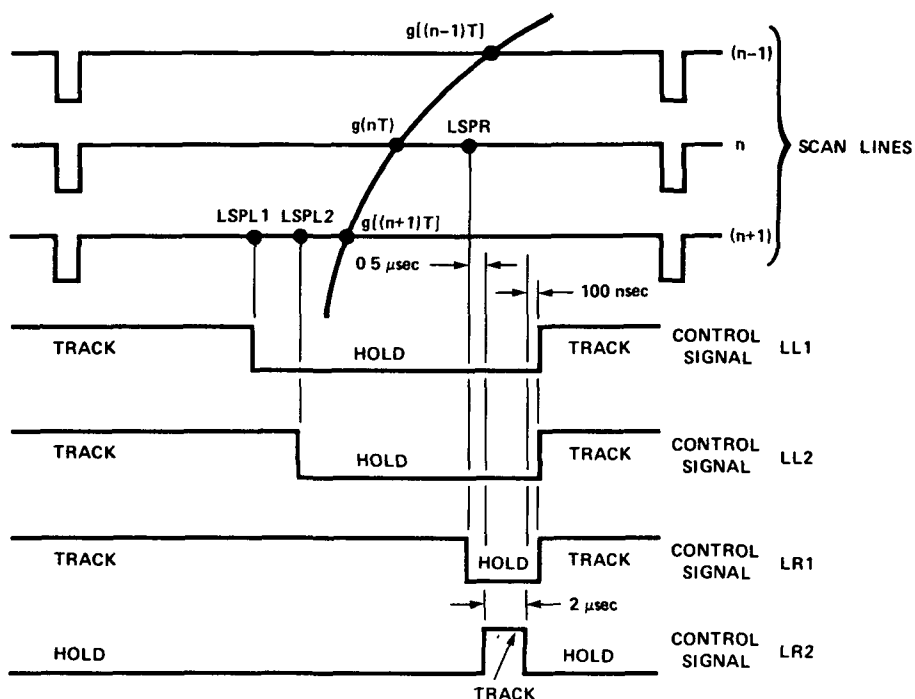

Figure 79.- Control signals track-and-hold amplifiers for the left border.

The hold command for S/H amplifier LR1 is given at LSPR and is held over a 2.6-μsec period. The first 0.5 μsec of this period allows the S/H switching transient to settle down. The following 2 μsec is the allowed acquisition time for S/H amplifier LR2, for which a slower type of S/H amplifier can be used. LR2 then samples the output voltage of LR1. An additional 100 nsec is allowed for the aperture time of S/H amplifier LR2. The hold commands for S/H amplifiers

LL1 and LL2 are given at LSPL1 and LSPL2, respectively, and are being held until the end of the hold period for LR1. As a result, all four video samples are available for further processing (dynamic expectation window width) during the last 100 nsec of this hold period.

The 1-MHz low-pass filtered video signal from the analog preprocessing circuitry (chapter 5) is applied to the input of S/H module LR1 and the positive input of the analog comparator (OP AMP 6) (see fig. 78). By use of an accurate resistive divider, the clamped video signal with half the amplitude of the original signal is applied to the inputs of S/H modules LL1 and LL2, resulting in output signals VL1/2 and VL2/2, respectively.

The video samples V_R, VL1/2, and VL2/2, and the negative error signal are applied to the negative input of OP AMP 1, which is used as a -1 amplifier. The output of this operational amplifier is therefore

$$V_{01} = -\left(VR + \frac{VL1}{2} + \frac{VL2}{2} - V_{error}\right) \qquad (242)$$

The error term is or is not included in this equation, depending on the setting of switch S1. The $\alpha/2$ factor in the formula for the reference level is implemented with a resistive divider at the output of OP AMP 1. Voltage follower OP AMP 2 acts as a buffer and its output signal equals

$$V_{02} = -\frac{\alpha}{2}\left(VR + \frac{VL1}{2} + \frac{VL2}{2} - V_{error}\right) \qquad (243)$$

where $0 \le \alpha \le 1$. The negative adjustable dc level of $-V_c$ volts is obtained with a potentiometer connected to a zenerdiode stabilized reference voltage of -6.2 V. The $-V_c$ volts and the output signal from OP AMP 2 are applied to the negative input of OP AMP 3, which is used as a

197

-1 amplifier. The output of this operational amplifier then equals

$$V_{03} = \frac{\alpha}{2} \left(VR + \frac{VL1}{2} + \frac{VL2}{2} - V_{error} \right) + V_c \qquad (244)$$

which is the required dynamic reference level. This signal is connected
to one of the inputs of a single-pole, double-throw junction FET switch.
Depending on the state of the switch, the output is then either the
dynamic reference level or the output signal from OP AMP 4, which
provides an adjustable dc level. This dc level is applied when a con-
stant reference level is selected for the border detection and for the
detection of the first left-border point when the dynamic reference
level mode is selected. The desired switch setting is achieved by apply-
ing the appropriate logic signal at the input of the high-speed switch
driver.

OP AMP 5 functions as a buffer for the reference level signal from
the FET switch. The buffered reference level is connected to the nega-
tive input of the high-speed comparator AM685 (OP AMP 6). This is a very
fast analog comparator with a maximum 6.5-nsec propagation delay at 5 mV
overdrive, a 3.0-nsec latch setup time, and complementary ECL outputs.
The latch function allows the comparator to be used in the S/H mode;
with the latch enable input high, the comparator functions normally.
When the latch enable is driven low, the comparator outputs are locked
in their existing logical states. The comparator is reset at each video
line during the horizontal synchronization pulse. As described in
chapter 5, when the left ventricle appears as a bright structure against
a dark background (cineangiogram), the video signal is clamped at ground.
During the horizontal synchronization pulse, the reference level is then

198

always higher than the video signal and enabling the comparator with the RESET pulse resets the comparator. If the ventricle appears as a dark structure against a lighter background (positive image from video disc/tape), the video signal is clamped at +2 V in the analog preprocessing circuitry. To reset the comparator under these circumstances, a reference level above +2 V is needed. The reference level is then pulled toward +3.3 V by saturating transistor Q1 during the horizontal sync pulse. The RESET pulse then again enables the comparator, which returns to the reset state.

To detect the left ventricular border, the comparator is enabled during the expectation window period only (explained in chapter 8 for the right border). For the left border, the comparator changes state as soon as the video signal becomes higher than the reference level, and the comparator is immediately disabled. The moment the comparator state changes, indicates the detected border position. The transition of the output signal results in the triggering of a monostable multivibrator (not shown in fig. 78), which generates a 100-nsec wide pulse for mixing into the video signal, so that a brightened point appears on the TV monitor.

Implementation of Error Term

The error term is generated with operational amplifiers OP AMP 7 and OP AMP 8. The sampled video level VL1/2 is applied to the positive input of OP AMP 7 and VL2/2, to the negative input. OP AMP 7 is used as a difference amplifier, resulting in an output voltage

$$V_{07} = \frac{VL1}{2} - \frac{VL2}{2} \qquad\qquad (245)$$

199

We are now interested to know when V_{07} is positive, that is (VL1/2) > (VL2/2). This is determined by use of the precision limiter circuit (appendix B). With the positive input of OP AMP 8 connected to ground, the output of the precision limiter is

$$V_{08} = -\left(\frac{VL1}{2} - \frac{VL2}{2}\right) = -V_{error} , \qquad \text{if } \frac{VL1}{2} > \frac{VL2}{2} \left.\begin{array}{c} \\ \\ \\ \\ \end{array}\right\}$$

and

$$V_{08} = 0 \qquad , \qquad \text{if } \frac{VL1}{2} < \frac{VL2}{2}$$

(246)

For an accurate limiter performance, an ultrafast operational amplifier (LH 0032) and hot carrier diodes are required. The video lines for which (VL1/2) > (VL2/2) can be indicated on the monitor screen with a brightened bar if a control signal is generated with the high-speed analog comparator NE 529 (OP AMP 9) (see fig. 80).
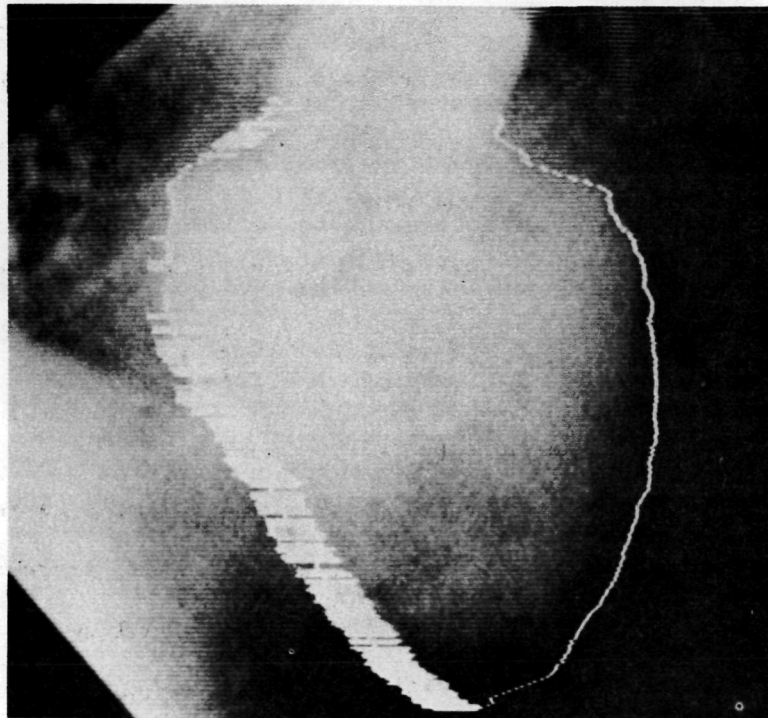

Figure 80.- The horizontal brightened bars indicate the video lines for which (VL1/2) > (VL2/2) for the left border.

200

At places of low contrast along the left ventricular border, forced border points may be generated at the beginning or end points of the expectation window. As explained in chapter 3, this occurs when the video signal does not cross the reference level during the expectation window period. If these forced border points are generated over a number of consecutive video lines, then the defined border is a straight line when the zeroth-order line extrapolation principle is used and a parabola for the first-order line extrapolation principle. The changes in border positions from line to line are determined by the selected expectation window width. It is clear that, after a few lines, the defined border may be too far from the actual border to be able to return if the contrast improves.

This instability can be avoided by automatically narrowing the expectation window width under low contrast conditions so that only limited excursions from previous border points are allowed. The chosen criterion for this dynamical adjustment is that the voltage levels $(VL1/2) + (VL2/2)$ and V_R are of comparable magnitude, that is,

$$VR - \left(\frac{VL1}{2} + \frac{VL2}{2}\right) < K \qquad (247)$$

where K is an adjustable positive dc level.

Because the new expectation window widths must be known before the positions of LEPL, LSPL1, and LSPL2 for line $(n+1)$ are calculated at the end of line n, the sampled video levels on line n are used in equation (247). This means that the applied expectation window width on a line is determined by the video samples on the previous line. The

fact that no video sample at the current line is used can be justified since the difference between the video samples on either side of the contour changes very little from line to line. Also, in this simple case, only a binary value is assigned to the calculated difference VR − [(VL1/2) + (VL2/2)]; if this difference satisfies equation (247), then the width is adjusted; otherwise, it is not.

The above described criterion has been implemented with OP AMP's 10 and 11 (fig. 78). Operational amplifier OP AMP 10 is used as a difference amplifier with the output voltage of S/H amplifier LR1 applied at its positive input and VL1/2 and VL2/2 at its negative input. The output voltage is given as

$$V_{010} = VR - \left(\frac{VL1}{2} + \frac{VL2}{2}\right) \tag{248}$$

which is connected to the B input of the analog comparator NE 529. The adjustable dc level of K volts is obtained from a zenerdiode-stabilized dc level of 6.2 V with a 1k potentiometer. The S/H control signal for LR2 is used as a strobe signal for the comparator. This pulse appears inverted at the A output of the comparator if VR − [(VL1/2) + (VL2/2)] > K volts; in this case, the width of the expectation window need not be adjusted. For sample levels satisfying equation (247), the A output remains high.

The actual implementation for dynamically adjusting the expectation window width is given in figure 81. With the output voltage of the analog comparator OP AMP 11 (fig. 78) applied to the D input of flip-flop DFN1a, this voltage level is sampled at 100 nsec after the beginning of the strobe signal for the comparator, resulting in a high output
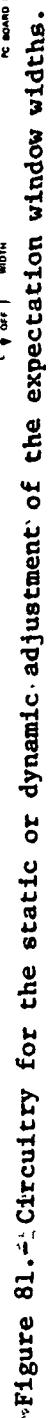
202

Figure 81.—Circuitry for the static or dynamic adjustment of the expectation window widths.

level, if $VR - [(VL1/2) + (VL2/2)] < K$ and remaining low otherwise.

Flip-flop DFN1a is cleared by the low level from switch DWS if one does not want to use this dynamic adjustment of the expectation window width and by the signal from ANM2c, which prevents it from using during the initial detection period, where necessary large excursions occur (mitral valve) under often fairly low contrast conditions.

The Q output of DFN1a functions as the SELECT signal for multiplexers MUN1 and MUN2. The A channel is selected if no dynamic expectation window width is required and the B channel if it is required. The expectation window widths LEWL and LEWR, each represented in 4 bits, are connected to the A-channel inputs of MUN2 and MUN1, respectively. With the A channel selected, the expectation points LEPL and LEPR are determined in the usual way as described in chapter 8 for the right border. The 4-bit binary full adder ALN1 provides LEWL + LEWR, necessary to determine LEPR.

In case of a dynamic adjustment of the expectation window width, the expectation window is chosen symmetrically around its center. The width is adjustable manually in four steps with rotary switch LAEW: each position change of the switch corresponds to a 40-nsec change in actual width. Under practical conditions the static expectation window widths LEWL and LEWR are adjusted to a much wider width than 4×40 nsec = 160 nsec; therefore, limiting the dynamic width to a maximum of 160 nsec certainly means a much more restricted expectation window width. The switch position of LAEW is again converted to a 3-bit binary number in a similar manner as for the other rotary switches. This 3-bit number plus a fourth bit, which is always zero, is selected

by MUN1 and MUN2 if the Q output of DFN1a is high, and the new expectation points LEPL and LEPR on the following video line are determined according to this new width. The current implementation of the dynamic expectation window width is clearly a relatively simple adjustment since only one threshold level is checked. The four possible widths, as presently selected manually with LAEW, can be determined automatically by implementing four different threshold levels. Before implementing this more complex system, more experience with the system is required to determine its feasibility. The implemented dynamic system has proven to be effective in obtaining a more stable outline under low-contrast conditions.

Page intentionally left blank

CHAPTER 11: EVALUATION OF THE CONTOUR DETECTION AND DATA

ACQUISITION SYSTEM

A quantitative evaluation of the success of the border algorithm has been carried out. For this purpose, eight aluminum ellipses are used, as well as four post-mortem dog casts and two series of canine left ventricular angiograms. The ellipses range in size from 17.73 to 71.36 cm^2, with major-to-minor axis ratios of 2:1. These sizes correspond to the projections of eight prolate ellipsoids with circular cross sections, ranging in volume from 40 to 320 cm^3 in steps of 40 cm^3.

Because the output from both the contour detector and the conventional manual method are the absolute coordinates of the detected structures, the areas and the distances from the border points to the chord, connecting the left-hand side of the aortic valve and the apex, are calculated and compared for both methods.

Image Analysis System

Figure 82 is a block diagram of the image analysis system as implemented in the Cardiovascular Research Laboratory at Ames Research Center (ref. 59).

The left ventricular outline is manually traced using an Adage Graphpen System. The cineangiograms of a left ventricular study to be processed are mounted on a film editor and a selected frame is projected onto the transparent graphic tablet. The pen position may be sampled in a single point or in a continuous (40 points/sec) mode, so that discrete points can be selected or smooth curves drawn. The resolution of the sonar stylus position is 0.25 mm over the entire 35- by 35-cm tablet
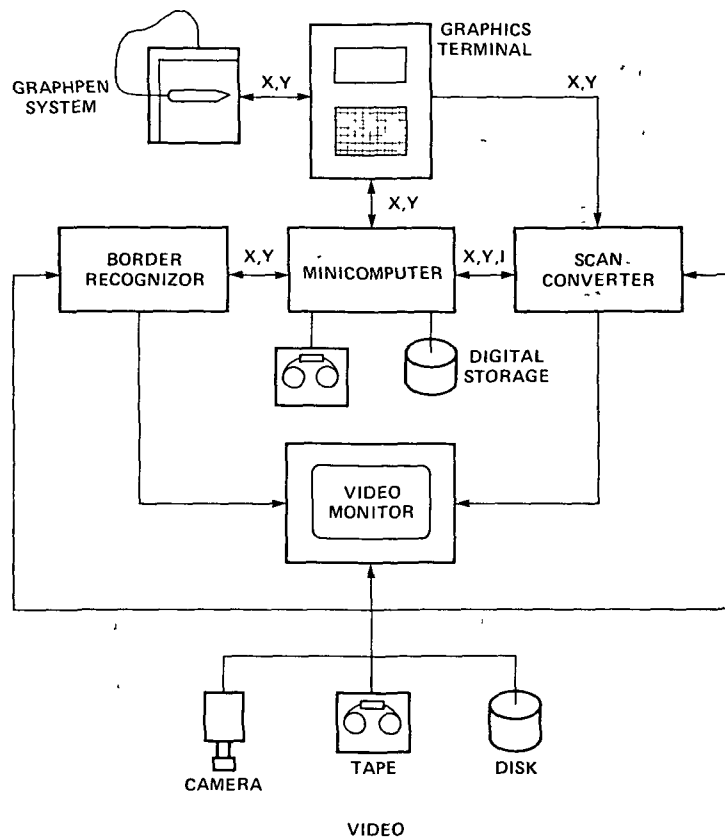
Figure 82.- Image analysis system. Left ventricular outlines can be
stored in computer memory in two input modes: (1) manually using
graph pen on either projected cine frame or displayed video image and
(2) real time using the border recognizer.

area. The coordinates obtained are stored in the minicomputer and dis-

played simultaneously on the screen of the Adage 100B Graphics Terminal.

By use of the Ampex DR10 video disc in the stop-action mode, a

selected video frame can also be analyzed manually by mixing the x-y

cathode ray tube signal from the graphics terminal into the video signal

by way of the Hughes 639 scan converter.

For the contour detector, the coordinates of the detected border

points are stored in computer memory through the computer interface (as

described in chapter 4). It was explained in chapter 4 that consecutive

208

memory locations contain alternately the x coordinates of the left and right borders, respectively, while the y coordinates of the starting point and outpulse are the last transferred coordinates per video field. The beginning and end points of the aortic valve are distinguished from the rest of the x and y coordinates by means of an extra flag bit. The x and y coordinates of the two discrete points are stored in the first four memory locations of a particular field file.

The data sequence from the manual editor is somewhat different. For a selected angioframe, the x and y coordinates of the two discrete points are stored first. After this, the outline is traced from the end point of the aortic valve, along the right border to the apex, and back to the beginning point of the valve along the left border. For each sample point, the x and y coordinates are stored; the number of sample points per outline depends on the speed with which the outline is being traced. Finally, the x and y coordinates of the beginning and end points of the aortic valve plane are stored as discrete points. The aortic valve plane is only defined by these two points.

Because of the different data formats for both systems, a reformatting program was written for the contour detector, which translates the stored data into the same format as obtained from the manual editor (ref. 60). This reformatting is initiated from the teletype by the operator after all the required data are stored in the computer. The program checks at the same time to see if the number of x coordinates per video field equals twice the difference in the y coordinates of the starting point and outpulse plus two; an "illegal frame" has been stored if this condition is not satisfied. Now that the video detected

outline is in the same format as defined for the manual editor, all existing programs for subsequent data processing of the ventricular margin can be applied and a comparison between the automated and manual method is possible.

To compare the two methods, it is important to recognize potential sources for errors.

Possible Error Sources

The errors that might occur in the automatic and manual border recognition methods are categorized as follows:

(1) Parallax

(2) Border-tracking jitter

(3) Border definition criteria

(4) Inaccuracies in the obtained border coordinates as a result of the limited resolution

(5) Linear and nonlinear magnification in the x-ray and optical system.

Parallax- Generally, parallax can be described as an apparent change in the direction of an object by a change in observational position, which provides a new line of sight. This error is applicable for the manual editor, where the image is projected from underneath onto a transparent plate. The border coordinates are computed by pointing the sonar stylus at the left ventricular margin from the viewing side. It is clear that parallax errors occur if the tablet is viewed from different angles. A correct border coordinate is obtained if the eyes of the observer are in a plane perpendicular to the tablet with the selected point lying in this plane and the distances from the eyes to the point being equal. This error is not applicable for the contour

210

detector because the detected border points and the starting point (for computing the discrete points) are mixed into the video signal and displayed at the same physical level as the left ventricular image.

The percentage of error caused by parallax can be estimated by pointing repeatedly at a discrete point from different viewing angles and comparing the resulting coordinates. In practice, this error will be very small if one is aware of this problem and therefore views the outline from the correct angles.

Border-tracking jitter- Assuming we have a well-defined margin, multiple manually tracings of the same margin will result in slightly different results. The human hand is not steady enough to exactly trace the same outline each time. In the video system, border jitter occurs because of the limited signal/noise ratio.

The magnitude of this error can be estimated by tracing a well-defined margin repeatedly. For the manual method, one should then view the border each time from the same angle. The differences in the obtained border coordinates are then a measure for the border-tracking jitter.

Border definition criteria- In actual angiograms, contrast is often fairly low, making it difficult to define exactly where the border is. An investigator may want to draw the outline slightly different from where the automatic method detects the border. This error will be even more important if different investigators trace the same angiogram. This error is, of course, small if we have well-defined borders as for the x-ray films of the aluminum ellipses. However, for actual angiograms, this type of error will be the largest of the five possible errors.

Inaccuracies in border coordinates as a result of limited resolution- Inaccuracies occur because of the limited number of bits available to determine a border coordinate. The Graphpen System determines each position in 12 bits, resulting in an accuracy of 1 in 4096. For the video system, the x and y coordinates are each determined in an 8-bit format, giving an accuracy of 1 in 256. To calculate the size and shape of the left ventricular cavity, this accuracy is sufficient because the resulting error will be small compared with other possibly occurring errors.

Linear and nonlinear magnification in x-ray and optical systems- To correct for linear and nonlinear (from nonparallel x-ray beams and distortion due to recording or projection systems) magnification, a magnification factor must be determined. Generally this magnification factor will be position dependent. The techniques used to handle these problems will be described later in this chapter. The detected outline can then be reconstructed spatially - as it occurs inside the chest - using an appropriate computer program. This method will effectively compensate for the errors due to nonlinearities in the recording and projection systems.

From this short discussion on the possibly occurring errors, it is clear that repeatedly tracing a well-known, well-defined outline, as for the x-rayed aluminum ellipses, will provide an estimate of the over-all error that results from categories 1, 2, 4, and 5. Because these four possibly occurring errors are expected to be small and of about the same magnitude, no attempt has been made to separate them. In the day-to-day routine with actual left ventricular angiograms, the error due

212

to the border definition criteria will be the largest of the five
possible errors.

X-ray Coordinate System

The single-plane fluoroscopic system in the Cardiovascular Research
Laboratory at Ames is illustrated in figure 83. It consists of a vari-
able 15/22.5-cm image intensifier with both 35 mm film and video
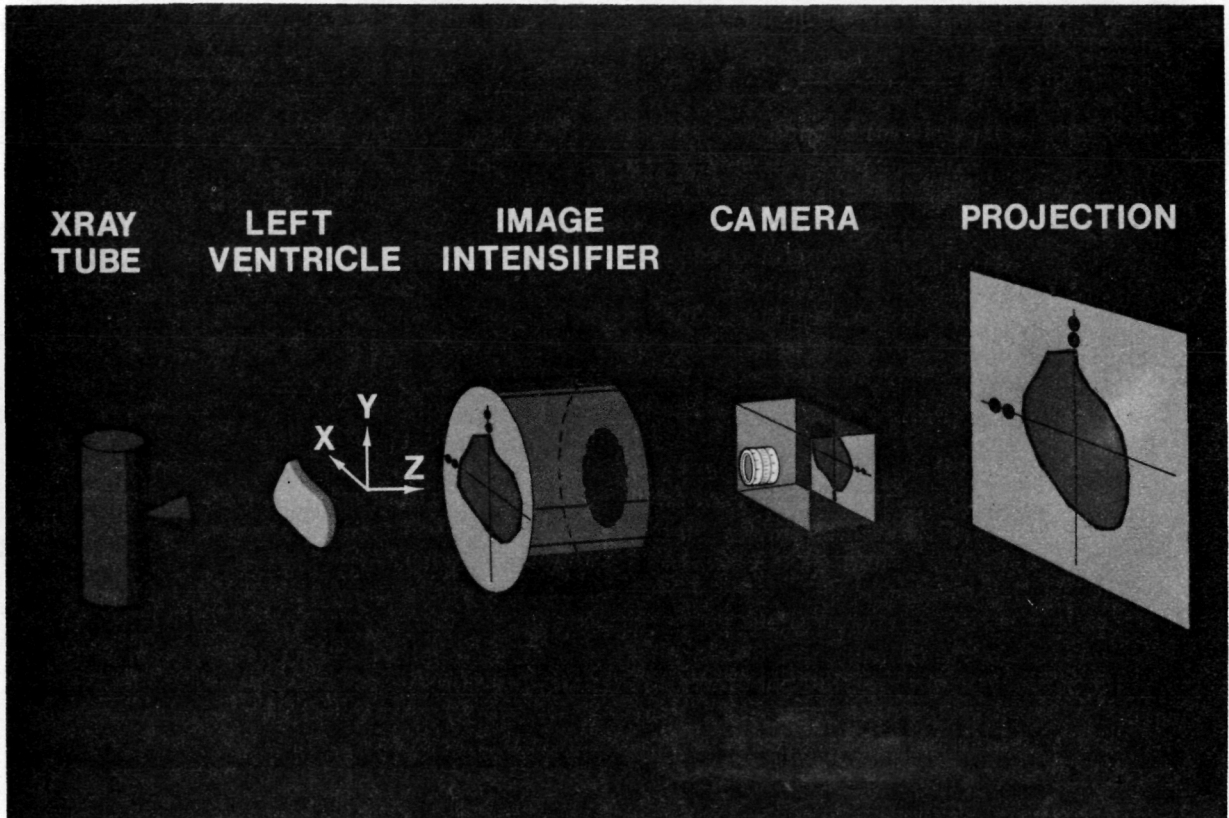recording.

Figure 83.- Single-plane fluoroscopic system in the Cardiovascular
Research Laboratory. The x-rayed structure undergoes linear and
nonlinear magnifications before it is projected on a viewing screen.

To accurately measure the changes in left ventricular size and
shape over a heart cycle, an external x-y-z coordinate system must be

213

used. This coordinate system is defined by the positions of lead beads on a calibration plate attached to the face of the image intensifier (fig. 83). Actually, only two lead beads are required, one on the x axis and the other on the y axis; both points are placed 6.35 cm from the origin of the plate. These two positions are used to calculate the position of the origin and to indicate the angular position of the object with respect to this coordinate system.

The reasons for not simply providing a lead bead at the origin are: (1) the resulting dot in the projected image has such a high brightness level that it may interfere with the border algorithm and (2) it may not be possible to distinguish the projected lead bead in the contrast-filled left ventricular cavity. By placing the two lead beads sufficiently far from the origin, the abovementioned situations will not occur, if one assures that the contrast-filled structure is about in the center of the image. Originally, lead-filled crosshairs were provided on the calibration plate, as shown in figure 83. With the manual editing system the origin was simply defined by pointing at the center of the crosshairs with the sonar stylus. However, the high brightness projections of the crosshairs interfered with the automatic border algorithm, giving reason to remove them from the calibration plate.

The projections of the two earlier defined lead beads are the discrete points whose coordinates must be stored in computer memory (chapter 4). Assuming that the calibrated (projected back to face of image intensifier) values of the x and y coordinates of the two lead beads are determined as (x1, y1) and (x2, y2), respectively, the origin of the external coordinate system is computed as

$$x0 = \frac{x1 + x2}{2} - \frac{y2 - y1}{2} \qquad (249)$$

$$y0 = \frac{y1 + y2}{2} + \frac{x2 - x1}{2} \qquad (250)$$

as shown in figure 84. Note that the calibrated values of the x and y coordinates should be used in this calculation because the video-defined x and y coordinates do not have exactly the same dimensions. The order in which the two discrete points are stored in memory should always be the same.
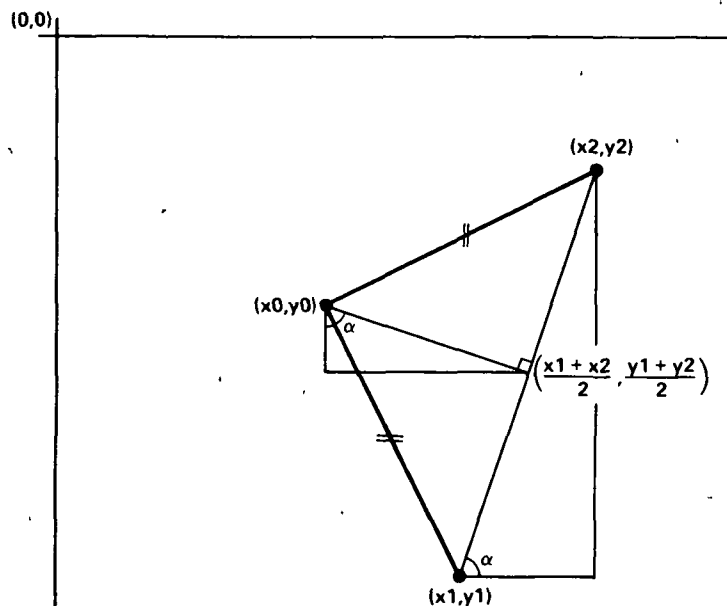

Figure 84.- The origin of the external coordinate system can be calculated from the two lead bead positions (x1, y1) and (x2, y2), respectively.

Image Transformations

A projected angiogram, displayed on a video monitor or on the transparent tablet of the manual editor, has been subjected to linear and nonlinear magnifications. First, the x-rayed structure is linearly magnified by the diverging x-rays before it is recorded on the image

215

intensifier. This magnification factor is defined as the ratio of the distances from the x-ray tube to the image intensifier and from the x-ray tube to the object. Second, linear and nonlinear magnifications occur from the image intensifier to the projection screen, caused by the curvature of the image intensifier face, lenses of recording and projection systems, and nonlinearities in the scanning systems for video recordings. To accurately correct the obtained left ventricular outlines back to actual or real dimensions, it is important to account for these linear and nonlinear magnification factors. Although modern recording and projection systems are nearly linear, it is still important to consider the slight nonlinearity for an accurate determination of the spatial or actual coordinates of the object being measured. This is particularly true for volume calculations where readjusted or corrected values are cubed.
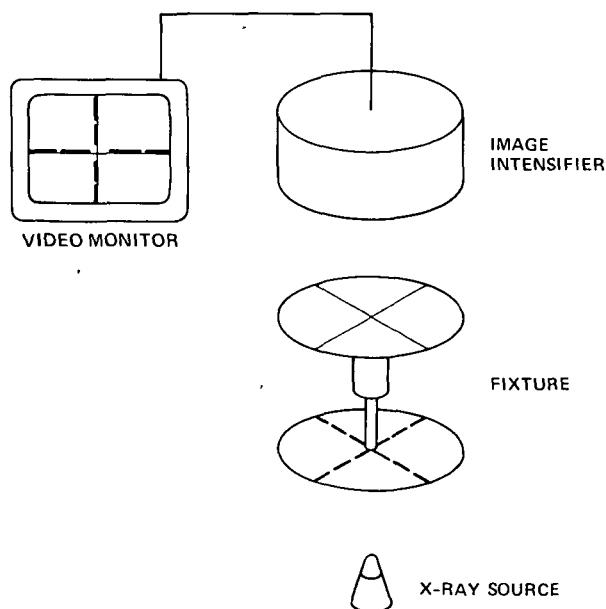
The image intensifier must be aligned to reduce nonlinearity and skew by attaching the fixture shown in figure 85 to the face of the image intensifier instead of the calibration plate before a left ventricular study is performed. The crosshairs on the two plates will line up on the video monitor only when the focal axis of the

Figure 85.- The image intensifier is aligned with respect to the geometric center of the x-ray beam by an alignment fixture.

image intensifier coincides with the central beam of the x-ray source. The origin of the calibration plate is coincident with that of the fixture. It is important that the fixture and the calibration plate be nonmagnetic to prevent distortion caused by interference with the electromagnetic field of the image intensifier.

An overall magnification function from the face of the image intensifier to the projection screen can be obtained by attaching a different calibration plate to the face of the image intensifier. This calibration plate is provided with lead beads placed on concentric circles with respect to the focal center of the image intensifier. An x-ray film is taken of this configuration and placed on the manual editor so that the position of the center of the calibration plate coincides as accurately as possible with the center of the projection screen. Because the distances from the lead beads to the center of the calibration plate are known in cm, the magnification factor of each lead bead can be determined, expressed in coordinates/cm. For the manual editor, it was shown (ref. 13) that the overall magnification factor M can be moduled to consist of two terms: a constant M_0 and a term $M_1 \cdot R$, which is directly proportional to the distance from a point to the origin of the x-y axis (fig. 86). The magnification factor is constant for the positions on a concentric circle.

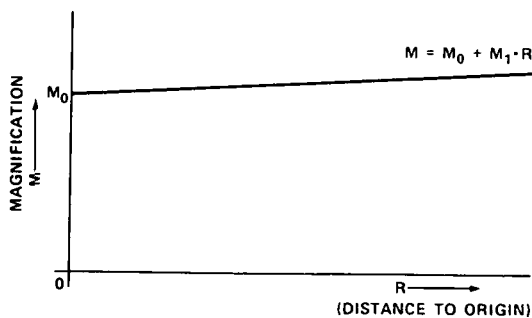For the video system, we must distinguish two

Figure 86.- The overall magnification factor M from the image intensifier to the projection screen is a linear function of the distance from a point to the origin of the calibration plate.

magnification factors, one for the x coordinates and one for the y coordinates, because the x and y coordinates are not expressed in the same units. The x coordinate of a point is determined by counting the number of 5-MHz clock pulses from the horizontal synchronization pulse to this border point, and the y coordinate is the video line number. This will clearly result in different magnification factors.

The same film of the calibration plate with lead beads on concentric circles is used for the video system. This film is positioned on the light table so that the projected origin of the calibration plate coincides with the center of the horizontal and vertical video scans and the x, and y axes of the plate coincide with and are perpendicular to the scan lines, respectively. With the contour detector in the DISCRETE POINTS mode, the starting point is positioned at each projected lead bead and enabling the computer interface over a one-field period results in the storage of the x and y coordinates of a selected point in the computer. This procedure is followed five times to average out possible pointing errors. To calculate the magnification function for the x coordinates, only the computed magnification factors for the points on the x axis (y = 0) are used. The regression equation for the obtained factors is defined as the magnification function. The regression equation is now assumed to be valid for each x coordinate, independent of the y value. This can be justified by projecting the lead beads on the concentric circles back to the face of the image intensifier using the obtained regression equations. The x coordinates of the calculated and actual lead bead positions agreed within 1 mm for all cases, which is sufficiently accurate. In exactly the same way, the regression

equations are determined for the y magnification function using only the lead bead positions on the y axis. Again, these equations are assumed to be independent of the x coordinate, which was checked by comparing the positions of the projected points and the actual lead beads. The positions again agreed within 1 mm. This procedure is equally applicable if the stored data on the video disc are used.

For the actual evaluation, the areas of the ellipses, casts, and left ventricular angiograms are computed for both systems as well as the distances from the borders to the defined chord. The necessary programming steps are described briefly (refs. 60 and 61).

After the detected outline has been stored in computer core memory and thereafter on the disk, the data are reformatted into the required format with program FORM3. The next step is then to project the outline back to the face of the image intensifier and to define the outline with respect to a new coordinate system, formed by the x and y axes of the calibration plate. This projection is done with a program called CVRT, and is achieved by applying the appropriate magnification factor for each point along the outline. The area, longest chord, and volume (according to the area/length method) are then computed with program VOL1. This program asks for the linear magnification factor from the object to the image intensifier face so that the final results will be in actual or real dimensions.

For the comparison between the video and manual system, the outline is rotated so that the chord from the left-hand side of the aortic valve plane to the apex is vertical; for this, a program CONMAN is executed. This separates the outline into a left and a right side. The chord is

now divided into 100 equidistances and, for both sides of the outline, the distances from the outline to the chord are calculated. This is done in exactly the same way for the manually traced outline, and the mean and standard deviations of the differences in the distances are calculated for each side, resulting in a measure of the accuracy with which the two outlines agree; this final step is done with the program called HANSAL. The mean and standard deviations are given in millimeters. Also, the difference in area involved is calculated for each side in cm^2 and in a percentage of the average value of the complete left ventricular areas, determined by both the video and manual methods.

It is clear that this kind of comparison depends very much on the positions of the left-hand side of the aortic valve and the apex. At the time that the cineangiograms were processed with the video system, the starting point and simulated aortic valve plane were positioned very precisely, so as to coincide as accurately as possible with the manually defined positions. An obvious solution would be to use the external coordinate system to overlay the outlines. This works perfectly if we compare outlines from the same system, but additional shifts and rotations in the positions of the outlines occurred when corresponding outlines from the two systems were mathematically overlayed. Apparently, this is a result of differences in the calculated origin due to pointing errors and slight differences in the magnification factors. More work must be done to determine exactly the error sources in this case and to solve this problem. Because of these additional shifts and rotations, this method was not applied for comparing the outlines, but the distances to the defined chords were compared instead.

220

Finally, the results of the evaluation are described in the last part of this chapter.

Evaluation Data

Ellipses- The x-ray images of the eight aluminum ellipses were processed by both the manual and video systems and the calculated areas were compared with the true areas. The results are given in table 1. Figure 87 is a photograph of one of the x-rayed ellipses as viewed on a TV monitor.
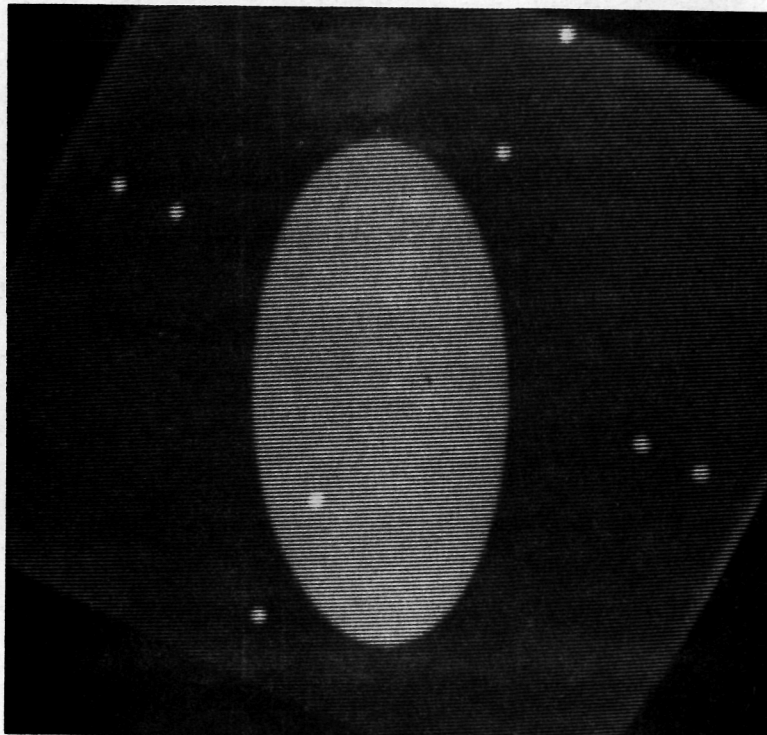

Figure 87.- X-ray picture of aluminum ellipse.

For the manual method, the areas are determined within an accuracy of 1.18 percent for the first six ellipses and 2.27 percent for the two largest ellipses. For the video method, the accuracy of all but the largest ellipse is better than 0.64 percent. Only the largest ellipse

TABLE 1.- CALCULATED AREAS FROM MANUAL AND VIDEO PROCESSING FOR THE EIGHT ALUMINUM ELLIPSES

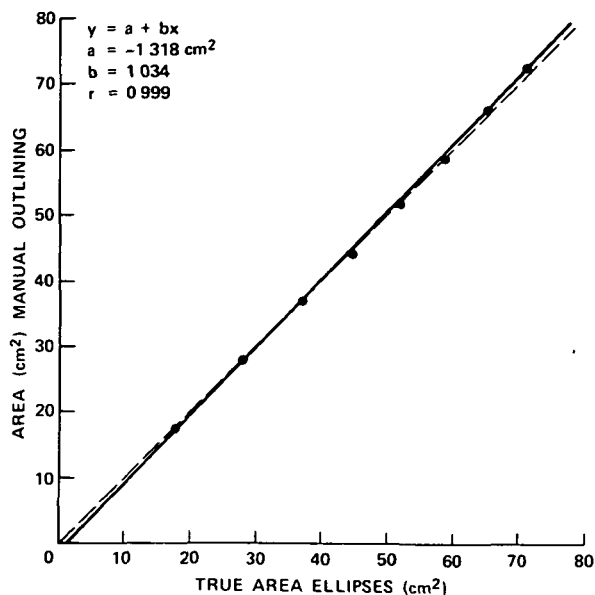| Ellipse	True area, cm^2	Manual processing		Video processing	
		Measured area, cm^2	Percentage difference	Measured area, cm^2	Percentage difference
1	17.73	17.61	-0.68	17.76	+0.17
2	28.24	27.95	-1.03	28.42	+.64
3	37.10	36.88	-0.59	37.10	+.00
4	44.79	44.26	-1.18	44.94	+.33
5	52.12	51.98	-0.27	52.34	+.42
6	58.83	59.25	+0.71	58.84	+.02
7	65.15	66.51	+2.09	64.91	-.37
8	71.36	72.98	+2.27	70.40	-1.35

Figure 88.- Comparison of calculated areas from manual outlining with true areas for the aluminum ellipses. The dashed line is the line of identity and the solid line is the regression line.
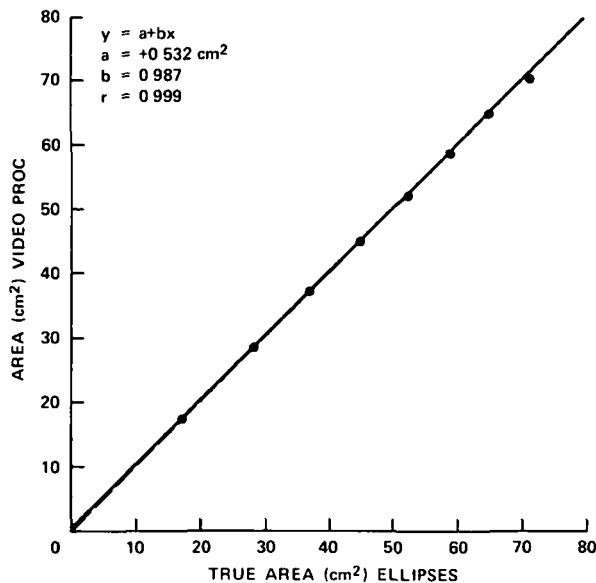

Figure 89.- Comparison of calculated areas from video processing with true areas for the aluminum ellipses. The dashed line is the line of identity and the solid line is the regression line.

is off by 1.35 percent. Note that the areas of the largest ellipses are much greater than the areas encountered for normal left ventricular cavities, or those with mild disease states.

The regression analysis of the computed areas from the manual and video methods with the true areas are given in figures 88 and 89, respectively. The correlation coefficients for both methods is $r = 0.999$.

To determine the reproducibility with which an area can be determined, the smallest, middle, and largest ellipses were each processed five times. The calculated standard deviation was then used as a measure for this reproducibility. The results are given in table 2. These results show that the reproducibility for the video system is an order of magnitude better than for the manual method.

223

TABLE 2.– THREE ELLIPSES WERE EACH PROCESSED FIVE TIMES WITH THE MANUAL AND VIDEO METHODS. THE STANDARD DEVIATION OF THE CALCULATED AREAS IS A MEASURE FOR THE REPRODUCIBILITY.

Ellipse	True area, cm^2	Manual processing			Video processing		
		Measured area, cm^2, mean	Standard deviation, cm^2	Standard deviation, percentage of mean	Measured area, cm^2, mean	Standard deviation, cm^2	Standard deviation, percentage of mean
1	17.73	17.61	0.20	1.14	17.76	0.02	0.11
4	44.79	44.26	.66	1.49	44.94	.07	.16
8	71.36	72.98	.45	0.62	70.40	.02	.03

On the average, the inaccuracy in the determination of the area of a normal-sized angiogram due to errors of categories 1, 4, and 5 will be less than 1 percent for manual processing and less than 0.64 percent for video processing. Repeatedly processing the same outline results in a standard deviation of less than 1.49 and 0.16 percent for manual and video processing, respectively.

Casts- Four post-mortem canine left ventricular casts were positioned in a specially constructed fixture under the image intensifier so that the orientation would be the same as during life in a dog. The casts were x-rayed and the resulting images processed by both methods. The outline of each cast was determined five times so that the reproducibility could be assessed at the same time. *The obtained outlines were projected back into space using the appropriate magnification factors.*

The results are given in table 3.

The areas of the obtained outlines agree within 1.20 percent and the reproducibility for the video system is, on the average, a factor of 7.5 times better than for the manual system. The regression analysis of the computed areas from video processing with the areas from manual outlining is given in figure 90. The correlation coefficient is 0.999.

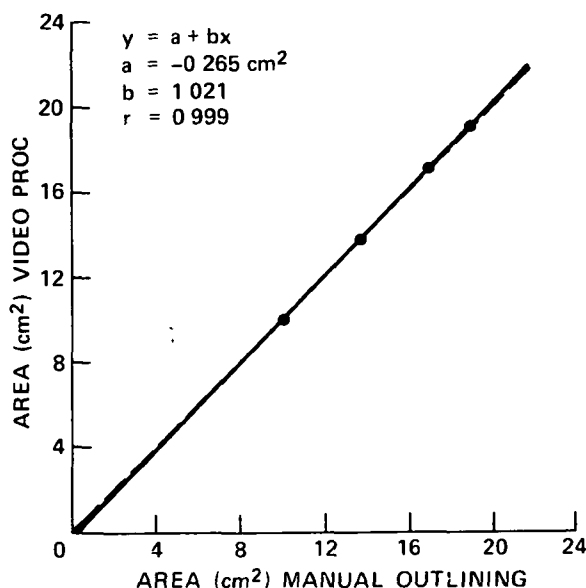The results of the border comparisons are given in table 4.

Figure 90.- Comparison of calculated areas from video processing with areas from manual outlining for four post-mortem casts. The dashed line is the line of identity and the solid line is the regression line.

$y = a + bx$
$a = -0\ 265\ cm^2$
$b = 1\ 021$
$r = 0\ 999$

AREA (cm^2) VIDEO PROC

AREA (cm^2) MANUAL OUTLINING

225

TABLE 3.- CALCULATED MEAN AREAS AND STANDARD DEVIATIONS FOR FOUR POST-MORTEM DOG CASTS

Cast number	Manual outlining			Video processing			
	Mean area, cm^2	Standard deviation, cm^2	Standard deviation, percentage of mean area	Mean area, cm^2	Percentage difference with manual method	Standard deviation, cm^2	Standard deviation, percentage of mean area
1	18.92	0.16	0.85	19.03	+0.58	0.02	0.08
2	16.88	.15	.89	16.94	+.36	.02	.12
3	13.64	.24	1.76	13.79	+1.10	.04	.28
4	10.03	.30	2.99	9.91	-1.20	.05	.53

TABLE 4.- STATISTICAL ANALYSIS OF THE DIFFERENCES IN LEFT- AND RIGHT-BORDER COORDINATES FOR

CORRESPONDING MANUALLY AND VIDEO PROCESSED OUTLINES

Cast number	Left border				Right border			
	Mean deviation, mm	Standard deviation, mm	Area deviation, cm^2	Percentage area deviation of mean total area	Mean deviation, mm	Standard deviation, mm	Area deviation, cm^2	Percentage area deviation of mean total area
1	-1.32	1.59	-0.77	-4.06	+1.60	0.79	+0.93	+4.90
2	-2.66	1.25	-1.39	-8.22	+3.40	1.11	+1.79	+10.59
3	-0.81	1.43	-0.43	-3.14	+0.37	0.79	+0.20	+1.46
4	+0.90	1.68	+.45	+4.51	-.04	1.70	-.02	-0.20

For both sides of the outlines, the mean and standard deviations of the differences in the distances from the border points to the corresponding chord, measured at equidistances along these chords, are given in millimeters. With the total area for each outline divided in this way into 99 slices, each with the same width, for both the left and right sides, the differences in area between the two outlines are also given in cm^2 and as a percentage of the average value of the total areas of the two outlines. For both the distance and area comparisons, a negative sign means that the video-detected outline is "inside" the manually traced outline. With each cast being processed five times for the manual and video methods, only the first outline of each series of five was used for the above described comparisons.

These data need to be interpreted with caution. For cast 2, for example, relatively large deviations result with comparable magnitude and of different signs. This is really the result of slightly different positions for the aortic and/or apex points for both outlines. The apex point is determined with a software routine as the point farthest removed from the left-hand side of the aortic valve plane. Consider the case when the defined aortic valve points coincide but the positions of the apex points are slightly different. For the comparison routine, this is as if one outline had been rotated about the aortic valve point, resulting in positive and negative deviations. If this rotation is not negligible, then the magnitude of these deviations will be comparable because the deviations due to border inaccuracies are generally relatively small.

228

There are several reasons for the inaccuracy in the determination of the apex point. First, the sampling rate of the stylus position for the manual method is low (40 samples/sec), usually resulting in a number of coordinates per outline between 50 and 70. The number of coordinates per outline from the video system was greater than 140 for the casts, depending on the size of the x-ray shadow. Second, the distance between the left and right border at the apex for the video system was relatively wide. The casts were positioned in a fixture between metal pins, two at the aortic valve plane and one at the apex. These pins appeared in the x-rayed images as structures with a higher brightness level than the casts, so that the distance between the borders at the apex could not be made as small as is usually possible.

The above described inaccuracies make clear that the optimum solution will be to overlay the two outlines mathematically. It was explained earlier in this chapter that shift and rotational problems must be solved before this improved method can be applied.

If we omit the results of cast 2 from these evaluations, because it is obvious that the relatively large deviations result from a rotational problem, then we can say that the mean and standard deviations of the borders for both sides are within 1.60 and 1.70 mm, respectively. The area deviation per side is then better than 4.90 percent in the remaining cases. The calculated deviations are expressed in millimeters and cm^2, respectively, because the outlines were corrected back to actual dimensions. Note that the contrast of the x-rayed casts was generally relatively low, clearly resulting in differences between the two methods.

Figure 91(a) shows a hard copy of the five outlines of cast 3, mathematically overlayed, as determined by the manual system. The five video-detected outlines of the same casts are shown in figure 91(b). These figures clearly show the much better reproducibility of the video system.
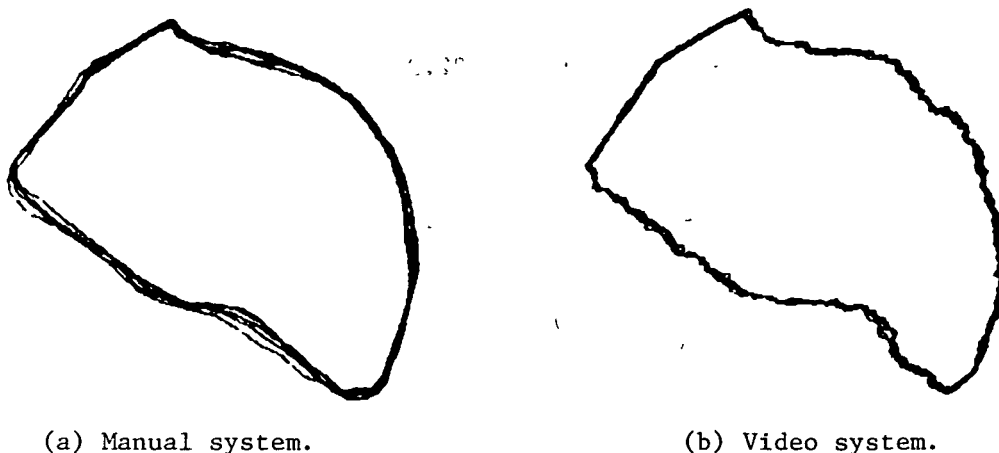

(a) Manual system.   (b) Video system.

Figure 91.- With an external coordinate system the obtained outlines can be mathematically overlayed. This figure shows the results when cast 3 is processed five times for the manual and video systems.

Left ventricular angiograms- Two series of left ventricular angiograms were processed by both methods. Every other cine frame from diastole to systole was used for this purpose. The obtained outlines were corrected for linear and nonlinear magnifications. The calculated areas for the first series of angiograms are given in table 5. For most outlines, the video system determines the area about 2 to 4 percent smaller than for the manually traced contours. The regression analysis of the computed areas from video processing with the areas from manual outlining is given in figure 92. The correlation coefficient is 0.996. The volume vs. time curves are shown in figure 93; the solid function represents the calculated areas from video processing and the dashed

230

TABLE 5.- CALCULATED AREAS FROM MANUAL AND VIDEO PROCESSING FOR

14 FRAMES OF THE FIRST SERIES OF LEFT VENTRICULAR ANGIOGRAMS

Frame	Manual outline measured area, cm^2	Video processing measured area, cm^2	Percentage difference with manual method
123	20.29	19.71	-2.86
125	20.91	20.15	-3.63
127	21.32	20.47	-3.99
129	21.52	21.05	-2.18
131	23.00	22.31	-3.00
133	23.86	23.39	-1.97
135	22.98	22.27	-3.09
137	21.33	20.43	-4.22
139	18.71	18.32	-2.08
141	16.90	16.02	-5.21
143	14.42	14.27	-1.04
145	13.28	13.65	+2.79
147	13.96	12.98	-7.02
149	13.34	12.77	-4.27

LEFT VENTRICULAR ANGIO'S 123-149

$y = a + bx$
$a = +0\,087\,cm^2$
$b = 0\,965$
$r = 0\,996$
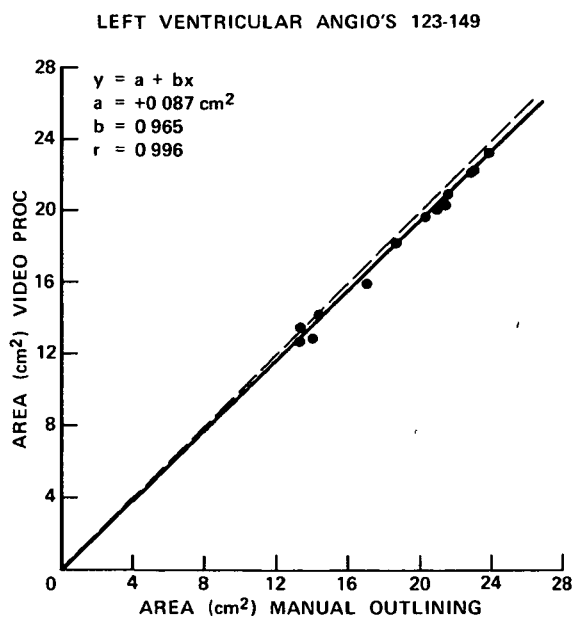
Figure 92.- Comparison of calculated areas from video processing with areas from manual outlining for 14 frames of the first series of left ventricular angiograms. The dashed line is the line of identity and the solid line is the regression line.

231
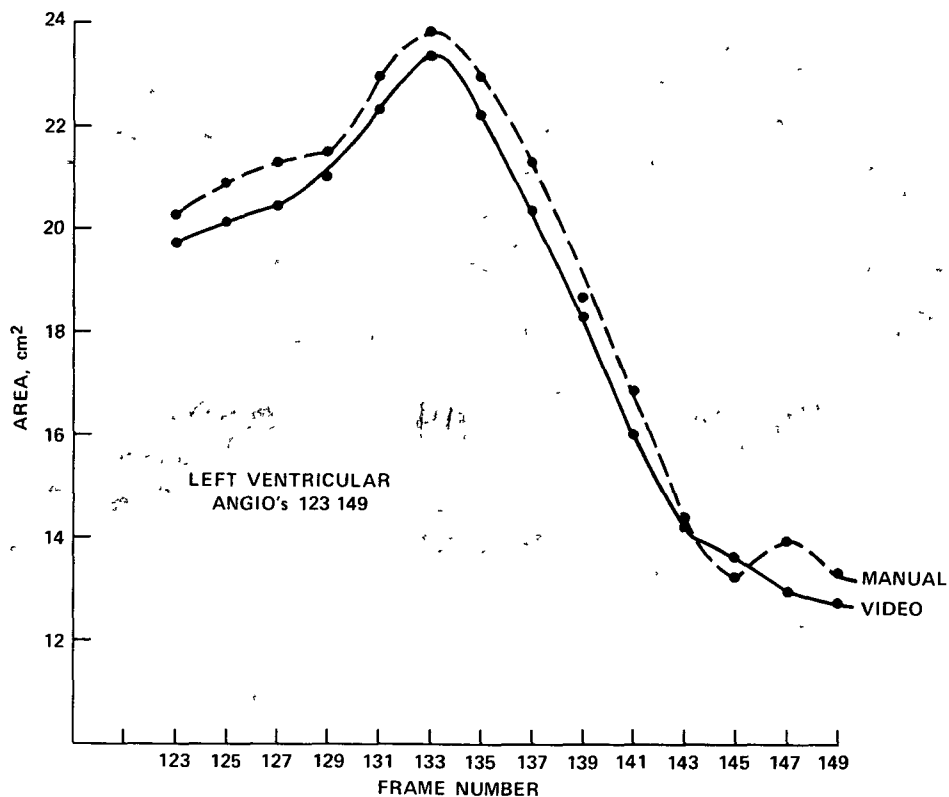
Figure 93.- Area vs. time plots of the calculated areas for the first
series of left ventricular angiograms. The solid line indicates the
calculated areas from video processing and the dashed line from
manual, outlining.

function, from manual outlining. Except for the differences in magnitude,
the video curve is smoother than the manual curve.

For each method separately, the detected contours were mathemati-
cally overlayed using the external coordinate system and displayed on
the graphics terminal. Such a display of outlines, corresponding to
different sample points in the cardiac cycle, is called a contourgraph.
The contourgraph in figure 94(a) gives the results from the manual
editor and, in figure 94(b), from the video system. It is clear that
smooth curves result when the outline is traced manually.

232
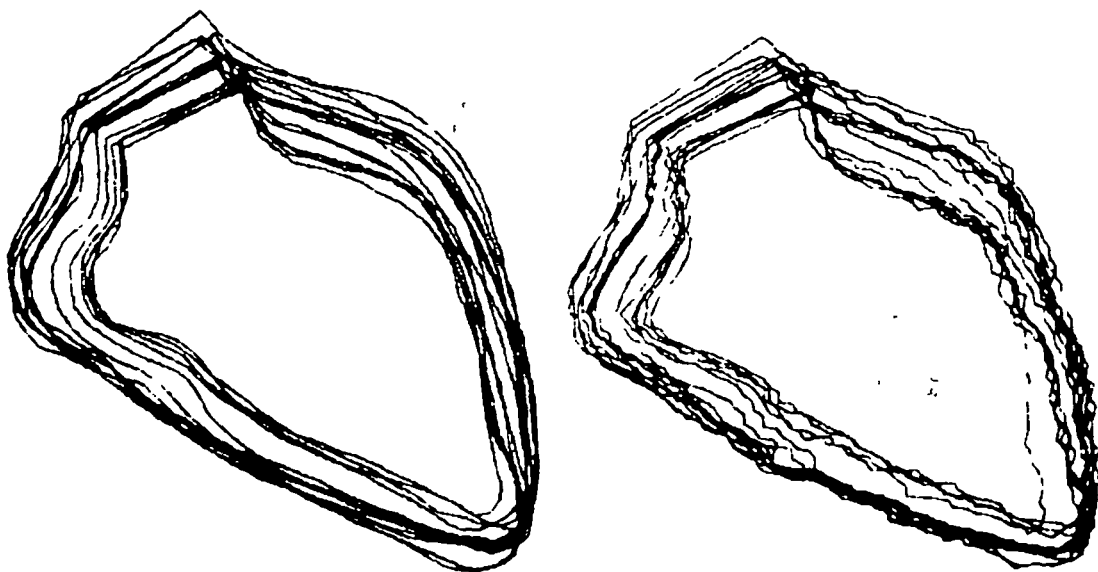
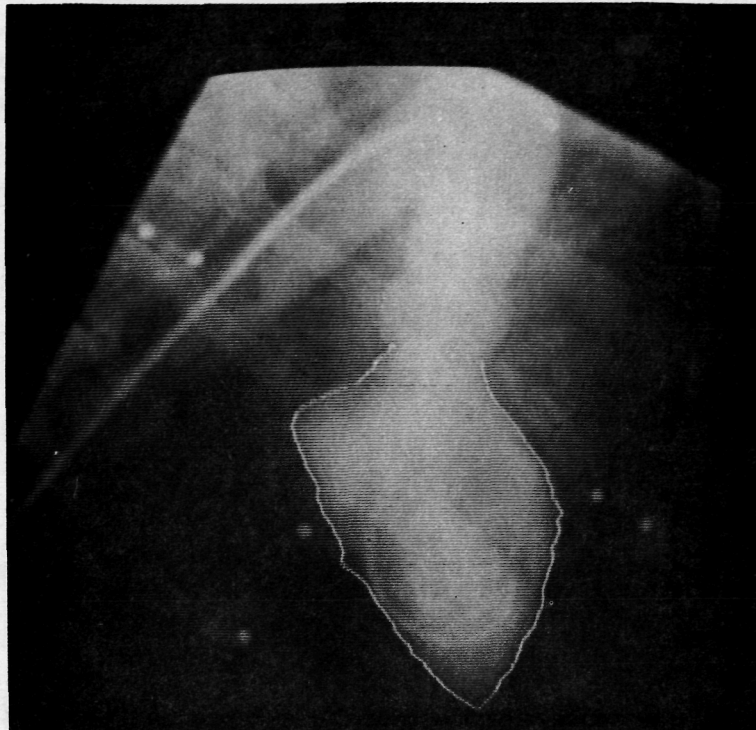(a) Manual processing.   (b) Video processing.

Figure 94.- The 14 left ventricular outlines, obtained at different
instances from diastole to systole, are mathematically overlayed
using an external coordinate system.

For four frames, the outlines were again determined five times; the
resulting mean area and standard deviations are given in table 6. The
standard deviation (expressed as a percentage of the mean area) is better
than 2.83 and 0.31 percent for the manual and video systems, respec-
tively. The reproducibility of the video system is on the average a
factor of 8.2 times better. The video-detected outlines of these four
frames are illustrated in figure 95.

The results of the border comparisons are given in table 7. The
comparisons are done with the outlines corrected back to actual dimen-
sions. For most frames, the mean deviation per side is well within 1 mm
and the standard deviations are all within 1.60 mm. The differences in
area, given as a percentage of the mean of the entire areas determined
by both methods, for both sides is, for most frames, within 4 percent.

TABLE 6.- FOUR FRAMES WERE EACH PROCESSED FIVE TIMES WITH THE MANUAL AND VIDEO METHODS. THE STANDARD DEVIATION OF THE CALCULATED AREAS IS A MEASURE FOR THE REPRODUCIBILITY.

| Frame	Manual outlining			Video processing		
	Mean area, cm^2	Standard deviation, cm^2	Standard deviation, percentage of mean area	Mean area, cm^2	Standard deviation, cm^2	Standard deviation, percentage of mean area
125	20.93	0.29	1.39	20.23	0.04	0.20
133	24.22	.23	0.95	23.28	.04	.17
141	17.34	.49	2.83	16.12	.04	.25
149	13.34	.30	2.25	12.77	.04	.31

Angio 125
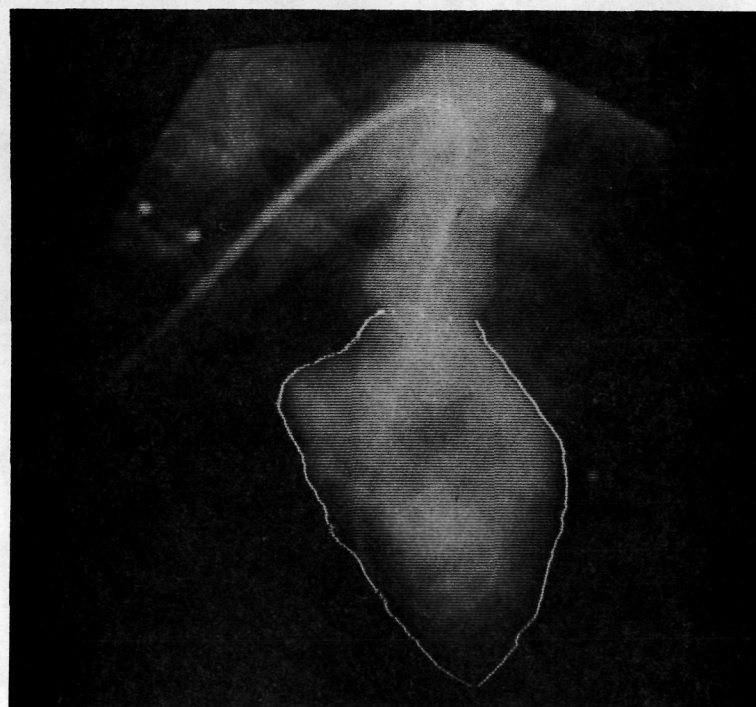
Angio 133

Figure 95.- Video-detected outlines for four selected frames from
diastole to systole.
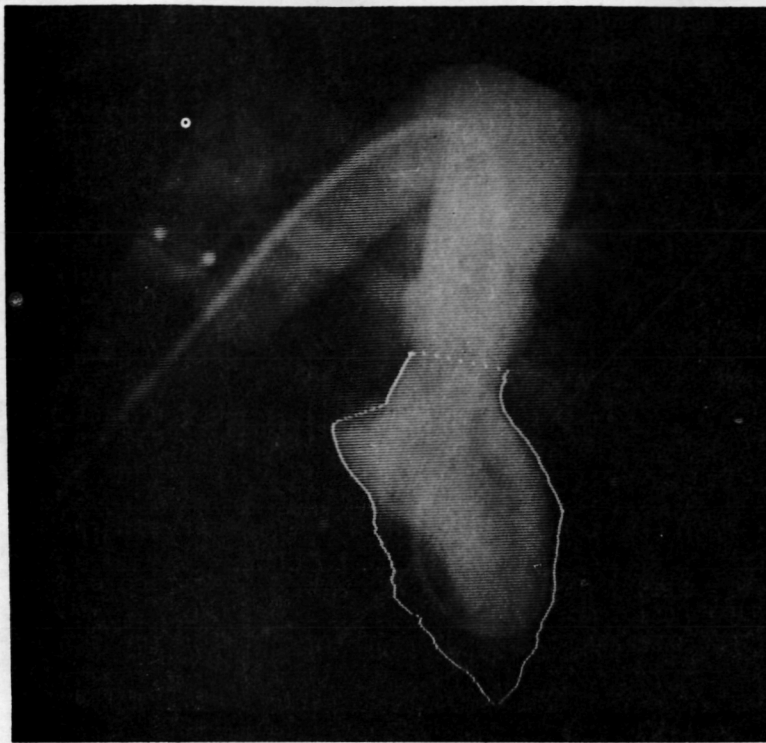
Angio 141
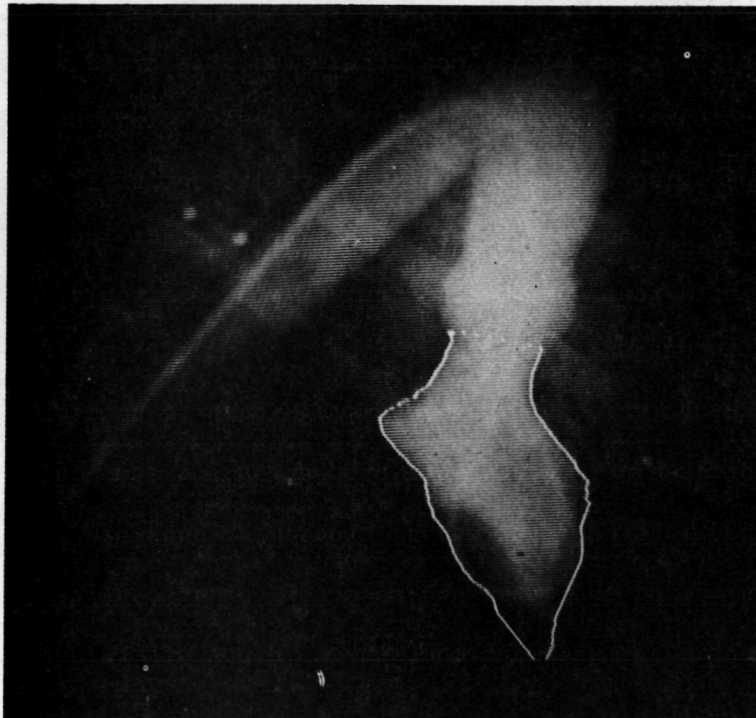
Angio 149

Figure 95.- Concluded.

236

TABLE 7.- STATISTICAL ANALYSIS OF THE DIFFERENCES IN LEFT- AND RIGHT-BORDER COORDINATES FOR

CORRESPONDING MANUALLY AND VIDEO PROCESSED OUTLINES.

Frame	Left border				Right border			
	Mean deviation, mm	Standard deviation, mm	Area deviation, cm²	Percentage area deviation of mean total area	Mean deviation, mm	Standard deviation, mm	Area deviation, cm²	Percentage area deviation of mean total area
123	+0.66	1.40	+0.45	+2.25	-1.00	0.87	-0.68	-3.40
125	-.34	0.83	-.24	-1.17	-0.11	.64	-.08	-0.39
127	+.04	.87	+.03	+0.14	-.20	1.22	-.14	-.67
129	+.72	.60	+.49	+2.30	-.53	1.04	-.36	-1.69
131	-.07	1.29	-.05	-0.22	+.18	1.60	+.12	+0.53
133	+.38	1.01	+.27	+1.14	-.43	1.10	-.31	-1.31
135	+.49	0.60	+.34	+1.50	-.83	0.54	-.59	-2.61
137	+.43	.55	+.29	+1.39	-1.18	.72	-.82	-3.93
139	+.23	.56	+.16	+0.86	-0.06	.87	-.04	-0.22
141	-1.15	1.30	-.76	-4.62	+.27	.94	+.18	+1.09
143	+0.43	0.90	+.27	+1.88	-.34	1.25	-.22	-1.53
145	+1.85	.78	+1.17	+8.69	-.63	0.96	-.40	-2.97
147	-0.46	.94	-0.29	-2.15	-.99	1.25	-.63	-4.68
149	+.42	.75	+.25	+1.91	-.86	1.04	-.52	-3.98

The remarks about the inaccuracies in the determination of the chord are, of course, also applicable here. The inaccuracies in the apex position now mainly result from the limited number of sample points and the differences in the definition of the apex for both systems. It is clear that situations occur when the investigator will draw the apex slightly different from the automatically detected apex.

For the second series of left ventricular angiograms, 13 outlines were processed from diastole to systole. The results are given in table 8. For 7 of the 13 frames, the correlation in areas between the two systems is very good (within 2 percent), but for the remaining six frames the video system determined the areas on the average 7.11 percent too low. These frames have fairly low contrast, so that it was often hard to tell exactly where the actual border was. Under these circumstances, the differences between the two methods will, of course, increase.

TABLE 8.- CALCULATED AREAS FROM MANUAL AND VIDEO PROCESSING FOR THE
FIRST 13 FRAMES OF THE SECOND SERIES OF LEFT VENTRICULAR
ANGIOGRAMS

Frame	Manual outline measured area, cm^2	Video processing measured area, cm^2	Percentage difference with manual method
1	32.80	32.70	-0.30
3	34.30	34.05	-.73
5	33.96	34.44	+1.41
7	34.21	34.30	+0.26
9	32.48	31.82	-2.03
11	28.54	28.75	+0.74
13	26.33	25.18	-4.37
15	23.24	23.24	+0.00
17	21.57	20.25	-6.12
19	19.90	17.95	-9.80
21	18.97	16.85	-11.18
23	18.07	16.62	-8.02
25	17.50	16.95	-3.14

The regression analysis of the computed areas from video processing
with the areas from manual outlining is given in figure 96. The correla-
tion coefficient is 0.997. Figure 97 shows the computed areas plotted
vs. time. The solid function represents the calculated areas from video
processing and the dashed function, from manual outlining. The results
of the border comparisons are given in table 9. For 10 of the 13 frames,
the mean deviation in the borders is within 1.68 mm for both sides and
the standard deviation is within 2.52 mm for all frames. The differ-
ences in area, expressed as a percentage of the mean of the entire areas
determined by both methods, is within 6.12 percent for both sides in 9 of
13 frames.
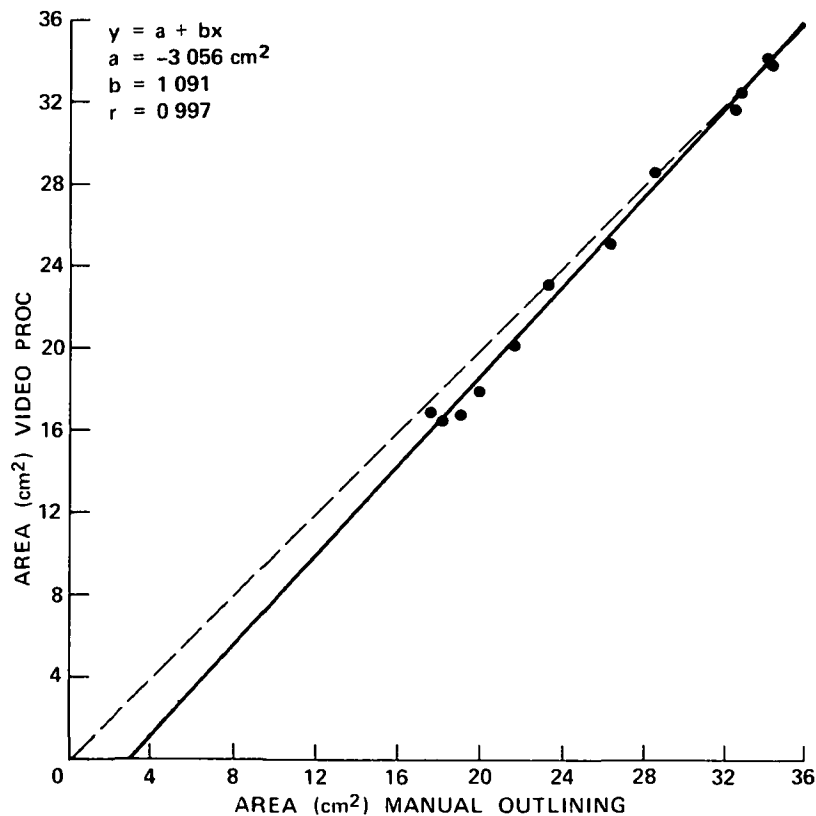
Figure 96.- Comparison of calculated areas from video processing with
    areas from manual outlining for 13 frames of the second series of
    left ventricular angiograms. The dashed line is the line of identity
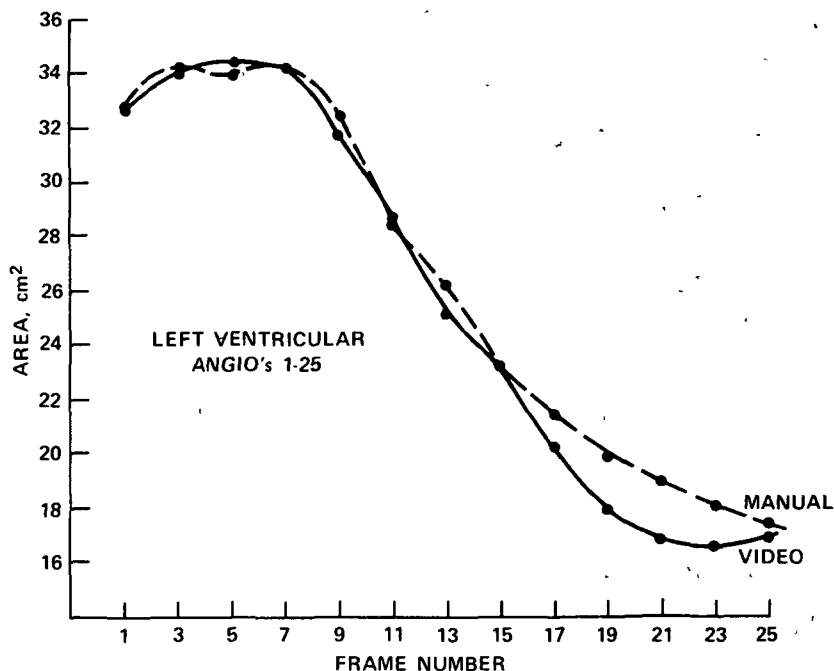   and the solid line is the regression line.

Figure 97.- Area vs. time plots of the calculated areas for the second
series of left ventricular angiograms. The solid line indicates the
calculated areas from video processing and the dashed line from
manual processing.

The earlier remarks about the apex inaccuracies (made in the

sections on the casts and the first series of left ventricular angio-

grams) are again applicable. For this second series, the contrast at

the apex was often fairly low, resulting in relatively wide distances

between the left and right borders at the apex.

TABLE 9.- STATISTICAL ANALYSIS OF THE DIFFERENCES IN LEFT- AND RIGHT-BORDER COORDINATES

FOR CORRESPONDING MANUALLY AND VIDEO PROCESSED OUTLINES

Frame	Left border				Right border			
	Mean deviation, mm	Standard deviation, mm	Area deviation, cm²	Percentage area deviation of mean total area	Mean deviation, mm	Standard deviation, mm	Area deviation, cm²	Percentage area deviation of mean total area
1	+0.38	2.52	+0.32	+0.98	-0.29	1.08	-0.25	-0.76
3	-2.08	0.88	-1.80	-5.27	+2.32	0.94	+2.01	+5.88
5	-0.37	.85	-0.33	-0.96	+0.77	.89	+0.68	+1.99
7	-1.08	1.18	-.93	-2.71	+1.10	.99	+.96	+2.80
9	+0.39	2.46	+.33	+1.03	-1.57	1.90	-1.33	-4.14
11	+.86	1.89	+.71	+2.48	+0.20	1.40	+0.17	+0.59
13	+1.10	2.39	+.85	+3.30	-2.97	2.06	-2.31	-8.97
15	-2.25	1.22	-1.75	-7.53	+1.63	0.73	+1.27	+5.46
17	+0.93	1.85	+0.71	+3.40	-1.68	1.78	-1.28	-6.12
19	-.38	1.68	-.28	-1.48	-1.42	2.00	-1.07	-5.65
21	-1.67	1.59	-1.27	-7.09	-0.45	2.13	-0.34	-1.90
23	-1.71	1.07	-1.30	-7.49	-.13	1.76	-.10	-0.58
25	-0.82	2.09	-0.60	-3.48	-.61	2.17	-.44	-2.55

Page intentionally left blank

CHAPTER 12:   FUTURE IMPROVEMENTS

It has been shown that the proposed detection and data acquisition
system for the left ventricular outline can detect the outline accurately.
However, while working with the system, new ideas came up, which should
result in: (1) improved border-tracking capability, (2) less operator
interaction, and (3) improved on-line use.   In this chapter, the follow-
ing new ideas are discussed:

(1) Edge enhancement

(2) Detecting the first right-border point

(3) Dynamic determination of the aortic valve plane

(4) Dynamic adjustment of the sampling distances to the border

(5) Microprocessor control

Edge Enhancement

In the present system, the border positions are detected using a
dynamic thresholding technique.   As explained in chapter 9, under all
reasonable conditions there is a value for α ($0 \leq \alpha < 1$) such that
acceptable border points are detected along the left ventricular border
with the equilibrium reference level V_{equil} satisfying

$$b_{min} + c < V_{equil} < b_{min} + c + \Delta\gamma_1 \qquad (251)$$

where b_{min} is the lowest dc level per field for the video lines
traversing the left ventricle, c is the incremental dc level for a
particular equilibrium situation, Δ is the one-sided sample window
width, and γ_1 is the ventricular slope.   Assuming that $V_c = b_{min}(1 - \alpha)$,
the equilibrium reference level is given by

$$V_{equil} = \frac{\frac{\alpha}{2}(\Delta\gamma_1 + b_{min} + c)\left(1 - \frac{\gamma_2}{\gamma_1}\right) + b_{min}(1 - \alpha)}{1 - \frac{\alpha}{2}\left(1 + \frac{\gamma_2}{\gamma_1}\right)} \qquad (252)$$

where γ_2 is the background slope $(0 \leq \gamma_2 < \gamma_1)$. It is clear that the reference level will be different from the calculated equilibrium level V_{equil} at those places along the border where sudden changes in dc level and/or slopes from the last equilibrium situation occur, because the new equilibrium level will be reached only with a finite time constant.

However, the left ventricular border is characterized not only by a certain threshold level but also by a slope. This parameter has not been used explicitly so far and it will certainly be worthwhile to study the possibilities of using the slope as an additional factor in determining the actual border positions.

Generally, measuring or extracting the slope in images is a problem associated with scene analysis and image enhancement (refs. 62 and 63). For this particular application in angiograms often with low contrast, it will be necessary to use a principle that does not introduce significant amounts of additional noise and is electronically relatively easy to implement.

An edge or line in a particular direction can be emphasized while all others are attenuated or suppressed by performing a suitable differentiation or differencing operation in the orthogonal direction. If we assume that the longest chord of the left ventricle is approximately vertical on the monitor screen, then at the average the direction along the ventricular border will be perpendicular to the scan lines. This

244

then suggests differentiating the video signal or taking the difference of video lines which have been delayed over a short period T_D with respect to each other.

Differentiating the video is not a practical solution because it introduces a lot of noise. This can easily be seen in the frequency domain by taking the Fourier-transform of the derivative of a general function $v(t)$. Define $\mathcal{F}[v(t)] \triangleq V(s)$, then:

$$\mathcal{F}\left[\frac{d\ v(t)}{dt}\right] = 2\pi is\ V(s) \qquad (253)$$

that is the original function $V(s)$ is multiplied by $2\pi is$, which is a linear function of the frequency s. Therefore, the high frequency noise components are very much amplified.

Differencing however, is less noisy than differentiating and may be a practical tool for this problem. Taking the difference of $v(t)$ and $v(t-T_D)$ amounts to applying the convolution of $v(t)$ with $[\delta(t) - \delta(t-T_D)]$, where $\delta(t)$ is the impulse function. In formula:

$$v(t) - v(t-T_D) = v(t) * [\delta(t) - \delta(t-T_D)] \qquad (254)$$

Taking the Fourier-transform yields:

$$\mathcal{F}[v(t) - v(t-T_D)] = (1 - \cos 2\pi sT_D + j \sin 2\pi sT_D) \cdot V(s) \qquad (255)$$

The magnitude of the coefficient of $V(s)$ is now

$$|1 - \cos 2\pi sT_D + j \sin 2\pi sT_D| = \sqrt{2(1 - \cos 2\pi sT_D)} \qquad (256)$$

which is a cosine function with a maximum value of 2 and a minimum value of 0. The frequency components with $s = (2m+1)/2T_D$ $(m = 0, 1, 2, \ldots)$ are multiplied by a factor of two, while the frequency components with $s = m/T_D$ $(m = 0, 1, 2, \ldots)$ cancel out. This shows the much better noise

245

behavior of the difference operator as compared with differentiating. Clearly, the actual border information is also less amplified using the difference operator, but that poses no problem. Schematically, the difference operation is shown in figure 98.
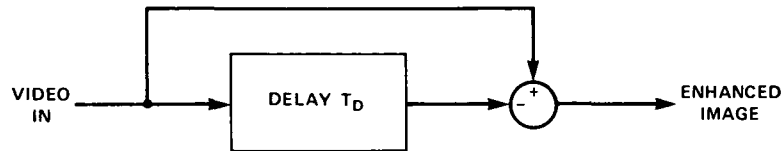

Figure 98.- Subtracting the delayed video signal from the original signal results in image enhancement.

Taking the linear border model defined in chapter 9 as an example, the wave forms in figure 99 result when the input signal is delayed over a period T_D and then subtracted from the original signal. For a left ventricular slope of γ_1 V/sec, the amplitude of the difference
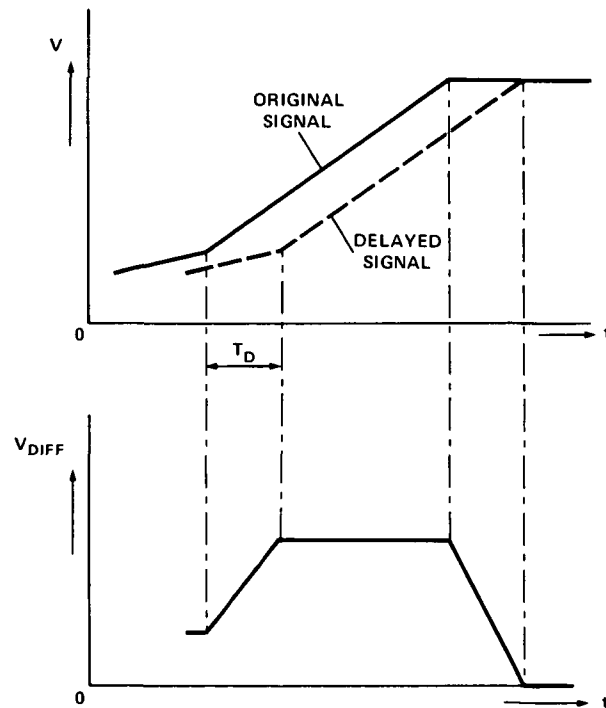
Figure 99.- Resulting wave forms when applying the difference operator to the linear border model.

signal is T_D tg γ_1. It follows from figure 99 that the maximum of the difference signal is reached at the knee point of the delayed video signal. This particular point is the position where one would want to detect the border in the ideal case. The amplitude of the difference signal is a measure for the slope of the ventricular border. The problem of detecting the ventricular border then amounts to determining the point in time where the maximum of the difference signal is reached (discussed later).

It will be advantageous in generating the difference video signal to use the 1-MHz, low-pass filtered video, which is also applied to the analog comparators. This signal contains all the relevant border information and will produce a less noisy difference signal than would be the case with the original 5-MHz signal. Applying the principle of figure 98 to actual angiograms results in the images shown in figure 100. Figures 100(a) and (b) show the original and enhanced images of an angiogram near diastole and systole, respectively. The applied delay, clearly visible at the outermost boundaries in the picture, is about 1 μsec. The slope of the left ventricular image being positive for the left border results in a positive difference signal (bright edge), while the negative slope for the right border results in a negative difference signal (dark edge).

There are several ways to determine the border point from the difference signal in figure 99. In the description of these possible methods, it will always be assumed that the detection will be allowed only within the expectation window. Especially with the slightly more noisy difference signal compared with the 1-MHz filtered video, it will
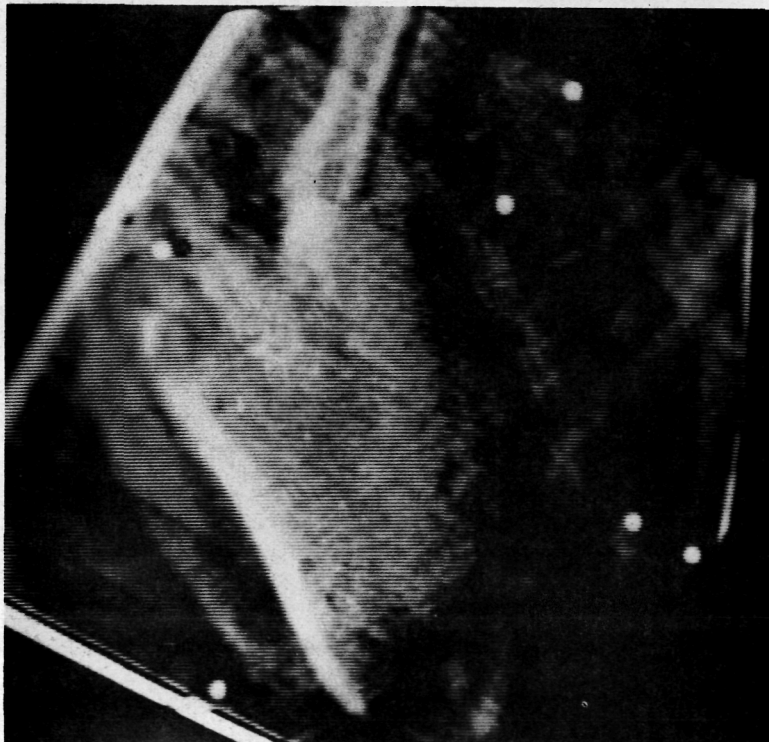
(a) Original and enhanced angiogram near diastole.

Figure 100.- Applying the difference operator to actual angiograms
results in the enhanced images shown.

248
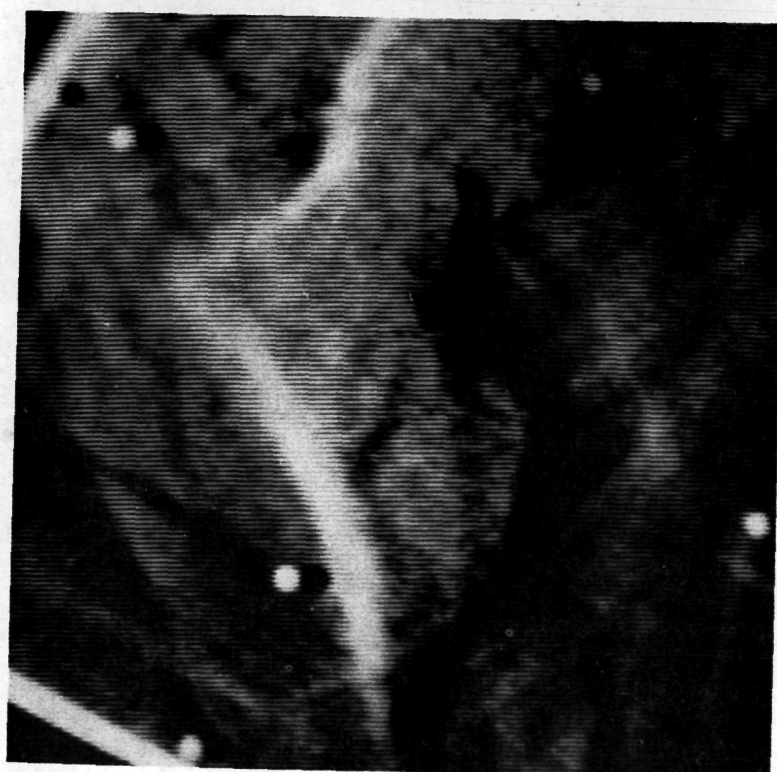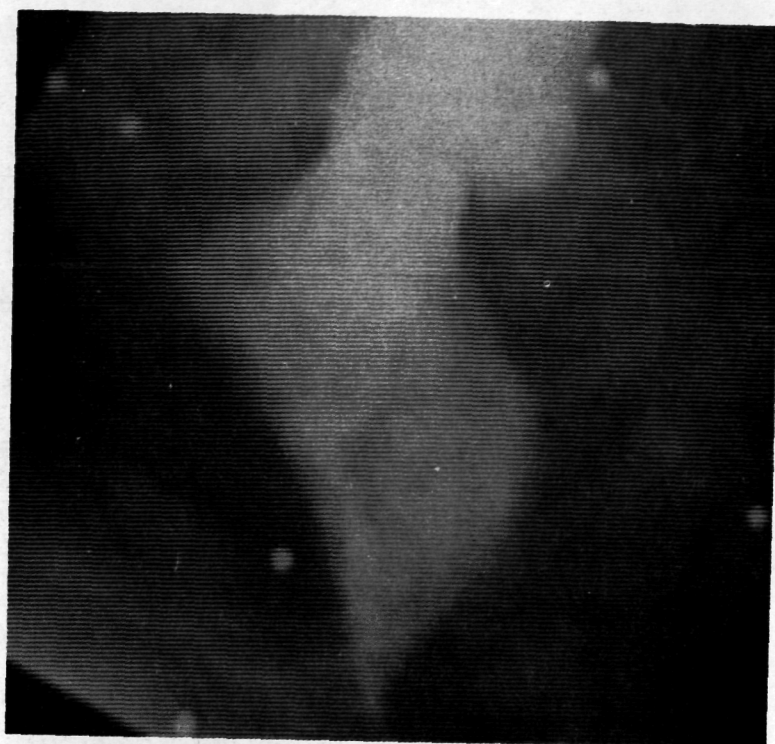
(b) Original and enhanced angiogram near systole.

Figure 100.- Concluded.

be important that the center of the expectation window approximates the actual border point as accurately as possible, allowing a relatively narrow expectation window. This again favors the first-order line extrapolation principle above the zeroth-order principle. Some of the possible detection methods are:

(1) Apply adjustable dc thresholding technique to the difference signal. This results in the detection of a border point where the density gradient becomes greater than a preset gradient. However, the gradient changes appreciably along the ventricular border so that a relatively low preset value would have to be chosen. This may result in erroneous border points due to noise and intervening structures. Also, the position of the detected border point with respect to the knee in the border model depends on the preset level.

(2) Apply a dynamic thresholding technique. It is clear that the amplitude of the difference signal is a function of the difference of the video samples $V_R(n)$ and $V_L(n+1)$ (as·defined in fig. 62, chapter 9). The threshold level should therefore be adjusted on a line-to-line basis according to the difference $V_R(n) - V_L(n+1)$. Forced border points are again generated at the beginning and end of the expectation window if the difference signal is already above the threshold level at the beginning of the expectation window and if the difference signal is below the threshold level during the entire expectation window, respectively.

The above described two principles are usually referred to as threshold gradient principles.

(3) Detect the trailing edge of the double difference signal. Ideally, we would like to determine the position where the maximum of

the difference signal is reached. There is no easy solution for this

directly in real time. Indirectly, this can be solved by applying the

difference principle again to the difference signal, resulting in the

generation of a double-difference signal $V_{2,DIFF}$. This operation is

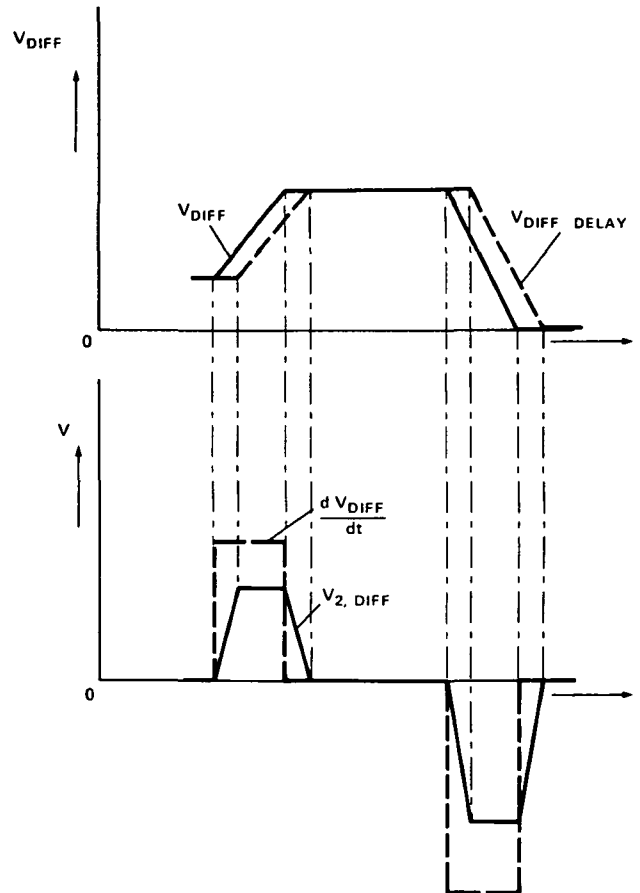shown in figure 101 with the difference signal in figure 99.

Figure 101.- Taking the difference of the difference signal in figure 99
and the delayed signal results in the wave form of $V_{2,DIFF}$. The
time derivative of V_{DIFF} is also shown.

It follows from figure 101 that the beginning of the trailing edge

of the first trapezoid-shaped pulse indicates the position where the

difference signal reaches its maximum. However, the trailing edge can

be detected only by using a dynamic thresholding technique. This will

251

result in a detected border point slightly to the right of the actual border point, which is acceptable. The derivative of the difference signal is also given in figure 101. Applying the thresholding technique to dV_{DIFF}/dt gives the actual border point, but taking the derivative will introduce too much noise.

If this edge enhancement principle proves useful for the contour detection, then both this principle and the presently used dynamic thresholding technique will be applied simultaneously. The actual border position can then be defined as the average position of the positions determined by both principles separately.

The result of the above described edge enhancement is that edges that are perpendicular to the scan lines are maximally enhanced and edges parallel to the scan lines are not enhanced. For an edge making an angle of ϕ degrees with the scan lines, the percentage of enhancement is given by $|\sin \phi| \times 100$ percent.

Somewhat more complex electronic circuits have been reported, which enhance details, contours, and structures regardless of whether they run parallel, perpendicular, or at any angle ϕ to the scan lines. One of these schemes (ref. 64) produces an all-directional second derivative signal (detail signal). Detail enhancement is effected by adding the detail signal to the unchanged main signal. The detail signal, which contains the edges and fine structures of the original picture, is produced by a sharp-unsharp subtraction. This signal for low sharpness is generated in two steps. At first, the sharpness of the mainly horizontal edges and structures (low angles of inclination ϕ) is reduced by means of two supersonic delay lines for the duration of one scan line

252

(63.5 μsec). In the second step, the sharpness of mainly vertical edges (angles of inclination ϕ up to 90°) is lowered by means of a low-pass Thomson filter. Adjustable amounts of the detail signal and the main signal are added together to form the output signal. The transfer characteristics show that the transition between unchanged low spatial frequencies and enhanced high frequencies is shifted toward higher frequencies with decreasing angle of inclination ϕ.

A scheme that enhances the edges perpendicular to the scan lines by delaying the density signal and subtracting it from itself in a video subtractor is given in reference 65. The density signal is defined as $D = \log(1/T) = \text{const} - (1/\gamma)\log E$, where T is the transmittance of the film, γ is the gamma for the vidicon tube, and E is the TV camera output. To obtain the density signal, the video signal must be logarithmically amplified with a log amplifier.

For the general case that an image is processed in both x and y directions, twice differentiating in each direction results in the so-called Laplacian operator $\nabla^2 = (\partial^2/\partial x^2) + (\partial^2/\partial y^2)$ (ref. 66). If it is assumed that the original picture can be described by $f(x,y)$ and the resulting picture by $F(x,y)$, the operation

$$F(x,y) = f(x,y) - k^2 \left(\frac{\partial^2 f}{\partial x^2} + \frac{\partial^2 f}{\partial y^2} \right) \tag{257}$$

where k is a constant, is referred to as contour enhancement. The detail image, which results by applying the Laplacian operator multiplied by k^2, is subtracted from the original image. This overall operation is an approximation of a standard photographic technique known as unsharp masking.

Detecting the First Right-Border Point

It was explained in chapter 8 that the generation of the simulated aortic valve plane is halted and the first right-border point is detected as soon as the video level reaches a preset reference level within the defined expectation window. This preset reference level is set by the operator. However, contrast near the outflow tract for the right border is often fairly low (fig. 102), making it difficult to set
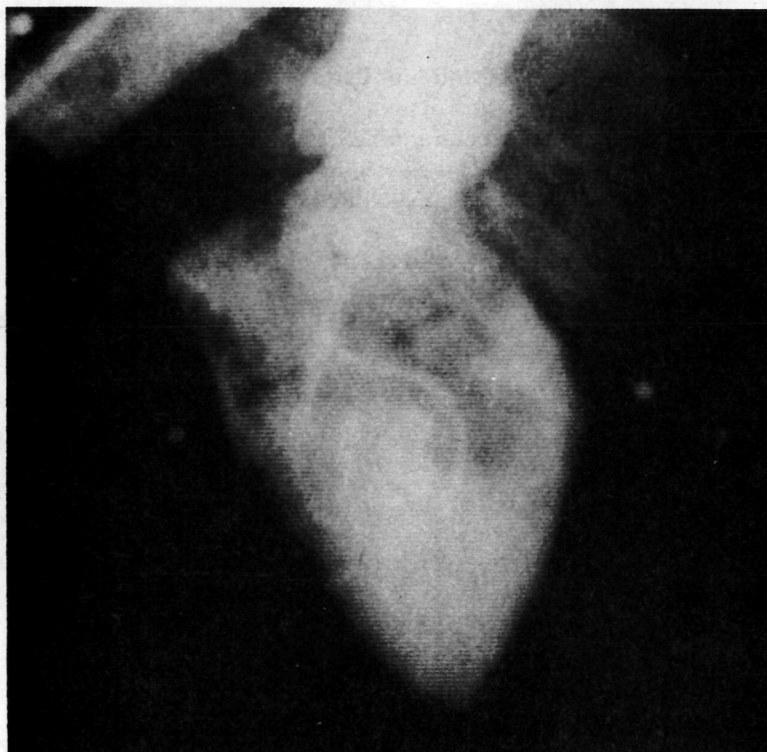

Figure 102.- Angiogram with fairly low contrast near outflow tract.

this level. If the preset level is adjusted slightly too high, then the aortic valve generation is halted too early and, if it is slightly too low, then it extends too far into the background area. Also, the video level at this right-border point generally changes during a cardiac cycle, requiring readjustments of this preset level.

254

To make this adjustment less critical, it is proposed to use the difference of the normally defined video samples as a measure to determine the first right-border point (fig. 103). In this figure, the sample
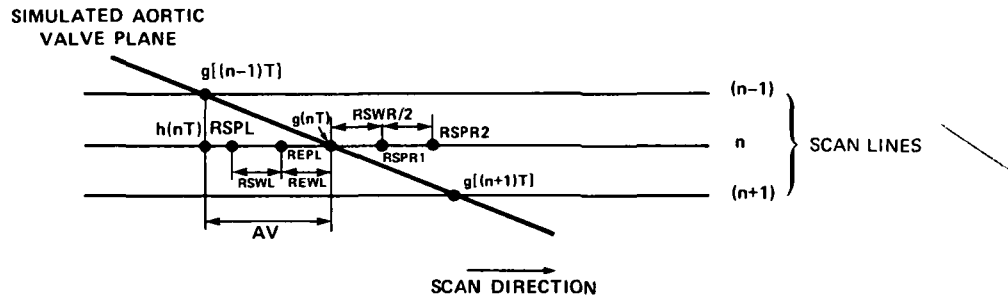

Figure 103.- First right-border point is detected when the difference between the left- and right-hand sample levels on the same line exceeds a preset level.

and expectation points are defined during the aortic valve plane generation. To calculate the reference level for line (n + 1), the sample levels at RSPR1 and RSPR2 on line n and at RSPL on line (n + 1) are used. However, to detect the first right-border point, we will use the difference of the sample levels on the same line. Assume that the current line number is n, then we are interested in the magnitude of the difference

$$V_D = VL - \left(\frac{VR1}{2} + \frac{VR2}{2} \right) \tag{258}$$

where VL is the sample level at RSPL and VR1 and VR2, the sample levels at RSPR1 and RSPR2, respectively, all determined on line n. So long as the samples are taken in the contrast-filled outflow tract, the magnitude of V_D is small. However, when g(nT) is generated in the neighborhood of the actual border so that RSPR1 and RSPR2 are positioned

255

in the background area, the difference will increase. The end point of the aortic valve is then defined where V_D crosses a preset level for the first time per field; after this, the AV is set to zero to determine the expectation window for the next line. The first right-border point is then detected in the usual way. This principle allows limited changes in contrast during a cardiac cycle. If contrast is very low, then this principle fails, but that is certainly true for the old threshold method. At one time, this principle was tested and proved to be feasible and successful on a trial basis. However, it has not been incorporated in the contour detector II. Further experiments are necessary before this can be implemented.

Dynamic Determination of the Aortic Valve Plane

In the present system, the starting point is positioned by the operator at the aortic valve by means of a joystick. However, during a cardiac cycle, the aortic valve plane is not fixed, but moves (as clearly shown in fig. 94 of chapter 11 where the detected borders are overlayed using an external coordinate system). This makes it clearly evident that the starting point must be repositioned automatically when on-line use is contemplated.

It is also clear that automatic repositioning the starting point is a very difficult problem. The reason for using the starting point has always been to generate the simulated aortic valve plane, which cannot be determined with a threshold technique. The position of the aortic valve plane is necessary to calculate the area and volume of the left ventricular cavity, but not necessarily to detect the left ventricular outline. The contour detector can detect the outline plus the aortic

valve by positioning the starting point in the aortic region above the valve (as shown in fig. 104). Therefore, it is proposed to determine the simulated aortic valve plane using a software routine. This can be done in the minicomputer (PDP-12) or with a microprocessor built in the contour detector (see section on microprocessor control in this chapter).
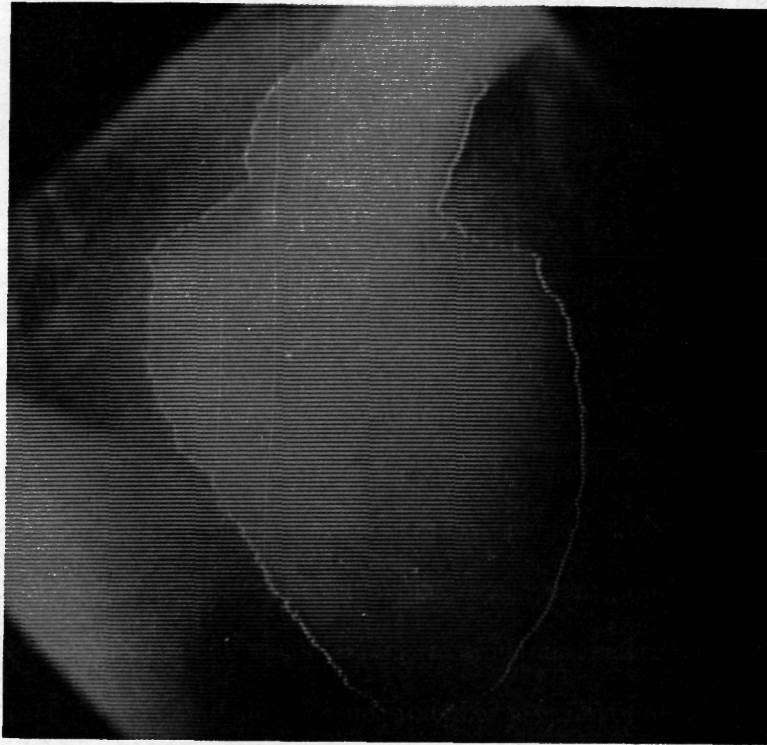

Figure 104.- Aortic valve and left ventricular cavity are detected when the starting point is positioned above the aortic valve (human left ventricle).

The procedure for calculating the area and volume of a left ventricular cavity then requires the execution of one extra software routine, compared with the present setup. Data will be handled as previously described. Outline coordinates are stored first in core memory and thereafter on a digital disk, assuming a minicomputer is used for this purpose. The aortic valve algorithm will be applied before the

257

reformatting is done; the algorithm finds, of course, only the beginning and end points of the simulated aortic valve plane. Once the valve points have been determined, the border coordinates above the valve plane can be deleted and the formatting routine can be applied. Note that the number of left-border x coordinates is generally no longer equal to the number of right-border x coordinates because the right-border points on the simulated aortic valve plane have not been generated. This can be solved by calculating new right-border points on the valve line by linear interpolation; this format is necessary for the reformatting program presently used. Otherwise, the reformatting program must be changed. After the reformatting, the data file is again in the required format to execute the remaining programming steps.

If a microprocessor is being used in the contour detector, the aortic valve plane can probably be determined in the remaining time of a field period.

An applicable software routine has been reported in the literature (ref. 37) and was described in chapter 2. This algorithm uses the following properties of the aortic valve:

(1) The valve line is one of the shortest lines that will connect the right and left boundaries of the ventricle-aorta outline.

(2) The valve line is roughly perpendicular to the centerline of the ventricle-aorta silhouette.

(3) There is usually a large right turn angle at one or both of the valve line ends.

Another reported algorithm searches for the minimum distance between any of the first 20 points of the left border and any of the

first 20 points on the right side (ref. 41). A similar algorithm would probably best suit our requirements without restricting to the first 20 points.

Because of the particular shape of the aortic valve, it is clear that the designated valve plane can be determined by searching for a local minimum in the distances between the two sides of the ventricular outline. With the starting point always positioned above the aortic valve, for each left-border point the minimum distance to the right border can be calculated. A plot of these shortest distances as a function of the video line number is shown in figure 105. The position of the designated aortic valve plane should then be easy to recognize. If the starting point is always positioned approximately in the middle of the aorta, then fairly large movements of the aorta can be allowed without disturbing the contour detection.
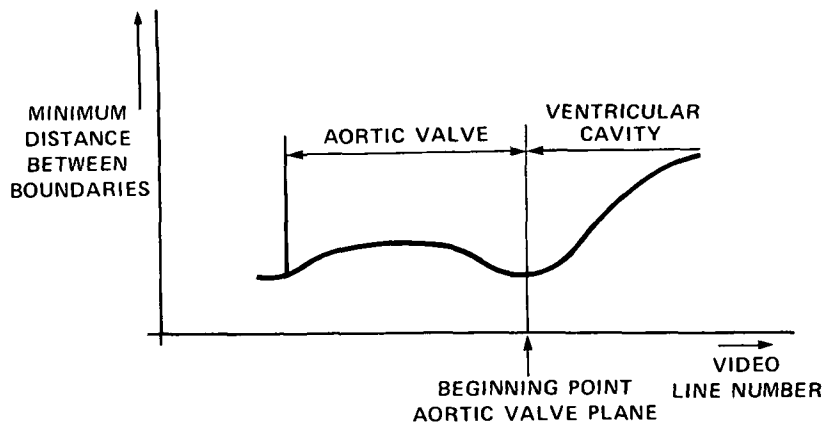

Figure 105.- The beginning point of the simulated aortic valve plane is the left border point for which the function of minimum distances between boundaries has a minimum, following the maximum of the aortic valve.

259

Dynamic Adjustment of the Sampling Distances

In the theoretical analysis of the dynamic reference level, it was assumed that the sample points are taken at a distance Δ from the border point and that the direction of the left ventricular outline is perpendicular to the scan lines, resulting in maximum density changes along a video line. However, in actual angiograms, the direction of the left ventricular outline changes appreciably over a frame and with that the maximum density changes on a video line. Figure 106 shows a canine left ventricular angiogram with the positions of the sample points LSPL1, RSPL, and RSPR2 superimposed in the video signal. Although the sample window widths are constant over this frame, the sample points at the mitral valve, for example, are closer to the actual border because of the direction of the outline.
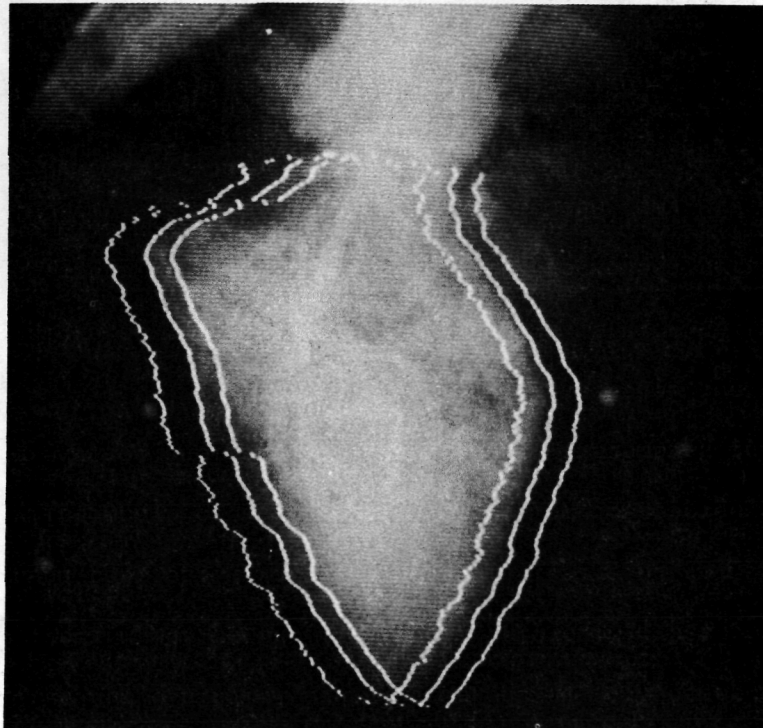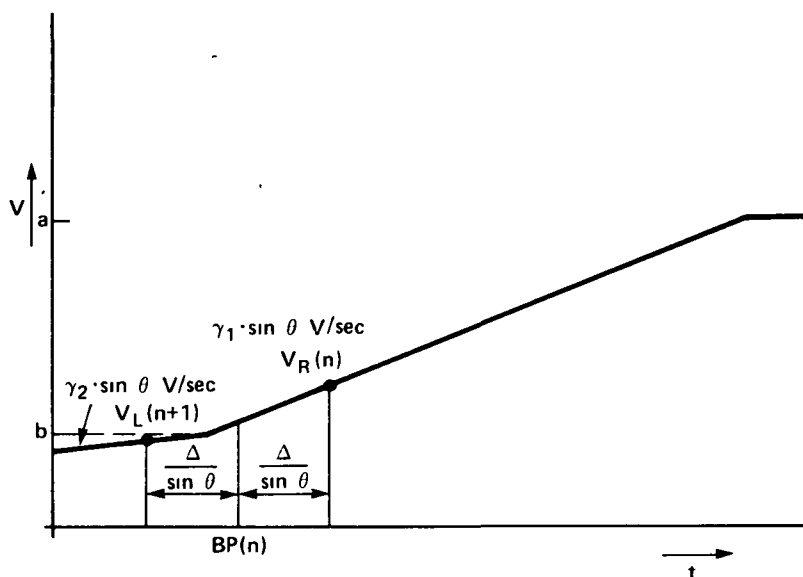

Figure 106.- Positions of the sample points LSPL1, LSPR, RSPL, and RSPR2 superimposed in the left ventricular image.

Figure 107(a) shows the linear border model proposed in chapter 9;
it is assumed for this model that the direction of the left ventricular

(a) Assumed linear border model with sample window widths Δ under the
condition that the direction of the left ventricular outline is
perpendicular to the scan lines.
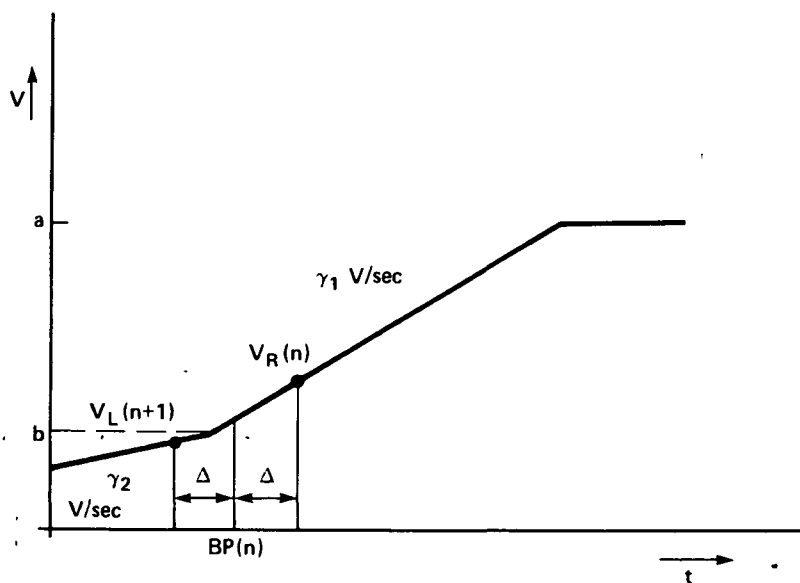
(b) The sample window widths must be adjusted to $\Delta / \sin \theta$, when the
direction of the outline makes an angle of $\theta°$ with the scan
lines.

Figure 107.- Dynamic adjustment of the sample window widths.

outline is perpendicular to the scan lines. Consider the case that the direction of the outline makes an angle θ° with the scan lines. The border model then changes so that the new slopes are $\gamma_1 \sin \theta$ and $\gamma_2 \sin \theta$, respectively, as shown in figure 107(b). To sample the same video levels, the sample window widths must be changed to $\Delta' = \Delta/\sin \theta$, a change in width of $\Delta/\sin \theta - \Delta = \Delta[(1/\sin \theta) - 1]$.

It follows from this discussion that the sample window widths should be adjusted dynamically according to the direction of the outline to always sample the correct video levels. A possible solution for implementing this dynamic sample window width principle is described in this section.

Figure 108 shows the situation that the straight line through $g(nT)$ and $g[(n-1)T]$ makes an angle θ° with the scan lines. Assuming
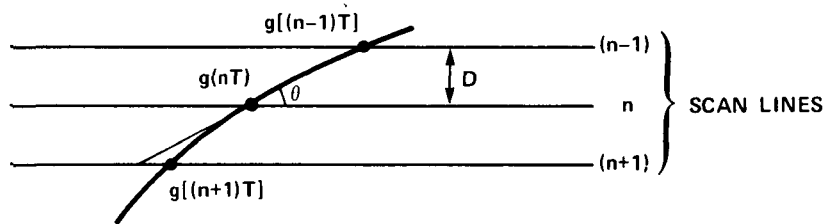

Figure 108.- Direction of the outline makes an angle of θ° with the scan lines.

$g(nT)$ is the last detected border point, the position of $g[(n+1)T]$ can again be approximated using linear extrapolation. The difference in horizontal position between $g(nT)$ and $g[(n-1)T]$ is therefore a measure for angle θ and should be used to adjust the sample window widths on line $(n+1)$. Mathematically, this can be written as

$$g(nT) - g[(n-1)T] = D \cot g\ \theta \tag{259}$$

where D is the vertical distance between consecutive video lines in the same field, expressed in 50-MHz clockpulses. The value for D can be derived by assuming $\theta = 45°$; then

$$g(nT) - g[(n-1)T] = D \qquad (260)$$

Each field has 262-1/2 lines, including the vertical retrace lines; let us estimate the actual number of lines during the nonblanking period to be 250. The horizontal line period is 63.5 μsec, including the horizontal retrace time; the actual nonblanking line time is then approximately 57 μsec. Because of the 4:3 aspect ratio, the effective line period for calculating D is $3/4 \times 57$ μsec. The value of D, expressed in 50-MHz clock pulses, follows by dividing the effective line period by the number of video lines, that is,

$$D = \frac{3/4 \times 57 \text{ μsec}}{250} = 171 \text{ nsec} \approx 8.5 \text{ clock pulses} \qquad (261)$$

Table 10 gives $g(nT) - g[(n-1)T]$ expressed in clock pulses as a function of θ using formula (259). Now that we have an equivalent value for D, the measured difference $g(nT) - g[(n-1)T]$ allows the calculation of the corresponding angle θ so that the new width $\Delta / \sin \theta$ can be determined.

To implement this procedure, it is proposed to use a look-up table consisting of ROM's. The size of this ROM memory can be derived by considering the maximum number of bits, used for Δ, $\Delta / \sin \theta$, and $\{g(nT) - g[(n-1)T]\}$. The sample window width Δ is given in a 4-bit binary format; allowable values for Δ are from 0 to 12 (chapter 8). The dynamic window width is limited to a 5-bit format; otherwise, the samples are taken too far from the actual border, possibly resulting in

TABLE 10.- DIFFERENCES IN CONSECUTIVE BORDER POSITIONS $g(nT)$ AND $g[(n-1)T]$ (EXPRESSED IN 50-MHz CLOCK PULSES) AS A FUNCTION OF THE ANGLE BETWEEN THE LINE CONNECTING $g(nT)$ AND $g[(n-1)T]$ AND THE DIRECTION OF THE SCAN LINES

θ, deg	cotg θ	$g(nT) - g[(n-1)T] = D \cdot cotg\ \theta$
90	0.000	0.00
80	.176	1.50
70	.364	3.09
60	.577	4.90
50	.839	7.13
45	1.000	8.50
40	1.192	10.13
30	1.732	14.72
20	2.747	23.35
10	5.671	48.21

erroneous sample levels due to intervening structures. In practice, a five-bit format for $g(nT) - g[(n-1)T]$ will be sufficient. The address of the ROM memory will be formed by Δ and $\{g(nT) - g[(n-1)T]\}$, totaling nine bits. Therefore, we need per border five ROM's each 512×1 bits; the right- and left-hand window width for a border side can be accessed sequentially. The ROM configuration is shown schematically in figure 109.
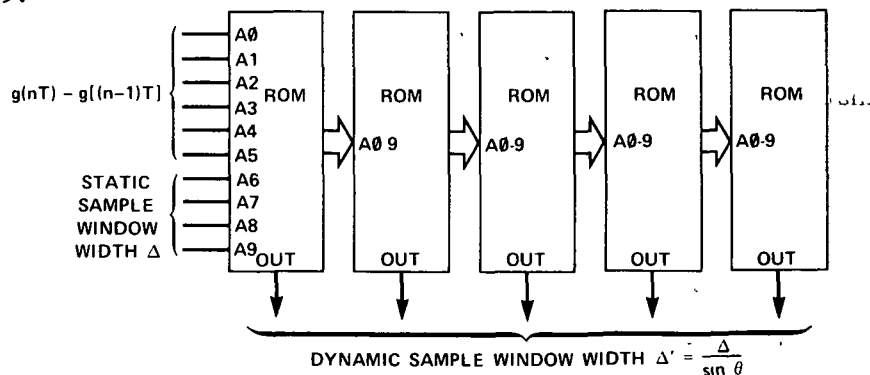

Figure 109.- ROM configuration for the dynamic adjustment of the sample window widths.

Clearly, the presently implemented system is already quite complex and there certainly will be an increase in the complexity after all proposed improvements have been implemented. With this kind of a complexity, it will be necessary to design the total system as a real-time, special purpose computer system, whereby the dynamic adjustments of the different parameters are controlled as much as possible by a central processor. This approach will result in an optimization of the performance of the system. The contour detector prototype II has been designed so that the border points, expectation, and sample window widths are determined in a binary format suitable for use with a microprocessor.

With the technology advances in the microprocessor area developing rapidly, this seems to be the approach of choice for the next generation contour detector. In the near future (within 6 months), a very fast microprocessor (Motorola M10800) will be on the market, which may be suitable for this real-time control task. The idea then will be to use the microprocessor mainly as a controller to dynamically adjust the different parameters. Some possible functions for the microprocessor in the contour detector are:

(a) *Dynamic expectation window width-* It was explained in chapter 10 that making the expectation window width narrow under low contrast conditions was very successful. In the present system, only one threshold level is used and the minimum width of the window must be set manually. Converting the difference of the sample levels in a digital format will allow the microprocessor to select the appropriate minimum expectation window width using more threshold levels.

265

(b) *Selection of zeroth- or first-order line extrapolation principle-* In the present system, either the zeroth- or first-order line extrapolation principle can be selected manually. The zeroth-order principle is usually selected under low contrast conditions if the longest chord is approximately perpendicular to the scan lines. In most cases, areas with low contrast (e.g., where the diaphragm crosses the heart border) and with higher contrast occur along the same outline. This suggests that the appropriate principle should be enabled automatically, depending on contrast and the direction of the outline; a measure for the direction of the outline is, of course, $g(nT) - g[(n-1)T]$. This automatic selection can be controlled very well by a microprocessor.

(c) *Dynamic adjustment sample window width-* This was explained in some detail earlier in the chapter.

(d) *Dynamic determination of the aortic valve plane-* This was also explained earlier in the chapter.

(e) *Calculation of area, longest chord, and volume-* Presently, the correction of the detected outline to actual values and the calculation of area, longest chord, and volume are done in a minicomputer (PDP-12). It is clear that this can also be done with a microprocessor, making the total system a stand-alone system. The minicomputer can then be assigned for other tasks.

(f) *Improved reliability-* If a microprocessor is used as the controller for the contour detector, the total IC count will be reduced, resulting in a more reliable system and one that is easier to service. Although the microprocessor will play an important role in the proposed next generation contour detector, it will still constitute only a

266

relatively small portion of the total system from the hardware point of
view. The ECL circuitry, for example, for determining the positions of
the expectation and sample points along a video line will still be
necessary, as well as the implemented arithmetic units, because of the
large number of arithmetic operations that must be done in a relatively
short time period. This will also allow the microprocessor to perform
other control functions in the meantime.

CONCLUSIONS

Results to date with the system have been extremely good. In most
cases, an accurate outline can be obtained, even in pictures with rela-
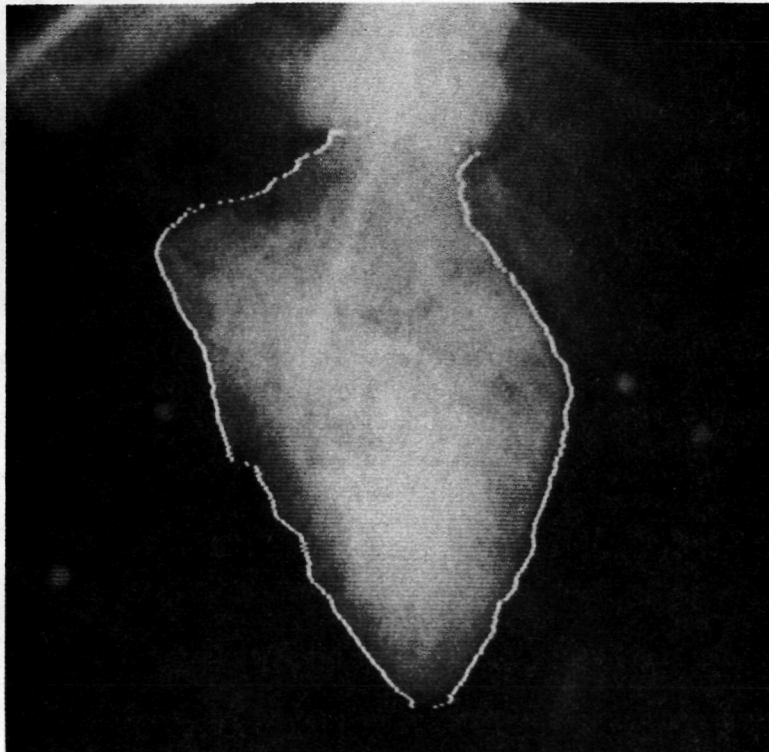tively low contrast. Figure 110 shows the detected contour for a left

Figure 110.- Resulting contour for a left ventricular angiogram of a dog
when applying the described algorithm.

267

ventricular angiogram of a dog when the described algorithm is applied.

The detector contour for a human left ventricle is shown in figure 111.

The obtained contours agree very well with the outline drawn by an

experienced investigator. An accurate outline is obtained in figure 111,

even at places of low contrast, as represented by the area where the
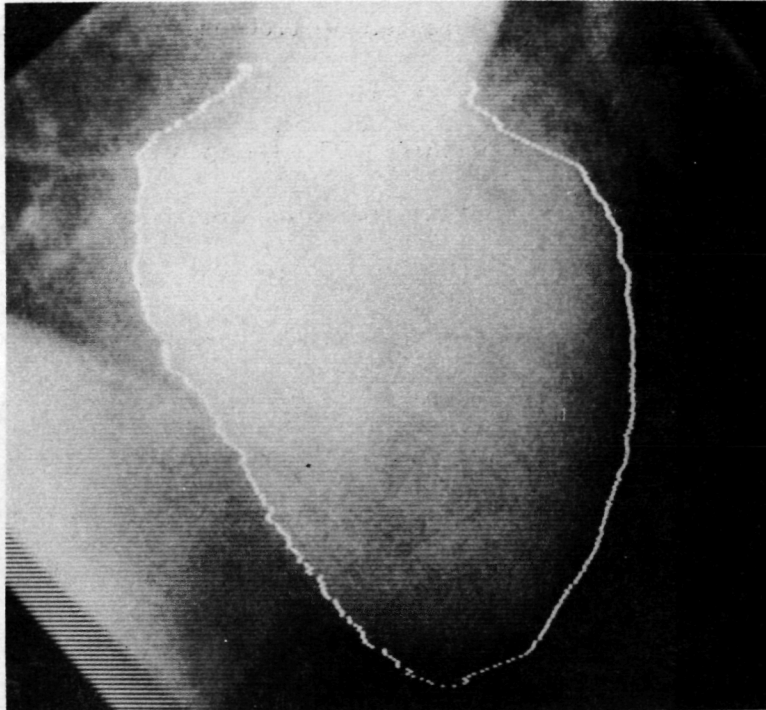
diaphragm crosses the left ventricular chamber.

Figure 111.- Resulting contour for a human left ventricle when apply-
ing the described algorithm. An accurate outline is obtained, even
at places of low contrast, as represented by the area where the
diaphragm crosses the left ventricular border.

The quantitative evaluation of the success of the border algorithm

showed the high accuracy of the system and the good agreement with manu-

ally drawn outlines. For this purpose, eight aluminum ellipses are used,

as well as four post-mortem dog casts and two series of canine left

ventricular angiograms. The areas and the distances from the border

points to the chord, connecting the left-hand side of the aortic valve

268

plane and the apex, are being calculated and compared for the automatic and manual border outlining. The video system determined the actual areas of the ellipses within 0.64 percent for all but the largest ellipse and the manual system within 1.18 percent for all but the two largest ellipses. For the casts, the areas computed by both methods agreed within 1.20 percent with maximum values for mean and standard deviations in border differences of 1.60 and 1.70 mm, respectively, for three of the four casts. For the first series of left ventricular angio- grams, the areas agreed within 4.27 percent for 12 of the 14 processed frames; in all cases the maximum values for mean and standard deviations in border differences were 1.85 and 1.60 mm, respectively. Thirteen frames were processed for the second series of left ventricular angio- grams; the areas agreed within 6.12 percent for 10 frames with maximum values for mean and standard deviations of 1.71 and 2.52 mm, respec- tively. In the overall evaluation, reproducibility of the video system was shown to be much greater than for manual tracings of the border.

A limited number of experiments has been done with the contour detector working on-line using the stored data on the video disc. In these cases, the system detected the outlines on-line. However, a more extensive evaluation of the system in a clinical or investigative envi- ronment on a day-to-day basis is necessary to determine which improve- ments remain to be made. Some improvements already have been proposed in chapter 12, which will result in: (1) improved border tracking capability, (2) less operator interaction, and (3) improved on-line use. Especially, the automatic determination of the aortic valve plane will be important for on-line use of the system.
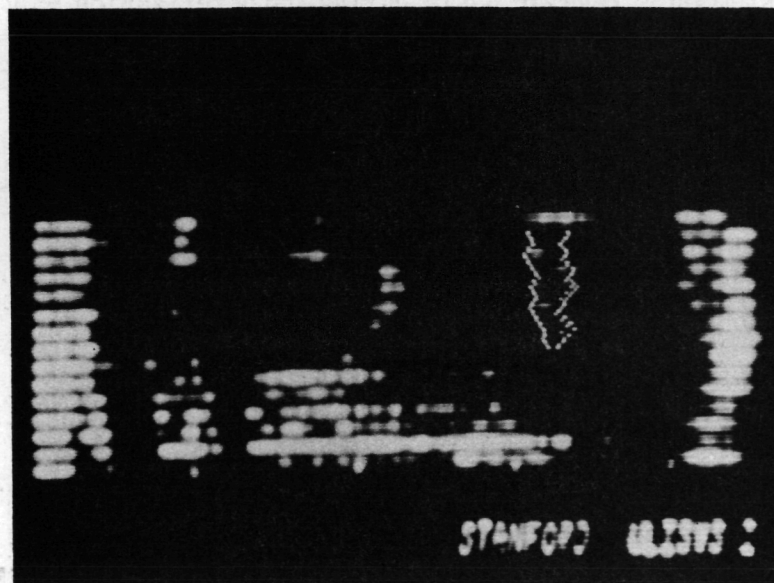
It is clear that the threshold detection technique is also applicable to other fields, for example, echocardiography. A cineframe of a human heart study using a multielement array was scanned with the contour detector and resulted in the contours shown in figure 112 (ref. 67). The left border in figure 112(a) indicates the left ventricular epicardial surface at the posterior wall; the detected structure in figure 112(b) is the anterior leaflet of the mitral valve. Only a small portion of the total image could be selected for contour detection because of the particular implementation of the contour detector, but it clearly shows that the structures can be recognized by use of threshold detection.

The application of the presently proposed data acquisition system for on-line, real-time detection of left ventricular outlines has many advantages over presently used manual or semiautomatic procedures in a clinical or investigative environment. Conventional methods require time-consuming and tedious techniques of recording on film, manually drawing the outline, and storing the information in computer memory. The associated time delays can be days, if not weeks, and the reproducibility often is poor, especially if the margins are drawn by different investigators.

Projected use of the system during a catheterization will require the storage of the obtained video angiograms on a video disc; cineangiograms may be used as a secondary storage medium. Use of the disc will allow for selection of the initial frame to be studied and for the initial setting of the system parameters, such as the positioning of the starting point, the expectation and sample window widths, and the adjustment of the α factors for the reference levels. After this,

270
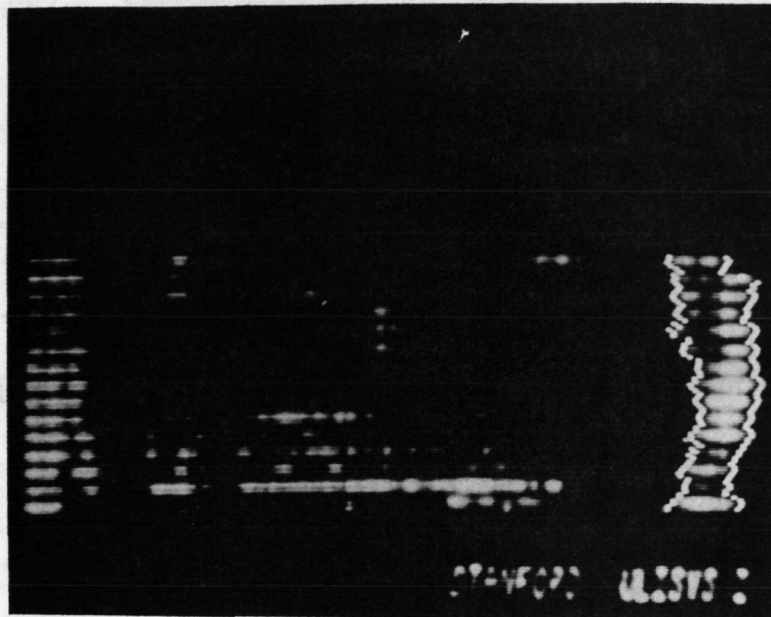
(a) Left border indicates the epicardial surface of the posterior wall of the left ventricle.

(b) Detected contour of the anterior leaflet of the mitral valve.

Figure 112.- The threshold detection technique applied to Echocardiography.

271

the disc can be run at 60 fields/sec and the system will automatically detect the contour. By limiting the display on the viewing monitor to the detected outline of the left ventricular chamber, the investigator can concentrate on its dynamic changes. A hard copy of a contourgraph and the calculated areas, longest chords, and volumes will be available within a few minutes as computer output functions. At the same time, these data can be correlated with simultaneously occurring pressure and flow events. If necessary, individual angiographic frames or the whole cycle can be replayed. With all the information now available, the investigator can verify the validity of the study and provide a diagnosis before the patient has left the table. This will obviously result in better patient care and decreased cost, which justifies the use of this system on a regular basis during catheterization studies.

When using a biplane x-ray system whereby both projections are displayed side by side on the video monitor, the most practical and economical solution will be to process the two projections sequentially.

Ames Research Center

National Aeronautics and Space Administration

Moffett Field, Calif. 94035, November 17, 1975

The video rectangle generator is an electronic circuit that generates the video signal for a rectangle. The polarity of the rectangle can be selected so that it is displayed on the viewing monitor as a bright structure against a dark background or as a dark structure against a bright background. The rectangle can be positioned arbitrarily on the TV monitor screen. The height and width can be adjusted independently, but they are always vertical and horizontal. Figure 113 shows the rectangle as a bright structure against a dark background.
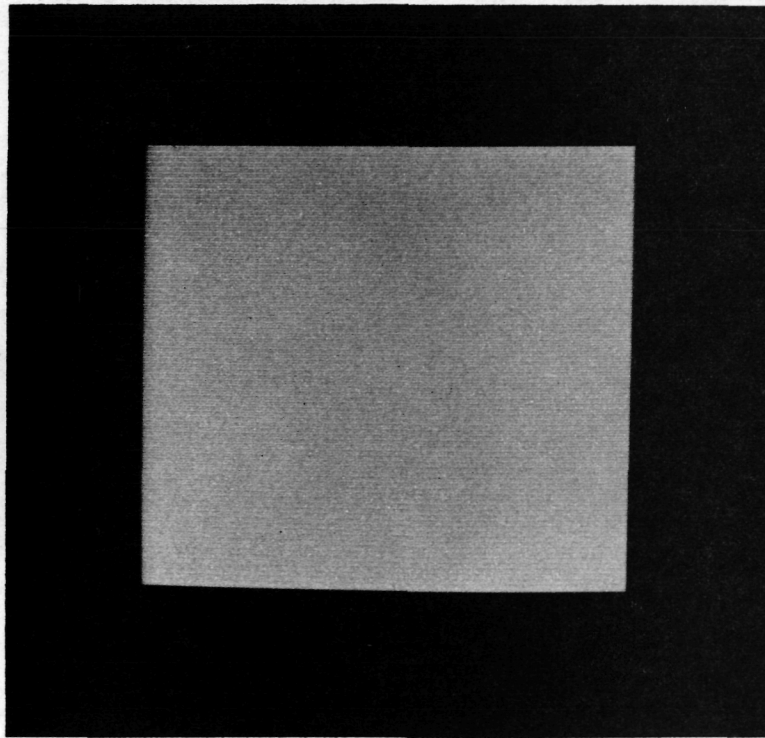

Figure 113.- The video rectangle as viewed on a TV monitor.

This ideal model can be seen as a very rough approximation for a ventricle. When using negative cineangiograms, the left ventricle is shown as a bright chamber against a dark background. A video angiogram

from video disc or tape, on the contrary, displays the left ventricle on the viewing monitor as a dark cavity with a brighter background. Thus both situations can be simulated with this video rectangle generator.

Such a simple repetitive signal has proven to be very helpful during the design of the contour detector and the computer interface. It is clear that the contour detector finds a very stable contour around this rectangle. This is very advantageous for the initial adjustments of the different parameters in the contour detector. Stable oscilloscope displays result because of the ease of triggering a repetitive signal. Actual time delays, for example, can be measured very accurately and the design of the system can be optimized according to the obtained information. Figure 114 is an example of a detected contour. The first part
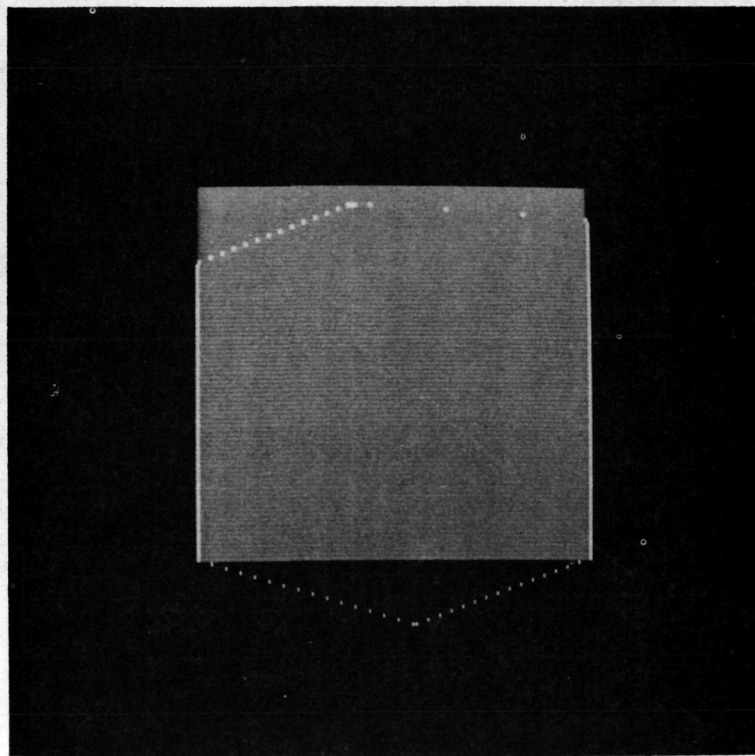

Figure 114.- Detected contour for the video rectangle.

274

of the right border from the starting point to the right side of the rectangle is again the aortic valve plane. The slopes of the other non-vertical parts of the contour are determined by the corresponding expectation window widths. An outpulse is again generated in the normal way as described in chapter 7. It is also possible to terminate the detection at the last line of the rectangle by applying an outpulse, generated by the video rectangle generator at the end of that line (fig. 115).
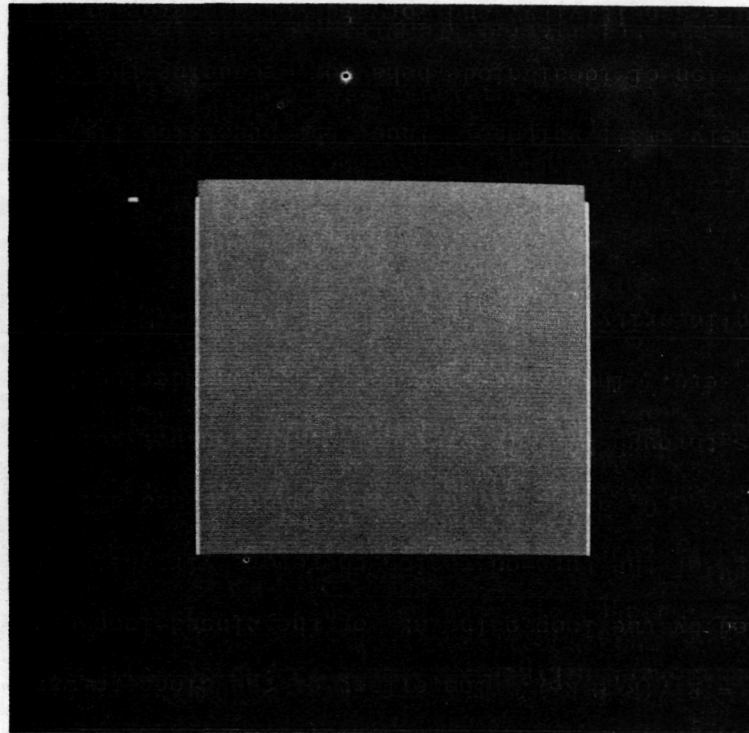

Figure 115.- Contour detection is halted at the bottom of the rectangle by applying an internally generated outpulse.

The actual implementation of the circuiting is shown in figure 116. Required input signals are the vertical, horizontal, and composite synchronization pulses from a sync generator.
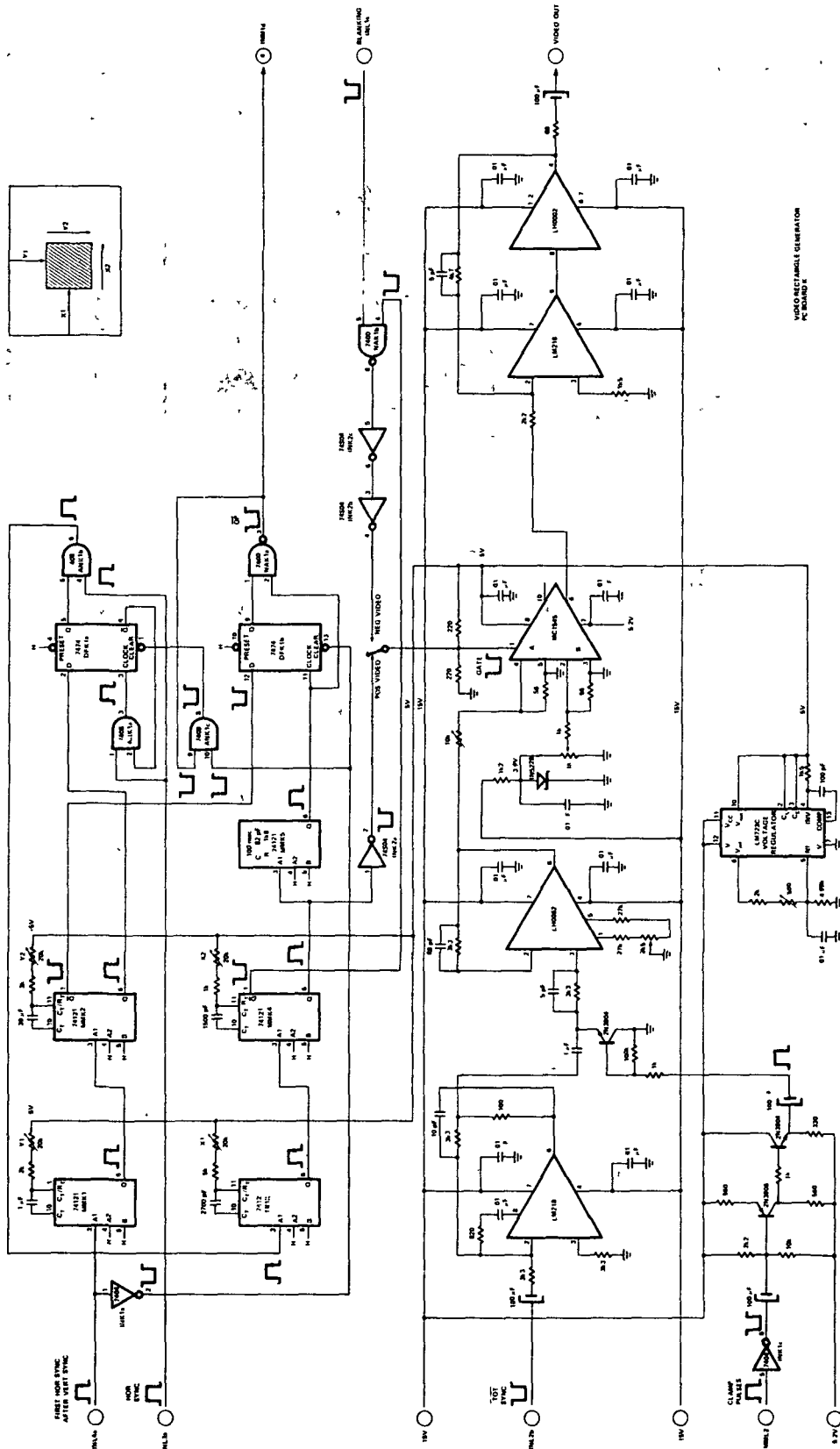
Figure 116.— Circuit diagram of the video rectangle generator.

Basically, the precision limiter implemented in the analog preprocessing circuitry is as shown in figure 117.   In this circuit, the
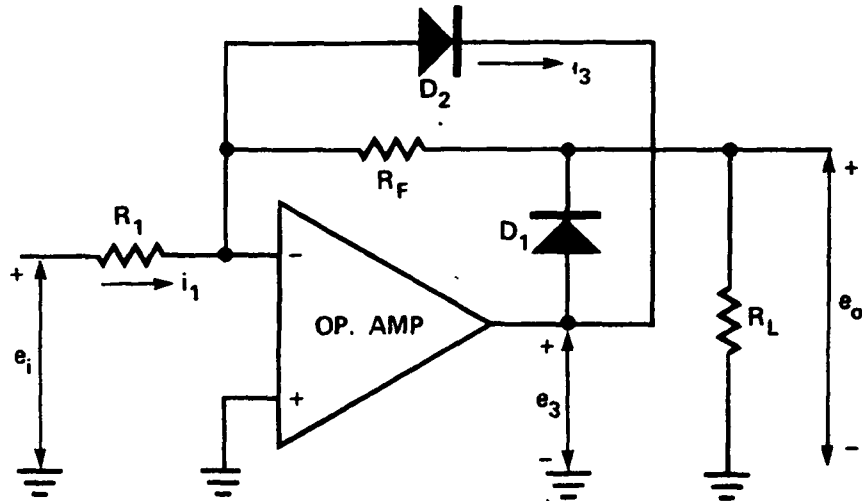

Figure 117.- Basic circuit of the precision limiter.

high open-loop gain of the operational amplifier is used to reduce the effect of the diode nonlinearity and the temperature sensitivity.   Using the usual op. amp. relationships and the formula for the diode voltage as a function of the current through the diode,

$$V_f = \frac{nkT}{q} \left[\ln(i_f - I_o) - \ln I_o \right] = f(i_f) \tag{262}$$

the circuit can be analyzed.

For $e_3 > 0$ ($e_1 < 0$), the current i_3 will be zero because $e_2 \approx 0$ and D2 is back-biased.   Essentially all input current i_1 flows through R_F, generating an output voltage

$$e_0 = -R_F i_1 = -\frac{R_F}{R_1} e_i \ , \qquad e_i < 0 \tag{263}$$

If the finite amplifier gain and diode nonlinearity are considered, the expression becomes

$$e_0 = \frac{\left(-\frac{R_F}{R_1}\right) e_i}{1 - \left(\frac{1}{A\beta}\right)\left[1 + \frac{f(i_2)}{e_0}\right]} \; , \tag{264}$$

where $\beta = R_1/(R_1 + R_F)$. The effect of the diode forward voltage $f(i_2)$ is reduced by the loop gain $A\beta$ of the closed-loop circuit. The "rounding" of the turn-on region therefore virtually disappears.

For $e_3 < 0$, diode D1 no longer conducts and all the input current i_1 flows through D2. Theoretically, the output voltage is then exactly equal to zero. The expression for e_0, considering finite gain and the diode nonlinearity, is

$$e_0 \approx - \frac{f(i_1)}{A} \cdot \frac{R_L}{R_F + R_L} \; , \quad e_i > 0 \tag{265}$$

an extremely small voltage. Thus, the precision limiter provides a good approximation of ideal diode behavior, reducing the diode nonlinearity, temperature sensitivity, and forward voltage drop by a factor equal to the loop gain of the amplifier. The transfer curve for the precision limiter is given in figure 118. In the actual implementation, hot carrier diodes were used, necessary in switching the high-frequency video signal.
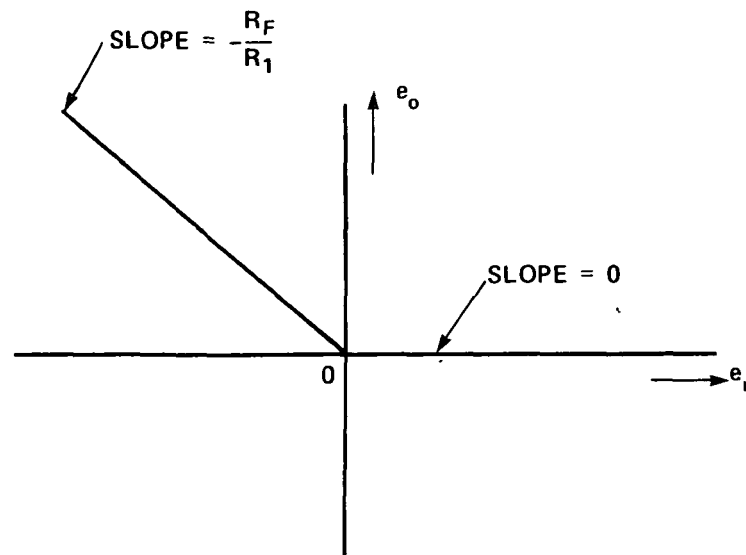
278

Figure 118.- Transfer curve of precision limiter.

Page intentionally left blank

The transfer function of the applied low-pass filter in the analog preprocessing circuitry is a three-pole Bessel function with a cutoff frequency at 1 MHz. The considerations for choosing this type of filter are given here.

Ideally, the magnitude of the transfer function is constant within the desired frequency range ω_c (called the passband) and zero over the rest of the frequency range (referred to as the stopband). Such an ideal magnitude response for a low-pass filter is shown in figure 119.
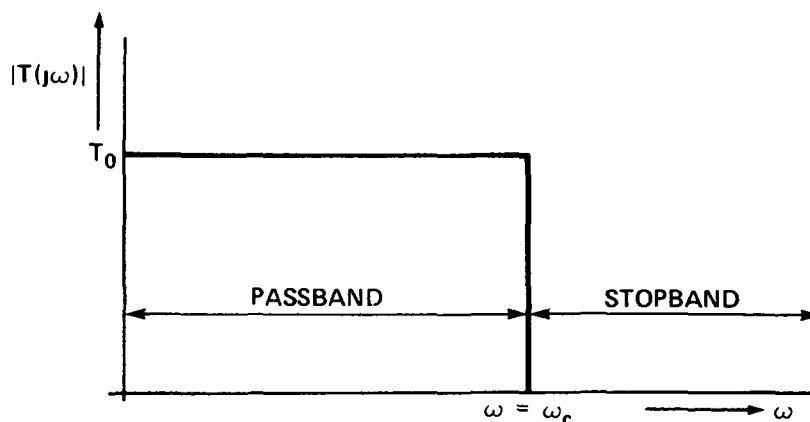
Figure 119.- Ideal low-pass filter transmission.

Clearly, such a transfer function is not physically realizable; the best one can do is to approximate the ideal transfer function as accurately as possible. Except for this steady-state frequency response, the transient response to a step input may also be of interest. Real video signals are more nearly characterized as a sequence of pulses or a series of step changes in signal amplitude and, as a result, a certain pulse or step response in the time domain will be a more important

requirement in this application than a flat transfer function in the frequency domain. In practice, the transient response of a linear circuit is usually specified in terms of the rise time. τ_R, the delay time τ_D, and the overshoot γ. These parameters are defined as follows:

(1) Rise time τ_R is defined as the time for a transient response to rise from 10 to 90 percent of its final (steady-state) value for a step input.

(2) Delay time τ_D is defined as the time required for a transient response to reach 50 percent of its final value for a step input.

(3) Overshoot γ is the difference between the peak value and final value of the step response expressed as a percentage of the final value.

Generally, it is true that the higher the overshoot the better the rise time. For pulse and video applications, usually an overshoot of higher than 5 percent is not desirable since it causes distortion of the transient signal. It is shown in reference 68 for linear circuits how the steady-state magnitude and/or phase distortion leads to a transient distortion, and that the approximation of linear phase leads to a better replica of the input signal than the approximation of maximally flat magnitude. For as little overshoot as possible, it is necessary to have a maximally flat delay (MFD) function rather than a maximally flat magnitude (MFM) function. The maximally flat delay response corresponds to a linear phase response; the rise time for this response will be somewhat poorer than for a MFM response.

For pulse and video applications, where the transient response must have low overshoot (approximately linear phase), there is an approximate

relationship between the rise time and the bandwidth (ref. 69). This empirical relationship is of the form

$$B \cdot \tau_R = 0.35 \text{ to } 0.45 \tag{266}$$

where B is the bandwidth from zero to the upper 3-dB cutoff frequency f_c. If the rise time for a particular application is known, then the required bandwidth can be determined using the above empirical relationship.

A calibration bar was placed under the x-ray image intensifier and x-rayed to determine the minimum rise time of the x-ray system. The resulting video signal was displayed on a Tektronix Waveform Monitor and a minimum rise time of 222 nsec was measured, which gives a required upper 3-dB frequency of

$$f_{3dB} = \frac{0.35}{222 \times 10^{-9}} = 1.574 \text{ MHz}$$

This measured rise time will always be much shorter than the rise times that occur in actual left ventricular angiograms. After having studied several angiograms, it was found that a typical left ventricular border has a rise time of approximately 640 nsec. This results in an upper 3-dB frequency of 546 kHz.

Because of the abovementioned requirements, a third-order Bessel filter was chosen with a cutoff frequency at 1 MHz. This filter has a linear phase response and the magnitude of the transfer function falls off at a rate of 18 dB/oct. beyond the cutoff frequency. The impulse and step response for low-pass filters with various numbers of poles in the complex frequency function are given in reference 70.

Page intentionally left blank

REFERENCES

1. Dodge, H. T.; Sandler, H.; Baxley, W. A.; et al.: Usefulness and
   limitations of radiographic methods for determining left ventricu-
   lar volume. *Am. J. Cardiol.*, 18:10-24, July 1966.

2. Sandler, H.: Dimensional analysis of the heart - A review. *The Am.
   J. of the Medical Sciences 260,* 1:56-70, July 1970.

3. Heintzen, P. H. (ed.): *Roentgen-, Cine-, and Video-Densitometry*:
   Fundamentals and applications for blood flow and heart volume
   determination. Stuttgart: Georg Thieme Verlag, 1971.

4. Sandler, H.; and Alderman, E.: Determination of left ventricular
   size and shape. *Circulation Research 18*, 1:1-8, Jan. 1974.

5. Bove, A. A.; Ziskin, M. C.; and Freeman, E.: Selection of optimum
   cineradiographic frame rate. Relation to accuracy of cardiac
   measurements. *Investigative Radiology*, 5:329-335, Sept.-Oct., 1970.

6. Chapman, C. B.; Baker, O.; Reynolds, J.; et al.: Use of biplane
   cinefluorography for measurement of ventricular volume. *Circula-
   tion*, 18:1105-1117, Dec. 1958.

7. Dodge, H. T.; Sandler, H.; Ballew, D. W.; et al.: The use of
   biplane angiocardiography for the measurement of left ventricular
   volume in man. *Am. Heart Journal 60*, 5:762-776, Nov. 1960.

8. Davila, J. C.; and Sanmarco, M. E.: An analysis of the fit of
   mathematical models applicable to the measurement of left ventricu-
   lar volume. *The Am. J. of Cardiol.*, 18:31-42, July 1966.

9. Sandler, H.; and Dodge, H. T.: The use of single plane angiocardio-
   grams for the calculation of left ventricular volume in man. *Am.
   Heart Journal 75*, 3:325-334, March 1968.

10. Tsakiris, A. G.; Donald, D. E.; Sturm, R. E.; et al.: Volume, ejection fraction and internal dimensions of left ventricle determined by biplane videometry. *Federation Proceedings 28*, 4:1358-1367, July-Aug. 1969.

11. Santamore, W. P.; DiMeo, F. N.; and Lynch, P. R.: A comparative study of various single-plane cineangiocardiographic methods to measure left-ventricular volume. *IEEE Transactions on Biomedical Engineering, BME-20*, 6:417-421, Nov. 1973.

12. Baker, O.; Khalaf, J.; and Chapman, C. B.: 'A scanner-computer for determining the volumes of cardiac chambers from cinefluorographic films. *Am. Heart Journal 62*, 6:797-803, Dec. 1961.

13. Rasmussen, D.: A method for spatial measurement of dynamic cardiac dimensions using single or biplane cinefluoroscopy. To be published in Investigative Radiology.

14. Rasmussen, D.: Clinical evaluation of a new method of obtaining spatial cardiac dimensions from sequential single plane cineangiograms. To be published in Investigative Radiology.

15. Sandler, H.; and Rasmussen, D.: Angiographic analysis of heart geometry. In *Roentgen-, Cine, and Video-Densitometry*: Fundamentals and applications for blood flow and heart volume determinations, edited by P. H. Heintzen. Stuttgart: Georg Thieme Verlag, 1971, pp. 212-223.

16. Greenleaf, J. F.; Ritman, E. L.; Coulam, C. M.; et al.: Computer graphic techniques for study of temporal and spatial relationships of multidimensional data derived from biplane roentgen videograms with particular reference to cardioangiography. *Computers and Biomedical Research*, 5:368-387, 1972.

17. Robb, R. A.; Johnson, S. A.; Greenleaf, J. F.; et al.: An operator-interactive, computer-controlled system for high fidelity digitization and analysis of biomedical images. *Proceedings of the Society of Photo-optical Instrumentation Engineers. Seminar, Quantitative Imagery in the Biomedical Sciences*, 40:11-24, Aug. 1973.

18. Johnson, S. A.; Robb, R. A.; Greenleaf, J. F.; et al.: The problem of accurate measurement of left ventricular shape and dimensions from multiplane roentgenographic data. *European Journal of Cardiology, Excerpta Medica*, I/3:241-258, 1974.

19. Robb, R. A.; Greenleaf, J. F.; and Ritman, E. L.: Three dimensional visualization of the intact thorax and contents: A technique for cross-sectional reconstruction from multiplanar x-ray views. *Computers and Biomedical Research*, 7:395-419, 1974.

20. Robb, R. A.: Three-dimensional reconstruction of the working heart and lungs by multiplanar x-ray scanning videodensitometry. *Proceedings of the Society of Photo-optical Instrumentation Engineers. Cardiovascular imaging and image processing, Theory and Practice - 1975*, 72: July 1975.

21. Ritman, E. L.; Johnson, S. A.; Sturm, R. E.; et al.: The television camera in dynamic videoangiography. *Radiology 107*, 2:417-427, May 1973.

22. Williams, J. P.; Sturm, R. E.; Tsakiris, A. G.; et al.: Biplane videoangiography. *Journal of Applied Physiology 24*, 5:724-727, May 1968.

23. Sturm, R. E.; and Wood, E. H.: The video quantizer: An electronic photometer to measure contrast in roentgen fluoroscopic images. *Mayo Clinic Proc.*, 43:803-806, Nov. 1968.

24. Wood, E. H.; and Sturm, R. E.: Use of videometry and electronic data processing for hemodynamic investigations by angiographic techniques. In: *Pathophysiology of congenital heart disease,* edited by Adams, F. H., Swan, H. J. C., and Hall, V. E., 1970, pp. 419-435.

25. Ritman, E. L.; Sturm, R. E.; and Wood, E. H.: A biplane roentgen videometry system for dynamic (60/sec) studies of the shape and size of circulatory structures, particularly the left ventricle. In: *Roentgen-, Cine-, and Video-Densitometry*: Fundamentals and applications for blood flow and heart volume determination, edited by P. H. Heintzen. Stuttgart: Georg Thieme Verlag, 1971, pp. 179-211.

26. Wood, E. H.; Ritman, E. L.; and Sturm, R. E.: The problem of determination of the roentgen density, dimensions and shape of homogeneous objects from biplane roentgenographic data with particular reference to angiocardiography. *Proceedings of the San Diego Biomedical Symposium*, 11: Feb. 1972.

27. Greenleaf, J. F.; Ritman, E. L.; and Wood, E. H.: Dynamic computer generated displays for study of the human left ventricle. *Proceedings of the Society of Photo-optical Instrumentation Engineers. Seminar, Developments in Electronic Imaging Techniques*, 32:111-119, Oct. 1972.

288

28. Ritman, E. L.; Sturm, R. E.; and Wood, E. H.: Biplane roentgen videometric system for dynamic (60/sec) studies of the shape and size of circulatory structures, particularly the left ventricle. *The Am. J. of Cardiology*, 32:180-187, Aug. 1973.

29. Dumesnil, J. G.; Ritman, E. L.; and Frye, R. L.: Quantitative determination of regional left ventricular wall dynamics by roentgen videometry. *Circulation*, 50:700-708, Oct. 1974.

30. Covvey, H. D.: Measuring the human heart with a real-time computing system. *Data Processing Magazine*: 27-32, May 1970.

31. Marcus, M. L.; Schuette, W. H.; and Whitehouse, W. C.: An automated method for the measurement of ventricular volume. *Circulation*, 45:65-76, Jan. 1972.

32. Marcus, M. L.; Schuette, W. H.; and Whitehouse, W. C.: Use of a video system in the study of ventricular function in man. *The Am. J. of Cardiology*, 32:175-179, Aug. 1973.

33. Chow, C. K.; and Kaneko, T.: Automatic boundary detection of the left ventricle from cinangiograms. *Computers and Biomedical Research*, 5:388-410, 1972.

34. Kaneko, T.; and Mancini, P.: Straight-line approximation for the boundary of the left ventricular chamber from a cardiac cineangiogram. *IEEE Transactions on Biomedical Research*, BME-20, 6:413-416, Nov. 1973.

35. Tasto, M.: Guided boundary detection for left ventricular volume measurement. *Philips Forschungslaboratorium GmbH*, Hamburg, 1973.

36. Modestino, J. W.; and Kaufman, H.: Digital image processing with application to angiocardiograms. Presented at Eascon, 1974.

37. Griffith, R. L.; Grant, C.; and Kaufman, H.: An algorithm for locating the aortic valve and the apex in left-ventricular angiocardiograms. *IEEE Transactions on Biomedical Engineering*, *BME-21*, 5:345-349, Sept. 1974.

38. Robb, R. A.: Computer-aided contour determination and dynamic display of individual cardiac chambers from digitized serial angiocardiographic film. In *Roentgen-, Cine-, and Video-Densitometry*: Fundamentals and applications for blood flow and heart volume determination, edited by P. H. Heintzen. Stuttgart: Georg Thieme Verlag, 1971, pp. 170-178.

39. Robb, R. A.: *Computer aided analysis of cardic dynamics using roentgenographic and videometric techniques.* Ph.D. Dissertation, University of Utah, Aug. 1971.

40. Wiscomb, W. K.: A hardware system for man-machine interaction in the study of left ventricular dynamics. In *Roentgen-, Cine-, and Video-Densitometry*: Fundamentals and applications for blood flow and heart volume determination, edited by P. H. Heintzen. Stuttgart: Georg Thieme Verlag, 1971, pp. 165-169.

41. Clayton, P. D.; Harris, L. D.; and Rumel, S. R.: Left ventricular videometry. *Computers and Biomedical Research*, 7:369-379, 1974.

42. Beckenbach, E. S.; and Desilets, D. T.: The computerization of high speed cineangiocardiographic left ventricular volume determination. *Proceedings of the Society of Photo-optical Instrumentation Engineers. Seminar, Pattern Recognition*, 18:173-192, 1969.

43. Newell, J. D.; Keller, R. A.; and Bailey, N. A.: A simple method for the generation of organ and vessel contours from roentgeno-graphic or fluoroscopic images. *Medical Physics 2*, 2:73-75, March/April 1975.

44. Heintzen, P. H.; Malerczyk, V.; and Pilarczyk, J.: On-line pro-cessing of the video-image for left ventricular volume determina-tion. *Computers and Biomedical Research*, 4:474-485, 1971.

45. Heintzen, P. H.; Malerczyk, V.; and Pilarczyk, J.: A videometric technique for automated processing of pressure-volume-diagrams. *Computers and Biomedical Research*, 4:486-492, 1971.

46. Heintzen, P. H.; Brennecke, R.; Bürsch, J. H.; et al.: Automated videoangiocardiographic image analysis. *IEEE Computer, 8*, 7:55-64, July 1975.

47. Alderman, E. L.; Sandler, H.; and Brooker, J. Z.: Light-pen com-puter processing of video image for the determination of left ventricular volume. *Circulation*, 47:309-316, Feb. 1973.

48. Slager, C. J.; and Verbeek, B. E. J. M.: *Automatische detectie van de linkerventrikelcontour m.b.v. op rontgenfoto's toegepaste televisie technieken.* Thesis, Electronics Laboratory, Technolo-gical University, Delft, April 1971, pp. 1-70.

49. Groeneweg, W. H.: *Hartcontourdetectie m.b.v. videotechniek.* Thesis, Electronics Laboratory, Technological University, Delft, March 1972, pp. 1-78.

50. Veen, van, B. L. J.: *Verbeteringen aan een schakeling voor automatische detectie van de linkerventrikelcontour.* Thesis, Electronics Laboratory, Technological University, Delft, March 1973, pp. 1-53.

51. Noz, W. A.: *Hartcontourdetectie.* Thesis, Electronics Laboratory, Technological University, Delft, June 1974, pp. 1-146.

52. de Jong, L. P.; and Slager, C. J.: Automatic detection of the left ventricular outline in angiographs using television signal processing techniques. *IEEE Transactions on Biomedical Engineering, BME-22,* 3:230-237, May 1975.

53. Reiber, J. H. C.: *Rekenautomaat voor de real-time bepaling van de linkerventrikel volumina.* Thesis, Electronics Laboratory, Technological University, Delft, Nov. 1971, pp. 1-123.

54. Anon.: *PDP-12 system reference manual.* Digital Equipment Corporation. Maynard, Mass., 1972.

55. McCluskey, E. J.: Error detecting and error-correcting codes. Notes Switching Theory (EE 181), Stanford University, Oct. 1972.

56. Linford, J.: *Error detection and correction using exclusive-or gates and parity trees.* Motorola Application Note AN-496A. Motorola Semiconductor Products Inc., 1973, pp. 1-10.

57. Hamming, R. W.: Error-detecting and error-correcting codes. *Bell System Technical Journal,* 29:147-160, April 1950.

58. EIA Standard, RS-330: *Electrical performance standards for closed circuit television camera 525/60 interlaced 2:1.* Nov. 1966.

59. Rasmussen, D.: Computer measurement and representation of the heart in two and three dimensions. *Proceedings of the Society of Photo-optical Instrumentation Engineers. Cardiovascular Imaging and Image Processing, Theory and Practice - 1975,* 72: July 1975.

60. Charlton, K. E.: *Reform.* Programming Methods, Inc., Mountain View, Calif., Feb. 1975, pp. 1-33.

292

61. Gordon, R.: *The RPP-package.* Programming Methods, Inc., Mountain View, Calif., Sept. 1975.

62. Duda, R. O.; and Hart, P. E.: *Pattern classification and scene analysis.* John Wiley and Sons, Inc., New York., 1973.

63. Rosenfeld, A.: *Picture processing by computer.* Academic Press, 1969.

64. Fuchs, W. A.; Messerschmid, U.; Herren, U.; et al.: Electronic detail enhancement in roentgen television. *Investigative Radiology,* 7:140-146, May-June 1972.

65. Vary, A.: Investigation of an electronic image enhancer for radiographs. NASA Technical Memorandum TM X-68,025, 1972.

66. Kovásznay, L. S. G.; and Joseph, H. M.: Image processing. *Proceedings IRE,* 43:560-570, May 1955.

67. Plummer, J. D.; Meindl, J. D.; and Maginness, M. G.: An ultrasonic imaging system for real-time cardiac imaging. *Proceedings 1974 IEEE International Solid-State Circuits Conference,* 162-163, Feb. 1974.

68. Ghausi, M. S.: *Principles and design of linear active circuits.* McGraw-Hill Book Co., Inc., New York, Chapters 4 and 16, 1965.

69. Gibbons, J. F.: *Semiconductor Electronics.* McGraw-Hill Book Co., Inc., New York, Chapter 18, 1966.

70. Henderson, K. W.; and Kants, W. H.: Transient responses of conventional filters. *IRE Transactions on Circuit Theory,* 333-347, Dec. 1958.

"The aeronautical and space activities of the United States shall be conducted so as to contribute . to the expansion of human knowledge of phenomena in the atmosphere and space The Administration shall provide for the widest practicable and appropriate dissemination of information concerning its activities and the results thereof"
—NATIONAL AERONAUTICS AND SPACE ACT OF 1958

NASA SCIENTIFIC AND TECHNICAL PUBLICATIONS

TECHNICAL REPORTS Scientific and technical information considered important, complete, and a lasting contribution to existing knowledge

TECHNICAL NOTES Information less broad in scope but nevertheless of importance as a contribution to existing knowledge

TECHNICAL MEMORANDUMS Information receiving limited distribution because of preliminary data, security classification, or other reasons Also includes conference proceedings with either limited or unlimited distribution

CONTRACTOR REPORTS Scientific and technical information generated under a NASA contract or grant and considered an important contribution to existing knowledge

TECHNICAL TRANSLATIONS Information published in a foreign language considered to merit NASA distribution in English

SPECIAL PUBLICATIONS Information derived from or of value to NASA activities Publications include final reports of major projects, monographs, data compilations, handbooks, sourcebooks, and special bibliographies

TECHNOLOGY UTILIZATION PUBLICATIONS Information on technology used.by NASA that may be of particular interest in commercial and other non-aerospace applications Publications include Tech Briefs, Technology Utilization Reports and Technology Surveys

Details on the availability of these publications may be obtained from·
SCIENTIFIC AND TECHNICAL INFORMATION OFFICE
NATIONAL AERONAUTICS AND SPACE ADMINISTRATION
Washington, D.C. 20546